UNIVERSITE D'ABOMEY - CALAVI (UAC)

ECOLE DOCTORALE SCIENCES DE LA VIE ET DE LA TERRE

Registered under N°: …385….

A DISSERTATION

Submitted

In partial fulfillment of the requirements for the degree of

DOCTOR of Philosophy (PhD) of the University of Abomey-Calavi (Benin Republic)
In the framework of the
Graduate Research Program on Climate Change and Water Resources (GRP-CCWR)

By
Daniel KWAWUVI
Public defense on: 04/24/2023

======

INTRA-SEASONAL RAINFALL VARIABILITY AND ITS IMPLICATIONS ON STREAMFLOW IN THE OTI BASIN, WEST AFRICA

======

Supervisors:
Daouda Mama, Professor, Université d'Abomey-Calavi, Benin
Sampson K. Agodzo, Professor, Kwame Nkrumah University of Science and Technology (KNUST), Kumasi, Ghana
Andreas Hartmann, Professor, Technical University of Dresden, Germany

======

Reviewers:

Expédit W. VISSIN, Prof. Université d'Abomey-Calavi, Benin
Philip G. OGUNTUNDE, Prof. The Federal University of Technology, Nigeria
Kwasi PREKO, Prof. Kwame Nkrumah University of Science and Technology, Ghana

======

JURY

CODO Francois de Paule	Full Professor, University of Abomey Calavi, UAC, Benin	President
VISSIN Expédit	Full Professor, University of Abomey-Calavi, UAC, Benin	Reviewer
OGUNTUNDE Gbenro Philip	Full Professor, Federal University of Technology, Akure, Nigeria	Reviewer
PREKO Kwasi	Full Professor, Kwame Nkrumah University of Science and Technology (KNUST), Kumasi, Ghana	Reviewer
ALAMOU A. Eric	Full Professor, UNSTIM, Benin	Examiner
MAMA Daouda	Full Professor, University of Abomey Calavi, UAC, Benin	Supervisor
AGODZO K. Sampson	Full Professor, Kwame Nkrumah University of Science and Technology (KNUST), Kumasi, Ghana.	Co-supervisor

Dedication

This work is dedicated to my Dad EX-WOI James Kwawuvi, my brothers and sisters and friends who supported me either materially or through inspiration during my PhD study at WASCAL, Universite d'Abomey-Calavi in the Republic of Benin.

Acknowledgement

This PhD work is realized in the framework of the West African Science Service Center on Climate Change and Adapted Land use (WASCAL) and funded by the German Federal Ministry of Education and Research (BMBF) in collaboration with the Benin Ministry of High Education and Scientific Research (MESRS).

My profound gratitude goes to my supervisors, Prof. Dr. Daouda Mama (Université d'Abomey Calavi, Republic of Benin), Prof. Sampson K. Agodzo (Kwame Nkrumah University of Science and Technology, Kumasi, Ghana) and Prof. Dr. Andreas Hartmann (Technical University of Dresden, Germany), for their exceptional supervision. I am grateful for their time, constructive critiques, suggestions and encouragements.

My appreciation also goes to Dr. Isaac Larbi and Dr. Andrew Limantol (University of Environment and Sustainable Development, Ghana), Tesfalem Abraham (University of Freiburg, Germany, and Hawassa University, Ethiopia) Dr. Enoch Bessah (Kwame Nkrumah University of Science and Technology, Ghana), Mr. Benjamin Bonkoungou, Mr. Max Gustav, Ms. Luo Lichuan, Kübra Özdemir Çalli and all staff of the Institute of Groundwater Management, Technical University of Dresden, Germany who assisted me in a way or the other during the execution of this research and during my stay in Germany.

My respect to the staff of WASCAL Graduate school, Climate change and water resources at Université d'Abomey Calavi as well as my colleagues who in their various ways assisted me.

Finally, my sincere admiration goes to my father, EX-WOI James Kwawuvi, my siblings and Ms. Yetunde Mojisola Rasaq for their constant support granted me throughout this programme.

Abstract

This study assessed the intraseasonal rainfall variability and its implications on streamflow in the Oti River Basin in West Africa. The specific objectives were to: (i) determine the intra-seasonal rainfall variability and trends for the historical period (1981-2010) and future period (2021-2050) in the Oti basin. (ii) determine the projected changes in intra-seasonal rainfall variability indicators in the Oti basin for the future period (2021-2050) and (iii) assess the impact of intra-seasonal rainfall variability on streamflow using the Hydrologiska Byråns Vattenbalansavdelning (HBV) model. The analysis was performed using high-resolution and quality-controlled climate data from the Ghana Meteorological Agency, National Meteorological Service of Togo, Meteorological Department of Benin, Climate Hazards Infrared and Precipitation Stations (CHIRPS), and NASA-POWER. The analysis for the future period was performed under RCP4.5 and RCP8.5 scenarios using a multi-model mean ensemble of eight bias-corrected regional climate models based on the quantile-quantile mapping method and from the Coordinated Regional Climate Downscaling Experiment (CORDEX-Africa). The study also used discharge data from the Water Resources Commission, Ghana, Water Resources Directorate (Togo), National Hydrological Service (DGIRH) of Burkina Faso and the Direction Generale de L'eau, Benin. The study revealed a likely decline in mean rainfall in the future by about 103.6 mm/yr (RCP4.5) and 45.9 mm/yr (RCP8.5). It also projected a decline in mean rainfall during the rainy season by about 90.8 mm/yr (RCP4.5) and 34.6 mm/yr (RCP8.5). The study further found a late onset of rains in the basin by about +16 days (RCP4.5) and +15 days (RCP8.5) which would possibly have a rippling effect on rainfall cessation in the basin causing it to occur earlier by a decrease of about 21 days under both RCP4.5 and RCP8.5 scenarios, with regards to the historical period. This subsequently resulted in shortening the length of rainy season by about 37 days (RCP4.5) and 36 days (RCP8.5). The number of wet and dry days are projected to increase and decrease respectively. Additionally, the streamflow of the basin was evaluated and projected for the future using the HBV hydrologic model. The mean multi-model ensemble predicted an increase in mean monthly streamflow at all sub-basins in the future (2021-2050) relative to the historical period (1981-2010) except Arly which is anticipated to have a decrease in its streamflow by about 2.79% (RCP4.5) while it will increase by about 31.17% (RCP8.5). The anticipated variations in the rainfall could affect the scheduling of agriculture, its sustainability and could place the basin a water-related stress.

Key words: Oti River Basin, HBV model, rainfall variability, onset, cessation, anomaly.

Synthèse de la Thèse

Résumé

Cette étude a évalué la variabilité intrasaisonnière des précipitations et ses implications sur le débit dans le bassin de la rivière Oti en Afrique de l'Ouest. Les objectifs spécifiques étaient de (i) déterminer la variabilité intrasaisonnière des précipitations pour la période historique (1981-2010), la période future (2021-2050) dans le bassin de l'Oti. (ii) déterminer les changements prévus dans les indicateurs de variabilité intra-saisonnière des précipitations dans le bassin de l'Oti pour la période future (2021-2050) et (iii) évaluer l'impact de la variabilité intra-saisonnière des précipitations sur le débit en utilisant le modèle HBV. L'analyse a été réalisée à l'aide de données à haute résolution et de qualité contrôlée provenant de stations météorologiques (données climatiques et de débit), les données de précipitations CHIRPS (*Climate Hazards Group Infrared Precipitation with Station*) et NASA-POWER (Prévision de la National Aeronautics and Space Administration Concernant les Ressources Énergétiques Mondiales). L'analyse pour la période future a été réalisée dans le cadre des scénarios RCP4.5 et RCP8.5 à l'aide d'un ensemble moyen multi-modèle de huit modèles climatiques régionaux corrigés sur la base de la méthode de cartographie quantile-quantile et issus de l'expérience CORDEX-Africa (Coordinated Regional Climate Downscaling Experiment). L'étude a révélé une baisse probable des précipitations moyennes dans le futur d'environ 103,6 mm/an (RCP4.5) et 45,9 mm/an (RCP8.5). Elle prévoit également une baisse des précipitations moyennes pendant la saison des pluies d'environ 90,8 mm/an (RCP4.5) et -34,6 mm/an (RCP8.5). L'étude a également révélé un décalage vers l'avant du début des pluies dans le bassin d'environ +16 jours (RCP4.5) et +15 jours (RCP8.5), ce qui pourrait avoir des répercussions sur l'arrêt des pluies dans le bassin, entraînant une diminution d'environ 21 jours dans les scénarios RCP4.5 et RCP8.5 par rapport à la période historique, et raccourcissant ensuite la durée de la saison des pluies à environ 37 jours (RCP4.5) et 36 jours (RCP8.5). Contrairement à la baisse prévue de la quantité de précipitations annuelles, la moyenne d'ensemble des modèles prévoit que le nombre de jours humides et secs dans le bassin augmenterait et diminuerait respectivement à l'avenir. En outre, le débit du bassin a été évalué et projeté pour l'avenir à l'aide du modèle hydrologique HBV. Les modèles prévoient une augmentation générale du débit mensuel moyen dans tous les sous-bassins à l'avenir (2021-

2050) par rapport à la situation de référence (1981-2010), à l'exception de l'Arly, dont le débit moyen devrait diminuer d'environ 2,79 % (RCP4.5) tandis qu'elle augmentera d'environ 31,17% (RCP8.5). A l'échelle annuelle, la moyenne de l'ensemble multi-modèle prévoit une augmentation de 5,24% à 41,94% du débit de pointe, et de 3,83% à 46,83% du débit d'étiage dans les sous-bassins.

Mots clé: Bassin de l'Oti, modèle HBV, variabilité des précipitations, début des précipitations, arrêt des précipitations, anomalie des précipitations.

Introduction

La sous-région de l'Afrique de l'Ouest est confrontée à de fortes variations des précipitations à la fois dans le temps et dans l'espace. Les fluctuations des précipitations restent une menace pour le bassin (Oti) partagé par le Ghana, le Burkina Faso, le Togo et le Bénin. Le bassin contribue à la production agricole (tant arable que pastorale) et sert à générer des revenus pour les pays dépendants de la région. Cependant, en raison de l'évolution constante du climat, les variations des précipitations dans le bassin ont conduit la région à subir des événements catastrophiques tels les sécheresses et les inondations, qui ont eu un impact négatif sur les vies humaines, les biens et les sources de revenus. Pour une gestion efficace de l'hydrologie du bassin, il est nécessaire de comprendre la distribution spatiotemporelle des précipitations dans le bassin à travers l'étude d'indicateurs tels que le total des précipitations annuelles, le total des précipitations saisonnières, le début et la fin des pluies, la durée de la saison des pluies et le nombre de jours humides et secs. Pour ces raisons, l'étude se concentre sur l'investigation des variations intrasaisonnières des précipitations dans le bassin de l'Oti, et comment ces variations pourraient avoir un impact sur le débit du bassin. De cette façon, l'étude fournira une meilleure compréhension de la distribution des précipitations et de ses variations anticipées dans le bassin sous les futurs scénarios de changement climatique, RCP4.5 et RCP8.5. Les objectifs spécifiques de l'étude étaient de : (i) déterminer la variabilité intra-saisonnières des précipitations pour la période historique (1981-2010), la période future (2021-2050) et leurs tendances dans le bassin de l'Oti. (ii) déterminer les changements prévus dans les indicateurs de variabilité intra-saisonnière des précipitations dans le bassin de l'Oti pour la période future (2021-2050) et (iii) évaluer l'impact de la variabilité intra-saisonnière des précipitations sur le débit en utilisant le modèle HBV.

Zone d'étude

Le bassin de la rivière Oti est situé dans quatre pays d'Afrique de l'Ouest à savoir le Ghana, le Burkina Faso, le Togo et le Bénin. Le bassin du fleuve Oti est partagé entre le Ghana, le Burkina Faso, le Togo et le Bénin. Il se situe entre les longitudes 6^0W et 2^0E et les latitudes 0^0 et 15^0N (figure 1). Il est l'un des sous-bassins du système du bassin de la Volta en Afrique de l'Ouest avec une superficie estimée à environ 72 000 km^2. Les précipitations annuelles varient de 1 010 mm (Nord) à 1 400 mm (Sud), avec une évaporation moyenne de 2,540 mm par an et un ruissellement d'environ 254 mm par an. Le bassin connaît un régime pluvial unimodal, avec un pic maximal en août. Les précipitations de la saison des pluies représentent environ 90 % des précipitations annuelles totales du bassin. La saison des pluies s'étend d'avril à octobre (AMJJASO) tandis que la saison sèche va de novembre à mars (NDJFM).

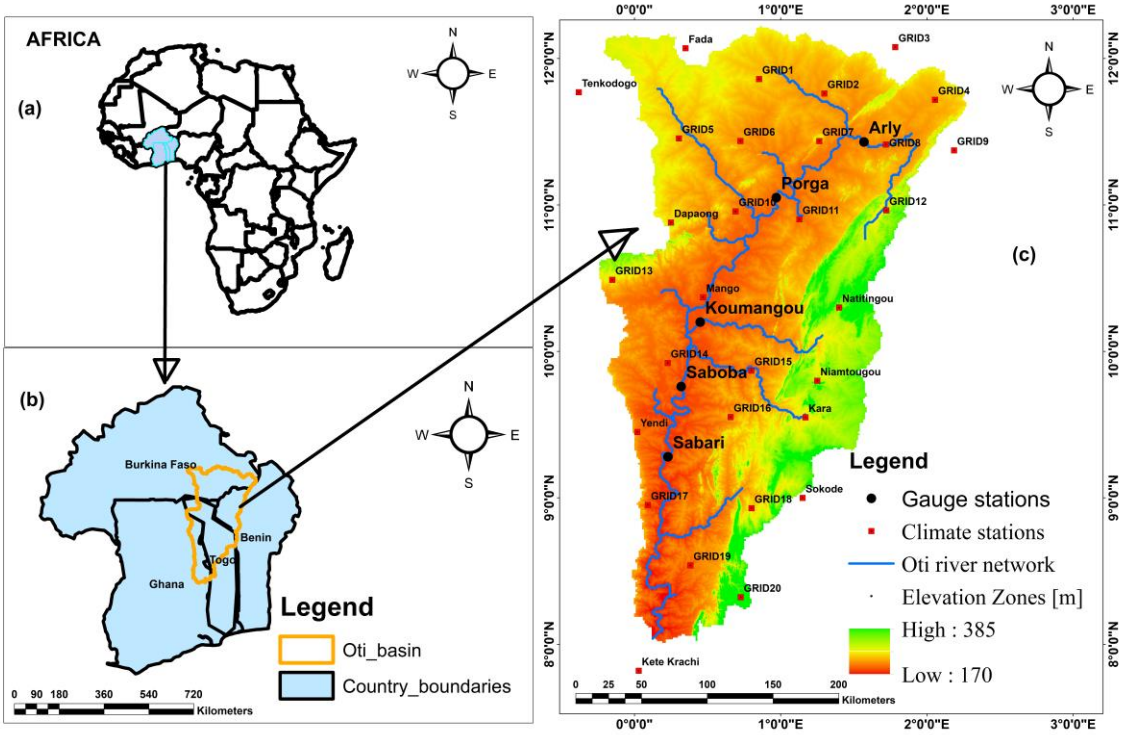

Figure 1 : Carte de la zone d'étude montrant (a) la localisation des pays riverains de l'Oti en Afrique, (b) le bassin de l'Oti (en jaune) partagé par le Ghana, le Burkina Faso, le Togo et le Bénin et (c) le modèle numérique d'élévation, les stations climatiques et de jaugeage, et le réseau fluvial dans le bassin de l'Oti.

Matériel et méthodes

L'étude a utilisé une combinaison de données climatiques de stations, de jeux de données CHIRPS et NASA POWER pour la période observée, 1981-2010, et ensemble moyen de 8 modèles RCA4 dynamiques à échelle réduite (Modèles Climatiques Régionaux, MCR) dans le cadre de l'expérience CORDEX-Africa (Expérience régionale coordonnée de réduction

d'échelle du climat) sous les scénarios RCP4.5 et RCP8.5 pour la période future, 2021-2050. Les MCR ont été obtenus à une résolution spatiale de $0,44^{o}\times0,44^{o}$ (~50km×50km). L'analyse pour la période future a été effectuée à l'aide d'un ensemble moyen multi-modèle des huit modèles climatiques régionaux corrigés des biais. Avant d'utiliser les données CHIRPS et NASA POWER pour d'autres analyses, elles ont été validées avec les données climatiques météorologiques à l'échelle mensuelle moyenne. Après validation, ils ont montré leur capacité à reproduire la climatologie du bassin. L'étude a ensuite analysé les indicateurs de variabilité intrasaisonnière des précipitations tels que le total des précipitations annuelles, le total des précipitations saisonnières (pluvieuses et sèches), le début et la fin des précipitations, la durée de la saison des pluies et le nombre de jours humides et secs dans le bassin pour les périodes historiques et futures. Les totaux des précipitations annuelles et saisonnières ont été déterminés comme la somme des précipitations pour chaque jour pour la période historique (1981-2010) et la période future (2021-2050). Les totaux des précipitations saisonnières ont été calculés sur la base des périodes de la saison des pluies (AMJJASO) dans le bassin. La sortie des précipitations journalières simulées, provenant de l'ensemble des MCR corrigés des biais pour le futur proche (2021-2050) sous les scénarios RCP4.5 et 8.5 et les précipitations journalières observées (1981-2010) ont été utilisées pour calculer le début, la fin et la durée de la saison des pluies à l'aide d'Instat+v3.36. Le début des pluies a été défini comme le début de la saison, le jour le plus précoce étant le 1er avril, et pendant cette période, les 5 premiers jours recueillent un cumul d'au moins 20 mm de pluie, sans sécheresse supérieure à 7 jours dans les 30 jours suivants. L'arrêt des pluies a été défini comme la fin de la saison qui se produit après le 1er octobre lorsque le bilan hydrique du sol a 0 mm de pluie. Pour calculer la date d'arrêt, l'évapotranspiration journalière moyenne de chaque station a été utilisée. En suivant la méthode de Penman-Monteith dans l'application Instat+v3.36, l'évapotranspiration moyenne journalière (ET_o) a été calculée en utilisant comme données d'entrée la température minimale et maximale journalière, l'humidité relative, la vitesse du vent et le rayonnement solaire. La durée de la saison des pluies (LRS) a été obtenue à partir de la différence entre le début et la fin des précipitations. Le nombre de jours de pluie et de jours secs a été déterminé en comptant tous les jours avec des précipitations $\geq 1,0$ mm comme pluvieux et les jours avec des précipitations $< 1,0$ mm comme secs. Le coefficient de variation (CV), l'écart-type (SD) et la moyenne ont été utilisés pour analyser les indicateurs de variabilité intrasaisonnière des précipitations passées et futures. Pour étudier la nature des précipitations au cours de la période d'observation de l'étude et pour déterminer les années sèches et humides, l'anomalie

des précipitations saisonnières (AMJJASO) a été calculée. La méthode d'interpolation pondérée par la distance inverse a été utilisée pour interpoler les indices pluviométriques calculés sur le bassin à l'échelle annuelle à partir des emplacements distincts. Pour évaluer l'impact de la variabilité intrasaisonnière des précipitations sur les débits et les projections de débits futurs, les variables d'entrée du modèle hydrologique Hydrologiska Byråns Vattenbalansavdelning (HBV) ont été préparées. La technique du polygone de Thiessen a été utilisée pour calculer les précipitations surfaciques à partir de mesures ponctuelles journalières des précipitations pour chacun des cinq sous-bassins discrétisés. Les données de température maximale et minimale de l'ensemble des huit modèles climatiques selon les scénarios RCP4.5 et RCP8.5 ont été utilisées pour estimer l'évapotranspiration potentielle pour la période future 2021-2050. Le modèle a été calibré (1981-1986) et validé (1987-1991), et la performance du modèle a été évaluée en utilisant un seuil d'efficacité de Nash-Sutcliffe ≥ 0,5. Le modèle HBV calibré a ensuite été piloté par la moyenne d'ensemble des projections climatiques des huit modèles climatiques régionaux corrigés des biais forcés par deux scénarios d'émissions de gaz à effet de serre (RCP4.5 et RCP8.5) et la moyenne d'ensemble historique des modèles. L'étude a appliqué les statistiques de tendance de Mann-Kendall (MK) pour évaluer les tendances des indicateurs de variabilité des précipitations analysés, ainsi que le débit projeté. L'estimateur de pente de Sen a été utilisé pour déterminer l'ampleur des tendances.

Résultats et discussion

Les résultats montrent que l'ensemble du bassin connaîtra probablement une baisse des précipitations, qui passeront de 1073,8 mm/an, soit la moyenne annuelle des précipitations pour la période historique (1981-2010), à environ 970,2 mm/an (RCP4.5) et 1027,9 mm/an (RCP8.5) dans le futur (2021-2050). La quantité de pluie pendant les périodes de la saison des pluies devrait également diminuer d'environ 90,8 mm/an (RCP4.5) et 34,6 mm/an (RCP8.5). En outre, l'étude a révélé que le début des pluies devrait être avancé, ce qui indique un retard dans le début des pluies. Ainsi, les pluies qui commençaient au tour du 8 mai (128 jours) au cours de la période historique, se déplaceraient probablement vers la période du 24 mai (144 jours) dans le cadre du scénario RCP4.5 et le 23 mai (143 jours) dans le cadre du RCP8.5 au cours de la période 2021-2050. Dans l'ensemble du bassin, on a découvert que l'arrêt des précipitations devrait se produire plus tôt dans le futur proche qu'au cours de la période historique. Ainsi, l'arrêt des précipitations se produira probablement autour du 7 octobre (280e

jour de l’année) dans les scénarios RCP4.5 et RCP8.5, ce qui indique un recul d'environ 21 jours par rapport à la période historique, qui s'est produite le 29 octobre (302e jour de l’année). La durée de la saison des pluies (LRS) dans le bassin serait probablement raccourcie par les changements prévus dans le début et la fin de la saison des pluies. Cela indique que la LRS serait raccourcie de 173 jours (historique) à environ 136 jours (RCP4.5) et 137 jours (RCP8.5) dans un futur proche. La moyenne d'ensemble des modèles prévoit une réduction du nombre de jours humides (NDD) du bassin inférieur vers le bassin supérieur dans le futur proche. Les analyses ont montré que le NDD augmenterait dans le bassin inférieur tandis qu'une diminution est prévue dans le bassin supérieur. En résumé, la moyenne des NDD dans l'ensemble du bassin montre une augmentation, ce qui contraste avec la diminution prévue des précipitations annuelles dans le bassin. Contrairement à la tendance à la sécheresse (dry-gets-drier) prévue par d'autres études, ces résultats prévoient une légère diminution du nombre de jours secs (NDD) dans l'ensemble du bassin. Cela pourrait être dû au fait que le modèle a surestimé l'influence du flux de la mousson d'été, ce qui explique pourquoi il a fourni une mauvaise approximation de la distribution spatiale du NDD. De la même manière, l'impact des vents maritimes et leur convergence sur le bassin peuvent être mis en évidence par la sous-estimation du NDD par le modèle. La diminution prévue des précipitations annuelles et les variations saisonnières projetées en termes de début et de fin des précipitations et de durée de la saison des pluies pourraient avoir de graves répercussions sur les activités sensibles au climat, telles que la planification de l'agriculture (cultures et élevage) et la production agricole, ainsi que sur le débit des cours d'eau du bassin. Des régimes pluviométriques inhabituels pourraient avoir un impact sur les cultures et entraîner des pertes de récolte.

En ce qui concerne la projection du débit du bassin, le modèle HBV a généré des valeurs NSE de (0,5 à 0,66) pour la calibration et de (-28,99 à 0,71) pour la validation. L'efficacité de Kling-Gupta (KGE) a également généré des valeurs de (0,49 à 0,75) pour la calibration et de (-4,09 à 0,72) pour la validation. Ces résultats ont montré un bon accord entre le débit observé et simulé dans les sous-bassins de Porga, Arly, Koumongou, Sabari et Saboba. L'analyse du cycle annuel du débit mensuel moyen a révélé que le débit moyen à Porga et Arly a diminué de 1,9 % et 31,9 % respectivement pour la période de validation (1987-1991), tandis que le débit moyen a augmenté d'environ 86 %, 66 % et 141,7 % à Koumongou, Sabari et Saboba respectivement pour la période de validation par rapport à la période d'étalonnage (1981-1986). Les projections du débit mensuel futur indiquent que le débit moyen augmenterait généralement dans tous les sous-bassins tant dans le scénario RCP4.5 que dans le scénario

RCP8.5, à l'exception de l'Arly qui devrait diminuer d'environ 2,79% dans le scénario RCP.45 tandis qu'elle augmentera d'environ 31,17% dans le scénario RCP8.5. En ce qui concerne le débit annuel futur, l'étude prévoit une augmentation de 5,24 % à 41,94 % du débit maximal et de 3,83 % à 46,83 % du débit minimal dans les sous-bassins.

Conclusion

En résumé, l'étude a mené des analyses sur un certain nombre d'indicateurs pluviométriques critiques, tels que le total des précipitations annuelles, le total des précipitations saisonnières (saisons humides et sèches), le début des pluies, la fin des pluies, la durée de la saison des pluies et le nombre de jours humides et secs dans le bassin de la rivière Oti pour les périodes historiques (1981-2010) et futures (2021-2050). Le modèle Hydrologiska Byråns Vattenbalansavedlning (HBV) modifié a été appliqué dans le bassin pour évaluer son débit et faire des projections pour la période future 2021-2050 selon les scénarios de changement climatique RCP4.5 et RCP8.5 (Representative Concentration Pathways). Ces études ont été réalisées pour examiner la variabilité intrasaisonnière des précipitations et ses implications sur le débit du bassin de la rivière Oti. L'étude prévoit une diminution future des précipitations annuelles dans le bassin, de 1 073,8 mm/an dans la période historique, d'environ 103,6 mm/an (RCP4.5) et 45,9 mm/an (RCP8.5). Les précipitations pendant la saison des pluies sont également susceptibles de diminuer, passant de 1038,6 mm/an pendant la période historique à environ 947. 7 mm/an (RCP4.5) et 1004 mm/an (RCP8.5). De même, pendant la saison sèche, la quantité de pluie qui était d'environ 35,3 mm/an devrait diminuer à environ 22,5 mm/an (RCP4.5) et 24 mm/an (RCP8.5). Bien que la quantité de précipitations annuelles et saisonnières projette une baisse générale, le nombre de jours humides et secs dans l'ensemble du bassin indique une augmentation et une diminution générales respectivement dans le futur selon l'ensemble du modèle. Le bassin devrait connaître un déplacement vers l'avant du début des pluies, du 8 mai (historique) au 24 mai environ (RCP4.5) et au 23 mai (RCP8.5). Ce déplacement du début des pluies aurait des répercussions sur la cessation et la durée de la saison des pluies, de sorte que les précipitations dans le bassin devraient cesser plus tôt, tandis que la durée de la saison des pluies deviendrait plus courte par rapport à la période historique.

L'étude a également révélé qu'après 10 ans de sécheresse exceptionnelle en 2027, le bassin connaîtra probablement une situation extraordinairement humide en 2037, pendant la saison des pluies, selon le scénario RCP4.5. Selon le scénario RCP8.5, une situation très humide se produirait probablement en 2028, tandis qu'une situation extrêmement sèche est attendue dans

le bassin en 2041 pendant la saison humide. Selon le scénario RCP4.5, le bassin connaîtra probablement une situation exceptionnellement humide en 2043 pendant la saison sèche, 17 ans après avoir connu une situation extrêmement sèche en 2026. En revanche, le scénario RCP8.5 prévoit que 2025 sera assez sec et que 2037 sera très humide. En outre, le débit du bassin a été évalué et projeté pour l'avenir en utilisant à la fois les données de la station et les données maillées du modèle hydrologique HBV. Les débits mensuels des cinq sous-bassins devraient augmenter à l'avenir, à l'exception de l'Arly, où l'on prévoit une diminution des débits. Toutes les stations auraient leurs pics maximum et minimum respectivement en août et en février.

L'étude a été confrontée à de nombreuses limitations, la plus importante étant la rareté et l'inadéquation des données recueillies par les stations pour le climat et le débit. Ceci a donc encouragé l'intégration des données CHIRPS, des données du projet NASA POWER pour les analyses dans le bassin de l'Oti. L'étude recommande donc que les études futures dans le bassin prennent en compte plus de MCR-GCM et de scénarios d'émission. Elle recommande également que le débit dans le bassin soit surveillé et enregistré de manière adéquate afin de soutenir la recherche qui offre des informations pour la mise en œuvre de mesures efficaces d'adaptation au changement climatique.

Table of Contents

List of Acronyms

AI	Aridity Index
CDF	Cumulative Distributive Function
CHIRPS	Climate Hazards Group Infrared Precipitation with Stations
CMhyd	Climate Model data for hydrologic modeling
CMIP5	Coupled Model Intercomparison Project
CORDEX	Coordinated Regional climate Downscaling Experiment
CV	Coefficient of Variation
DEM	Digital Elevation Model
DPHM-RS	Semi-Distributed Physically based Hydrological Model using Remote Sensing and GIS
ETo	Potential Evapotranspiration
GCMs	Global Climate Models
GDP	Gross Domestic Product
HBV	Hydrologiska Byrans Vattenbalansavedlning
IDW	Inverse Distance Weighted Interpolation
IPCC	Intergovernmental Panel on Climate Change
ITD	Inter-Tropical Discontinuity
JMA	Japanese Meteorological Agency
LRS	Length of Rainy Season
Max	Maximum
MERRA-2	Modern Era Restrospective-Analysis for Research and Applications, version 2
Min	Minimum
MISBA	Interactions Soil-Biosphere Atmosphere Model
MK	Mann-Kendall
MWH	Ministry of Works and Housing
NASA POWER	National Aeronautics and Space Administration Prediction of Worldwide Energy Resource
NDD	Number of Dry Days
NSE	Nash-Sutcliffe Efficiency
NWD	Number of Wet Days
ORB	Oti River Basin
PBIAS	Percentage Bias

PIHM	Penn State Integrated Hydrological Model
RCA4	Rossby Centre Regional Climate Models
RCMs	Regional Climate Models
RCP	Representative Concentration Pathway
RMSE	Root-Mean-Square Error
SD	Standard Deviation
SDGs	Sustainable Development Goals
SWAT	Soil and Water Assessment Tool
UN	United Nations
UNEP-GEF	United Nations Environment Programme-Global Environment Facility
VIC	Variable Infiltration Capacity
WASM	West African Summer Monsoon

List of figures

List of tables

Chapter 1: General Introduction

This chapter provides the background of the study, problem statement, literature review, research questions, objectives of the study, the hypothesis, novelty, scope of the thesis, the expected results and benefits and outline of the thesis.

1.1 Context and problem statement

Globally, variability in climate influences ecosystems and economic systems of countries, and in some cases results in disasters. Due to the high degree of climate variability, certain locations experience hot or cold spells, wet (more often than not, major rainstorms), or dry weather (Pabón & Dorado, 2008). The importance of lengthy climate series research has increased as a result of the hydrologic cycle's increased worldwide variation brought on by climatic change, which has made it more difficult to anticipate future climate patterns and their effects (Houghton et al., 1995).

In Africa, this variability in climate has an influence on crucial sectors like water, agriculture, energy, health, biodiversity (Kumi et al., 2020). Due to its extensive climatic susceptibility and little ability for adaptation, Africa ranks among the most susceptible continents. Considering poor climate surveillance and ongoing coverage limitations, information on recent global warming is constrained (IPCC, 2012). Consequently, (IPCC, 2014a) predicted that without efforts to mitigate climate change, there will be a substantial rise in temperature extremes, maximum wind speed, intense precipitation, extreme coastal high-water levels and droughts will intensify and last longer in the future. Hydrological and ecological processes will change in both time and space as a result of projected modifications in the water cycle caused by global warming (Mujere & Moyce, 2016).

West Africa is susceptible to severe floods and dry spells because of the region's substantial precipitation patterns over a wide range of scales (Thierry Lebel et al., 2009). According to Twisa & Buchroithner (2019) and Nhemachena et al. (2020), this can be attributed to the direct connection between rainfall and global climate. Variations in precipitation have led to severe floods and droughts in many locations in West Africa, presenting a serious risk to the sub-region (Ebi & Bowen, 2016). Particular instances are the 2017 flood which impacted approximately 1 million individuals (Adegoke et al., 2019; IFRC, 2017) as well as the 1983 drought episode, which resulted in deaths and destruction of farms and homes in Ghana (Ankrah et al., 2023). Climate fluctuations already affect the savannah and semiarid areas,

with droughts and flood events, particularly since the 1960s (Epule et al., 2017). Sadly, it is anticipated that climatic change will rise (Suleiman & Ifabiyi, 2015) with Sahel's precipitation projected to be more unpredictable (IPCC, 2014b). There have been reports of a 15%–30% decrease in precipitation during the 1960s and 1970s discontinuities (Oguntunde et al., 2006), and the 1980s were therefore described as an arid period of the twentieth centennial in West Africa (Nicholson & Palao, 1993).

Kasei et al. (2010) examined the drought frequency in the Volta Basin for 1961-2005, and revealed that the drought severity was below -2.0 which affected practically 75% of the area. Their study further denoted that the years 1961, 1970, 1983, 1992 and 2001 experienced serious droughts. The Oti River Basin, on the other hand, was flooded in 1998, 2007, 2008, 2010, and 2018, which caused significant human casualties and annihilation of infrastructure, particularly in 2007 claiming 23, 46 and 56 lives in Togo, Burkina Faso and Ghana respectively (Komi et al., 2016; Tschakert et al., 2010). The significant level of vulnerability of the basin-dependent communities is demonstrated by these estimates.

Although water and agriculture are crucial sectors for economic expansion and the achievement of sustainability in the region, the sectors are consistently affected due to variations in climate that continue to threaten them (Chemnitz & Hoeffler, 2011; Hope, 2009; Nhemachena et al., 2020). In sub-Saharan Africa, particularly in rainfed agriculture-dependent areas like West Africa, global warming and fluctuation are perceived as the greatest threats to food stability (Wheeler & Von Braun, 2013). Rainfed agriculture in the West African region, for instance, engages approximately 65% of the working force, covers around 95% of the area under cultivation, and makes for 30% to 70% of the region's Gross Domestic Product (GDP) (Blanc, 2012; Akumaga & Tarhule, 2018). According to Kasei et al. (2010) the primary causes of oscillations in producing food in the north of the basin, are the large variation of total precipitation in addition to trends in space and time throughout the watershed.

With the important nature of rainfall to the basin-dependent countries' economies, water managers and the agricultural sector must deal with fluctuations in rainfall, on a yearly and seasonal basis (Valerio, 2005). Their ability to adjust to the predictability of climatic fluctuation is a key component of their success (Nhemachena et al., 2020). It is worthy to note that the water resources of the Oti Basin aid in agricultural activities such as bush fallow cultivation, livestock grazing and fishing. Unfortunately, changes in climate may jeopardize the basin's hydrologic capabilities (Kasei et al., 2010). It must be noted that alterations in river

peak discharge and water volume can be brought on by climatic variations and change (Prowse et al., 2006). Therefore, forecasting is critical for future water resource supply and hazard management, as changes in streamflow can lead to increased disasters. Owusu et al. (2008) have also stated that rainfall variability and its negative impacts on water resource sharing such as the Oti Basin, could be a potential threat for conflict and hence requires necessary attention.

The Volta Basin and other areas of the Oti River Basin (ORB) have been the subject of numerous researches, each with a distinct spatial-temporal scope and yielding an entirely unique set of findings. In the Volta Basin, for instance, Kasei et al. (2010) examined the periodic aspects of climatological droughts. They discovered that between 1961 and 2005, a large portion of the area experienced severe drought, with an area-wide spread of around 90%. Komi et al. (2017) predicted the magnitude of flood risks in the Togo portion of the ORB. They discovered that when LISFLOOD, a hydrological model, and LISFLOOD-FP, a flood inundation model, were used, the simulated flood spread within the basin was more responsive to grid resolution. Klassou & Komi (2021) also analysed severe precipitation throughout the central portion of the ORB and focused on a few chosen high indicators. Their analysis showed that the majority of the heavy rainfall indices declined, whereas the dry spell indicator showed a growing tendency over a sizable part of the basin. In the Kara Basin, a sub-catchment of the ORB, Badjana et al. (2014) also studied the land-cover dynamics. They indicated that between 1972 and 2000, the area underwent transformation in its land cover, with a noticeably large loss of its native forests. Within the same Kara basin, Badjana et al. (2017) examined the long-term patterns in yearly precipitation, its length and the yearly maximum precipitation for seven stations from 1950 to 2010. According to their findings, the mean annual precipitation significantly dropped at several stations, while the interannual variability of annual precipitation decreased over time at all the stations studied. However, they also noted an increase in the length of annual precipitation, suggesting that precipitation was more frequent but less intense in areas where annual precipitation had decreased.

Prior researches like Komi et al. (2017), Klassou & Komi (2021) and Badjana et al. (2017) have been limited to a small number of geographically insufficient weather stations, and neither of these have given the main ORB its full attention in order to determine and project the intraseasonal precipitation variations in the basin. It is no doubt from literature that the continuous nature of the changing climate which triggers variability in rainfall will threaten

the basin. Additionally, severe precipitation incidents like floods in the Basin call for a clear understanding of the intra-seasonal rainfall variations in the ORB. Moreover, conducting this study at the intra-seasonal scale will reveal the occurrences within the seasons. As, widely known, within the broader concept of annual variability, there are also intra-seasonal factors such as timing of onset and cessation which profoundly influence the success or failure of crop planting/growing periods and these could impact rainfed agriculture in the basin Mugalavai et al. (2008). This will enable the basin management authorities to appreciate well, the consequences of changing climate and variations in the basin, and develop adaptation and mitigation measures that could safeguard sustainable livelihoods.

1.2 Literature review

1.2.1 Climate variability and change impacts on streamflow

All over the world, climatic variability and climate change continue to garner considerable attention from researchers due to their wide-ranging devastating effects (Jain & Singh, 2020). The effects of global climate change can already be seen all across the planet. Glacial ice is melting at a quicker rate (Coulson et al., 2021), increasing sea levels (Ramachandran et al., 2017), and natural disasters such as floods, cyclones, and storms have become more common and intense (Majumder et al., 2017). Global warming of 1.5 degrees Celsius has been reported by the Intergovernmental Panel on Climate Change (IPCC), which is a source of significant concern for all international bodies (IPCC, 2018). According to the IPCC (2018), humans are responsible for around 1.0 °C of global warming as of today since the beginning of the industrial age, and further indicates that global warming might reach 1.5 °C between 2030 and 2052 if current trends continue. Heat waves will linger longer and more frequently (IPCC, 2014b). Higher evaporation and air humidity, as well as variations in precipitation, are the result of this warming (Huang et al., 2013). The fluctuations have an impact on runoff and water availability, and consequently on river discharge regimes and vary across regions. Some areas are likely to have water shortages, while others are expected to have more devastating floods. Increased occurrence of floods could lead to significant economic losses including diminishing agricultural production (Abbaspour et al., 2009) and extensive infrastructural damage (Dang et al., 2016).

Above 60% of the populace in sub-Saharan Africa depends on rainfed agriculture and surface water to make a good living (World Bank, 2013). Due to its low adaptation capability and sensitivity, the continent is already noted as being uniquely subject to climate change (IPCC,

2014b). According to IPCC (2014a), the continent's weather patterns will become more varied, and severe weather occurrences will increase in frequency and severity, endangering people's lives and well-being more frequently. One of the most significant influences of climate change will be on the augmentation of the hydrologic cycle and land-based waterbodies especially on streamflow (Kiesel et al., 2019; Wu et al., 2020). Ecosystems made by long-living water-dependent vegetation, such as forests, are particularly susceptible to such changes. Climate change could generally jeopardize water resource management (JiménezNavarro et al., 2021). The quantity, timing, and type of rainfall will be affected by a warmer climate (Safeeq et al., 2013), which would also alter streamflow (Elsner et al., 2010; Hamlet et al., 2013), and stream temperature (Isaak et al., 2012; Luce et al., 2014). Interannual rainfall variability is substantial across most of Africa with the Sahel having a prominent multi-decadal variation (Hulme et al., 2001). For instance, droughts were severe in the region during the 1970s and 1980s due to low rainfall relative to the 1900-1970 period (Mahe et al., 2013; Hulme, 2002).

In recent times, studies with a focus on climate change impacts on streamflow are increasingly being conducted on various rivers in the study region. For instance, Dembélé et al. (2022) made a thorough assessment of the effects of climatic variations on the Volta River basin in West Africa and reported a potential shift in the timing of low flows and an earlier occurrence in high flows in the future. Rameshwaran et al. (2021) studied how climate change might impact discharge in West Africa; They projected that river flows could be 23% lower in the west (e.g., Senegal) and 80% higher across the eastern region (e.g., Chad) by the 2050s. Stanzel et al. (2018) also assessed the impact of climate change on the hydrology of the West Africa in the context of hydropower potential and reported relatively strong flow decrements for the region's north and east, and significant rises primarily for the southwest for the future periods 2026-2045 and 2046-2065. Sawai et al. (2014) have also assessed climate change effects over the Black Volta River basin by employing data generated from the atmospheric general circulation model with a 20-km resolution (AGCM20) from the Japanese Meteorological Agency (JMA) and the Meteorological Research Institute (MRI). They projected that outflow will drop between January to July at a maximum value of 50 percent and rise throughout August to December at a maximum value of 20 percent in future (2075-2099).

Li & Jin (2017), have opined that projecting hydrologic variation seems essential for regulating future water supplies and vulnerabilities as alterations in hydrology might result in further catastrophes as compared to a change in the mean state. Several studies such as Bürger et al. (2011), Hirabayashi et al. (2013), Arnell & Gosling (2016), Dankers et al. (2014), Prudhomme et al. (2014) and Schewe et al., (2014) have widely discussed the potential changes in hydrological extremes and regimes in the region. Nonetheless, the relationship between climate change and hydrological variance is yet to be fully explored. According to Hirabayashi et al. (2013), Arnell and Gosling (2016) and Schewe et al. (2014), multiple climatic and hydrological variables should be examined, when looking at the impact of climate change on hydrological extremes and hence it is not regarded as a simple function of change in precipitation. Several factors could account for changes in streamflow. For instance, in their studies on historical river flow patterns of the Yangtze River in China, Chen & Frauenfeld (2014) recorded a strong correlation with precipitation. In the same way, Bawden et al. (2014), in their study, found a strong correlation with precipitation but not temperature, when they analysed the trends in the historical streamflow of the Athabasca River basin in Canada. Yet, studies conducted by Leng et al. (2015), Qiao et al. (2014) and Li & Jin (2017) premised on future hydrologic predictions, revealing that changes in both temperature and rainfall contributed to hydrological variations.

1.2.2 Hydrological modeling

The spatiotemporal distribution of both precipitation and evaporation determine how accessible water supplies are for human consumption and ecosystems (Konapala et al., 2020). Nevertheless, climate change continues to have major implications for hydrological, biological, and ecological systems, including water quantity and quality (Liu et al., 2009). Most river stream flows have changed in the last decade, possibly as a result of climatic change (Dinpashoh et al., 2019). These observations suggest that future changes in climate will have substantial worldwide implications. In light of this, hydrologists and weather forecasters understood that simulating hydro-climatology for large rivers is essential for understanding the basin-scale water regime and, ultimately, managing water systems (Yu et al., 2013).

Due to its critical importance for integrated land and water resource management, the investigation of hydrological systems, particularly of river basins, has grown more common in recent decades (Badjana, Fink, et al., 2017). Hydrological models have evolved into critical

instruments for analyzing integrated river basin systems and, for that matter, managing sustainable water and ecological processes (Tessema, 2011). According to Xu (2002) and Yu (2002), hydrological models are frequently classified as lumped, semi-distributed, or distributed and can be conceptual or physically based. Conceptual models are hydrologic models that use a simplified mathematical conceptualization of a system using a series of interconnected reservoirs to represent various components of the hydrologic process through recharge and depletion. They are typically lumped in nature, with the same parameter values applied to the whole catchment and little consideration given to the geographic diversity of watershed characteristics. The outputs of conceptual models are strongly reliant on observed data, and the quality of the input data employed in the model is critical (Jaiswal et al., 2020). The physical models use mass, momentum, and energy conservation equations to depict various hydrological processes. In these models, the governing partial differential equations are usually solved using finite difference or finite computation approaches. Physical models may be able to account for the geographic heterogeneity of land use, slope, soil, and climate in order to cope with semi- or completely dispersed hydrological processes within the watershed (Jaiswal et al., 2020). Some of the most commonly applied conceptual models by hydrologists across the globe are the HBV model (Rusli et al., 2015; Seibert & Vis, 2012), HYMOD (Quan et al., 2015), TANK model (Suryoputro et al., 2017), SIMHYD (Chiew et al., 2018), GR4J (Perrin et al., 2003), ARNO model (Lane et al., 2019).

The nature of physical models needs a substantial quantity of topographic, soil, land use, and weather data in order to establish a foundation for investigating differences in the hydrologic processes due to human involvement and climate change for water resource management (Chokkavarapu & Mandla, 2019; Dwarakish & Ganasri, 2015). The following are some of the semi- or fully distributed physical models that have been recently used by hydrologists: Variable Infiltration Capacity (VIC) (Droppers et al., 2020), MIKE SHE (M. Zhang et al., 2019); Soil & Water Assessment Tool (SWAT) (Guug et al., 2020), Semi-Distributed Physically based Hydrologic Model using Remote Sensing and GIS (DPHM-RS) (Biftu & Gan, 2001); TOPNET (Singh et al., 2020), Penn State Integrated Hydrological Model (PIHM) (Yu et al., 2013), Interactions Soil-Biosphere Atmosphere model (MISBA) (Elsanabary & Gan, 2015), etc.

Although the application of rainfall-runoff models has been extensively used across the globe, the use of these models is limited in the West African sub region due to the lack of data, and

partly because these models were made for the temperate environments (Kwakye, 2016). For example, Paturel et al. (2003) used a semi-distributed empirical model to produce reasonable rainfall-runoff modeling results for various catchments in West Africa. In their climate research, Niel et al. (2003) also used a lumped hydrological model to investigate parameter stability in several watersheds in the west and central Africa and discovered that non-stationarity in rainfall or runoff series does not imply non-stability of model parameters. Jung & Kunstmann (2007) utilized the mesoscale meteorological model MM5 and the hydrological model WaSiM to evaluate the effect of human influence on West Africa's Volta Basin. According to their findings, precipitation decreased at the start of the rainy season, increased at its peak, and clearly increased in temperature. Amisigo et al. (2008) used the statistical model NARMAX for various river basins in West Africa to evaluate the effect of diverse hydrological modeling techniques and source grids on discharge prediction and achieved remarkable month-to-month river flow performance in the Volta River basin. In their study on hydrological modeling over West Africa's White Volta Basin, Wagner et al. (2009) used both the joint meteorological model (MM5) and WaSiM, and revealed a strong performance for the year 2004 and a weaker performance for 2005 due to rainfall overestimation. Abubakari et al. (2017) have also investigated the spatial variation of Volta basin's hydrology under projected impacts of climate change using SWAT and showed a higher spatial variability, with variability much higher at the end of the century (2071-2100). The study also reported that although rainfall is projected to increase in the entire basin, some of the sub-basins in the north and south parts would decrease in the future. Again, Abubakari et al. (2019) used SWAT model to model river flow reaction to climate change over White Volta River basin and discovered that there would be a transition in monthly maximum streamflow from September to August, whereas in future the extremely dry seasons (December, January and February) showed unmodified. Hydrological modeling is consequently critical for quantifying climatic change and variability impacts over a catchment's hydrology.

1.2.3 Climate variability, change and climate models

Climatic change is described as a shift in the atmosphere's state that can be seen across period, typically generations or even more, in alterations to the average and/or variation of its properties (IPCC, 2014). Due to its devastating and widespread effects, climate change impact studies are based on climate model estimates of future climate (IPCC, 2014; Lutz et al., 2016). They are the most significant instruments for analyzing the climate system's response to diverse forcings, establishing seasonal to decadal climate predictions, and generating climate

projections for the next century and beyond (Flato et al., 2013). The model used is directly related to the science subject understudy (Collins et al., 2006; Held, 2005). The outputs from Global Climate Models (GCMs) are usually directly downscaled to higher resolution due to their coarse spatial resolution. The downscaling employs empirical-statistical downscaling methods or serves as a set of boundary conditions for regional climate models (RCMs), whose results are then downscaled to a greater resolution (Lutz et al., 2016). When the objective was to apply a realistic forcing scenario and the realized forcings are qualitatively comparable to the projection forcings, these projections are frequently considered as plausible future outcomes (Hausfather et al., 2020).

The number of global climate models (GCMs) available for climate change projections is steadily growing with RCMs having downscaled many GCMs. RCMs are extremely effective where GCMs seem unable to rectify small details and local drivers of regional climate (e.g., convection), in regions with highly diversified land cover or topography, and in areas with inland lakes, despite their inability to enhance the simulation abilities of large-scale fields beyond those simulated by GCMs (Giorgi, 2019; Rummukainen et al., 2015). Numerous studies have also assessed the pattern of future climate change in the West African region from these climate models. Some of these studies are Ilori & Balogun (2022), Yeboah et al. (2022), Attogouinon et al. (2020), Dosio et al. (2020), Ogega et al. (2020), Gnitou et al. (2019), Adeniyi & Dilau (2018), Heinzeller et al. (2018), Akinsanola et al. (2017), Diasso & Abiodun (2017), Nikiema et al. (2017), etc. All these have been done as part of large-scale coordinated attempts in the West African sub-region to examine their potential for regional climate projection research (Giorgi et al., 2009; Jacob et al., 2014) ever since the IPCC (2007) reported the region to be highly vulnerable to the adverse effects of weather and climate variability. It is worthy to note that the ability of GCMs involved in the Coupled Model Intercomparison Project (CMIP5) and Regional Climate Models (RCMs) within the World Climate Research Programme, Coordinated Regional-climate Downscaling Experiment (CORDEX) to replicate the basic characteristics of the African rainfall weather patterns has been well demonstrated (Giorgi & Gutowski, 2015; Taylor et al., 2012).

In addition to the above, various researches have looked into how the CMIP5 model, in particular, simulates rainfall patterns and climatology of the West African region. For instance, Nikiema et al. (2017) analyzed and evaluated summer rainfall and temperature simulations from the CMIP5 and CORDEX multimodel ensembles over West Africa. They

discovered that while CORDEX did not surpass the CMIP5 ensembles predicted mean climatology of temperature, it significantly improved the simulation of rainfall. The responses of the West African Summer Monsoon (WASM) rainfall and several other key atmospheric aspects to global warming were also explored, and it was discovered that the climate models' ensemble mean accurately matched the WASM rainfall features (Akinsanola & Zhou, 2018). In addition, Akinsanola et al. (2017) assessed the capacity of a number of Rossby Centre Regional Climate Models (RCA4) driven by global circulation models (GCMs) to simulate essential attributes of rainfall climatology throughout West Africa. Their results showed that the RCA4 effectively reflected the spatial and interseasonal rainfall pattern, but performed poorly over the Guinea coast. According to Akinsanola et al. (2017), the application of the models' ensemble mean improved the representation of rainfall characteristics in the region. Okafor et al. (2019) evaluated the performance of several CMIP5-GCM-driven ensembles of RCMs from the CORDEX-Africa project over the Volta Basin. Their findings revealed that the models accurately matched the key features of the West African climate, such as its variation in sign, amplitude, and spatial extent. They were quick to mention that the model simulations for a few specific measures, areas, and seasons have known flaws. In their study, Agyekum et al. (2018) also evaluated how some global climate models (GCMs) from the Coupled Model Intercomparison Project (CMIP5) simulate rainfall over the Volta Basin. They discovered that, while all of the models simulated rainfall differently, the ensemble mean outperformed the individual models across a range of timescales. These investigations have made significant contributions towards the evaluation of CMIP5 GCM-RCMs' efficiency in mimicking the climate of West Africa and the Volta Basin, and hence climate models from CMIP5 can be applied in the Oti River Basin.

1.2.4 Hydrologiska Byråns Vattenbalansavedlning (HBV)

Hydrologiska Byråns Vattenbalansavedlning (HBV) is a popular water balance model. It is well known for its ability to conduct hydrological analysis related to water balance (Bergström, 1992). The model's key strengths are its physically based parameters, which are beneficial because of the ease with which they can be linked to physical attributes; the reasonable number of free parameters in comparison to other models (the HBV model has only eight parameters) parameters (Gan et al., 1997); simple data requirements; user-friendliness; simplicity of operation; and high-performance levels (Lindstrom et al., 1997). The model has seen widespread application in operational hydrological forecasting and water budget analyses (Abebe et al., 2010). In particular, Rusli et al. (2015) examined the impacts of

temporal changes with regard to optimization of the Hydrologiska Byråns Vattenbalansavedlning (HBV) model, as well as the calibration efficiency employing manual adjustment and mean estimated values in China. Their study revealed that choosing extended temporal calibration durations for hydrological analysis results in simulations that are generally more accurate for water balance assessment. Pervin et al. (2021) also used the HBV model to project the future water levels and streamflow of the Mackenzie River in Canada using precipitation, temperature and potential evapotranspiration data as input. Singh & Marcy (2017) have also investigated the effects of applying a simplified hydrological model like the HBV against two other complex hydrological models (TOPNET and WASiM-ETH) to predict discharge and to quantify the uncertainty of results in the Waiokura catchment, in the North Island of New Zealand. Their study also investigated the effects of using simple versus complex hydrological models in climate change studies. They discovered that the due to the different input data, discharge differed significantly between the models used, and also concluded that a simple to moderately complex model is undoubtedly sufficient for most climate change studies. Abraham et al. (2018) also used the HBV model to predict future runoff conditions under changing climate over Lake Ziway Catchment in Ethiopia. Koutsouris et al. (2017) also investigated the possibility of bias correction of global precipitation datasets to assist river discharge computation in the central valley of Tanzania using the HBV model, and their findings indicated a potential benefit of incorporating river discharge and weather data to correct biases (GPDs) throughout the model calibration procedure inside a hydrological modeling structure.

In west Africa, however, only few studies have applied the HBV model. For example, Götzinger (2007) applied the modified HBV model in the Ouémé basin, a West African basin in the republic of Benin. It was found from the study that the overall simulated discharge fitted the magnitude and variability of the observations sufficiently well for water resources management planning, and the general seasonal trend. In addition, a Nash-Sutcliffe efficiency of 0.77 was obtained for calibration at the catchment's Bonou outlet. Given the available data and their limitations, the water balance of the entire Ouémé basin could be reasonably replicated. According to Götzinger (2007) the modified HBV model is suitable for global change impact studies. Badou (2016) also used the HBV-light model in four poorly gauged basins in the Benin portion of the Niger River Basin and stated that the HBV model best simulated streamflow in the Coubéri and Gbassè basins. In their study, Kwakye & Bárdossy (2020) also investigated the performance of the HBV-IWS version on the Black Volta Basin

in West Africa. They found that the model performed well with an average Nash-Sutcliffe efficiency (NSE) of 0.75 and 0.6 for calibration and validation respectively for Lawra and Chache sub-basins. They also discovered that giving the low-flows more weight during the optimization increased the model's performance and that the model responds well to rainfall signals.

1.3 Research questions

- How has intra-seasonal variations influenced rainfall in the Oti River basin from the period 1981 to 2010?
- What will be the intra-seasonal rainfall pattern in the future period (2021-2050) in the Oti River basin?
- What impact does intra-seasonal rainfall variability has on streamflow in the Oti River basin?
- How well does the HBV model simulate the Oti River basin's streamflow?

1.4 Thesis objectives

1.4.1 Main objective

The aim of this work is to assess the intra-seasonal rainfall variability; its patterns and its repercussions on streamflow in West Africa's Oti River Basin.

1.4.2 Specific objectives

I. To determine the intra-seasonal rainfall variability and trends for the historical period (1981-2010) and future period (2021-2050) in the Oti basin.
II. To determine the projected changes in intra-seasonal rainfall variability indicators in the Oti basin for the future period (2021-2050).
III. To assess the impact of intra-seasonal rainfall variability on streamflow.

1.5 Hypothesis

a. Hypothesis 1: Intra-seasonal rainfall variability would decrease in the future period.
b. Hypothesis 2: Variability in intra-seasonal rainfall would decrease future streamflow.

1.6 Novelty

Regarding the Volta River Basin to which the Oti River Basin is a sub-catchment, several studies have been conducted on it, ranging from investigating the effects of climate change on basin's water supplies to exploring the consequences of climate change and land use and cover modifications on the availability of water. Nonetheless, limited research is found on the Oti River Basin most importantly with regards to modelling intra-seasonal rainfall variability and its implications on the Basin's streamflow. The study is therefore relevant as it seeks to reveal crucial information for policymakers to ensure feasible management and conservation of the basin, thereby intensifying understanding about climate change and creating verifiable evidence of how climate change is altering the Basin and its streamflow. The findings from the study will also provide an indication for stakeholders to strengthen proactive measures where necessary towards catastrophic conditions like floods and water stress that can be associated with rainfall variability. The study will also prompt stakeholders on the need for water sustainability planning since the basin-fringed communities rely on the water supply for domestic and agricultural activities.

1.7 Scope of the thesis

The study focuses on the analysis of intra-seasonal rainfall variability in the Oti catchment. Rainfall-based indices such as rainfall totals, onset, cessation, length of the rainy season, number of rainy and dry days were examined. To study the variability in rainfall, climate change analysis was performed on the rainfall indices, as well as the seasonal period (thus, rainy season) and subjected to descriptive statistics.

1.8 Expected results and benefits

The study presented: (i) illustrations of the past and future scenarios (from outputs of diverse climate models) of the rainfall variability indicators examined at the Oti River basin which are of great relevance to policy makers in the water and agricultural sectors and subsequently towards the attainment of Sustainable Development Goals (SDGs) 1, 2, 3 and 6 (These are 1: No Poverty; 2: Zero Hunger; 3: Good health and well-being and 6: Clean Water and Sanitation). (ii) information on how intra-seasonal rainfall variability could affect streamflow in the Oti River basin in the future.

Variability in rainfall, and intra-seasonal rainfall in particular, has been associated with extreme events ranging from floods, droughts, famine and destruction of properties among

others in most countries in the West African region. Sadly, these events continue to heighten causing adverse impacts on human livelihoods, water resources management, displacement of people from their homes, properties and gravely, the stability of economies in the region. The salient information presented in this work would greatly contribute towards the design of a demand specific adaptation and mitigation strategies for effective water resources management and sustainable agricultural production.

1.9 Outline of the thesis

Seven chapters make up the organization of this dissertation. Chapter 1 provides a general introduction, literature review, the research problem, objectives of the study, the novelty, the scope of the study, and expected outcomes. Chapter 2 presents an extensive description of the Oti catchment including location, relief, vegetation, climate, hydrography, soil and land use, as well as the demography, environmental, social and economic activities. Chapter 3 provides a detailed description of the data collected, tools and method of analysis. Additionally, the chapter discusses the reliability of climate models and satellite climate datasets in the Oti River Basin. The chapter 3 finally details the climatic and hydrological stations, as well as the rainfall, potential evapotranspiration and streamflow data employed in the hydrological modelling. Chapter 4 present results and discussions on the past and future intra-seasonal rainfall variability in the basin. Chapter 5 communicates the results of the projected changes in the rainfall variability indicators across the basin. Chapter 6 discusses intraseasonal rainfall variability's impact on streamflow. Chapter 7 presents the general conclusion and perspectives.

Chapter 2: Study Area

This chapter describes the study area (i.e., Oti River Basin) in detail by focusing on such characteristics as location, relief, vegetation, climate, hydrography, soil and land use. The chapter also highlights the demography, environmental, social and economic activities of the catchment.

2.1 Location

The Oti River Basin is shared by Ghana, Burkina Faso, Togo and Benin. It lies between longitudes 6^0W and 2^0E and latitudes 0^0 and 15^0N (Figure 2.1). It is part of the Volta basin system in West Africa. It is estimated to be about 72,000 km^2 (Barry et al., 2005; Kasei, 2009). The basin's weather patterns are influenced by the Inter-Tropical Discontinuity (ITD) and the West African Monsoon. The precipitation patterns in the study area exhibit spatial variability, characterized by an annual precipitation range of 1,010 mm (northern region) to 1,400 mm (southern region). Furthermore, the potential evaporation rate is estimated to be approximately 2,540 mm per year, while the annual runoff rate is approximate 254 mm (Kasei, 2009), and the basin experiences a unimodal rainfall pattern, with the maximum peak in August. Rainfall in the rainy season covers about 90% of the total annual rainfall in the Basin. The wet season spans from April to October (AMJJASO) whereas the dry period starts from November to March (NDJFM) (Klassou & Komi, 2021). Between 25.9 ^oC and 34 ^oC is the average yearly temperature range. The contribution from surface runoff to the annual total flow into the Volta Lake is estimated to be approximately 25%, which can be attributed to the basin's steep topography and considerable precipitation (Barry et al., 2005).

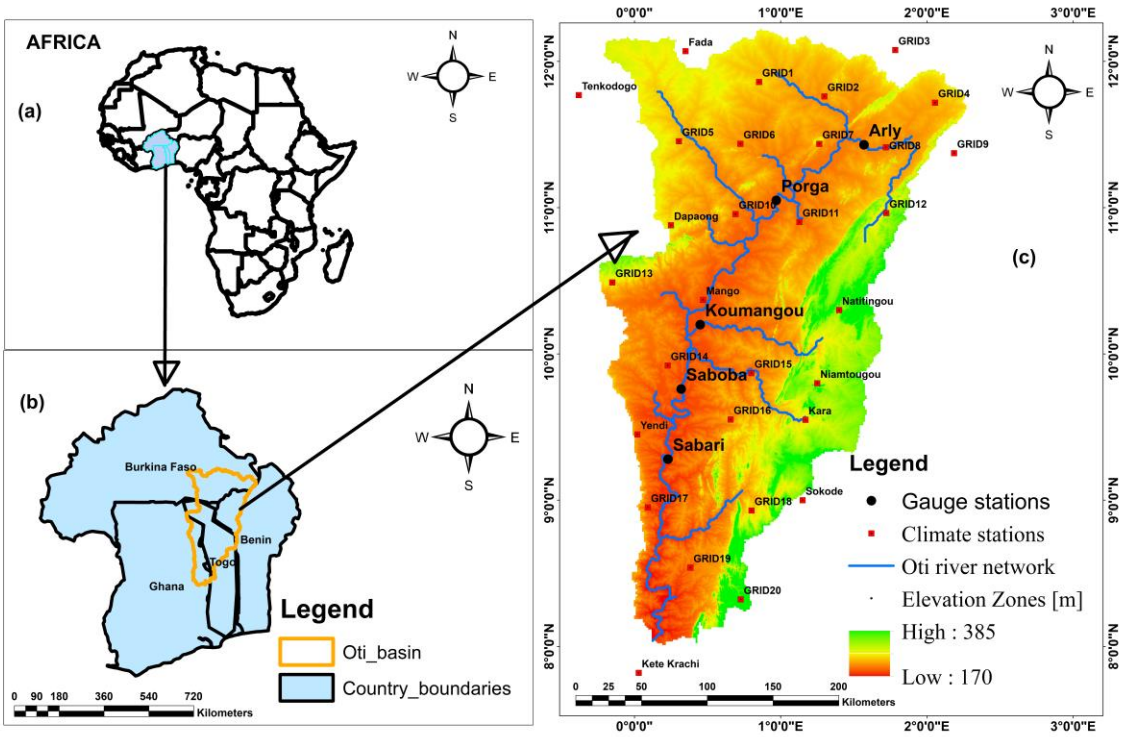

Figure 2. 1: Map of the study area showing (a) location of Oti Riparian countries in Africa highlighted, (b) Oti River Basin (highlighted in yellow) shared by Ghana, Burkina Faso, Togo and Benin and (c) Digital elevation model, climate and gauge stations, and river network in the Oti River Basin

2.2 Relief

Surface runoff contributes to around 25% of the yearly flow rate inputs into the Volta Lake since the basin's terrain is high with a lot of precipitation (Barry et al., 2005). It has an elevation that ranges between 60 m and 874 m (Figure 2.2). The Oti River, which starts in Benin's Atakora Mountain, runs northeast before turning west to form the boundary. It travels via Burkina Faso and Benin, then briefly through Togo and Benin, continues southward through Togo's north, along its borders with Ghana, and finally meets the Volta River close to Kete-Krachi in Ghana (MWH, 1998). Koumongou, Kéran, Kara, Mô, Kpanlé, Wawa, Ménou, and Danyi Rivers are headwaters. The Oti River has an annual average flow of approximately 500 m^3/s, thanks to the Kompienga Dam in Burkina Faso. During the dry season, virtually all of the tributaries cease to flow, and their annual average flows are only 5 m^3/s.

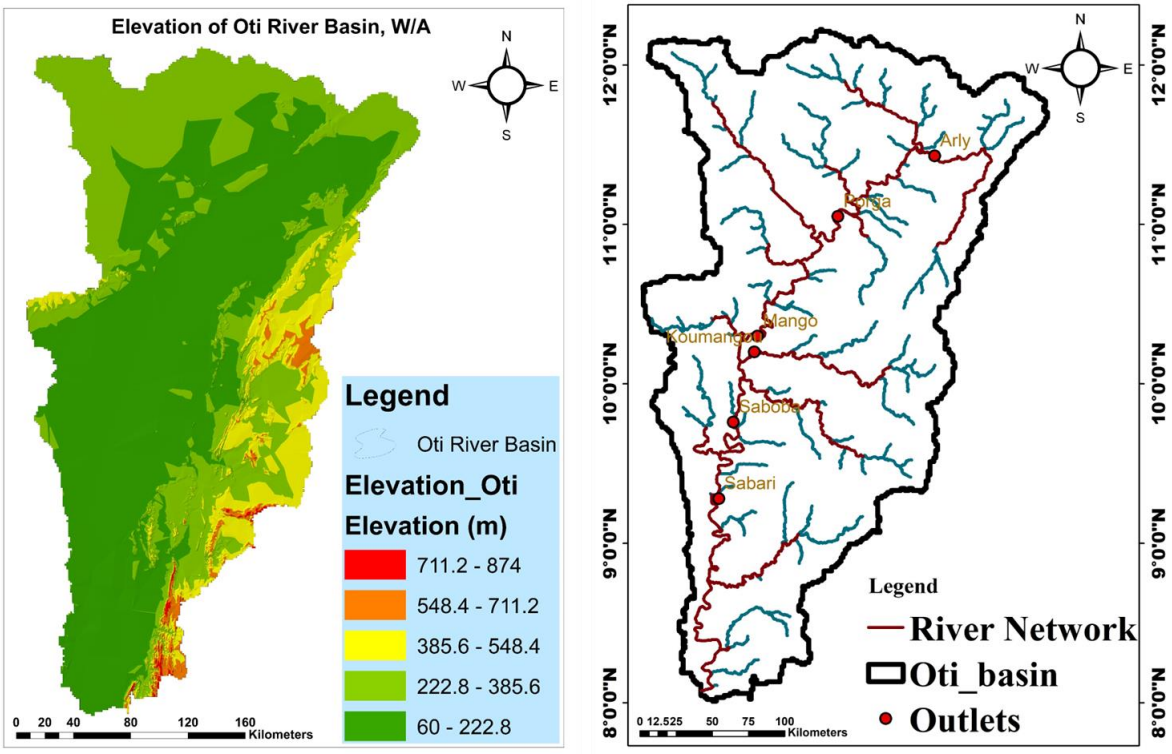

Figure 2. 2: Elevation and drainage pattern of the Oti River basin

2.3 Vegetation

Savannah, which covers 75% of the basin's surface and is primarily made up of grassland mixed with shrubs and trees, represents the most prevalent vegetation cover in the basin (Dembélé et al., 2020). Corresponding to the precipitation patterns, the vegetation has a south-to-north diminishing gradient in its richness and vigor. The basin's northern regions are primarily covered with grassy savannah, while its southern regions are covered with woody savannah. Sorghum, maize, millet, yam, rice, and groundnuts are among the main farmed staple crops in the basin (Lemoalle & de Condappa, 2010).

2.4 Climate

The Inter-Tropical Discontinuity (ITD) and its related West African Monsoon migrate and cooperate to shape the basin's weather. The yearly precipitation ranges between 1,010 mm north to 1,400 mm south. It has a pan evaporation of 2,540 mm per year and flow of about 254 mm per year (Kasei, 2009). The mean annual temperature ranges between 25.9^{o}C and 34 ^{o}C. The basin falls within the Sudano-Sahelian zone, Sudanian zone and Guinean eco-climatic zones (Dembélé et al., 2022) and experiences a unimodal rainfall pattern which peaks in

August. April through October is the wet season, whereas November through March is the summer months (Klassou & Komi, 2021) (Figure 2.3).

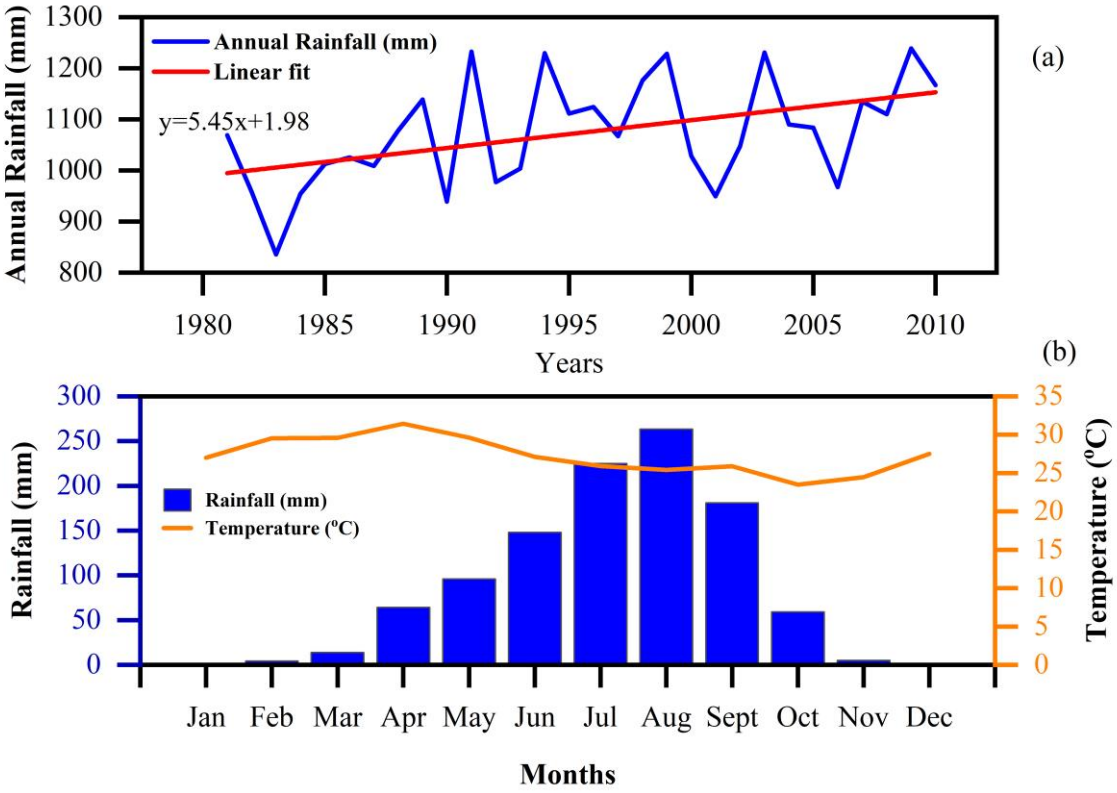

Figure 2. 3: (a) Mean annual rainfall (b) monthly rainfall and temperature in the Oti Basin at Dapaong using in-situ data

2.5 Hydrography

Among the main drainage systems of the Volta Basin is the Oti Basin. The easterly branch, called Oti River, rises 600 meters above sea level in Benin's north (Moniod et al., 1977). This is recognized as the Pendjari River and runs close to the wet Atakora Mountains in Benin, that is a continuation of the Akwapim Hills in Togo. It travels through Togo, and is referred to as Oti River. It then runs toward Ghana's border and joins the Volta River close to Kete-Krachi before flowing into Lake Volta. Koumongou, Kara, Mô, Kpanlé, Wawa, Ménou, Danyi, Afram, Obosom, Sene, Pru, Kulurakun, Daka, and Asukawkaw streams are its principal headwaters. Approximately 0.012 km^2 is the Oti River's flow rate. The Oti River has a constant flow with an estimated yearly flow of 100 to 300 m^3s^{-1}, although it can occasionally exceed 500 m^3s^{-1} attributable to flow control by the Kompienga Dam in Burkina Faso. Owing to its steep slope and comparatively high precipitation, the Oti River Basin supplies around 25% of the total annual discharges to the Volta Lake. Within the basin, overall storage sites

totaling around 406 million m^3 have already been found. These sites may control the basin production at a minimal flow of roughly 37 m^3/s (Barry et al., 2005). Mostly during the dry period, nearly all of the tributaries stop flowing. It flows at a mean rate of 11.215 x 106 m^3yr^{-1} (MWH 1998).

The Oti basin in northern Togo obtains approximately 1000 and 1200 mm of precipitation each year, whereas the southwestern gets around 1000 and 1500 mm. The basin's surface water resources are projected to be 4.71 x 109 m^3 annually. As a result of excessive water loss during the dry seasons, many streams run dry. The Oti, which is made larger by its tributaries and the Mô, exceeds a flow rate of 100 m^3/s within the Savannah region and 100 to 300 m^3/s in the Kara region in the northern section of the watershed. Dependence on surface water for irrigation purposes during the dry and wet months is challenging due to the significant flow unpredictability. The Menou, Wawa, and Danyi have substantially lower flows of between 1 and 6 m^3/s in the south-west region of the basin, however these flows remain perennial because the weather is more humid (Barry et al., 2005).

The Oti River Basin in Benin receives about 1,100 mm of precipitation on a yearly average. The average yearly flow rate is 58.6 m^3/s and the yearly flow volume is calculated to be roughly 1.85 x 109 m^3 (UNEP-GEF Volta Project, 2013).

2.6 Soil and Land Use

The Voltaian and Buem rock formations are beneath the Oti River Basin, which is wholly contained within the Inner Savanna Ecological Zone. Savannah Ochrosols, Groundwater Laterites, Savannah Ochrosol-GWL Intergrades, Savannah Lithosols, Savannah Gleysols, and Forest Lithosols are the soil types found in the Oti Basin (Barry et al., 2005).

Grazing and vast bush fallow agriculture are the contemporary modes of land use and vegetation cover, including tree savannah regeneration and small sections of protected forest on the southeasterly hills. In the basin, yams, guinea corn, maize, rice, millet, and groundnuts are the principal crops farmed. Along the river, fishing is prevalent, and pasture is also widespread, as it is across the rest of the savannah (Barry et al., 2005). Small towns can be found inside the basin (Barry et al., 2005). Additionally, slash-and-burn agriculture and bushfires during the dry periods cause annual losses in soil quality and vegetation quality (UNEP-GEF Volta Project, 2013). Figure 2.4 illustrates the soil and land use types in the Oti Basin.

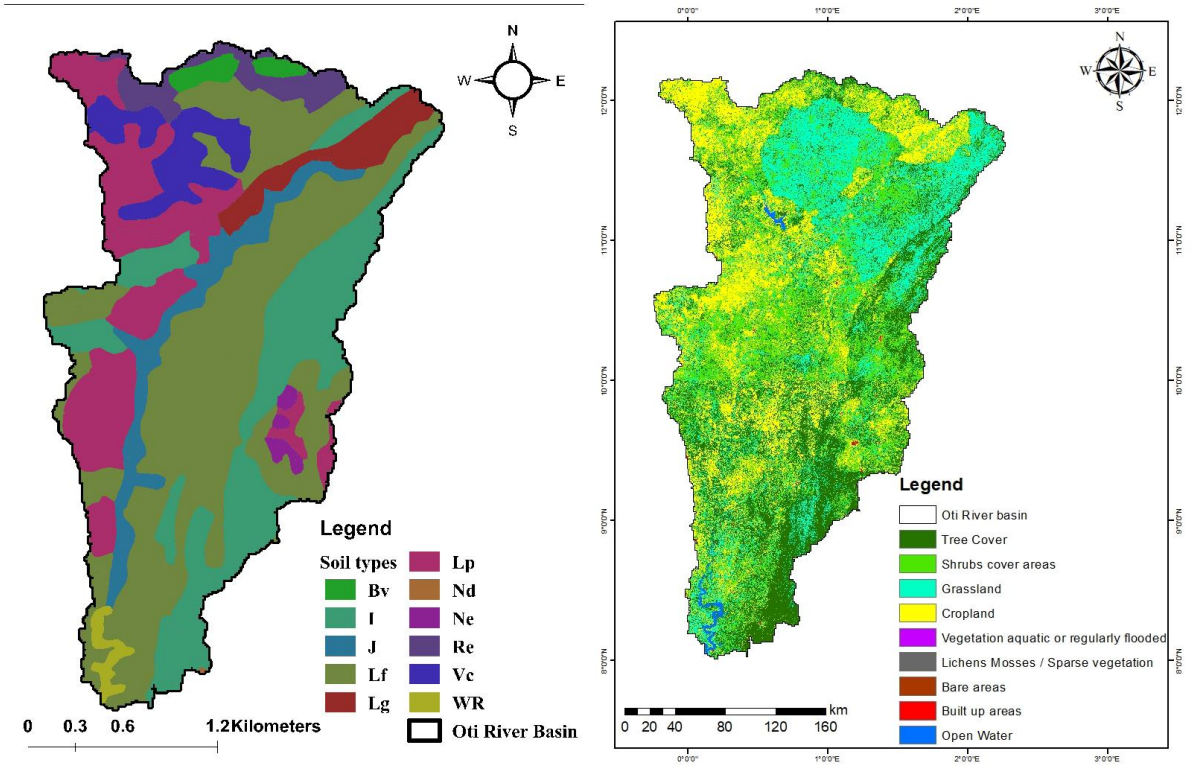

Figure 2. 4: Oti River Basin showing (a) soil types: Bv (Vertic Cambisols), I (Lithosols), J (Fluvisols), Lf (Ferric Luvisols), Lg (Gleyic Luvisols), Lp (Plinthic Luvisols), Nd (Dystric Nitisols, Ne (Eutric Nitisols), Re (Eutric Gleysols), Vc (Chromic Vertisols), WR (Inland water); (b) Sentinel-2 (S2) 2016 Prototype land cover map at 20 m for Africa by the European Space Agency (ESA)

2.7 Demography, environmental, social and economic activities

Population density within the riparian countries where the Volta basin to which the Oti is a sub-basin, varies with Togo having the greatest population levels (125 persons km^{-2}) and Mali having the least (13 persons km^{-2}) (Barry et al., 2005). There are 114, 92, 64, and 62 people per square kilometer in Ghana, Benin, Côte d'Ivoire, and Burkina Faso, accordingly. Different countries have different population levels (Obuobie & Barry, 2010).

Being a sub-catchment of the Volta basin (West Africa), the Oti basin has its population to be mainly rural and strongly depends on land resources for subsistence agriculture and livestock breeding (UNEP-GEF Volta Project, 2013). The Oti sub-basin in Ghana for instance, had its population increased from 106, 423 in 1960 to 557, 910 in the year 2000. In addition to this, the period 1984-2000 saw a 59% increase in the population of the sub-basin (Codjoe, 2006). Population movement occurs throughout the river catchment and is driven by a variety of reasons including hardship, rising population strain, and environmental deterioration (UNEP-GEF Volta Project, 2013). Due to geopolitical upheaval, residents of Togo's Savannah and

Kara areas who relocated to the south of the nation before 1990 are already coming back (Obuobie & Barry, 2010).

The Oti Basin is characterised by agricultural activities. One very significant source of earnings in the basin is farming, which includes raising animals, fishing, and forestry. Farming also accounts for a significant portion of the economic growth in partner countries (Mul et al., 2015). Agriculture creates nearly 40 percent of the basin's revenue and is largely dependent on available water supplies (Biney, 2010).

2.8 Conclusion of the chapter

This chapter has described and discussed the study area with focus on the location, relief, vegetation, climate, hydrography, soil and land use as well as the demography, environmental, social and economic activities. With a unimodal rainfall pattern, the basin has its rainfall peak in August, and the precipitation in the rainy season covers about 90% of the total annual rainfall in the basin. The basin is one of the primary drainage systems of the Volta River Basin. Completely within the Interior Savanna Ecological zone, the basin is covered by the Voltaian and Buem geological formations. The source of livelihood in the area is agriculture (crop farming, fish farming and livestock rearing) with agricultural extension based on slash-and-burn. The populace in the area remains mainly rural and strongly dependent on subsistence.

Chapter 3: Data, Materials and Methods

This chapter gives an explanation of the data collected, tools as well as methods. There are two parts to this chapter. The initial part outlines the climate datasets collected and methods used for the analysis of the past and future intraseasonal rainfall variability studies. The second section describes the characteristics of the sub-basins, the required data for input into HBV model, their preparation and setup of the hydrologic model, and calibration and validation methods.

3.1 Data

3.1.1 Station and satellite climate dataset

Observed daily rainfall and, maximum and minimum temperature data for eight climate stations within the Oti basin for the period 1981-2010 were obtained from the Ghana Meteorological Agency, the National Meteorological Service, Togo, and Benin Meteorological Department. Additionally, due to the basin's limited spatial distribution of climate stations, gridded daily rainfall data for 22 gridded points were extracted from Climate Hazards Group Infrared Precipitation with Stations (CHIRPS) (https://data.chc.ucsb.edu/products/CHIRPS-2.0/). CHIRPS is developed by the US Geological Survey and the Climate Hazards Group at the University of California at Santa Barbara (Fenta et al., 2018). CHIRPS incorporate satellite imagery with in-situ station data to create gridded rainfall time series and it has a spatial resolution of 5km, and a daily/pentad/monthly temporal resolution (Funk et al., 2015). The daily rainfall data from CHIRPS were extracted with the aid of R software using the respective geographical coordinates of the 22 gridded stations for the historical period of 1981-2010. Also, daily maximum and minimum temperature, relative humidity, windspeed, and solar radiation data were obtained from the National Aeronautics and Space Administration Prediction of Worldwide Energy Resource (NASA POWER) project for the period 1981-2010. The data from the NASA POWER project are derived from Modern Era Retrospective-Analysis for Research and Applications (MERRA-2) assimilation model products and GEOS 5.12.4 near-real-time products (https://power.larc.nasa.gov/data-access-viewer/) (Stackhouse et al., 2018). NASA supports satellite systems and research by providing data, including long-term estimates of meteorological quantities and surface solar energy fluxes, for the study of climate

and climate processes (Stackhouse et al., 2018). NASA-POWER data is available as a single point, regional, and global coverage with daily, interannual, and climatology temporal averages. It provides access to near real-time datasets with a grid resolution of one-half arc degree longitude by one-half arc degree latitude (Stackhouse et al., 2018). The NASA-POWER datasets (daily maximum and minimum temperature, relative humidity, wind speed and solar radiation) were also extracted for each gridded location from the NASA POWER website in the form of MS excel (.csv) format. Table 3.1 presents the climate data type used for the historical period (1981-2010).

Table 3. 1: Climate data type used for the historical period (1981-2010)

Stations	Longitude (degree)	Latitude (degree)	Relative location	Rainfall data type	Temperature data type
GRID1	0.85	11.86	Upper basin	Gridded	Gridded
GRID2	1.30	11.76	Upper basin	Gridded	Gridded
GRID3	1.78	12.08	Upper basin	Gridded	Gridded
GRID4	2.06	11.72	Upper basin	Gridded	Gridded
GRID5	0.31	11.45	Upper basin	Gridded	Gridded
GRID6	0.73	11.44	Upper basin	Gridded	Gridded
GRID7	1.26	11.44	Upper basin	Gridded	Gridded
GRID8	1.72	11.41	Upper basin	Gridded	Gridded
GRID9	2.19	11.37	Upper basin	Gridded	Gridded
GRID10	0.69	10.96	Upper basin	Gridded	Gridded
GRID11	1.13	10.90	Upper basin	Gridded	Gridded
GRID12	1.72	10.96	Upper basin	Gridded	Gridded
GRID13	-0.15	10.49	Middle basin	Gridded	Gridded
GRID14	0.23	9.92	Middle basin	Gridded	Gridded
GRID15	0.80	9.87	Middle basin	Gridded	Gridded
GRID16	0.66	9.55	Middle basin	Gridded	Gridded
GRID17	0.09	8.95	Lower basin	Gridded	Gridded
GRID18	0.80	8.93	Lower basin	Gridded	Gridded
GRID19	0.38	8.54	Lower basin	Gridded	Gridded
GRID20	0.73	8.32	Lower basin	Gridded	Gridded
Natitingou	1.40	10.30	Middle basin	Station	Station
Fada	0.35	12.07	Upper basin	Gridded	Gridded
Tenkodogo	-0.38	11.77	Upper basin	Gridded	Gridded
Kete-Krachi	0.03	7.82	Lower basin	Station	Station
Yendi	0.02	9.45	Lower basin	Station	Station
Dapaong	0.25	10.88	Upper basin	Station	Station
Kara	1.17	9.55	Middle basin	Station	Station
Mango	0.47	10.37	Middle basin	Station	Station
Niamtougou	1.25	9.80	Middle basin	Station	Station
Sokode	1.15	9.00	Lower basin	Station	Station

3.1.2 Climate models' datasets

Rainfall and temperature simulations from eight Regional Climate Model under the Coordinated Regional Climate Downscaling Experiment (CORDEX-Africa) (https://climate4impact.eu/) (Kjellström et al., 2016; Samuelsson et al., 2011) were used in this study. Table 3.2 shows the Global Circulation Models (GCMs) downscaled by RCA4, and the institutions that produced them. These RCMs were obtained at a spatial resolution of $0.44^{o}\times0.44^{o}$ (~50km×50km). The selection of the GCMs-RCMs was based on the fact that they have been extensively applied over the Volta basin (e.g. Annor et al., 2017; Kunstmann & Jung, 2005). Also, Akinsanola et al. (2017) and Agyekum et al. (2018) have performed an evaluation of rainfall simulations over West Africa using these GCMs and have attested to their suitability in the use for impact studies in the field of climate change and variability over the West African region. The study considered climate change scenario datasets for the future period (2021-2050) under RCP 4.5 and RCP 8.5 emission scenarios.

Table 3. 2: Description of Climate Model Intercomparison Project 5 GCMs downscaled by RCA4

GCM Name	Short Name	Institution	Reference	Country
CCCma-CanESM2	CanESM2	Canadian Centre of Climate Modelling and Analysis	Giorgi et al. (2009); Chylek et al. (2011)	Canada
CNRM-CERFACS-CNRMCM5	CNRM-CM5	Centre National de Recherches Météorologiques-Groupe d'études de l'Atmosphère Météorologique and Centre Européen de Recherche et de Formation Avancée	Voldoire et al. (2013)	France
ICHEC-EC-EARTH	EC-EARTH	A Consortium of European research institutions and researchers	Hazeleger et al. 2012	Europe
IPSL-IPSL-CM5A-MR	IPSL-CM5A-MR	Institut Pierre-Simon Laplace	Giorgi et al. (2009); Déandreis et al. (2014)	France
MIROC-MIROC5	MIROC5	National Institute for Environmental Studies, and Japan Agency for Marine-Earth Science and Technology	Watanabe et al. (2010)	Japan
MPI-M-MPI-ESM-LR	MPI-ESM-LR	Max-Planck-Institut für Meteorologie (Max Planck Institute for Meteorology)	Giorgetta et al. (2013)	Germany
NCC-NorESM1-M	NorESM1-M	The Norwegian Climate Center	Norwegian Climate Centre (2017)	Norway
NOAA-GFDL-GFDL-ESM2M	GFDL-ESM2M	NOAA Geophysical Fluid Dynamics laboratory	Dune et al. (2013)	USA

NB: *Models hereafter shall be referred to by the short names in Table 3.2.*

3.2 Analysis of climate change scenarios

3.2.1 CHIRPS product evaluation and quality verification

The CHIRPS rainfall products were evaluated using observed rainfall data from six meteorological stations in the Oti River Basin over the period 1981-2010. The stations considered for the validation include, Natitingou, Yendi, Dapaong, Kara, Mango and Sokode. The assessment was done on a monthly and annual basis. For each validation, the gridded

values of CHIRPS rainfall were compared with that of the meteorological station data rainfall values following the commonly used statistical measures, such as Pearson correlation coefficient (*R*), bias, root-mean-square error (RMSE), Nash-Sutcliffe efficiency (NSE) and standard deviation. The position of the CHIRPS gridded data within the acceptable range of the time-series metric [(r = -1 to 1), (Bias = 0 to ∞), (RMSE= 0 to ∞, with 0 being the perfect fit) and (NSE = -∞ to 1)], and the mean range across the six stations ascertained their ability to reproduce rainfall in the basin, and hence their approval for further studies (Bessah et al., 2020; Dembélé & Zwart, 2016; Moriasi et al., 2007). Similarly, the NASA POWER temperature data were compared with the meteorological stations' temperature data at both monthly and annual scale, based on the climate stations that had a complete data for the period 1981-2010.

$$r = \frac{\sum_{i=1}^{n}\left(G_i - \overline{G}\right)\left(S_i - \overline{S}\right)}{\sqrt{\sum_{i=1}^{n}\left(G_i - \overline{G}\right)^2}\sqrt{\sum_{i=1}^{n}\left(S_i - \overline{S}\right)^2}} \quad (1)$$

Where G_i *and* S_i represents climate station and satellite-observed rainfall values respectively; $\overline{G}$ and $\overline{S}$ are mean value of climate station and satellite-observed data, and n is the number of points.

$$\text{Bias} = \frac{\sum_{i=1}^{n} S_i}{\sum_{i=1}^{n} G_i} \quad (2)$$

Where G_i *and* S_i represents climate station and satellite-observed rainfall values respectively

$$RMSE = \sqrt{\frac{1}{n}\sum_{i=1}^{n}\left(S_i - G_i\right)^2} \quad (3)$$

Where S and G are climate station and satellite-observed rainfall data respectively.

$$NSE = 1 - \frac{\sum_{i=1}^{n}\left(Q_o - Q_s\right)^2}{\sum_{i=1}^{n}\left(Q_o - \overline{Q}_o\right)^2} \quad (4)$$

Where Q_o is climate station rainfall, $\overline{Q}_o$ is mean value of climate station rainfall, Q_s is satellite-observed rainfall

$$\sigma = \sqrt{\frac{\sum (x_i - \bar{x})^2}{N}} \quad (5)$$

Where X_i represents each value from the data, $\bar{X}$ is the data mean N is the size of the data.

Afterwards, with the aid of MS Excel and RClimDex, the CHIRPS rainfall data were used to accurately fill data gaps in rainfall detected in the Kete-Krachi (1st – 30th June 1984) and Niamtougou (2006). Also, for temperature data, missing gaps found in Natitingou (1st January - 31st Dec 1992), Kete-Krachi (1st - 30th June 1984), Niamtougou (21st July - 30th Sept. 1996; 1st Jan - 31st Dec 2006) and Sokode (29th Mar - 31st Dec 1998; 1st Jul – 31st Dec 2006) stations were directly filled with the daily maximum and minimum temperature from NASA POWER project (Aguilar et al., 2009; Larbi et al., 2018).

3.2.2 Bias-correction of climate models

The simulated daily rainfall and daily minimum and maximum temperature dataset in this study were extracted and bias-corrected using CMhyd application. The bias-correction method employed was the quantile-quantile mapping technique (Distribution mapping of temperature and precipitation) (Boe´ et al., 2007; Johnson & Sharma, 2011). The CMhyd considered the observed and the simulated rainfall data (thus, the historical and future scenarios) and used the overlapping period 1981-2005 to calculate the correction parameters for the future period (2021-2050) under RCP4.5 and RCP8.5 scenarios. The Bias-correction technique helps to adjust the simulated RCM climate values to fall in line with the observed (Teutschbein & Seibert, 2012). Many times, it is presupposed that the Gamma distribution (Thom, 1958) with shape parameter (α) and scale parameter (β) (Eq. (6)) is appropriate for rainfall distribution incidents and is given as:

$$f_\gamma(x \mid \alpha, \beta) = x^{\alpha-1} \cdot \frac{1}{\beta^\alpha \cdot \Gamma(\alpha)} \cdot e^{\frac{-x}{\beta;}} \; X \geq 0;\; \alpha, \beta > 0 \quad (6)$$

The distribution's structure is determined by its form parameter α: (1) α < 1 shows a gamma distribution with an exponential shape that is infinite on both dimensions, an exponential distribution is characterised by the special situation where (2) α = 1 and (3) α > 1 produces a skewed unimodal distribution curve. β defines the dispersion of the Gamma distribution. The probability of extreme occurrences decreases when β is reduced because the distribution is more compressed. In contrast, a larger β, results in a stretched distribution, which suggests a higher likelihood of extreme occurrences (Teutschbein & Seibert, 2012).

A Gaussian distribution with location and scale parameters is generally considered best for temperature data over time (Cramér, 1999; Schoenau and Kehrig, 1990):

$$f_N\left(x \mid \mu, \sigma^2\right) = X^{\alpha-1}.\frac{1}{\sigma.\sqrt{2\Pi}}.\mathrm{e}\frac{-\left(x-\mu\right)^2}{2\sigma^2}\ ; X \in \Re \qquad (7)$$

The Gaussian distribution's range is extended or constricted depending on the scale parameter σ, which controls the standard deviation. Smaller values of σ compress the distribution, making extreme values less likely. Conversely, larger values of σ denotes a stretched shape with a greater likelihood for extreme values. The location parameter μ directly controls the mean and distribution location (Teutschbein & Seibert, 2012).

For both observed and simulated RCM-simulated climatic variables, a cumulative distribution function was generated. The Gamma CDF can be used to logically describe this process for rainfall (F_γ) and its inverse (F_γ^{-1}) as demonstrated in Thom (1958) is as:

$$P^*_{contr}\left(d\right) = F_\gamma^{-1}\left(F_\gamma(\mathrm{P}_{contr}\left(d\right)\middle|\alpha_{contr,m},\beta_{contr,m}\right)\middle|\alpha_{obs,m},\beta_{obs,m}) \qquad (8)$$

$$P^*_{scen}\left(d\right) = F_\gamma^{-1}\left(F_\gamma(\mathrm{P}_{scen}\left(d\right)\middle|\alpha_{contr,m},\beta_{contr,m}\right)\middle|\alpha_{obs,m},\beta_{obs,m}) \qquad (9)$$

Where P^*_{Contr} is the corrected value for the RCM control run (1981-2005) for the day (d), with month (m), P^*_{scen} the simulated precipitation under historical climate scenario, F_γ is the Gamma Cumulative Distribution Function (CDF), α shape parameter and $\beta_{obs,m}$ is the scale parameter for the month.

For temperature, the same procedure can be expressed in terms of the Gaussian (normal) Cumulative Distribution Function (F_N) and its inverse (F_N^{-1}) as:

$$T^*_{contr}\left(d\right) = F_N^{-1}\left(F_N(\mathrm{T}_{contr}\left(d\right)\middle|\mu_{contr,m},\sigma^2{}_{contr,m}\right)\middle|\mu_{obs,m},\sigma^2{}_{obs,m}) \qquad (10)$$

$$T^*_{scen}\left(d\right) = F_N^{-1}\left(F_N(\mathrm{T}_{scen}\left(d\right)\middle|\mu_{contr,m},\sigma^2{}_{contr,m}\right)\middle|\mu_{obs,m},\sigma^2{}_{obs,m}) \qquad (11)$$

Where: T^*_{contr} is the corrected value for the RCM control run (1981-2005) for the day (d), within a month (m), T^*_{scen} is the simulated temperature under historical climate scenario, F_N is the Gaussian Cumulative Distribution Function, μ is location parameter and $\sigma_{obs,m}$ is the scale parameter for the month.

3.2.3 Evaluation of climate models

To evaluate the efficiency of the RCMs and their ensemble, the simulated rainfall and observed rainfall were compared while the simulated temperature was also compared with the

observed temperature at the mean monthly scale using the Taylor diagram. The Taylor diagram is a visual representation of how well a pattern (or a series of patterns) matches observations. It is measured in terms of correlation, centered root-mean-square difference, and standard deviations (Taylor, 2005). The performance evaluation was done on a monthly scale because it best shows the rainfall and temperature characteristics of the basin (Gulacha & Mulungu, 2016). The HydroGOF package in R software was utilized for the computation of the statistical measures that were used to evaluate the models. With a primary emphasis on hydrological modeling, the package points to Goodness-of-fit (GoF) functions for numerical and graphical comparison of simulated and observed time series. The commonly used statistical measures like Pearson correlation coefficient (*r*), relative standard deviation (rSD), Nash-Sutcliffe efficiency (NSE), root-mean-square error (RMSE), and Percentage Bias (PBIAS) were employed to evaluate the effectiveness of the RCMs. The position of each model and the ensemble mean in the acceptable range of the statistical measures [(r = -1 to 1), and (RMSE= 0 to∞, with 0 being the perfect fit), (PBIAS = -$\infty$to ∞, with 0 being the optimal value), showed how well it simulates rainfall and temperature in the basin (Bessah et al., 2020; Dembélé and Zwart, 2016; Moriasi et al., 2007).

3.3 Intra-seasonal rainfall variability indicators

3.3.1 Annual and seasonal rainfall totals

Annual and seasonal rainfall totals were determined as sum of rainfall for each day (Hadgu et al., 2013; Tegegn, 2015) for the historical period (1981-2010) and the future period (2021-2050). The seasonal rainfall total was calculated based on the rainy season [AMJJASO] period in the basin.

3.3.2 Rainfall onset, cessation and length of the rainy season

The output of simulated daily rainfall, from the ensemble of the bias-corrected RCMs for the near-future (2021-2050) under RCP4.5 and RCP8.5 scenarios and the observed daily rainfall and temperature for the historical (1981-2010) were used in computing the onset, cessation and the length of the rainy season. This computation was done with Instat+v3.36 (Stern et al., 2006). The relative humidity, wind speed, solar radiation and daily minimum and maximum temperature were used in the Instat+v3.36 to compute rainfall cessation dates. The onset of rains was defined as the start of the season with the earliest starting day as 1st April and during this period, the first 5 days collected an aggregate of at least 20 mm of rain, with no dryness

surpassing 7 days in the subsequent 30 days (Stern et al., 1981). Cessation of rain was defined based on the concept of water balance developed by Stern et al. (1981) (thus, the end of the season which occurs after 1st October when the soil water balance has 0 mm of rain). Length of the rainy season (LRS) was determined as the difference between onset and cessation dates of rainfall as applied in Amekudzi et al. (2015).

3.3.3 Number of wet and dry days

A threshold value of 1.0mm was set to define days as wet or dry. Thus, the number of rainy and dry days were determined by counting all days with rainfall ≥ 1.0mm as rainy and those days with rainfall < 1.0mm as dry days as demonstrated in Hadgu et al. (2013) and Tegegn (2015). The counting was done for each year of the data and this was done in MS Excel.

3.3.4 Variability analysis

The Coefficient of variation (CV) was computed using the formula in equation (12).

$$CV = \frac{\sigma}{\mu} \times 100 \qquad (12)$$

where σ is the standard deviation and μ is the mean rainfall for the temporal scales used. Degree of rainfall variations were: low (CV < 20), moderate (20 < CV < 30), and high (CV > 30) (Alemu & Bawoke, 2019).

3.3.5 Standard deviation

The square root of variance was used to calculate the standard deviation. The results were categorized in accordance with Tegegn (2015), who looked at the stability of rainfall in the following way: when standard deviation <10 as very high stabilities; 10-20 as high stability, and 20-40 as moderate stability and >40 as less stability. The standard deviation was computed as:

$$\sigma = \sqrt{\frac{\sum (x_i - \bar{x})^2}{N}} \qquad (13)$$

Where X_i represents each value from the data, $\bar{X}$ is the data mean N is the size of the data.

3.3.6 Rainfall anomaly index

Standardized anomaly index of rainfall was calculated using equation (14) below:

$$SAI_i = \frac{X_i - \overline{X}}{\sigma} \qquad (14)$$

where X_i stands for yearly rainfall for the period understudy; $\overline{X}$ represents the long-term average yearly rainfall for the observation period and σ corresponds to the standard deviation of yearly rainfall during the observed period (Alemu & Bawoke, 2019). Table 3.3 shows the SAI value classification used.

Table 3. 3: SAI value classification (McKee et al., 1993)

SAI value	**Category**
Above 2	Extremely wet
1.5 to 1.99	Very wet
1.0 to 1.49	Moderately wet
-0.99 to 0.99	Near normal
-1.0 to -1.49	Moderately dry
-1.5 to -1.99	Severely dry
-2 or less	Extremely dry

3.3.7 Inverse distance weighted (IDW) interpolation

Using the Inverse Distance Weighted (IDW) interpolation technique, the analyzed rainfall variability indicators across the basin were interpolated from the distinct locations at an annual timescale. The IDW technique uses the idea that there is more similarity in things that are nearby than things that are far from each other (Diodato & Ceccarelli, 2005; Lu & Wong, 2008).

3.3.8 Projected changes in rainfall indicators

The changes in rainfall variability indicators for the future period were computed. The projected changes in annual and seasonal rainfall, onset, cessation and LRS, and the number of wet and dry days were computed as the differences in yearly averages between these indicators during the observation (1981-2010) period and the near-future period (2021-2050).

3.3.9 Trend analysis for rainfall indicators

The study applied the Mann-Kendall (MK) trend statistics to assess trends in the annual and seasonal rainfall, rainfall onset, cessation, length of the rainy season, number of wet and dry

days. Sen's slope estimator was used to determine the magnitude of the trends over the ORB. The MAKESENS Software was used to compute the trends and the significance level was tested at 5%. The MK test compares the null hypothesis (H_o) of no trend to the alternative hypothesis (H_1) that there is a trend (Önöz & Bayazit, 2003). Positive values of the MK test show rising trends whereas negative values indicate declining trends. The Sen's slope (β) estimation test, computes the gradient (i.e., the linear rate of change) and it is a linear regression test. A positive value of β demonstrates an "upward trend" or an increase, while a negative value shows a "downward trend" or a decrease. No change is represented by a Zero value of β (Ayanlade et al., 2018). The MK trend test formula is given as follows:

$$S = \sum_{k=1}^{n-1} \sum_{j=k+1}^{n} Sgn\left(X_j - X_k\right) \qquad (15)$$

Where X_j and X_k are sequential rainfall or temperature values for the time series data of length n. The sum of the *Sgn* function and the mean-variance *Var (Smk)*, under the null hypothesis (H_o) of no trend and independence of the series terms are given in equations 16 and 17 correspondingly.

$$Sgn\left(X_j - X_k\right) = \begin{cases} 1 \, if \, X_j > X_k \\ 0 \, if \, X_j = X_k \\ -1 \, if \; X_j < X_k \end{cases} \qquad (16)$$

$$Var\left(S_{mk}\right) = \frac{N\left(N-1\right)\left(2N+5\right) - \sum_{i=1}^{m} U_i\left(i\right)\left(i-1\right)\left(2i+5\right)}{18} \qquad (17)$$

Where N represents length of the data set, m the number of tied groups and U_i the size of the M^{th} group.

The data trend was validated at a 5% significant level (Z_s α/2 = ± 1.96). When / ZS/ ≥ Zα/2 at α = 0.05 level of significance, the null hypothesis (H_o) of no trend is declined. The standard normal test statistic Z_S indicates a trend in the data series by displaying values that are positive or negative suggesting an increasing or decreasing trend. The trend test formula is as follows:

$$Z_S = \begin{cases} \frac{s-1}{\sqrt{VAR(s)}}, if\ s > 0 \\ 0 \quad if\ s = 0 \\ \frac{s+1}{\sqrt{VAR(s)}}, if\ s < 0 \end{cases} \tag{18}$$

Sen's slope estimator was used to determine the magnitude of the trend. Sen's slope (β) evaluation test merely calculates the gradient (i.e., the linear rate of change) and is a linear regression test. A positive value of β reveals an 'upward trend' or increase, while a negative value reveals a 'downward trend' or decrease. Zero β shows no change (Ayanlade et al., 2018). Sen's slope estimator is denoted as:

$$Q_i = \frac{\left(X_j - X_k\right)}{\left(j-k\right)} \ for\ all\ k < j\ and\ i = 1, .. \mathrm{N} \tag{19}$$

$$Q_{med} = \begin{cases} Q\left[\frac{(n+1)}{2}\right], where\ N\ is\ odd \\ Q\left(\frac{N}{2}\right) + Q\left[\frac{N+2}{2}\right], where\ N\ is\ even \end{cases} \tag{20}$$

Where Q_i is the slope between data points X_j and X_k, Qmed is median slope estimator that demonstrates the trend in the data.

3.4 HBV hydrologic model and its components

The research used the lumped HBV hydrologic model, a conceptual hydrological model, to predict streamflow at chosen stations in West Africa's Oti River Basin. It is well known for its ability to conduct hydrological analysis related to water balance (Bergström, 1992). Due to its adaptability, analytical accuracy, and demonstrated efficiency worldwide, the HBV hydrologic model was considered. Various research on hydrological modelling and climate change investigations have commonly applied the model (Al-Safi & Sarukkalige, 2017; Driessen et al., 2010). Having a reasonable number of free parameters with simple daily time steps data needed for input (thus, temperature, precipitation and potential evapotranspiration) (Pervin et al., 2021), the model becomes a suitable option for use in a data-scarce region like West Africa. Precipitation and discharge observation data are essential to calibrate the model and perform the simulation in a region with no major snow routine. For a region like West Africa, when the snow routine procedure is not taken into account, the HBV model comprises

of three primary box layers. In essence, it links the water flow channels in all three boxes, connecting precipitation in the soil box to runoff estimation as the simulation's output, as seen below:

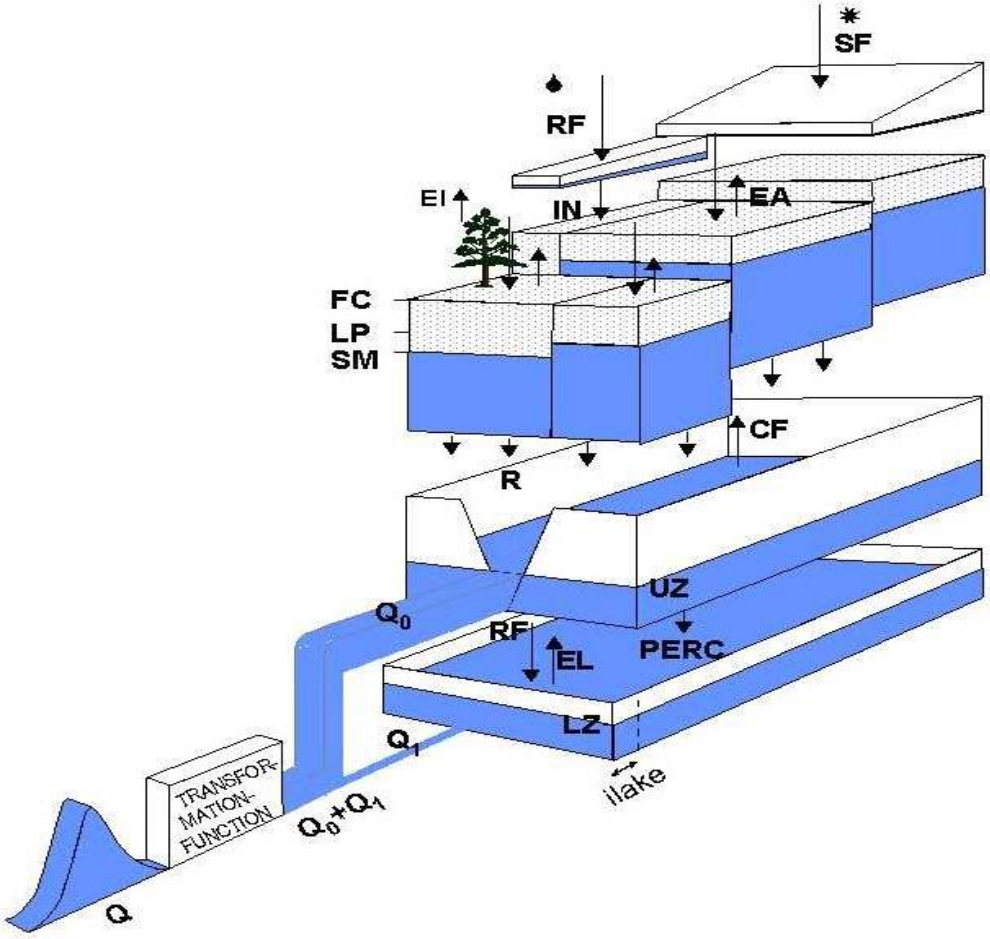

Figure 3. 1: HBV model structure (Adapted from Berglöv et al., 2009)

Being the initial box in the model, the soil box, represents the soil surface, where the precipitation falls and evapotranspiration occurs. The *ß*, FC, and LP, are the three parameters on which the soil moisture module of the HBV is based. Where *ß* regulates the contribution to the runoff response function or (dQ) the increase (dP-dQ) in soil moisture storage (S_{sm}) from each mm of rainfall. FC is the maximum soil moisture storage capacity (in mm) in the model. The soil moisture level (LP), which is expressed as a fraction of FC, is the level at which evapotranspiration (E_a) reaches its potential value (E_p). If S_{sm}/FC is higher than $LP \times FC$, the soil moisture zone's actual evaporation is equal to its potential evaporation. As demonstrated in Abraham et al. (2022), the parameters are computed using the following equations:

$$\frac{dQ}{dP} = (\frac{S_{sm}}{FC})^{\beta} \quad (21)$$

Where dQ = runoff [mm/d] and dP = precipitation [mm/d]

$$E_a = E_P.\min\left(\frac{S_{sm}}{FC.\mathrm{LP}},1\right) \quad (22)$$

The response function that converts extra water from the soil moisture zone to runoff is the runoff generation routine. It also considers how evaporation and direct precipitation impact a section that shows lakes, rivers, and other wet areas. The model has two reservoirs (tanks), the lower (linear) and upper reservoirs (non-linear) that disperse the created runoff concurrently in terms of rapid and delayed responses, accordingly. The upper reservoir's storage (P_{MAX}) will be increased by the output from the soil moisture zone. Water will infiltrate to the lower reservoir, S_{Lz} (mm) in accordance with the parameter PERC as long as there is water in the upper reservoir. In contrast, the lower reservoir is a representation of the groundwater storage of the catchment that contributes to the baseflow. The groundwater discharge, (Q_2) which is an output from the lower reservoir is regulated by the recession coefficient K_2 (d^{-1}) while the upper reservoir storage S_{UZ} (mm) is drained by two recession coefficients, K_0 (d^{-1}) and K_1 (d^{-1}), draining the quick flow Q_0 (mm/d) and slow flow portion Q_1 (mm/d) segregated by a threshold UZL (mm). The formula involved as demonstrated in Abraham et al. (2022) can be expressed as follows:

$$Q_0 = K_0\left(S_{uz} - UZL\right) \quad (23)$$

$$Q_1 = K_1\left(S_{UZ}\right) \quad (24)$$

$$Q_2 = K_2\left(S_{LZ}\right) \quad (25)$$

The upper reservoir will begin to fill up when the output dQ (mm/d) from the soil moisture routine surpasses its limit, and the response in times of flooding is modeled by this box. PERC, K_0, K_1, K_2, and UZL are the parameters calibrated using the runoff response function. The sum of inputs from the lower reservoir and upper reservoir at the individual sub-basins becomes the total runoff. For the hydrograph at the sub-basin's outlet to have the right shape, the runoff produced by the response routine is directed through a transformation function-a straightforward filter method with a triangular weight distribution with its time base expressed

as MAXBAS (d). Extensive elaboration on the HBV hydrologic model can be obtained from Bergström (1992) and Seibert & Vis (2012). The HBV model parameters used are displayed in Table 3.4

Table 3. 4: HBV model parameters subject to calibration (Beck et al., 2016)

		Range		Parameter
Parameter	Parameter explanation	Min	Max	Unit
BETA	Exponential parameter in soil routine	1	6	-
FC	Maximum soil moisture content	50	700	mm
K_0	Additional recession coefficient of upper groundwater store	0.05	0.99	d^{-1}
K_1	Recession coefficient of upper groundwater store	0.01	0.8	d^{-1}
K_2	Recession coefficient of lower groundwater store	0.001	0.15	d^{-1}
LP	Limit for potential evapotranspiration	0.3	1	-
MAXBAS	Transfer function parameter	1	3	d
PERC	Maximum flow from upper to lower tank	0	8	mmd^{-1}
UZL	Threshold parameter for extra outflow from upper zone	0	100	mm

3.5 HBV model input data

3.5.1 Daily discharge data

West Africa, like numerous other locations, struggles with a lack of data, particularly when it comes to records of observed discharge. The HBV model required daily discharge data for baseline period calibration of the model to generate future streamflow in the river basin. This data was obtained for five (5) stations in the Oti River Basin, from the Water Resources Commission, Ghana, Water resources directorate, Togo; General Directorate of Water Resources, Burkina Faso and National Directorate of Water (DG-Eau), Benin. The gauge stations for which the discharge data were obtained included Arly, Porga, Koumongou, Saboba and Sabari. The data set are provided for five streamflow gauging sites located in the ORB with varying completeness for each year and site. The data acquired were quality-checked and all data for each sub-basin had large missing records in the discharge data (Table 3.5). Daily discharge data from 1981 to 1991 were deemed suitable for the simulation in all five sub-basins after the few gaps detected in this period were filled using the regression-based estimating approach. A first step in the procedure is the estimation of regression equations that relate a variable with incomplete data to a collection of variables with complete data across all dataset observations. The equation generated is then used to predict the missing

values (Gao, 2017; Taylor et al., 2006). As indicated by Obahoundje et al. (2018), this method does not have any bias problem with the mean values. To find out if the available streamflow stations had good quality of data to be used, a linear regression analysis was performed between the annual discharge of each gauged station and their respective annual rainfall amount. The approach used followed the method of Taylor et al. (2006). In their study, they utilized the linear regression approach to identify stations that produced fair and accurate streamflow data. They further indicated that whilst good correlation coefficients may not assure that flow data are valid, poor correlations imply there are issues with the data. Similarly, in this study, all five (5) gauge stations had an R^2 value that was greater or equal to 0.5 and were considered for the simulation exercise.

Table 3. 5: Characteristics of streamflow gauging stations used in the study

	Co-ordinates (decimal degrees)		Drainage area	Mean Elevation	Period of	Missing data
Station	Lat	Long	(Km^2)	(m)	data	(%)
Porga	11.05	0.97	23134.61	212.32	1970-2019	10%
Arly	11.43	1.57	6487.93	307.74	1979-2005	49%
Koumongou	10.2	0.45	6684.92	323.81	1959-2017	48%
Sabari	9.28	0.23	60184.1	155.49	1959-2009	10%
Saboba	9.76	0.32	54038.96	140.13	1953-2009	16%

3.5.2 Precipitation data

The meteorological stations located in the five sub-basins were Natitingou, Fada, Tenkodogo, Yendi, Dapaong, Kara, Mango and Niamtougou. Owing to local area coverage, Climate Hazards Group Infrared Precipitation with Station data (CHIRPS) was employed to supplement the meteorological station data. The Thiessen polygon technique was used to calculate the areal precipitation. From daily point rainfall measures that are in and around the river Basin, the areal rainfall was determined. Twenty-four climate stations were used for modelling in the basin (i.e., GRID1-GRID16 in addition to the above-mentioned stations). The technique evaluates data across stations in relation to the distance between them. Abraham et al. (2018) and Pervin et al. (2021) applied the Thiessen polygon approach to generate areal mean of climate data for use in the HBV model and obtained good results. The Thiessen polygon method is given as:

$$P_{avg} = \sum_{i=1}^{n} W_i * P_i \quad (26)$$

$$W_i = \frac{A_i}{A_T} \quad (27)$$

Where A_i is Area of polygon, A_T is Total area of study area, and P_{avg} is average precipitation

3.5.3 Potential evapotranspiration

The daily potential evapotranspiration as one of the model inputs was estimated following the Penman-Monteith approach in Instat+v3.36 (Stern et al., 2006). Climate data such as daily maximum and minimum temperature, relative humidity, solar radiation and wind speed obtained from the National Aeronautics and Space Administration Prediction of Worldwide Energy Resource (NASA POWER) project (Stackhouse et al., 2018), for the period 1981-2010 were used in Instat+v3.36 to compute daily evapotranspiration. The ensemble maximum and minimum temperature data from 8 climate models under RCP4.5 and RCP8.5 scenarios were used to estimate the potential evapotranspiration (ETo) for the future period 2021-2050. The estimation was done following the Hargreaves-Samani method (Hargreaves & Samani, 1985). The method requires only maximum and minimum air temperature data and location latitude for estimating ETo (mm d^{-1}) (thus referred to as the HS-ETo). The HS equation can be expressed as:

$$HS - ET_O = a \times 0.408 \times R_a \times \left(T_{avg} + b\right) \times \left(T_{\max} - T_{\min}\right)^c \quad (28)$$

Where R_a is the extraterrestrial radiation (MJ m^{-2} d^{-1}), T_{max} is maximum air temperature (°C), T_{min} is the minimum air temperature (°C), T_{avg} is calculated as the average of T_{max} and T_{min} (°C), and the coefficient of 0.408 is used to convert from MJ m^{-2} d^{-1} to mm d^{-1}. Coefficients a, b and c are multiplier and offset parameters of the HS equation. The original values of empirical coefficients a, b, and c are 0.023, 17.8, and 0.5, respectively (Hargreaves & Samani, 1985).

3.6 Discretization and parameters of the gauged sub-basins

The Oti basin was split up into smaller units based on Digital Elevation Model and river systems of the watershed using SWAT+ and this resulted in 14 sub-basins. However, of the 14 sub-basins, only 5 were gauged sub-basins. After the delineation, the yearly average

rainfall, potential evapotranspiration, discharge, aridity index was determined for each sub-basin. Each of the sub-basin's land use and cover were categorized to correspond to their SWAT+ equivalents. Additionally identified were the slopes of the basin. Aridity index in each sub-basin demonstrates the precipitation to atmospheric water demand ratio. The fraction of potential evapotranspiration to yearly rainfall is known as the aridity index (AI) (Li et al., 2017; UNEP, 1992). It is frequently employed to measure humidity or dryness levels (Li et al., 2017; Sahin, 2012). It was determined as:

$$AI = \frac{MAP}{MAE} \tag{29}$$

Where MAP is Mean annual rainfall, and MAE is Mean annual evapotranspiration

The United Nations Environmental Program's (UNEP) global aridity classification scheme (UNEP, 1997, 1992) was employed. Table 3.6 shows the AI classification scheme used.

Table 3.6: Aridity index classification

Aridity Index	Classification
AI<0.03	Hyper arid
0.03≤AI<0.2	Arid
0.2≤AI<0.5	Semi-arid
0.5≤AI<0.65	Dry sub-humid
AI>0.65	Humid

3.7 HBV model calibration and validation

Calibration was performed with observed discharge data at five (5) available gauging stations. The calibration was performed on daily time steps. Historical daily flow from five (5) hydrological stations namely, Porga, Arly, Koumongou, Sabari and Saboba were used over the period January 1, 1981 to December 31, 1991. The time period selected for the calibration was January 1981 to December 1986 with the first year as a warm-up period (thus, 5 years of data for actual calibration (January 1981 to December 1986), and the behavioral parameter sets from the calibration chosen using a Nash-Sutcliffe Efficiency threshold of 0.5. The validation was executed for the period January 1987 to December 1991 (thus, 5 years of data) utilizing the obtained behavioural parameter values. The study generated simulated river

discharge combinations with the HBV model using a homogeneous random sampling technique. This was done using 20000 combinations of the nine HBV parameter sets used in the study to generate a uniform random Monte-Carlo sampling method. The NSE which indicates the model's efficiency and predictive relevance in simulating streamflow against the observed streamflow, was used to evaluate the performance of the HBV model as well as the Kling-Gupta efficiency. The NSE was calculated as expressed in equation (4).

The Kling-Gupta efficiency (KGE) prevents variability underestimation by considering the variability (α), bias (β), and correlation (r). Additionally, it allows bias comparison among catchments (Gupta et al., 2009). It is expressed as:

$$KGE = 1 - \sqrt{(r-1)^2 + (\alpha - 1)^2 + (\beta - 1)^2} \quad (30)$$

$$\alpha = \frac{\sigma_s}{\sigma_o} \text{ and } \quad \beta = \frac{\mu_s}{\mu_o}$$

Where KGE ranges from $-\infty$ to 1, with 1 being optimum.

3.8 Streamflow projection for future period and trend

To predict the effect of intraseasonal rainfall variations on streamflow in the basin for the near-future 2021-2050, the calibrated HBV model was subsequently driven by the ensembled mean of climate projections from eight bias-corrected regional climate models forced by two greenhouse-gas emission scenarios (RCP4.5 and RCP8.5), the historical observed (1981-2010) and the models' historical (1981-2005). The Mann-Kendall test and Sen's slope estimator were then employed to examine the trends of the projected streamflow at yearly scale.

3.9 Partial conclusion

This chapter discussed the various data kinds that were gathered as well as the tools and procedures utilized to analyze the data to meet the specified goals. Collected climate data, including Climate Hazards Group Infrared Precipitation with Station data (CHIRPS), National Aeronautics and Space Administration Prediction of Worldwide Energy Resource (NASA POWER) project data, discharge data, and estimates from regional climate models, are some of the different types of data used in this study. Applications such as CMhyd, Instat+, ArcGIS, R software, MATLAB, MAKESENSE, SWAT+ and the HBV model were used for the analyses.

Chapter 4: Historical and Future Intraseasonal Rainfall Variability Analysis

The findings of the analysis of intraseasonal rainfall variability indicators for the Oti River Basin are presented in this chapter. The findings include: (a) validation of CHIRPS rainfall and NASA POWER data for the Oti River Basin; (b) performance evaluation and bias-correction of climate models for the period 1981-2010; and (c) historical (1981-2010) and future (2021-2050) rainfall variability projections for the Oti River Basin under RCP4.5 and RCP8.5 scenarios.

4.1 Validation of satellite climate datasets for Oti River Basin

4.1.1 Comparison between the station and satellite rainfall and temperature data

The comparison of the station and satellite CHIRPS rainfall and NASA POWER temperature data was done at both mean monthly and yearly scale for the period 1981-2010 and presented in Table 4.1. From the comparison between CHIRPS data and station rainfall data, the CHIRPS rainfall was able to reproduce the unimodal nature of rainfall in the Oti River Basin with its peak which is known to be in August. A very high agreement with all the station data was shown with a correlation coefficient (r =0.99), and a Nash-Sutcliffe efficiency of 0.98 for Yendi and Dapaong stations and 0.99 for Kara, Mango, Sokode and Natitingou stations (Table 4.1). The CHIRPS dataset accurately predicted the mean monthly distribution of precipitation, a little overemphasizing the wettest period at Sokode, Dapaong and Yendi stations. It is observed that at the mean monthly scale, CHIRPS rainfall data was able to satisfactorily reproduce the mean monthly rainfall patterns for the six stations compared to the mean annual rainfall patterns. At annual scale, the variations in rainfall are well captured, for all the six locations. In general, CHIRPS showed a good agreement with the station data as confirmed by its high correlation values (0.99) at all the six stations and a minimum Nash–Sutcliffe efficiency of 0.98 (Table 4.1). Despite this, slight differences were observed in RMSE at Yendi, Dapaong, Kara and Sokode stations. This may be due to heterogeneity in the study locations but with relatively acceptable level of Bias. The performance of CHIRPS rainfall data against the rainfall data from meteorological stations at mean monthly and annual distribution are presented in Figure 4.1 and Figure 4.2 respectively.

In the same way, the comparison of NASA POWER temperature data with station temperature data at mean monthly and yearly scales showed good correlation values at Yendi, Dapaong, Kara and Mango stations in the Oti River Basin for the period 1981-2010. The

correlation values ranged between 0.71 to 0.99, an acceptable range of bias between 0.93 to 1.12 and a NSE of between 0.01 to 0.92 (Table 4.1). In summary, the outcomes of the evaluations suggest that the NASA POWER data matches the temperature pattern of the stations in the basin and, therefore, can be used for subsequent investigation.

Table 4. 1: Comparison of station and satellite climate datasets were compared at mean monthly and annual scale for the period 1981-2010

	Precipitation					
Monthly scale	Yendi	Dapaong	Kara	Mango	Sokode	Natitingou
Pearson correlation co-efficient (*r*)	0.99	0.99	0.99	0.99	0.99	0.99
Bias	0.97	0.93	0.97	1.03	1.03	0.99
Root-mean-square error (RMSE)	2.54	3.54	2.26	0.17	2.08	0.78
Nash-Sutcliffe efficiency (NSE)	0.98	0.98	0.99	0.99	0.99	0.99
Annual scale						
Pearson correlation co-efficient (*r*)	0.76	0.40	0.70	0.50	0.60	0.83
Bias	0.97	0.94	0.97	1.03	1.03	0.99
Mean annual rainfall (mm/yr)	1210.06	1061.47	1289.05	1045.2	1266.75	1187.48
	1178.20	**995.61**	**1256.66**	**1076.11**	**1300.63**	**1186.30**
Standard deviation	217.40	215.18	195.27	157.01	171.30	174.51
	129.51	**129.43**	**142.09**	**106.19**	**173.96**	**162.68**
Monthly scale	Temperature					
Pearson correlation co-efficient (*r*)	0.92	0.71	0.93	0.99		
Bias	0.93	0.99	1.12	0.99		
Root-mean-square error (RMSE)	0.67	0.49	0.92	0.01		
Annual scale						
Bias	0.93	0.99	1.12	0.94		
Mean annual temperature (^{o}C)	28.91	27.23	23.27	28.43		
	26.74	**26.90**	**25.45**	**26.82**		
Standard deviation	1.93	4.06	12.81	1.60		
	0.49	**0.41**	**0.47**	**0.44**		

NB: Values for CHIRPS and NASA-POWER are in bold

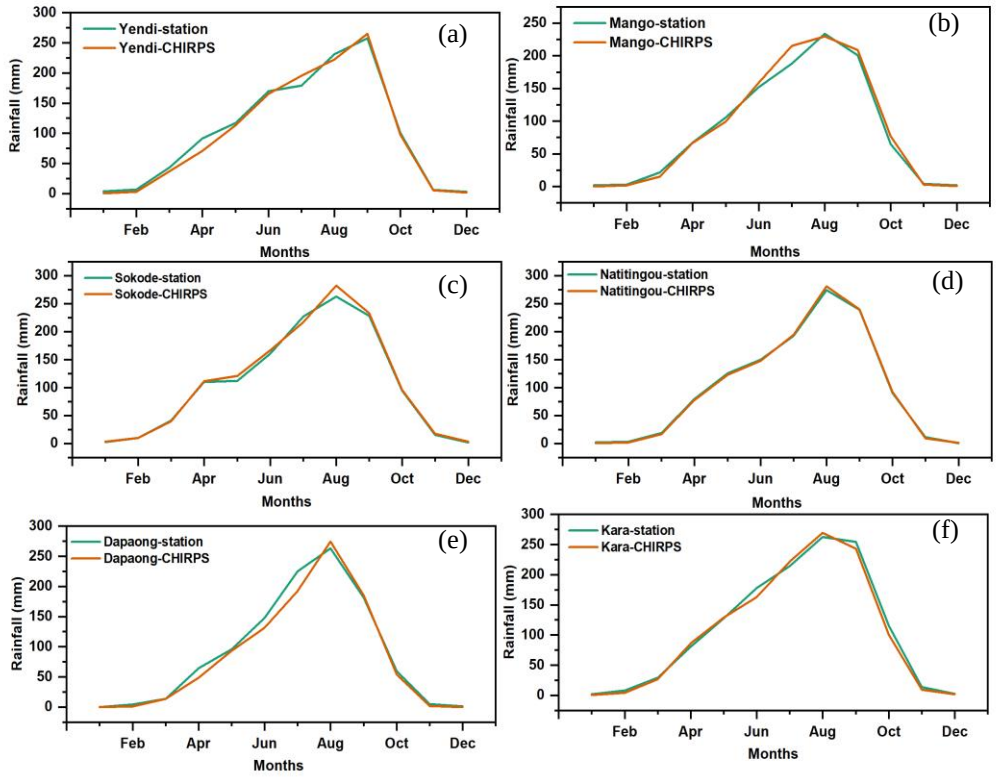

Figure 4. 1: Performance of CHIRPS rainfall data at mean monthly scale

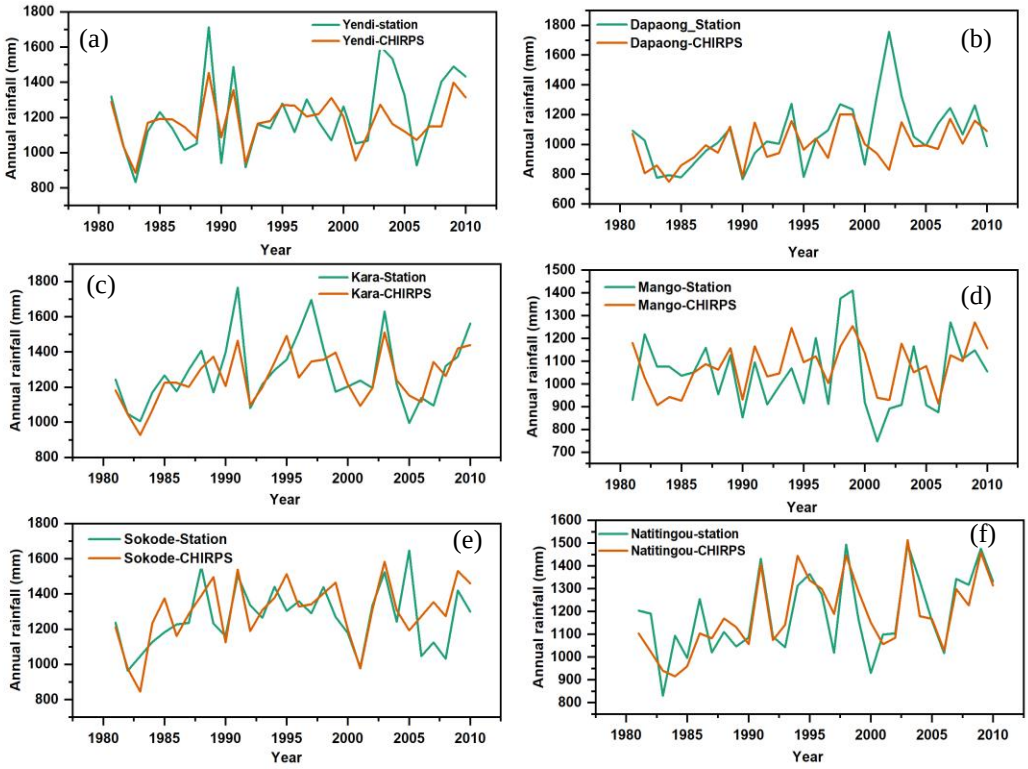

Figure 4. 2: Performance of CHIRPS rainfall data at mean annual scale

4.2 Bias-correction and performance of climate models

4.2.1 Rainfall and temperature

The bias-correction of the RCMs and their ensemble over the basin for simulated rainfall have been performed as presented in Figure 4.3 (a and b). It was revealed that the correlation between the raw models' ensemble and observation was moderate (r = 0.76) with a NSE value of 0.53 before bias-correction. The uncorrected models each showed clear variances in how they reproduced historical rainfall. However, after bias-correction, the individual models and their ensemble were enhanced. A strong correlation (r = 0.91) between the model's ensemble and the observed was obtained with an improved NSE of 0.98.

The results from bias-correction of simulated temperature are presented in Figure 4.3 (c and d). The results showed a correlation between the raw models' ensemble and observation was 0.82 and the NSE value was -0.38 before the bias-correction (Figure 3c). However, these improved after bias-correction (Figure 3d) with a strong correlation between the model's ensemble and observation (r = 1.00), and a NSE value of 0.99. Overall, the corrected

individual RCMs and their ensembles were shown to be better at reproducing the rainfall and temperature pattern shown by the observation at the monthly scale. Therefore, the bias-corrected RCMs and their ensemble can be stated to represent the basin, and are considered acceptable for further analysis. The performance of the models at the annual scale for both rainfall and temperature can be seen at annex 1c and annex 1d.

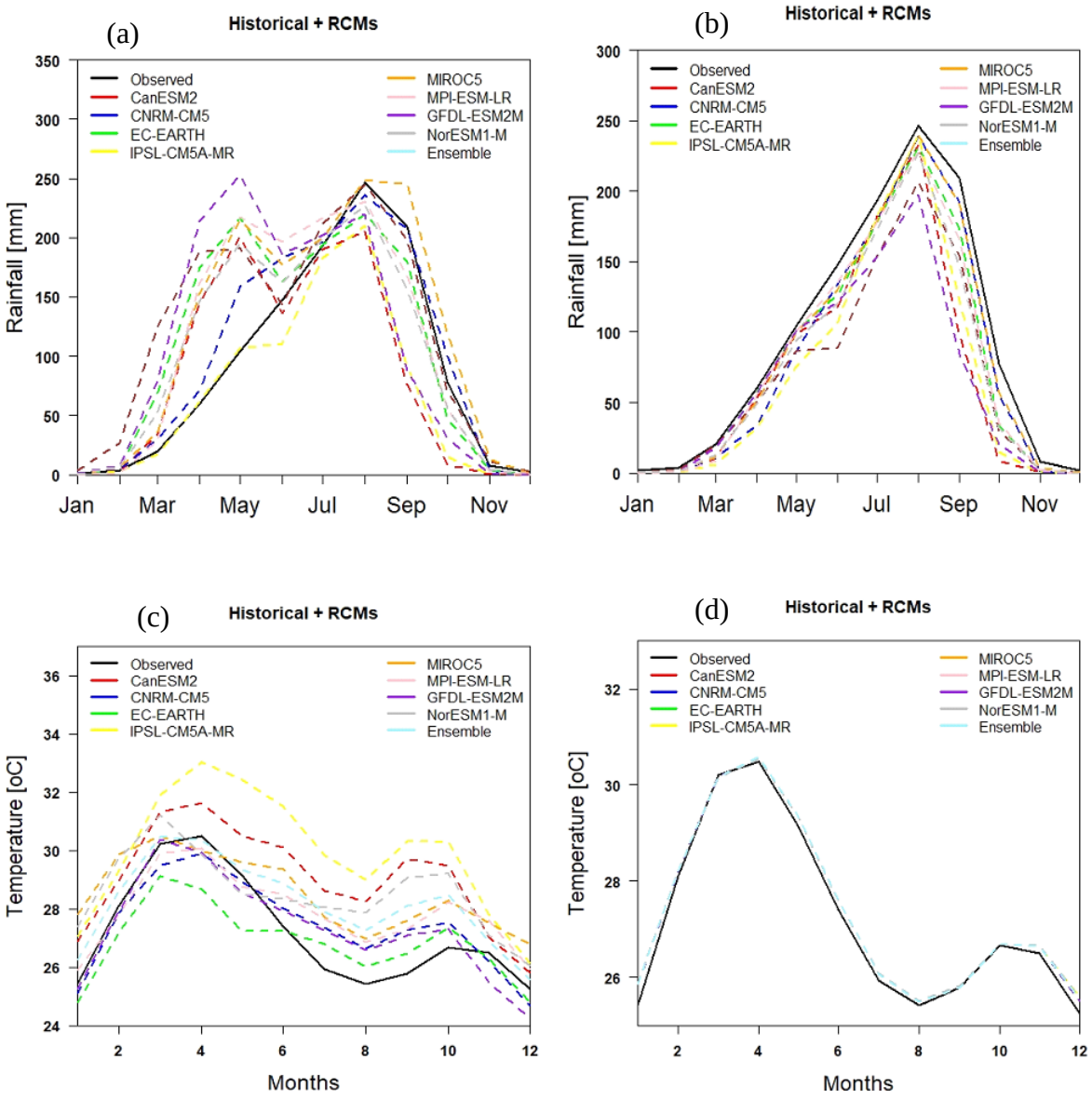

Figure 4. 3: Comparison at monthly scale between observation and simulated (a) rainfall before bias-correction, and (b) rainfall after bias-correction, (c) temperature before bias-correction, and (d) temperature after bias-correction

4.3 Climate models' performance evaluation

4.3.1 Rainfall at mean monthly scale

The performance of simulated rainfall by the CORDEX RCMs in reproducing the long term mean monthly rainfall patterns in the Oti river basin for the baseline period (1981-2005) was assessed and presented using the Taylor diagram (Taylor, 2005) as shown in Figure 4.4, and the models summary statistics presented in Table 4.2. All the RCMs including the ensemble mean captured the mean monthly rainfall distribution reasonably well with correlation (*r*) values above 0.9, a standard deviation value of less than 2.0 and a root-mean-square error (RMSE) value of less than 0.75. Generally, the results show a close match between the RCMs and ensemble simulated rainfall pattern and observation although all models showed an underestimation of rainfall.

Table 4. 2: Statistical analysis of climate models' performance in simulating mean monthly rainfall of the Oti River basin

Climate models	Statistical measures				
	PBIAS (%)	NSE	rSD	RMSE	*r*
CanESM2	-25.2	0.79	0.89	39.39	0.93
CNRM-CM5	-13.1	0.97	0.97	14.03	0.99
EC-EARTH	-14.3	0.95	0.92	18.84	0.99
IPSL-CM5A-MR	-27.4	0.83	0.91	35.66	0.95
MIROC5	-26.0	0.86	0.80	32.15	0.98
MPI-ESM-LR	-10.3	0.98	0.96	11.33	0.99
GFDL-ESM2M	-15.3	0.95	0.92	19.71	0.99
NorESM1-M	-29.7	0.73	0.76	44.36	0.93
Ensemble mean	-20.2	0.91	0.88	25.51	0.98

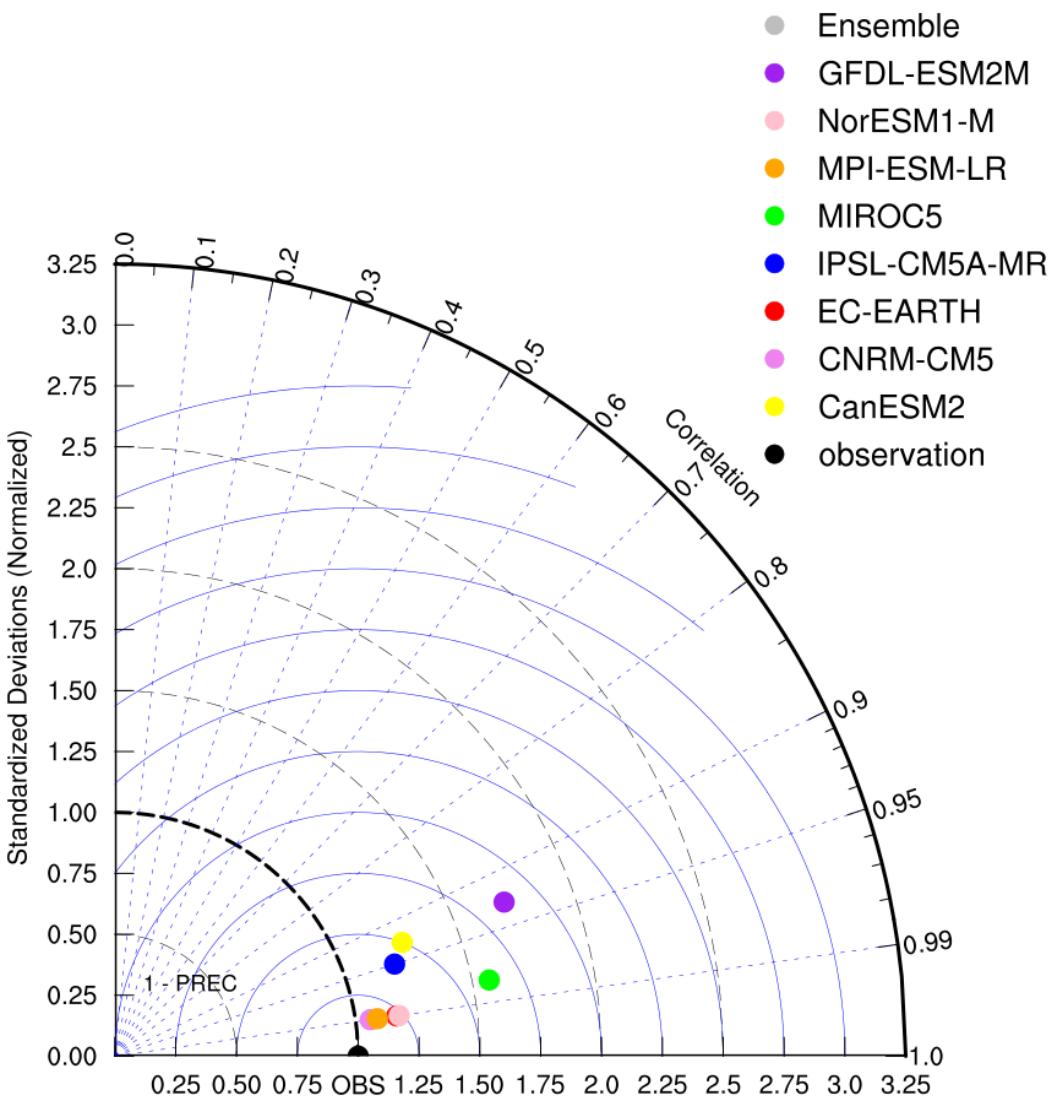

Figure 4. 4: Performance of simulated and observed mean monthly rainfall for Oti basin

4.3.2 Temperature at mean monthly scale

The performance of simulated temperature by the CORDEX RCMs in reproducing the long term mean monthly temperature patterns in the Oti river basin for the baseline period (1981-2005) was assessed and presented using the Taylor diagram (Taylor, 2005) as shown in Figure 4.5, and the models summary statistics presented in Table 4.3. All the RCMs including the ensemble mean captured the mean monthly temperature distribution very well with correlation (*r*) values not less than 0.99, a standard deviation value of not more than 1.25, and a root-mean-square error (RMSE) value below 0.25. Generally, the results show a close match between the RCMs and ensemble simulated temperature pattern and the observation.

Table 4. 3: Statistical analysis of climate models' performance in simulating mean monthly temperature of the Oti River basin

Climate models	Statistical measures				
	PBIAS (%)	NSE	rSD	RMSE	*r*
CanESM2	0.5	0.99	0.97	0.19	0.99
CNRM-CM5	0.5	0.99	0.97	0.19	0.99
EC-EARTH	0.5	0.99	0.97	0.19	0.99
IPSL-CM5A-MR	0.5	0.99	0.97	0.19	0.99
MIROC5	0.5	0.99	0.97	0.19	0.99
MPI-ESM-LR	0.5	0.99	0.97	0.19	0.99
GFDL-ESM2M	0.5	0.99	0.97	0.19	0.99
NorESM1-M	0.5	0.99	0.97	0.19	0.99
Ensemble mean	0.5	0.99	0.97	0.19	0.99

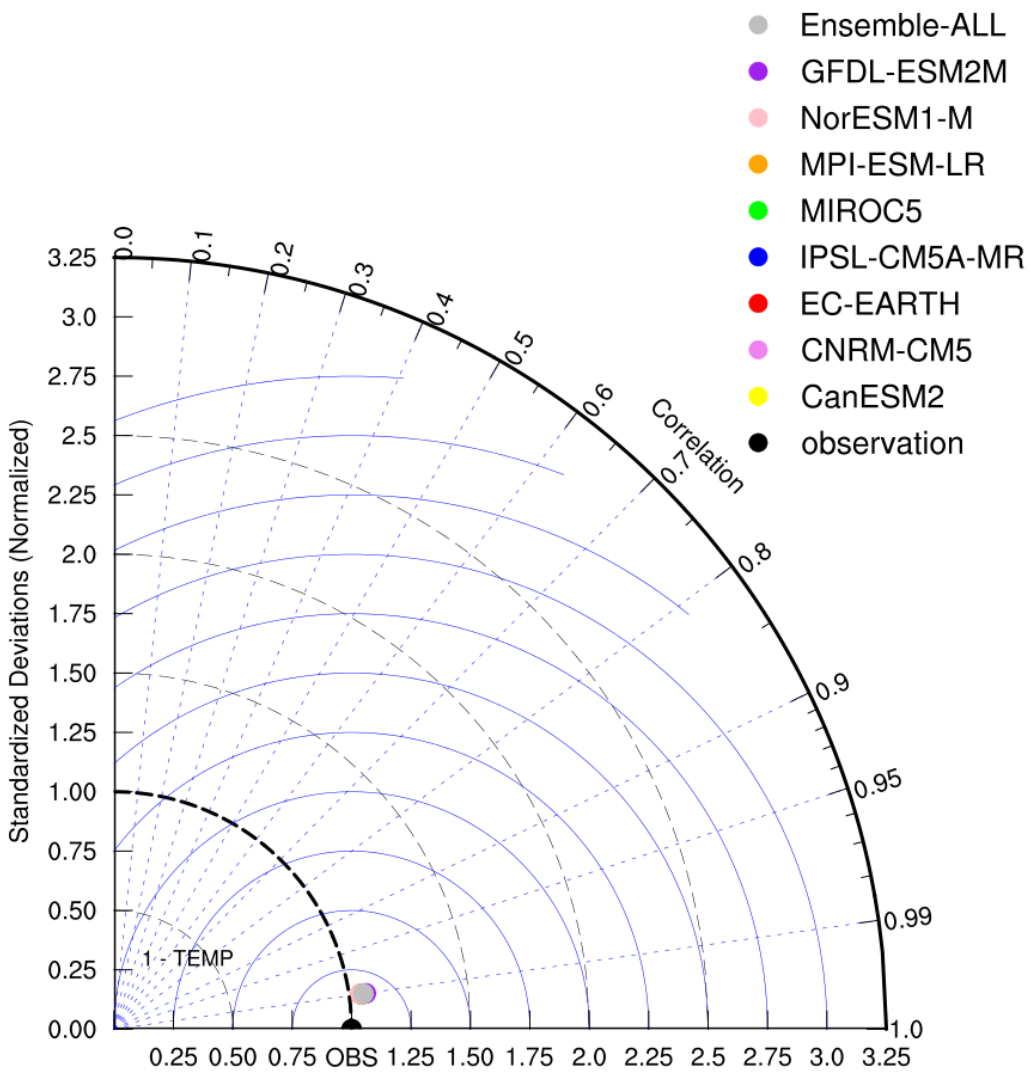

Figure 4. 5: Performance of simulated and observed mean monthly temperature for Oti basin

4.4 Spatial and temporal analysis of intraseasonal rainfall for Oti basin using ensemble mean

4.4.1 Annual rainfall projections in the Oti basin

The results for annual rainfall statistics in the basin for the historical (1981-2010), simulated historical (1981-2005) and future periods (2021-2050) under RCP4.5 and RCP8.5 are displayed in Table 4.4. During the historical period, the mean annual rainfall was 1073.8 mm/yr which ranged between 783.4 mm/yr at GRID3 and 1464.8 mm/yr at GRID20. However, for the models' historical period, the mean annual rainfall was 852.5 mm/yr which ranged between 1105.5 mm/yr at Sokode and 610.7 mm/yr at GRID3. The standard deviation (SD) ranged between 94.8mm/yr at GRID1 and 320.9mm/yr of rainfall at Kete-Krachi with a

mean value of 104.1mm/yr indicating that during this period rainfall was less stable. The SD values for the simulated historical also reveals that rainfall was less stable (Tegegn, 2015). The coefficient of variation (CV) varied from 10.2% at GRID16 to 23.6% at Kete-Krachi with a mean CV of 9.7% indicating less to moderate rainfall variability (10.2%<CV<23.6%) according to Asfaw et al. (2018) and Alemu and Bawoke (2019). With regards to the simulated historical, CV varied from 5.5% at GRID17 to 9.2% at Fada with a mean CV of 5.8%. The moderate variability in rainfall at Kete-Krachi (23.6%) and Dapaong (20.3%) suggests that the amount of water available in these areas was somewhat more erratic compared to the areas with low CV (Alemu and Bawoke, 2019).

The mean annual rainfall during the future (2021-2050) period would be around 970.2mm/yr under RCP4.5 which would range between 640.2mm/yr at GRID3 and 1408.3mm/yr at Sokode. The mean standard deviation recorded under RCP4.5 would be around 52.8mm/yr for the basin, which would vary from 56.4mm/yr at Fada to 100.9mm/yr at Niamtougou. The SD values during the future period, under the RCP4.5 scenario reveals that rainfall would be less stable (Tegegn, 2015). The mean coefficient of variation in the basin recorded under RCP4.5 would be around 5.4% ranging between 5.4% at GRID19 and 9.7% at GRID3 showing a low variation among the stations in the basin (5.4%<CV<9.7%) as demonstrated in Asfaw et al. (2018) and Alemu & Bawoke (2019).

The mean annual rainfall in the future period, under RCP8.5 would be around 1027.9mm/yr which would range between 758.4mm/yr at GRID3 and 1287.1mm/yr at Sokode. The mean standard deviation would be around 51.4mm/yr for the entire basin, ranging between 54.5mm/yr at GRID3 and 91.2mm/yr at Sokode. The SD values during the future period, under this scenario reveals that rainfall would be less stable (Tegegn, 2015). The mean coefficient of variation in the basin under the RCP8.5 scenario would be about 5% which would range between 5% at GRID16 and 9% at Natitingou. This shows a low variation of rainfall (5%<CV<9%) as demonstrated in Asfaw et al. (2018) and Alemu & Bawoke (2019).

Table 4. 4: Summary statistics of annual rainfall in Oti River Basin

Station	Observed (1981-2010)			Sim-historical (1981-2005)			RCP4.5 (2021-2050)			RCP8.5 (2021-2050)		
	Mean [mm]	SD [mm]	CV [%]	Mean [mm]	SD [mm]	CV [%]	Mean [mm]	SD [mm]	CV [%]	Mean [mm]	SD [mm]	CV [%]
GRID1	792.9	94.8	12	635.8	52.2	8.2	684.1	59.6	8.7	834.3	65.8	7.9
GRID2	815.6	115.6	14.2	649.4	47.3	7.3	693.4	63.3	9.1	839.2	55.4	6.6
GRID3	783.4	120.4	15.4	610.3	49.8	8.2	640.2	62	9.7	758.4	54.5	7.2
GRID4	853.6	130.4	15.3	685.2	55.2	8.1	712.7	62.9	8.8	835.9	64.7	7.7
GRID5	891.6	110.5	12.4	716.4	52.0	7.3	774.7	65	8.4	922	76.9	8.3
GRID6	877.2	107.2	12.2	695.7	45.8	6.6	773.1	62	8	896.1	76	8.5
GRID7	886	134.1	15.1	700.5	43.7	6.2	792	58.5	7.4	898.7	74.7	8.3
GRID8	928.6	137.5	14.8	756.7	48.3	6.4	829.3	69.2	8.3	915.9	68.5	7.5
GRID9	974.9	129.5	13.3	802.7	50.8	6.3	866.8	64.2	7.4	927.5	63.3	6.8
GRID10	941.8	113.3	12	768.7	54.4	7.1	885.7	63.9	7.2	1006.3	74.6	7.4
GRID11	943.7	126.4	13.4	770.7	47.3	6.1	872.7	60.8	7	957.5	63.7	6.7
GRID12	1074.7	141.2	13.1	895.3	53.3	6.0	932.1	70.8	7.6	1006.6	70.8	7
GRID13	982.5	107.9	11	800.7	65.9	8.2	845.9	61.8	7.3	914.2	69.8	7.6
GRID14	1101.5	112.2	10.2	900.5	67.6	7.5	1038	70.2	6.8	1117.4	64.4	5.8
GRID15	1200.3	132.5	11	958.6	72.9	7.6	1108.6	62.8	5.7	1124.9	60.7	5.4
GRID16	1239.3	126.6	10.2	995.3	71.2	7.2	1174.1	81.9	7	1193.7	59.5	5
GRID17	1330.6	170.1	12.8	1087.6	60.4	5.5	1279	95	7.4	1266.1	72.4	5.7
GRID18	1363.5	163.8	12	1031.5	87.5	8.5	1164.4	88.6	7.6	1128	70.4	6.2
GRID19	1360.3	194.4	14.3	1071.8	71.0	6.6	1295.4	69.5	5.4	1227.5	73.3	6
GRID20	1464.8	207.2	14.1	1105.6	92.5	8.4	1293.5	90.3	7	1212.1	77.9	6.4
Natitingou	1187.5	174.5	14.7	967.2	60.4	6.2	1045.2	64.9	6.2	1091.7	87.8	8
Fada	819.4	137.8	16.8	651.9	60.1	9.2	688.9	65.2	9.5	852.2	76.9	9
Tenkodogo	819	119	14.5	670.2	55.4	8.3	740.3	56.4	7.6	887.4	78.4	8.8
Kete-Krachi	1358.6	320.9	23.6	1018.0	59.5	5.8	1332.6	94.3	7.1	1249.1	91.2	7.3
Yendi	1210.1	217.4	18	982.5	68.2	6.9	1153.2	81.6	7.1	1148.2	71.4	6.2
Dapaong	1061.5	215.2	20.3	820.7	47.4	5.8	894.7	63.2	7.1	1012.5	80.3	7.9
Kara	1289.1	195.3	15.1	1024.1	73.7	7.2	1134.2	81.1	7.1	1149	83.6	7.3
Mango	1045.2	157	15	883.3	60.9	6.9	986.1	66.4	6.7	1096.5	67.5	6.2
Niamtougou	1361.9	200.3	14.7	964.8	70.3	7.3	1067.7	78.9	7.4	1082.2	77.3	7.1
Sokode	1266.8	171.3	13.5	1103.4	82.1	7.4	1408.3	100.9	7.2	1287.1	73.3	5.7
Basin	1073.8	104.1	9.7	857.5	49.4	5.8	970.2	52.8	5.4	1027.9	51.4	5

Note: *SD is standard deviation; CV is coefficient of variation; sim-historical is simulated-historical*

Similarly, rainfall is expected to decline in future under both climate scenarios at the temporal scale (Figure 4.6). From the time series, it is detected that annual rainfall in the basin during the historical period (1981-2010) was between 835.5mm/yr (1983) and 1239.1mm/yr (2009). With respect to the simulated historical (1981-2005), annual rainfall in the basin ranged from 751.28mm/yr (1984) to 926.37mm/yr (1990). In the future period and under RCP4.5, annual rainfall is expected to range between 842.4mm/yr (2027) and 1082.3mm/yr (2037); and between 900.6mm/yr (2041) and 1126.1mm/yr (2028) of rainfall for RCP8.5.

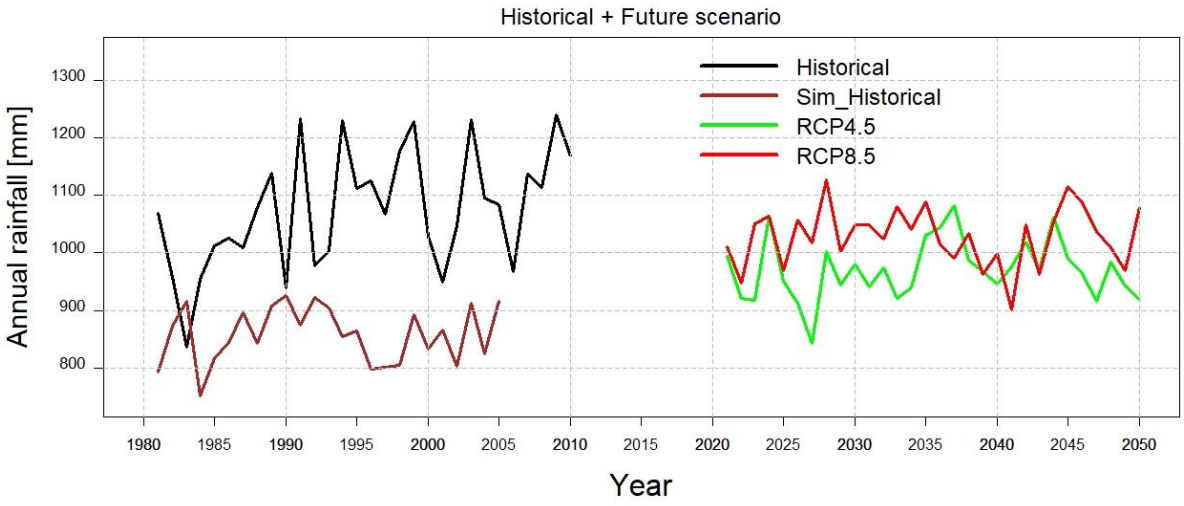

Figure 4. 6: Temporal variation in annual rainfall in Oti basin for historical (1981-2010), simulated historical (1981-2005) and future periods (2021-2050) under RCP4.5 and RCP8.5 scenarios

It is observed that the spatial variability of rainfall is more pronounced in the lower basin as compared to the middle and upper basins for the observed, simulated historical and future periods (Figure 4.7). Although rainfall in the lower basin would rise in the future period, the amount would be reduced. This could reflect the predictions of the IPCC (2007) that subtropical areas would experience a decreased rainfall due to the changing climate. The study discovered that rainfall would generally decrease by about 103.6 mm/yr across the entire basin under RCP4.5 scenario. Similarly, under RCP8.5, rainfall in the lower basin would further decrease by about 45.9 mm/yr while the upper basin would experience a slight recovery of rainfall (Figure 4.7). Majority of the stations in the basin would experience a

reduced amount of rainfall (particularly stations in the lower basin), except for a few stations which would record a little increment in rainfall.

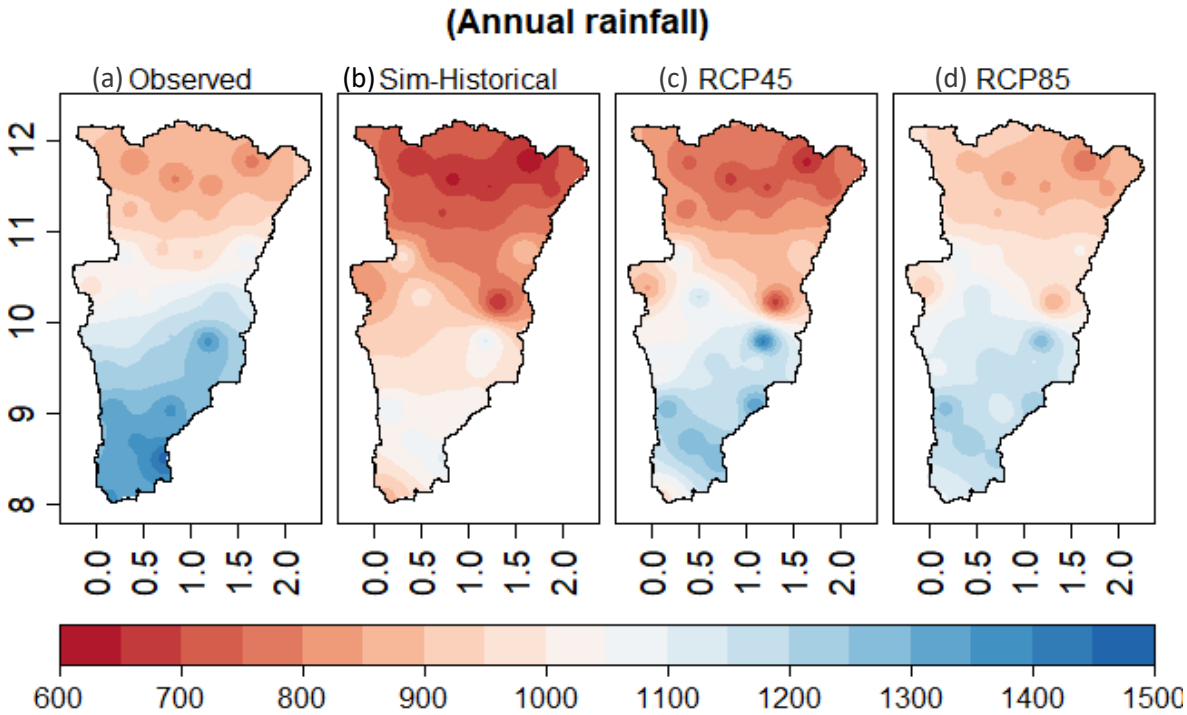

Figure 4. 7: Spatial distribution of annual rainfall (mm/yr) in the Oti basin during the (a) observed period (1981-2010), (b) simulated historical (1981-2005) and future period (2021-2050) under (c) RCP4.5 and (d) RCP8.5 scenarios

The trend for annual rainfall in the basin revealed a significantly increasing trend as well as stations such as GRID1- GRID12, GRID 15, Natitingou and Dapaong for historical period (1981-2010) (Table 4.5). These stations also revealed increasing magnitudes. For the simulated historical, it was observed that GRID3 was the only station that recorded a significant increasing trend, with the magnitude of increase at 3 mm annually. The MK test for the basin during the future period (2021-2050) under RCP4.5 exposed an insignificant increasing trend with a magnitude of 0.58 mm/yr at a 5% significant level. However, Niamtougou station revealed a significant increasing trend. Rainfall across the basin revealed insignificant decreasing trend with a negative magnitude (-0.05 mm/yr) in the future (2021-2050) for the RCP8.5 scenario (Table 4.5).

Table 4. 5: Mann-Kendall trend test and Sen's slope estimates for annual rainfall

Station	Observed (1981-2010)		Sim-historical (1981-2005)		RCP4.5 (2021-2050)		RCP8.5 (2021-2050)	
	Z value	Sen's slope	Z value	Sen's slope	Z value	Sen's slope	Z value	Sen's slope
GRID1	**2.36**	4.69	0.63	1.03	1.25	1.61	-1.21	-1.83
GRID2	**2.71**	5.28	1.52	1.75	1.28	1.81	-0.68	-0.79
GRID3	**2.82**	5.15	**2.36**	3.00	0.5	0.75	-0.64	-0.69
GRID4	**2.32**	4.98	1.05	1.49	0.57	1.2	-0.14	-0.32
GRID5	**2.53**	6.36	-0.21	-0.42	1.11	1.84	-1.32	-2.76
GRID6	**2.6**	6.14	0.30	0.41	1.61	1.71	-0.46	-0.93
GRID7	**3.03**	6.67	0.86	1.19	0.86	1.26	-0.71	-0.78
GRID8	**2.96**	7.69	0.26	0.66	0.61	0.99	0.64	1.33
GRID9	**3**	7.09	1.66	2.15	0.07	0.28	1.25	1.35
GRID10	**2.68**	6.63	0.07	0.16	0.25	0.63	0.43	0.58
GRID11	**3.28**	7.96	-0.86	-1.16	0.43	0.58	0.61	0.72
GRID12	**3.28**	8.7	1.05	1.30	1	1.63	1.03	2.25
GRID13	1.21	3.06	0.96	2.04	0.36	0.66	0.07	0.1
GRID14	1.25	3.38	0.00	0.03	0.14	0.16	1.25	1.59
GRID15	**2.11**	6.17	-0.02	-0.03	0.71	0.64	1	1.59
GRID16	1.89	5.87	0.07	0.17	-0.39	-0.93	0.82	1.22
GRID17	0.82	2.67	-0.86	-1.74	0.07	0.07	0.29	0.33
GRID18	1.57	4.82	0.30	0.95	1.46	3.18	1.18	2.21
GRID19	0.75	4.08	-0.86	-1.99	-0.25	-0.52	0.21	0.18
GRID20	1.75	7.37	-0.16	-0.53	0.86	2.22	1.57	2.81
Natitingou	**1.86**	6.69	-0.30	-0.81	1.03	2.01	0.57	1.16
Fada	2.28	8.2	0.00	-0.01	1.5	2.71	-0.93	-1.48
Tenkodogo	1.57	3.83	0.68	1.51	0.5	0.55	-1.53	-2.06
Kete-Krachi	0.82	4.93	-1.05	-1.81	-1.36	-2.7	-0.11	-0.43
Yendi	1.89	9.88	-0.02	-0.12	-0.86	-1.67	1.25	1.91
Dapaong	**2.68**	11.63	0.49	0.81	-0.11	-0.1	-0.96	-1.63
Kara	1	3.38	0.02	0.20	1.89	3.36	0.07	0.29
Mango	-0.5	-0.94	0.35	0.72	-0.04	-0.1	0.5	0.93
Niamtougou	1.75	7.77	-0.02	-0.10	**2.07**	3.35	0.14	0.33
Sokode	1.12	4.73	-0.54	-1.42	0.36	0.62	0.18	0.25
Basin	**2.5**	5.84	0.26	0.51	0.43	0.58	-0.04	-0.05

Note: *values in bold are significant at 5%; sim-historical is simulated-historical*

4.4.2 Seasonal rainfall predictions

4.4.2.1 Rainy season (AMJJASO)

Table 4.6 illustrates the summary results for the rainy season during the observed period (1981-2010), simulated-historical (1981-2005) and the future (2021-2050) under RCP4.5 and RCP8.5 scenarios. From the result, it can be deduced that during the observed period, the mean rainfall for the rainy season ranged from 778.1mm/yr at GRID 3 to 1324.5mm/yr at GRID 20 and a mean rainfall of 1038.6mm/yr for the entire basin. However, for the simulated historical period, the mean annual rainfall was 842.3 mm/yr which varied between 608.4 mm/yr at GRID3 and 1066.6 mm/yr at Sokode. The standard deviation (SD) also ranged from 95.0mm/yr at GRID1 to 304.4mm/yr at Kete-Krachi and a mean SD of 102.2mm/yr for the entire basin. The SD values for the observed period and simulated historical all reveal that rainfall was less stable across the basin (Tegegn, 2015). With regards to the simulated historical, CV varied from 5.7% at GRID17 and 9.3% at Fada with a mean CV of 5.8%. For the historical period (1981-2010), the coefficient of variation (CV) ranged between 10.3% at GRID16 and 23.9% at Kete-Krachi and with a mean CV of 9.8% for the entire basin, indicating a low to moderate variation among the stations (10.3% < CV < 23.9%) as demonstrated in Asfaw et al. (2018) and Alemu & Bawoke (2019).

In the future period, and under RCP4.5, it is observed that the mean rainfall for the rainy season would range between 637.1mm/yr at GRID3 and 1350.4mm/yr at Sokode with a mean for the entire basin that would be around 947.7mm/yr. The SD would range between 55.9mm/yr at Tenkodogo and 98.2mm/yr at Sokode with a mean SD of 51.4mm/yr. The SD values in the future period, under RCP4.5, reveal that rainfall in this period would be less stable (Tegegn, 2015). In addition, the CV would be in the ranges of 5.2% at GRID19 and 9.7% at GRID3, and a mean CV of 5.4% in the entire basin, indicating a low variation among the stations in the basin (5.2% < CV < 9.7%) (Asfaw et al., 2018; Alemu & Bawoke, 2019).

In the future period, and under RCP8.5, the mean rainfall for the rainy season would range from 753.9mm/yr at GRID3 to 1231.6mm/yr at Sokode and a mean of 1004.0mm/yr for the entire basin. The SD would also range from 54.2mm/yr at GRID3 to 91.0mm/yr at Kete-Krachi with a mean SD of 51.2mm/yr in the entire basin, indicating that rainfall in the rainy season would be less stable for the entire basin (Tegegn, 2015). The CV would range from 5.3% at GRID16 to 9.1% at Fada and a mean CV of 5.1% in the entire basin, indicating a low

variation among the stations in the basin (5.3% < CV < 9.1%) (Asfaw et al., 2018; Alemu & Bawoke, 2019).

Table 4. 6: Summary statistics of seasonal rainfall (AMJJASO) in Oti River Basin

	Observed (1981-2010)			Sim-historical (1981-2005)			RCP4.5 (2021-2050)			RCP8.5 (2021-2050)		
Station	Mean [mm]	SD [mm]	CV [%]	Mean [mm]	SD [mm]	CV [%]	Mean [mm]	SD [mm]	CV [%]	Mean [mm]	SD [mm]	CV [%]
GRID1	788.3	95.0	12.1	633.4	52.2	8.2	680.3	59.2	8.7	829.7	66.1	8.0
GRID2	809.7	115.3	14.2	647.0	47.5	7.3	689.4	62.6	9.1	834.1	55.5	6.7
GRID3	778.1	120.9	15.5	608.4	49.9	8.2	637.1	61.9	9.7	753.9	54.2	7.2
GRID4	847.4	130.9	15.4	682.7	54.8	8.0	708.3	62.3	8.8	830.5	64.5	7.8
GRID5	882.0	110.0	12.5	711.6	52.1	7.3	767.5	64.4	8.4	912.4	76.9	8.4
GRID6	869.1	106.6	12.3	691.8	45.4	6.6	768.2	61.1	8.0	888.2	76.3	8.6
GRID7	879.8	134.0	15.2	697.3	43.8	6.3	787.3	58.5	7.4	892.0	74.7	8.4
GRID8	917.7	137.5	15.0	753.0	48.4	6.4	823.5	68.9	8.4	907.8	68.0	7.5
GRID9	965.5	130.0	13.5	799.2	50.5	6.3	859.4	62.8	7.3	919.2	63.1	6.9
GRID10	930.5	114.4	12.3	762.6	53.9	7.1	875.0	64.3	7.3	993.7	74.8	7.5
GRID11	932.3	126.5	13.6	764.7	46.9	6.1	862.6	60.4	7.0	945.2	63.6	6.7
GRID12	1055.4	140.3	13.3	887.9	53.4	6.0	920.0	70.3	7.6	992.5	69.8	7.0
GRID13	963.0	107.0	11.1	792.0	64.9	8.2	833.7	61.5	7.4	899.6	68.6	7.6
GRID14	1071.6	111.7	10.4	885.2	67.0	7.6	1013.4	69.8	6.9	1088.9	64.1	5.9
GRID15	1163.6	130.0	11.2	938.7	73.7	7.8	1079.7	61.1	5.7	1093.5	60.9	5.6
GRID16	1189.6	122.4	10.3	968.2	69.1	7.1	1132.0	81.7	7.2	1149.6	60.6	5.3
GRID17	1264.4	161.8	12.8	1049.7	59.7	5.7	1225.0	93.6	7.6	1211.3	70.5	5.8
GRID18	1281.3	156.5	12.2	1003.0	84.7	8.4	1124.0	84.6	7.5	1086.9	70.1	6.4
GRID19	1274.4	182.3	14.3	1030.5	65.6	6.4	1239.7	64.8	5.2	1171.3	71.3	6.1
GRID20	1324.5	187.9	14.2	1062.7	87.4	8.2	1227.9	79.9	6.5	1147.6	76.8	6.7
Natitingou	1145.6	161.9	14.1	954.6	61.7	6.5	1026.5	63.4	6.2	1071.2	88.1	8.2
Fada	808.7	139.2	17.2	649.3	60.2	9.3	684.7	64.3	9.4	846.9	76.9	9.1
Tenkodogo	809.5	118.4	14.6	666.4	55.6	8.3	732.9	55.9	7.6	879.2	77.8	8.9
Kete-Krachi	1273.3	304.4	23.9	979.5	58.4	6.0	1282.7	96.3	7.5	1198.9	91.0	7.6
Yendi	1146.7	205.8	17.9	950.4	66.6	7.0	1105.7	80.8	7.3	1099.8	69.0	6.3
Dapaong	1037.2	214.1	20.6	811.0	47.3	5.8	880.1	63.0	7.2	995.4	79.8	8.0
Kara	1233.2	183.8	14.9	1005.7	73.7	7.3	1107.9	77.4	7.0	1120.8	84.0	7.5
Mango	1013.0	156.5	15.4	871.3	60.1	6.9	966.8	66.0	6.8	1074.7	67.2	6.3
Niamtougou	1304.9	186.4	14.3	945.6	70.2	7.4	1039.9	74.8	7.2	1052.6	77.7	7.4
Sokode	1196.6	175.6	14.7	1066.6	80.8	7.6	1350.4	98.2	7.3	1231.6	73.4	6.0
Basin	1038.6	102.2	9.8	842.3	48.6	5.8	947.7	51.4	5.4	1004.0	51.2	5.1

Note: *SD is standard deviation; CV is coefficient of variation; sim-historical is simulated-historical*

At the temporal scale, it is observed that rainfall for the rainy season in the basin during the historical period was between 804.9mm/yr (1983) and 1208.4mm/yr (1994). With respect to the simulated historical (1981-2005), rainfall in the basin during the rainy season ranged from 733.6 mm/yr (1984) to 911.1 mm/yr (1990). In the future period and under RCP4.5, rainfall in

the rainy season would range between 829.1mm/yr (2027) and 1057.1mm/yr (2037); and between 876.2mm/yr (2041) and 1094.6mm/yr (2028) of rainfall for RCP8.5 (Figure 4.8).

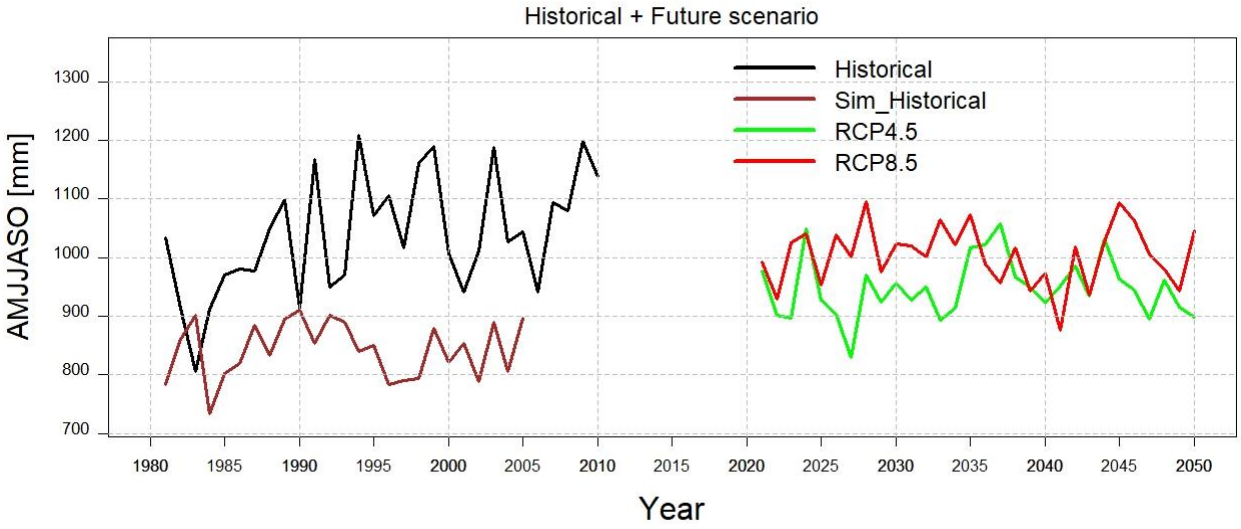

Figure 4. 8: Temporal variations in rainfall for rainy season (AMJJASO) during the historical (1981-2010), simulated historical (1981-2005) and future periods (2021-2050) under RCP4.5 and RCP8.5 scenarios

The spatial distribution of rainfall in the basin shows that rainfall in the basin increases from the upper basin towards the lower basin (Figure 4.9). It is discovered that the amount of rainfall in the lower basin was relatively high during the historical period (1981-2010) and in the near-future 2021-2050 under both RCP4.5 and RCP8.5 scenarios than it is shown by the simulated-historical (1981-2005) and moderate in the upper basin. Nonetheless, rainfall amount in the future period and under RCP4.5 would decline in the lower basin and in some parts of the upper basin. Under, RCP8.5, the amount of rainfall would further decline in the lower basin while the upper basin would generally neither increase nor decrease (Figure 4.9).

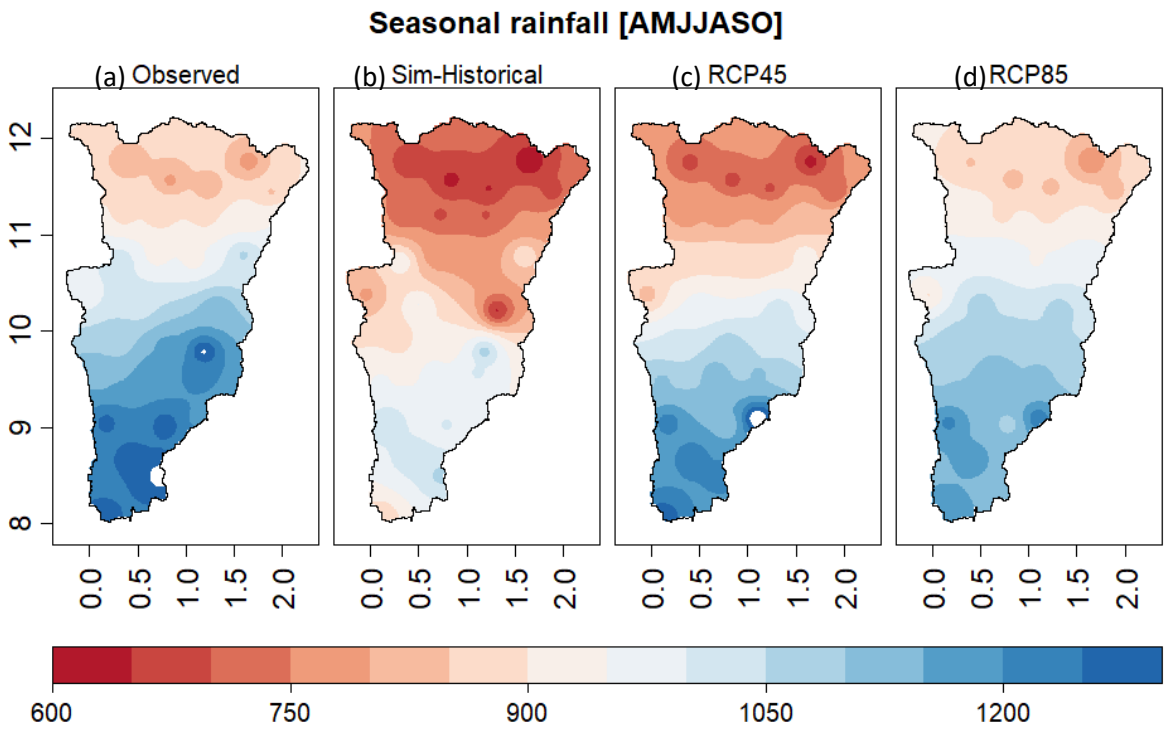

Figure 4. 9: Spatial distribution of seasonal rainfall (AMJJASO) (mm/yr) in the Oti basin during the (a) observed period (1981-2010), (b) simulated historical (1981-2005) and future period (2021-2050) under (c) RCP4.5 and (d) RCP8.5 scenarios

A significant and non-significant increasing trend were observed across the stations, and a significant increasing trend was discovered for the entire basin during the historical period (Table 4.7). Also, during this period, the magnitude of the increase was 5.91 mm per year in the entire basin. However, the simulated historical revealed a non-significant increasing trend for the entire basin with the magnitude of increase at 0.13 mm per year. Under RCP4.5, the stations revealed a mixture of increasing and decreasing trend across the stations, and a non-significant increasing trend with the magnitude of increase at 0.44 mm per year for the entire basin (Table 4.7). RCP8.5 also revealed a mixture of increasing and decreasing trend and a non-significant decreasing trend with the magnitude of decrease which would be around 0.33 mm per year for the entire basin (Table 4.7).

Table 4. 7: MK trend test for AMJJASO in Oti River Basin

	Observed (1981-2010)		sim-historical (1981-2005)		RCP4.5 (2021-2050)		RCP8.5 (2021-2050)	
Station	Z value	Sen's slope	Z value	Sen's slope	Z value	Sen's slope	Z value	Sen's slope
GRID1	**2.43**	4.77	0.63	1.34	1.18	1.49	-1.21	-1.92
GRID2	**2.78**	5.36	1.47	1.69	1.18	1.68	-0.82	-0.86
GRID3	**2.85**	5.14	**2.22**	3.04	0.54	0.64	-0.79	-0.91
GRID4	**2.36**	4.96	1.00	1.59	0.61	1.08	-0.32	-0.44
GRID5	**2.71**	6.27	-0.40	-0.59	1.21	1.72	-1.46	-2.73
GRID6	**2.68**	6.44	0.26	0.42	1.50	1.65	-0.61	-1.01
GRID7	**3.00**	6.73	0.77	1.36	0.82	1.11	-0.68	-0.75
GRID8	**3.21**	7.42	0.35	0.61	0.61	0.77	0.50	1.14
GRID9	**2.96**	7.08	1.70	1.96	0.00	0.05	1.03	1.12
GRID10	**2.64**	6.84	0.02	0.32	0.11	0.27	0.43	0.57
GRID11	**3.28**	7.97	-0.82	-1.22	0.39	0.53	0.46	0.57
GRID12	**3.18**	8.60	0.91	1.41	0.68	1.26	1.00	2.00
GRID13	1.28	3.23	0.91	1.96	0.39	0.76	-0.11	-0.05
GRID14	1.53	4.42	-0.16	-0.45	0.04	0.13	0.96	1.22
GRID15	**2.18**	6.40	-0.30	-0.77	0.21	0.29	0.68	0.97
GRID16	**2.03**	6.21	0.02	0.15	-0.68	-1.02	0.29	0.21
GRID17	0.75	3.35	-0.77	-1.43	-0.29	-0.36	-0.11	-0.18
GRID18	1.68	6.14	0.26	0.78	1.46	2.85	0.96	1.41
GRID19	1.00	3.75	-1.05	-1.89	-0.39	-0.58	-0.21	-0.23
GRID20	1.82	7.20	0.00	0.01	0.79	1.30	1.03	2.13
Natitingou	1.86	6.79	-0.63	-1.12	0.86	1.54	0.50	1.04
Fada	**2.46**	7.79	0.07	0.11	1.28	2.59	-0.96	-1.50
Tenkodogo	1.53	4.15	0.63	1.21	0.29	0.44	-1.61	-2.03
Kete-Krachi	0.18	1.37	-1.24	-1.71	-1.50	-2.97	-0.18	-0.48
Yendi	**2.25**	10.67	-0.21	-0.35	-1.28	-2.26	0.89	1.21
Dapaong	**2.71**	11.03	0.35	0.51	-0.07	-0.15	-1.18	-2.25
Kara	0.96	4.17	-0.07	-0.30	1.53	2.82	0.11	0.65
Mango	0.00	-0.01	0.30	0.56	-0.18	-0.21	0.25	0.51
Niamtougou	1.89	6.61	-0.12	-0.48	**1.93**	3.03	0.14	0.50
Sokode	1.14	4.97	-0.72	-1.87	-0.11	-0.29	-0.32	-0.57
Basin	**2.57**	5.91	0.16	0.13	0.29	0.44	-0.32	-0.33

Note: *values in bold are significant at 5%; Sim-historical is simulated-historical*

4.4.3 Rainfall onset

Table 4.8 presents the summary results for rainfall onset for the observed period (1981-2010), simulated historical (1981-2005) and the near-future (2021-2050) under RCP4.5 and RCP8.5. The onset of rainy season is found to be between 98 days (8 Apr) at GRID20 and 152 days (1 Jun) at Fada during the historical period with a mean onset of 128 days (8 May) for the entire basin. The simulated historical revealed onset to be between 120 days (30 Apr) at GRID19 and 179 days (28 Jun) at GRID3 with a mean onset of 149 days (29 May) for the whole basin. During the observed period, the SD ranged between 9 days at GRID20 and 29 days at Mango and a mean SD of 8 days for the entire basin. However, SD for the simulated historical ranged between 14 days at Kete-Krachi and 28 days at Tenkodogo, with a mean SD of 12 days. The recorded CV for onset would range between 8.9% at GRID20 and 21.1% at Sokode while a mean CV of 6.6% was recorded for the entire basin indicating a low to moderate variation (8.9%<CV<21.1%) for the observed period. The CV for simulated historical ranged between 11% at Kete-Krachi to 18% at GRID18, with a mean CV of 8% (Asfaw et al., 2018; Alemu & Bawoke, 2019) (Annex 1e).

In the future period and under RCP4.5 onset would be between 106 days (16 Apr) to 178 days (27 Jun) and with a mean onset of 144 days (24 May) for the entire basin. The SD would also range between 9 days at Sokode and GRID19, and 25 days at Natitingou and a mean SD of about 10 days in the entire basin. The recorded CV for onset would range between 8.2% at Sokode to 18.7% at Natitingou while a mean CV would be about 6.9% for the entire basin. This indicates a low variation in onset at the stations in the basin (8.2%<CV<18.7%) (Asfaw et al., 2018; Alemu & Bawoke, 2019).

Under RCP8.5 scenario, rainfall onset would range between 114 days (24 Apr) and 163 days (12 Jun) with a mean onset of 143 days (23 May) for the entire basin. The SD would also range between 13 days at GRID17 and GRID15, and 23 days at GRID3 and GRID4, and a mean SD of about 9 days for the entire basin. The recorded CV for onset would range between about 8.9% at Dapaong and Tenkodogo to about 16.3% at Natitingou while a mean CV would be about 6.3%. This shows a low variation of onset at the stations in the basin (8.9%<CV<16.3%) (Asfaw et al., 2018; Alemu & Bawoke, 2019) (Annex 1e).

Table 4. 8: Summary statistics of rainfall onset in Oti River Basin

Station	Observed (1981-2010)		Sim-historical (1981-2005)		RCP4.5 (2021-2050)		RCP8.5 (2021-2050)	
	Mean [days]	Date	Mean [days]	Date	Mean [days]	Date	Mean [days]	Date
GRID1	145	25 May	169	18 Jun	168	17 Jun	159	8 Jun
GRID2	146	26 May	177	26 Jun	168	17 Jun	159	8 Jun
GRID3	145	25 May	179	28 Jun	178	27 Jun	163	12 Jun
GRID4	145	25 May	174	23 Jun	170	19 Jun	155	4 Jun
GRID5	138	18 May	161	10 Jun	161	10 Jun	154	3 Jun
GRID6	139	19 May	158	7 Jun	164	13 Jun	152	1 Jun
GRID7	140	20 May	167	16 Jun	167	16 Jun	160	9 Jun
GRID8	138	18 May	159	8 Jun	156	5 Jun	149	29 May
GRID9	135	15 May	157	6 Jun	146	26 May	149	29 May
GRID10	132	12 May	151	31 May	149	29 May	149	29 May
GRID11	135	15 May	156	5 Jun	151	31 May	153	2 Jun
GRID12	127	7 May	153	2 Jun	153	2 Jun	151	31 May
GRID13	124	4 May	148	28 May	153	2 Jun	145	25 May
GRID14	116	26 Apr	149	29 May	136	16 May	143	23 May
GRID15	117	27 Apr	141	21 May	130	10 May	135	15 May
GRID16	107	17 Apr	137	17 May	122	2 May	129	9 May
GRID17	103	13 Apr	131	11 May	120	30 Apr	125	5 May
GRID18	102	12 Apr	134	14 May	124	4 May	128	8 May
GRID19	101	11 Apr	120	30 Apr	106	16 Apr	119	29 Apr
GRID20	98	8 Apr	124	4 May	115	25 Apr	114	24 Apr
Natitingou	124	4 May	131	11 May	134	14 May	138	18 May
Fada	152	1 Jun	167	16 Jun	169	18 Jun	160	9 Jun
Tenkodogo	143	23 May	169	18 Jun	163	12 Jun	159	8 Jun
Kete-Krachi	129	9 May	124	4 May	114	24 Apr	120	30 Apr
Yendi	124	4 May	139	19 May	132	12 May	138	18 May
Dapaong	138	18 May	157	6 Jun	160	9 Jun	159	8 Jun
Kara	123	23 May	129	9 May	127	7 May	132	12 May
Mango	146	26 May	142	22 May	140	20 May	143	23 May
Niamtougou	118	28 Apr	134	14 May	140	20 May	140	20 May
Sokode	113	23 Apr	125	5 May	109	19 Apr	118	28 Apr
Basin	128	8 May	149	29 May	144	24 May	143	23 May

Note: *SD is standard deviation; CV is coefficient of variation; Sim-historical is Simulated-historical*

From the temporal illustration of onset in the basin, it is observed that the onset for the historical period ranged between 115 days and 146 days. With respect to the simulated historical (1981-2005), rainfall onset in the basin ranged from 131 days (2005) to 173 days (1996), while for the future period, it is expected to range between 122 days and 162 days representing 2027 and 2033 correspondingly under RCP4.5. However, RCP8.5 scenario projects a further delay in onset of the rainy season which is expected to range between 128 days and 169 days for 2023 and 2038 respectively (Figure 4.10).

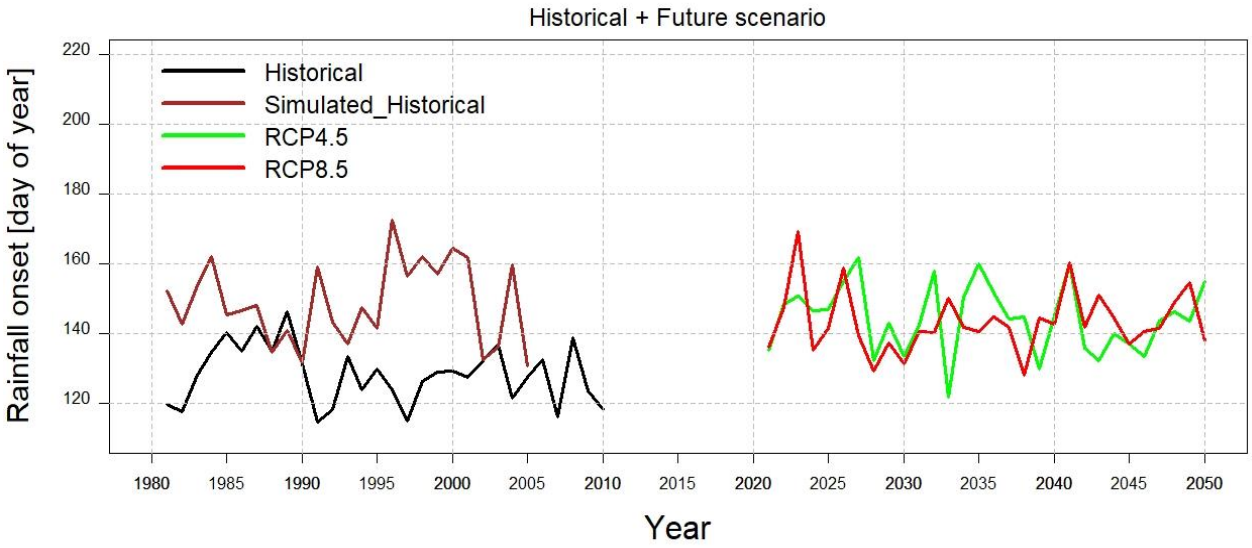

Figure 4. 10: Temporal variations in rainfall onset during the historical (1981-2010), simulated historical (1981-2005) and future periods (2021-2050) under RCP4.5 and RCP8.5 scenarios

Spatially, it is observed that the rains started early in the lower basin and later in the upper basin during the historical period with the same pattern observed for the future period under both RCP4.5 and RCP8.5 scenarios (Figure 4.11). This is because onset dates in the region usually increase northwards from the coast to inland as a result of moisture transport from the Gulf of Guinea into the sub-continent by the West African Monsoon (Kumi et al., 2020).

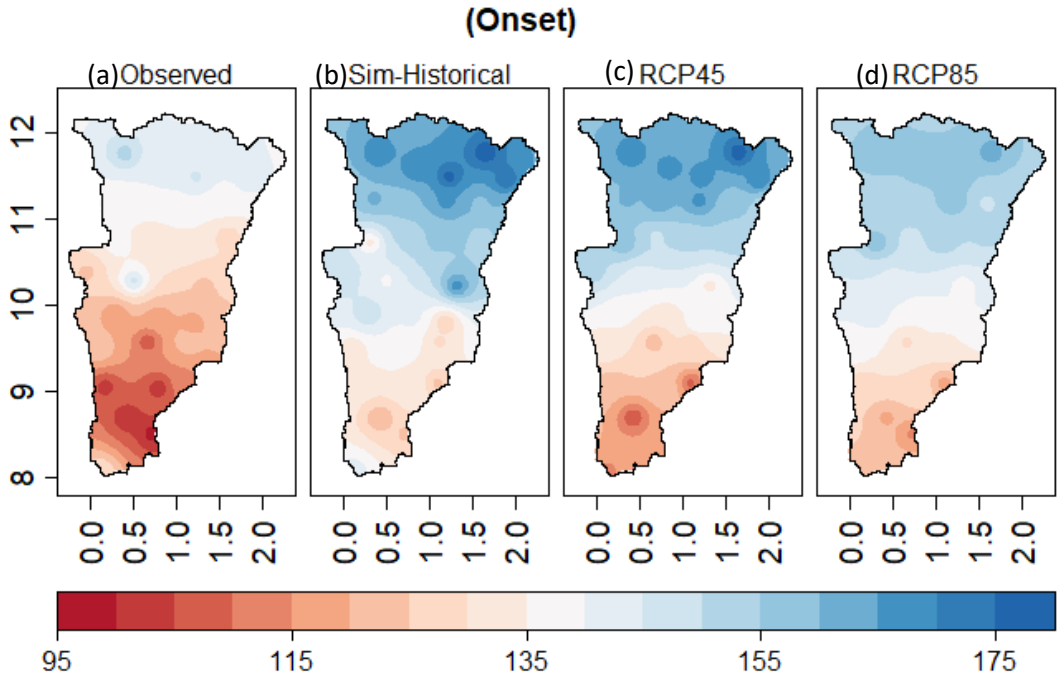

Figure 4. 11: Spatial distribution of onset (days) in Oti River Basin for (a) observed (1981-2010), (b) simulated historical (1981-2005) and future (2021-2050) under (c) RCP4.5 and (d) RCP8.5 scenarios

For the trend in rainfall onset, it is found that a mixture of increasing and decreasing trends was experienced among the basin's stations. Mostly, there is no significant trend found among the distinct stations except for Fada that was significantly negative (Table 4.9). However, for the entire basin, the trend was found to be non-significantly decreasing during the historical period. This indicates that rainfall onset dates experienced an earlier shift across the basin. Similarly, a mixture of increasing and decreasing trends is revealed to occur in the near-future under the RCP4.5 scenario, with GRID1, Kete-Krachi and Niamtougou decreasing significantly. This means that these stations are likely to have an earlier shift in their onset dates. In addition, a careful look at the Sen's slope shows that under RCP4.5, the entire basin has a greater magnitude (-0.14) than that of the historical period (-0.17) which indicates that the annual mean onset date for the entire basin under RCP4.5 would shift more speedily earlier than it did for the entire basin during the historical period. Under the RCP8.5 scenario, a mixture of increasing and decreasing trends would also be experienced across the stations in the basin. Yendi would likely be the only station whose decreasing trend would be significant. For the entire basin, the trend in rainfall onset would increase, although not significantly indicating that the onset date would shift to a later date (Table 4.9).

Table 4. 9: Mann-Kendall trend test for rainfall onset in Oti River Basin

	Observed (1981-2010)		Sim-historical (1981-2005)		RCP4.5 (2021-2050)		RCP8.5 (2021-2050)	
Station	Z value	Sen's slope	Z value	Sen's slope	Z value	Sen's slope	Z value	Sen's slope
GRID1	0.80	0.32	-0.42	-0.21	**-2.29***	-1.00	0.66	0.31
GRID2	-0.23	-0.14	0.00	0.00	-0.95	-0.33	-0.82	-0.27
GRID3	-0.12	-0.05	-1.33	-0.40	-0.86	-0.32	0.50	0.22
GRID4	0.84	0.30	-1.90	-0.86	-1.39	-0.50	0.18	0.00
GRID5	-0.79	-0.32	0.63	0.33	-1.09	-0.75	0.00	0.00
GRID6	-1.70	-0.56	-0.09	-0.03	0.79	0.33	0.98	0.35
GRID7	-0.64	-0.23	0.00	0.00	0.29	0.09	-0.09	0.00
GRID8	-0.25	-0.11	-0.23	-0.12	-0.21	-0.14	0.54	0.18
GRID9	-0.41	-0.15	-0.65	-0.28	0.93	0.29	0.14	0.07
GRID10	-0.59	-0.29	-1.15	-0.42	-0.61	-0.10	0.97	0.38
GRID11	-0.98	-0.39	-0.14	-0.03	-0.64	-0.38	0.25	0.00
GRID12	0.02	0.00	-0.12	0.00	-1.39	-0.56	-0.68	-0.25
GRID13	-0.77	-0.27	-0.51	-0.26	0.34	0.11	-0.02	0.00
GRID14	-0.82	-0.25	-0.42	-0.14	0.02	0.00	0.79	0.33
GRID15	-0.34	-0.13	0.12	0.00	-0.46	-0.08	0.25	0.00
GRID16	-0.46	-0.10	1.36	0.46	1.38	0.28	-0.57	-0.30
GRID17	0.25	0.00	0.00	0.00	-0.14	-0.04	0.29	0.07
GRID18	-0.91	-0.16	0.65	0.46	0.61	0.24	-0.39	-0.15
GRID19	-0.84	-0.08	1.97*	0.63	0.30	0.07	-0.70	-0.30
GRID20	-0.76	0.00	-0.19	-0.06	0.41	0.14	-0.45	-0.20
Natitingou	-1.54	-0.74	0.70	0.29	0.27	0.13	0.11	0.07
Fada	**-3.64**	-1.83	-0.63	-0.28	-1.57	-0.44	0.00	0.00
Tenkodogo	-0.98	-0.50	0.12	0.08	-0.30	-0.16	1.22	0.25
Kete-Krachi	0.68	0.46	1.92	0.50	**1.96**	0.60	0.80	0.29
Yendi	0.39	0.16	1.85	0.75	0.81	0.24	**-2.16**	-0.91
Dapaong	-1.00	-0.50	-0.33	-0.26	-0.46	-0.17	1.22	0.25
Kara	1.00	0.53	0.37	0.15	-1.27	-0.47	0.62	0.27
Mango	-0.46	-0.33	0.09	0.04	-0.84	-0.22	-0.13	0.00
Niamtougou	-0.02	-0.05	0.09	0.07	**-2.38**	-0.93	-0.05	0.00
Sokode	0.07	0.00	0.42	0.09	0.11	0.00	-0.52	-0.19
Basin	-0.87	-0.17	0.09	0.06	-0.68	-0.14	0.98	0.17

Note: *values in bold are significant at 5%; Sim-historical is Simulated-historical*

4.4.4 Rainfall cessation

Table 4.10 presents the summary results for cessation during the observed period (1981-2010), simulated historical (1981-2005) and the near-future (2021-2050) under RCP4.5 and RCP8.5. The shortest and longest days for cessation are seen in the ranges of 281 days (4 Dec) at GRID3 and 338 days (8 Oct) at GRID20 respectively, and a mean cessation of 302 days (29 Oct) for the entire basin during the historical period. The simulated historical revealed cessation to be between 275 days (2 Oct) at GRID1 to GRID8, GRID11 and Tenkodogo to 299 days (26 Oct) at Kete-Krachi with a mean cessation of 281 days (8 Oct) for the whole basin. The SD also ranged between 7 days at GRID7 and 20 days at Dapaong and Kete-Krachi and a mean SD of 6 days for the entire basin. However, SD for the simulated historical ranged between 0 day at GRID3, GRID6 and GRID7 and 10 days at Kete-Krachi with a mean SD of 2 days. The CV for cessation ranged between 2.4% at GRID7 and 6.6% at Dapaong while the mean CV was about 1.9% for the entire basin. This indicates less variation in cessation at the stations in the basin (2.4%<CV<6.6%). The CV for simulated historical ranged between 0% at GRID3, GRID6 and GRID7 and 3.3% at Kete-Krachi, with a mean CV of 0.8% (Asfaw et al., 2018; Alemu & Bawoke, 2019) (Annex 1f).

For the future period under RCP4.5 scenario, the rains are expected to end within the ranges of 275 days (2 Oct) at Fada, GRID1, GRID2, GRID3, GRID8 and GRID9 and 299 days (26 Oct) at Kete-Krachi and a mean cessation of 280 days (7 Oct) for the entire basin. The SD would also range between 0 days at GRID3 and 11 days at Kete-Krachi, GRID19 and GRID 17, and a mean SD of 3 days for the entire basin. The CV for cessation would range between 0% at GRID3 to 3.7% at GRID17, GRID19 and Kete-Krachi, while the mean CV for the entire basin would be about 1.0%. This indicates less variation in cessation at the stations in the basin (0%<CV<3.7%) (Asfaw et al., 2018; Alemu & Bawoke, 2019).

Under the RCP8.5 scenario, cessation is expected to be within the ranges of 275 days (2 Oct) at GRID3 and 294 days (21 Oct) at Kete-Krachi and a mean cessation of 280 days (7 Oct) for the entire basin. The SD would also range between 1 day at GRID3 and 11 days at GRID17 and a mean SD of 4 days for the entire basin. The CV for cessation would range between 0.4% at GRID3 and 3.8% at GRID17, and the mean CV would be about 1.4% for the entire basin. This indicates less variation in cessation at the stations in the basin (0.4%<CV<%) (Asfaw et al., 2018; Alemu & Bawoke, 2019) (Annex 1f).

Table 4. 9: Summary statistics of rainfall cessation in Oti River Basin

	Observed (1981-2010)		Sim-historical (1981-2005)		RCP4.5 (2021-2050)		RCP8.5 (2021-2050)	
Station	Mean [days]	Date	Mean [days]	Date	Mean [days]	Date	Mean [days]	Date
GRID1	291	18 Oct	275	2 Oct	275	2 Oct	279	6 Oct
GRID2	282	9 Oct	275	2 Oct	275	2 Oct	277	4 Oct
GRID3	281	8 Oct	275	2 Oct	275	2 Oct	275	2 Oct
GRID4	282	9 Oct	275	2 Oct	276	3 Oct	278	5 Oct
GRID5	283	10 Oct	275	2 Oct	278	5 Oct	276	3 Oct
GRID6	288	15 Oct	275	2 Oct	277	4 Oct	277	4 Oct
GRID7	283	10 Oct	275	2 Oct	276	3 Oct	277	4 Oct
GRID8	285	12 Oct	275	2 Oct	275	2 Oct	278	5 Oct
GRID9	285	12 Oct	276	3 Oct	275	2 Oct	278	5 Oct
GRID10	291	18 Oct	276	3 Oct	279	6 Oct	277	4 Oct
GRID11	289	16 Oct	275	2 Oct	278	5 Oct	276	3 Oct
GRID12	296	23 Oct	276	3 Oct	277	4 Oct	278	5 Oct
GRID13	297	24 Oct	277	4 Oct	278	5 Oct	279	6 Oct
GRID14	307	3 Nov	285	12 Oct	286	13 Oct	283	10 Oct
GRID15	306	2 Nov	283	10 Oct	281	8 Oct	282	9 Oct
GRID16	316	12 Nov	288	15 Oct	285	12 Oct	285	12 Oct
GRID17	323	19 Nov	294	21 Oct	288	15 Oct	292	19 Oct
GRID18	328	24 Nov	288	15 Oct	284	11 Oct	281	8 Oct
GRID19	332	28 Nov	294	21 Oct	290	17 Oct	291	18 Oct
GRID20	338	4 Dec	296	23 Oct	294	21 Oct	290	17 Oct
Natitingou	303	30 Oct	279	6 Oct	277	4 Oct	279	6 Oct
Fada	295	22 Oct	276	3 Oct	275	2 Oct	277	4 Oct
Tenkodogo	284	11 Oct	275	2 Oct	276	3 Oct	277	4 Oct
Kete-Krachi	328	24 Nov	299	26 Oct	299	26 Oct	294	21 Oct
Yendi	313	9 Nov	283	10 Oct	281	8 Oct	280	7 Oct
Dapaong	300	27 Oct	277	4 Oct	278	5 Oct	278	5 Oct
Kara	314	10 Nov	281	8 Oct	278	5 Oct	279	6 Oct
Mango	298	25 Oct	277	4 Oct	279	6 Oct	279	6 Oct
Niamtougou	316	12 Nov	280	7 Oct	278	5 Oct	279	6 Oct
Sokode	314	10 Nov	285	12 Oct	282	9 Oct	280	7 Oct
Basin	302	29 Oct	281	8 Oct	280	7 Oct	280	7 Oct

Note: *SD is Standard deviation; CV is Coefficient of variation; Sim-historical is Simulated-historical*

From the time series, it is observed that the cessation for the historical period ranged between 291 days to 314 days. With respect to the simulated historical (1981-2005), cessation in the basin ranged from 276 days (1994) to 285 days (1992), while for the future period, it is expected to range between 277 days and 291 days representing 2041 and 2022 correspondingly under RCP4.5. Under RCP8.5 scenario, it is expected to range between 276 days and 291 days representing 2044 and 2042 respectively (Figure 4.12).

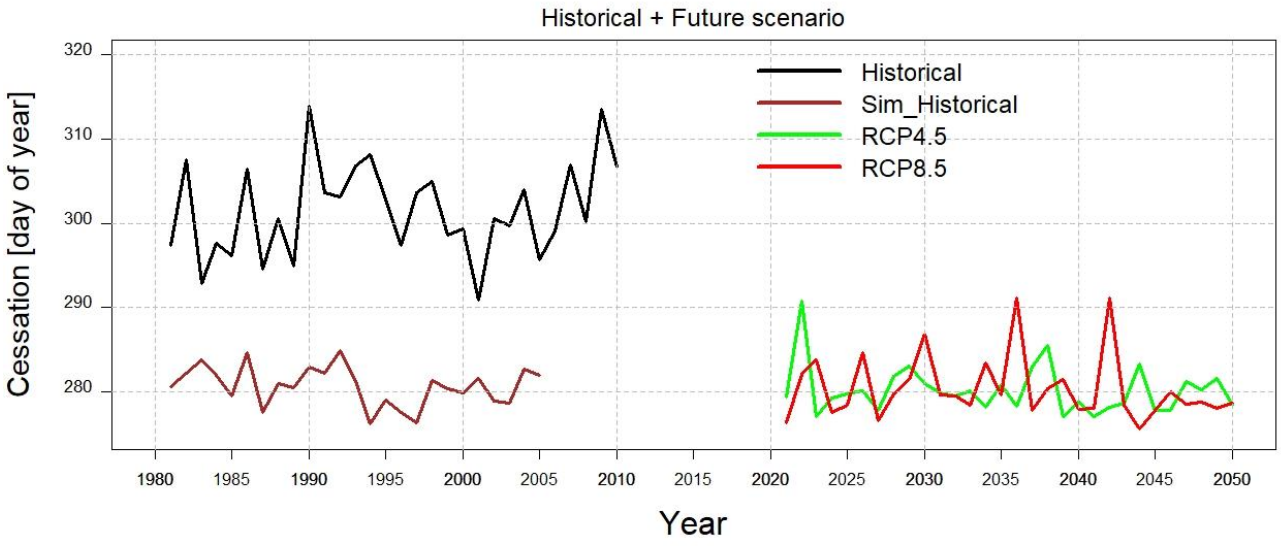

Figure 4. 12: Temporal variations in cessation during the historical (1981-2010), simulated historical (1981-2005) and future periods (2021-2050) under RCP4.5 and RCP8.5 scenarios

Spatially, it is found that the rains generally ended earliest in the upper basin, followed by the middle basin and finally the lower basin during the historical period. In the near-future under both RCP4.5 and RCP8.5 scenarios, a similar pattern of termination would be experienced over the basin although the suspension would be earlier than it happened during the historical period (Figure 4.13).

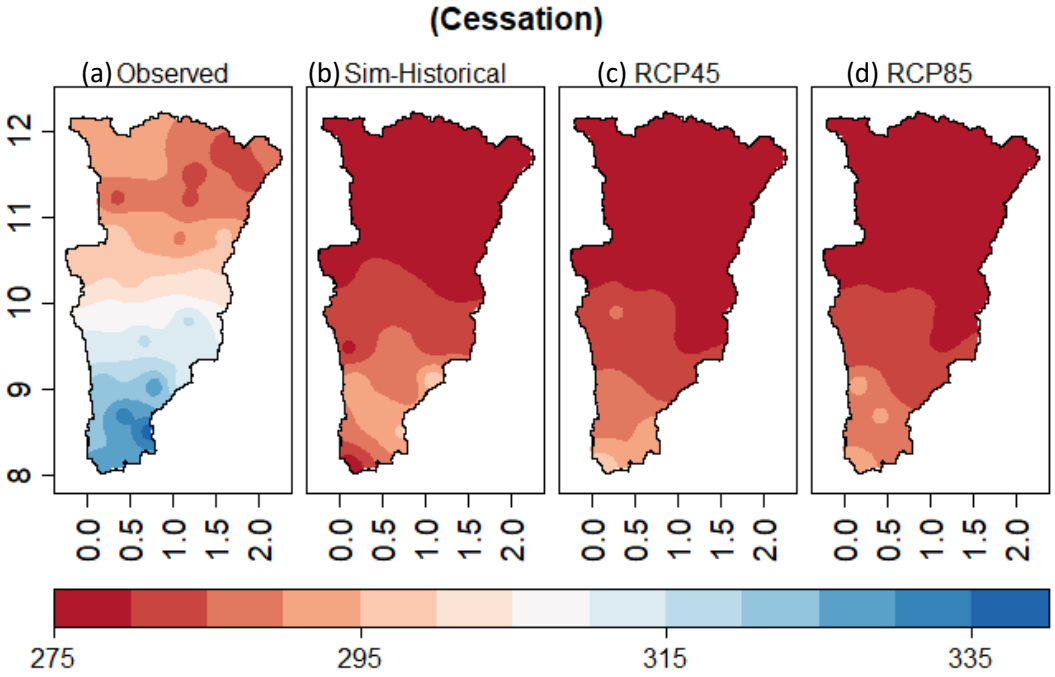

Figure 4. 13: Spatial distribution of cessation (days) in Oti River Basin for (a) observed (1981-2010), (b) simulated historical (1981-2005) and future (2021-2050) under (c) RCP4.5 and (d) RCP8.5 scenarios

The predicted early cessation is further emphasized by the MK test which reveals a decreasing trend in the basin in the near-future period (2021-2050) under both RCP4.5 and RCP8.5 scenarios (Table 4.11). The trends of cessation revealed that almost all the stations in the basin experienced an increasing trend except for Sokode, Kara, Yendi and GRID14 that had a non-significant decreasing trend (Table 4.11). Also, only GRID7 revealed a significant increasing trend, while for the entire basin, a non-significant increasing trend was exposed. This means during the historical period, cessation of rainfall at Sokode, Kara, Yendi and GRID14 trended earlier whereas at GRID7 and for the entire basin cessation date was later. In the near-future under RCP4.5, a mixture of non-significant increasing and decreasing trends would be observed among the stations in the basin except for Natitingou which could likely have a significant decreasing trend, indicating that cessation would be earlier at this station. The entire basin also reveals a non-significant decreasing trend under this scenario. Similarly, under RCP8.5, the entire basin shows a non-significant decreasing trend, while a mixture of non-significant increasing and decreasing trends exists among the individual stations. It is also found that the Sen's slope for the entire basin under RCP4.5 has a greater magnitude (-0.03)

than that under RCP8.5 (-0.05) which shows that the annual mean cessation date for the entire basin under RCP4.5 would shift more rapidly earlier than it would for the entire basin under RCP8.5 scenario (Table 4.11).

Table 4. 10: Mann-Kendall trend test for rainfall cessation in Oti River Basin

	Observed (1981-2010)		Sim-historical (1981-2005)		RCP4.5 (2021-2050)		RCP8.5 (2021-2050)	
Station	Z value	Sen's slope	Z value	Sen's slope	Z value	Sen's slope	Z value	Sen's slope
GRID1	0.89	0.23	-0.1	0.0	0.66	0.31	0.66	0.31
GRID2	1.28	0.11	-0.3	0.0	-0.82	-0.27	-0.82	-0.27
GRID3	1.04	0.00	-1.9	0.0	0.50	0.22	0.50	0.22
GRID4	1.20	0.14	-0.1	0.0	0.18	0.00	0.18	0.00
GRID5	0.00	0.00	-0.2	0.0	0.00	0.00	0.00	0.00
GRID6	0.32	0.05	-1.9	0.0	0.98	0.35	0.98	0.35
GRID7	2.39*****	0.36	-1.9	0.0	-0.09	0.00	-0.09	0.00
GRID8	1.34	0.29	-0.1	0.0	0.54	0.18	0.54	0.18
GRID9	0.45	0.00	-0.8	0.0	0.14	0.07	0.14	0.07
GRID10	0.73	0.14	-0.3	0.0	0.97	0.38	0.97	0.38
GRID11	1.25	0.23	1.3	0.0	0.25	0.00	0.25	0.00
GRID12	1.95	0.52	-0.5	0.0	-0.68	-0.25	-0.68	-0.25
GRID13	1.07	0.31	-1.6	0.0	-0.02	0.00	-0.02	0.00
GRID14	-1.45	-0.19	0.1	0.0	0.79	0.33	0.79	0.33
GRID15	1.66	0.32	-1.6	-0.3	0.25	0.00	0.25	0.00
GRID16	0.38	0.04	-0.6	-0.1	-0.57	-0.30	-0.57	-0.30
GRID17	0.38	0.08	-1.1	-0.3	0.29	0.07	0.29	0.07
GRID18	1.61	0.36	-1.1	-0.2	-0.39	-0.15	-0.39	-0.15
GRID19	0.57	0.07	0.4	0.1	-0.70	-0.30	-0.70	-0.30
GRID20	0.61	0.09	0.1	0.0	-0.45	-0.20	-0.45	-0.20
Natitingou	0.54	0.15	-0.3	0.0	-2.16*****	-0.91	-0.27	0.00
Fada	0.95	0.23	-0.3	0.0	0.11	0.07	0.11	0.07
Tenkodogo	1.52	0.22	0.0	0.0	0.00	0.00	0.00	0.00
Kete Krachi	1.04	0.50	-0.8	-0.3	-1.25	-0.26	-0.02	0.00
Yendi	-0.86	-0.33	-0.3	0.0	-0.40	0.00	-0.61	0.00
Dapaong	0.38	0.15	-0.8	0.0	1.22	0.25	1.22	0.25
Kara	-0.27	-0.13	-0.9	0.0	-1.19	0.00	-0.88	0.00
Mango	1.59	0.44	-1.8	0.0	0.80	0.29	0.80	0.29
Niamtougou	0.36	0.16	-0.5	0.0	-1.36	0.00	-0.88	0.00
Sokode	-1.00	-0.33	-1.4	-0.3	-0.47	0.00	-0.25	0.00
Basin	1.02	0.13	-1.1	-0.1	-0.45	-0.03	-0.66	-0.05

Note: *******values are significant at 5%; Sim-historical is Simulated-historical*

4.4.5 Length of the rainy season

Table 4.12 presents the summary results for the length of the rainy season (LRS) for the observed period (1981-2010), simulated historical (1981-2005) and the near-future (2021-2050) under RCP4.5 and RCP8.5. The length of the rainy season was found to range between 136 days at GRID2 and GRID3, 239 days at GRID20, and a mean LRS of 173 days for the entire basin during the historical period. The simulated historical revealed the length of the rainy season to be between 96 days at GRID3 and 175 days at Kete-Krachi with a mean LRS of 132 days for the whole basin. The SD also ranged between 13 days at GRID19 and 34 days at Mango and a mean SD of 12 days for the entire basin. However, SD for the simulated historical ranged between 17 days at GRID15, GRID16, GRID17, GRID20 and Yendi, and 28 days at Tenkodogo with a mean SD of 12 days. The CV for LRS ranged between 5.5% at GRID19 to 22.6% at Mango, while the mean CV was 6.8% for the entire basin. This indicates less to moderate variation in LRS at the stations in the basin (5.5%<CV<22.6%). The CV for simulated historical ranged between 10% at GRID17, GRID19 and GRID20, and 26% at GRID1 and Tenkodogo, with a mean CV of 9% (Asfaw et al., 2018; Alemu & Bawoke, 2019).

Under RCP4.5 scenario, LRS would be between 97 days at GRID3 to 185 days at Kete-Krachi with a mean LRS for the entire basin that would be around 136 days. The SD would range between 10 days at Sokode and 25 days at Natitingou, and a mean SD of 10 days for the entire basin. The CV for LRS would range between 6% at Sokode and 22% at GRID4, while the mean CV would be about 7.7% for the entire basin. This indicates a less to moderate variation in LRS at the stations in the basin (6%<CV<22%) (Asfaw et al., 2018; Alemu & Bawoke, 2019).

Under the RCP8.5 scenario, LRS would vary between 113 days at GRID3 and 176 days at GRID20, with a mean LRS of about 137 days for the entire basin. The SD would range between 12 days at GRID15 and 26 days at GRID4, and a mean SD of 10 days for the entire basin. The CV for LRS would range between 8.2% at GRID20 to 21.1% at GRID4, and the mean CV would be about 6.9% for the entire basin. This indicates a less to moderate variation in LRS at the stations in the basin (8.2%<CV<21.1%) (Asfaw et al., 2018; Alemu & Bawoke, 2019).

Table 4. 11: Summary statistics of LRS in Oti River Basin

Station	Observed (1981-2010)			Sim-historical (1981-2005)			RCP4.5 (2021-2050)			RCP8.5 (2021-2050)		
	Mean [days]	SD [days]	CV [%]	Mean [days]	SD [days]	CV [%]	Mean [days]	SD [days]	CV [%]	Mean [days]	SD [days]	CV [%]
GRID1	146	20	13.7	106	27	26	107	19	17.3	120	20	17.0
GRID2	136	21	15.3	98	22	22	107	22	20.2	118	23	19.3
GRID3	136	19	14.2	96	22	23	97	21	21.5	113	22	20.0
GRID4	138	20	14.7	102	25	25	106	23	22.0	123	26	21.1
GRID5	145	21	14.3	115	22	19	116	22	19.2	123	17	13.9
GRID6	149	21	13.9	117	20	17	112	24	21.2	125	21	17.2
GRID7	143	18	12.7	108	23	21	109	20	18.0	117	19	16.3
GRID8	148	19	13.0	116	23	19	120	23	19.0	129	21	16.2
GRID9	150	18	12.1	119	23	20	129	19	14.8	129	21	16.2
GRID10	158	23	14.8	124	18	14	131	21	15.9	129	16	12.2
GRID11	155	21	13.5	119	19	16	127	21	16.2	123	17	13.6
GRID12	169	23	13.6	123	18	15	125	17	13.7	126	18	14.0
GRID13	173	22	12.9	129	24	19	124	23	18.3	135	20	14.5
GRID14	190	22	11.3	137	21	15	150	21	13.8	140	21	14.8
GRID15	189	22	11.6	142	17	12	151	13	8.9	147	12	8.4
GRID16	209	23	11.1	151	17	11	163	15	9.2	156	18	11.8
GRID17	220	14	6.2	162	17	10	167	19	11.4	167	18	10.6
GRID18	226	18	7.9	155	26	17	160	14	9.0	153	20	13.3
GRID19	231	13	5.5	174	18	10	184	13	7.3	172	21	12.4
GRID20	239	15	6.3	172	17	10	179	17	9.6	176	15	8.2
Natitingou	179	23	12.7	148	19	13	143	25	17.8	141	24	17.1
Fada	143	29	20.1	108	22	21	106	15	14.5	117	20	16.9
Tenkodogo	142	25	17.4	107	28	26	114	21	18.8	119	15	12.6
Kete Krachi	200	32	15.9	175	18	10	185	19	10.4	173	19	10.7
Yendi	189	29	15.2	145	17	12	149	11	7.4	142	18	12.8
Dapaong	161	30	18.6	120	22	19	119	21	17.8	119	14	12.1
Kara	191	27	14.3	152	18	12	151	19	12.3	147	22	14.7
Mango	152	34	22.6	136	20	15	139	22	16.1	136	19	14.3
Niamtougou	198	30	15.0	146	21	14	138	19	13.8	139	20	14.5
Sokode	201	31	15.7	161	23	14	174	10	6.0	162	21	12.9
Basin	173	12	6.8	132	12	9	136	10	7.7	137	10	6.9

Note: *SD is Standard deviation; CV is Coefficient of variation; Sim-historical is Simulated-historical*

At the temporal scale, it is observed that the LRS for the historical period ranged between 149 days in 1989 and 191 days in 2007. With respect to the simulated historical (1981-2005), LRS in the basin ranged from 105 days (1996) to 151 days (2005), while for the future period, it is expected to range between 116 days in 2027 and 159 days in 2033 under RCP4.5. However, RCP8.5 scenario projects a further delay in LRS which is expected to range between 115 days and 156 days for the years 2023 and 2030 respectively (Figure 4.14).

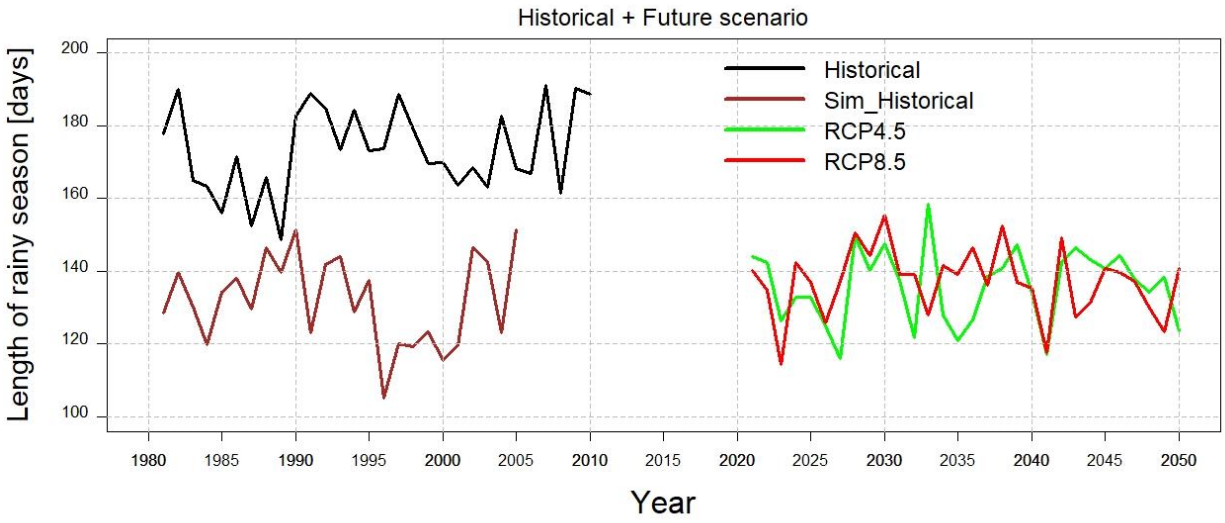

Figure 4. 14: Temporal variations in LRS during the historical (1981-2010), simulated historical (1981-2005) and future periods (2021-2050) under RCP4.5 and RCP8.5 scenarios

At the spatial scale, it is found that the LRS generally lasted for long in the lower basin and shorter in the upper basin. Although similar observation is made under RCP4.5 and RCP8.5 scenarios, almost all parts of the lower basin as well as most parts of the upper basin would experience an extreme reduction in the LRS (Figure 4.15).

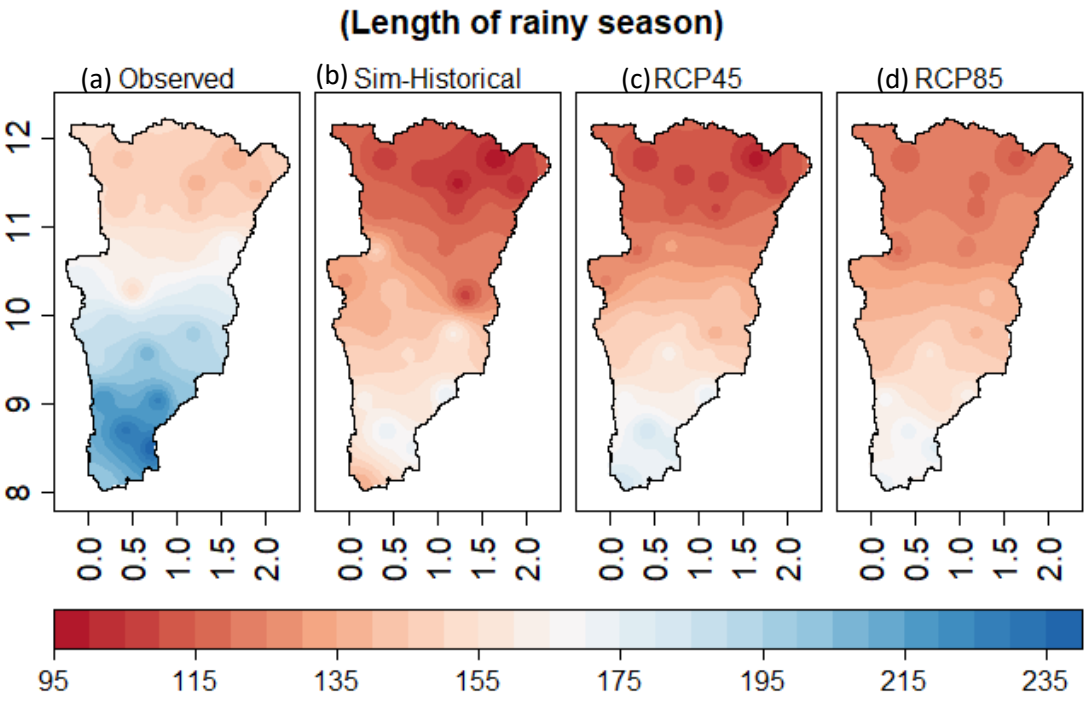

Figure 4. 15: Spatial distribution of LRS (days) in Oti River Basin for (a) observed (1981-2010), (b) simulated historical (1981-2005) and future (2021-2050) under (c) RCP4.5 and (d) RCP8.5 scenarios

For the trend in LRS, a mixture of non-significantly increasing, decreasing and no trend was found, except Fada which showed a significantly increasing trend. The entire basin indicated a non-significantly increasing trend during the historical period (Table 4.13). Similarly, a combination of increasing and decreasing trends would be observed among the stations, with the entire basin revealing a non-significantly increasing trend under the RCP4.5 scenario. However, GRID1 and Niamtougou would show a significantly increasing trend while Kete-Krachi would experience a significantly decreasing trend. Under the RCP8.5 scenario, a non-significantly increasing trend would be experienced for the entire basin, and a combination of increasing, decreasing and no trend among the stations. Furthermore, the slope for the entire basin under RCP4.5 has a greater magnitude (0.03) than that under RCP8.5 (-0.11) revealing that the annual mean LRS days for the entire basin under RCP4.5 would become more rapidly shorter than it would under the RCP8.5 scenario (Table 4.13).

Table 4. 12: Mann-Kendall trend test and Sen's slope estimates for LRS in Oti River Basin

	Observed (1981-2010)		Sim-historical (1981-2005)		RCP4.5 (2021-2050)		RCP8.5 (2021-2050)	
Station	Z value	Sen's slope	Z value	Sen's slope	Z value	Sen's slope	Z value	Sen's slope
GRID1	0.00	0.00	0.42	0.18	**2.00**	0.89	-0.80	-0.42
GRID2	0.84	0.45	0.00	0.00	0.84	0.33	0.96	0.31
GRID3	0.73	0.40	1.33	0.40	0.86	0.32	-0.36	-0.09
GRID4	-0.05	0.00	1.92	0.98	0.98	0.35	-0.21	0.00
GRID5	0.93	0.44	-0.68	-0.34	0.59	0.33	0.55	0.13
GRID6	1.64	0.79	0.09	0.03	-0.77	-0.33	-0.89	-0.33
GRID7	1.70	0.74	0.00	0.00	-0.34	-0.09	0.20	0.05
GRID8	1.39	0.54	0.33	0.20	0.34	0.18	-0.70	-0.36
GRID9	0.54	0.29	0.65	0.32	-1.02	-0.33	-0.25	-0.11
GRID10	0.70	0.33	0.94	0.42	0.36	0.06	-1.18	-0.42
GRID11	1.39	0.67	0.14	0.03	0.45	0.29	-0.13	0.00
GRID12	1.00	0.73	0.14	0.00	0.93	0.38	0.36	0.17
GRID13	1.64	0.75	0.07	0.00	-0.73	-0.38	-0.55	-0.16
GRID14	0.23	0.04	0.07	0.07	0.20	0.14	-1.09	-0.25
GRID15	0.82	0.43	-0.82	-0.34	0.80	0.22	-0.07	0.00
GRID16	0.38	0.17	**-1.99**	-0.83	-1.20	-0.33	0.07	0.00
GRID17	0.27	0.08	-0.77	-0.33	0.84	0.40	-0.09	-0.07
GRID18	1.34	0.33	-1.29	-0.84	-0.71	-0.21	-0.04	0.00
GRID19	1.57	0.29	-1.52	-0.77	0.80	0.25	0.55	0.25
GRID20	0.46	0.20	0.42	0.16	0.59	0.20	0.21	0.05
Natitingou	1.64	0.86	-0.59	-0.24	-0.98	-0.43	-0.16	-0.13
Fada	**3.27**	1.94	0.68	0.31	1.36	0.38	0.00	0.00
Tenkodogo	1.50	0.88	-0.07	-0.04	0.07	0.00	-1.23	-0.33
Kete-Krachi	0.04	0.07	**-1.99**	-1.07	**-2.32**	-0.92	-0.61	-0.31
Yendi	-0.89	-0.58	**-2.10**	-1.00	-1.50	-0.40	1.66	0.78
Dapaong	0.50	0.40	0.47	0.45	-0.18	-0.11	-1.75	-0.57
Kara	-1.00	-0.74	-0.07	0.00	1.00	0.44	-0.63	-0.22
Mango	0.95	0.86	-0.51	-0.28	0.00	0.00	0.00	0.00
Niamtougou	0.09	0.06	0.00	0.00	**2.16**	0.84	-0.23	-0.07
Sokode	-1.00	-0.67	-0.89	-0.50	-0.79	-0.18	0.55	0.20
Basin	0.54	0.18	-0.28	-0.12	0.18	0.03	-0.55	-0.11

Note: *values in bold are significant at 5%; Sim-historical is Simulated-historical*

4.4.6 Number of wet days

Table 4.14 illustrates the summary results wet days during the observed period (1981-2010), simulated historical (1981-2005) and the future (2021-2050) under RCP4.5 and RCP8.5. From the result, it can be deduced that during the observed period, the wet days ranged from 66 days at Fada to 135 days at GRID20 and a mean wet days of 95 days for the entire basin. With respect to the simulated historical, the wet days ranged between 133 days at GRID3 and 207 days at GRID19 and GRID20, with a mean wet days of 171 days in the basin. The standard deviation (SD) also ranged from 6 days at Dapaong to 18 days at GRID19 and Natitingou and a mean SD of 8 days for the entire basin during the observed period. However, for the simulated historical, mean standard deviation was 6 days, and ranged between 6 days at Sokode and Natitingou, and 11 days at Fada. The coefficient of variation (CV) ranged between 8% at Sokode and Dapaong to 20% at Fada and with a mean CV of 8% for the entire basin thus, indicating a less to moderate variation (8%<CV<20%). The CV for the simulated historical varied between 3% at Sokode to 8% at GRID3 and Fada, with a mean CV of 4% (Asfaw et al., 2018; Alemu & Bawoke, 2019).

In the future period, and under RCP4.5, it is observed that the mean for wet days would range between 135 days at GRID3 and 214 days at GRID19 with a mean for the entire basin that would be around 175 days. The SD would range between 5 days at GRID8 and 9 days at GRID20 and Tenkodogo with a mean SD of 5 days. In addition, the CV would be in the ranges of 3% at GRID8, GRID19 and Kete-Krachi to 6% at Tenkodogo, and a mean CV of 3% for the entire basin, indicating less variation among the stations in the basin (3%<CV<6%) (Asfaw et al., 2018; Alemu & Bawoke, 2019).

In the future period, and under RCP8.5, wet days would range between 139 days at GRID3 to 214 days at GRID19 and a mean of 175 days for the entire basin. The SD would also range between 6 days at GRID6, GRID7, GRID10, GRID11, GRID13, GRID14, Kara, Mango, Niamtougou and Sokode, and 10 days at GRID20 and Tenkodogo and, a mean SD of 5 days for the entire basin. The CV would range between 3% at GRID10, GRID14, GRID16, GRID17, GRID19, Kara, Niamtougou and Sokode, and 6% at GRID1, Fada and Tenkodogo and a mean CV of 3% for the entire basin, indicating less variation (Asfaw et al., 2018; Alemu & Bawoke, 2019).

Table 4. 13: Summary statistics for number of wet days in Oti River Basin

	Observed (1981-2010)			Sim-historical (1981-2005)			RCP4.5 (2021-2050)			RCP8.5 (2021-2050)		
Station	Mean [days]	SD [days]	CV [%]	Mean [days]	SD [days]	CV [%]	Mean [days]	SD [days]	CV [%]	Mean [days]	SD [days]	CV [%]
GRID1	78	11	14	138	9	7	141	7	5	144	9	6
GRID2	82	9	11	140	9	7	143	6	4	146	7	4
GRID3	78	9	12	133	10	8	135	7	5	139	8	5
GRID4	84	10	11	142	10	7	145	7	5	148	8	5
GRID5	83	10	12	147	8	6	152	8	5	154	8	5
GRID6	85	9	10	149	8	5	154	7	5	155	6	4
GRID7	87	11	13	147	8	5	153	6	4	154	6	4
GRID8	90	11	12	149	8	5	155	5	3	154	7	4
GRID9	91	10	11	153	8	5	155	6	4	156	7	5
GRID10	92	8	9	162	9	5	167	7	4	169	6	3
GRID11	100	11	11	161	7	5	166	7	4	165	6	4
GRID12	102	12	12	167	8	5	170	6	4	170	7	4
GRID13	98	11	11	169	8	5	170	7	4	170	6	4
GRID14	106	11	10	183	7	4	190	8	4	190	6	3
GRID15	119	14	12	190	8	4	196	8	4	195	7	4
GRID16	126	13	10	201	7	4	206	8	4	205	7	3
GRID17	123	14	11	206	7	4	209	8	4	208	7	3
GRID18	131	15	12	194	7	4	198	7	4	197	7	4
GRID19	133	18	13	207	9	4	214	7	3	214	7	3
GRID20	135	17	12	207	10	5	213	9	4	210	10	5
Natitingou	94	18	19	181	6	3	185	7	4	183	7	4
Fada	66	13	20	140	11	8	141	7	5	145	9	6
Tenkodogo	82	8	10	142	7	5	143	9	6	147	10	6
Kete Krachi	80	9	11	202	8	4	211	6	3	209	8	4
Yendi	78	8	10	195	9	5	199	8	4	198	8	4
Dapaong	67	6	8	165	8	5	169	7	4	171	7	4
Kara	93	9	10	188	7	4	193	8	4	190	6	3
Mango	69	8	12	177	8	5	181	8	4	182	6	4
Niamtougou	97	10	11	186	7	4	191	8	4	189	6	3
Sokode	94	8	8	205	6	3	212	8	4	209	6	3
Basin	95	8	8	171	6	4	175	5	3	175	5	3

Note: *SD is Standard deviation; CV is Coefficient of variation; Sim-historical is Simulated -historical*

At the temporal scale, it is observed that the wet days (NWD) in the basin during the historical period was between 69 days (1983) to 108 days (2009). For the simulated historical, the wet days in the basin was between 161 days (1996) to 185 days (1992). In the future period and under RCP4.5, the wet days would range between 163 days (2027) to 188 days (2028), and between 165 days (2039) and 183 days (2042) for RCP8.5 (Figure 4.16).

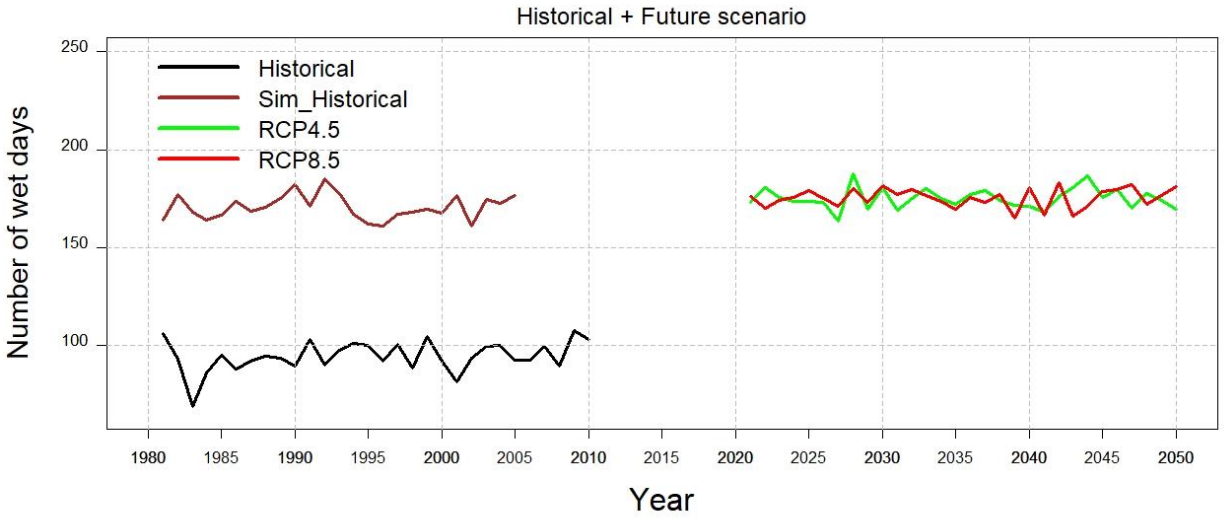

Figure 4. 16: Temporal variations in NWD during the historical (1981-2010), simulated historical (1981-2005) and future periods (2021-2050) under RCP4.5 and RCP8.5 scenarios

At the spatial scale, it is found that during the historical period, the lower basin had more number of wet days and this reduced towards the upper basin. Similarly, the wet days in the lower basin would be more and would decrease towards the upper basin in the near-future period under both RCP4.5 and RCP8.5 scenarios (Figure 4.16).

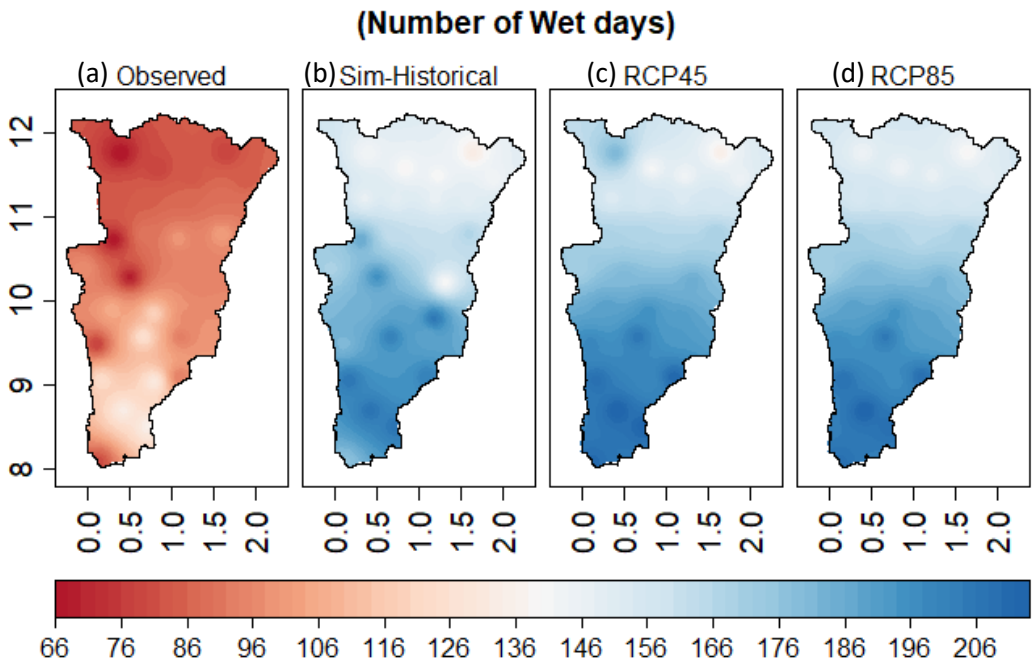

Figure 4. 17: Spatial distribution of NWD in Oti River Basin for (a) observed (1981-2010), (b) simulated historical (1981-2005) and future (2021-2050) under (c) RCP4.5 and (d) RCP8.5 scenarios

The Mann-Kendall trend test revealed a mixture of non-significantly positive and negative trends among the stations in the basin except for stations like GRID9, Natitingou, Fada, Yendi, and Dapaong that showed significantly positive trends during the observed period (Table 4.15). The entire basin however revealed a non-significantly positive trend (0.26 day per annual). The Simulated-historical period also revealed a mixture of non-significantly positive and negative trends among the stations whereas the entire basin showed a non-significantly positive trend (0.09 day per annual). Under the RCP4.5 scenario, there would be a mixture of non-significantly positive and negative trends among the stations in the basin, while the entire basin would show a non-significantly negative trend, with the magnitude of decrease being -0.01 day per annual. Similarly, under the RCP8.5 scenario, there would be a mixture of non-significantly positive and negative trends among the stations in the basin with the exception of only GRID12 that would reveal a significantly positive trend. The entire basin would reveal a non-significantly positive trend, with a magnitude of increase of about 0.08 day per annual (Table 4.15).

Table 4. 14: Mann-Kendall trend test and Sen's slope estimates for number of wet days

	Observed (1981-2010)		Sim-historical (1981-2005)		RCP4.5 (2021-2050)		RCP8.5 (2021-2050)	
Station	Z value	Sen's slope	Z value	Sen's slope	Z value	Sen's slope	Z value	Sen's slope
GRID1	1.14	0.35	0.89	0.21	0.09	0.00	-0.16	0.00
GRID2	1.07	0.30	0.56	0.18	0.45	0.05	0.52	0.08
GRID3	1.56	0.33	0.45	0.10	-1.31	-0.19	-0.81	-0.17
GRID4	1.32	0.32	1.24	0.31	-1.28	-0.20	-0.25	-0.04
GRID5	0.75	0.17	0.02	0.00	-0.09	0.00	-0.84	-0.15
GRID6	1.07	0.16	0.14	0.03	-1.04	-0.19	-0.61	-0.07
GRID7	0.71	0.21	0.80	0.25	-0.89	-0.11	0.32	0.00
GRID8	0.70	0.17	1.34	0.26	-0.34	0.00	0.82	0.11
GRID9	**2.07**	0.48	0.28	0.09	-0.34	0.00	0.36	0.05
GRID10	1.45	0.29	0.45	0.15	-0.46	-0.08	0.14	0.00
GRID11	0.86	0.27	-0.75	-0.15	-0.20	0.00	0.89	0.12
GRID12	1.18	0.33	-0.80	-0.13	0.57	0.08	**2.03**	0.27
GRID13	-0.14	0.00	0.98	0.21	0.14	0.00	1.17	0.12
GRID14	-0.34	-0.13	-0.12	0.00	0.48	0.06	0.18	0.00
GRID15	0.14	0.00	0.26	0.05	0.72	0.09	0.30	0.00
GRID16	0.61	0.20	0.26	0.06	0.88	0.15	0.43	0.00
GRID17	0.43	0.11	-0.56	-0.21	-0.63	-0.08	0.36	0.00
GRID18	-0.14	-0.05	-0.02	0.00	0.66	0.08	0.18	0.00
GRID19	0.11	0.09	-0.33	-0.10	1.41	0.17	0.84	0.13
GRID20	0.07	0.00	-0.65	-0.18	0.82	0.17	1.05	0.29
Natitingou	**3.72**	1.31	0.16	0.00	-0.22	0.00	0.72	0.12
Fada	**3.81**	1.10	0.26	0.10	0.59	0.13	0.00	0.00
Tenkodogo	1.29	0.21	0.23	0.03	-0.77	-0.13	-0.29	0.00
Kete Krachi	-1.57	-0.29	-0.96	-0.25	-0.34	0.00	0.91	0.15
Yendi	**2.94**	0.50	0.91	0.29	0.91	0.14	0.16	0.00
Dapaong	**2.78**	0.31	-0.05	0.00	-0.09	0.00	0.79	0.17
Kara	0.54	0.08	0.40	0.11	0.27	0.05	0.21	0.00
Mango	1.57	0.30	-0.28	-0.06	0.74	0.13	1.22	0.18
Niamtougou	1.89	0.37	0.35	0.08	0.43	0.08	0.39	0.05
Sokode	1.96	0.31	-0.33	-0.06	1.41	0.21	0.82	0.14
Basin	1.32	0.26	0.51	0.09	-0.02	-0.01	0.64	0.08

Note: *values in bold are significant at 5%; S. slope=Sen's slope; Sim-historical=Simulated historical*

4.4.7 Number of dry days

Table 4.16 illustrates the summary results for number of dry days during the observed period (1981-2010), simulated historical (1981-2005), and the future (2021-2050) under RCP4.5 and RCP8.5. From the result, it can be deduced that during the observed period, the dry days ranged from 230 days at GRID20 and 299 days at Fada, and mean dry days of 270 days for the entire basin. With respect to the simulated historical, the dry days ranged between 158 days at GRID19 and GRID20, and 232 days at GRID3, with mean dry days of 194 days in the basin. The standard deviation (SD) also ranged from 6 days at Dapaong to 18 days at GRID19 and Natitingou, and a mean SD of 8 days for the entire basin. However, for the simulated historical, mean standard deviation was 6 days, and ranged between 6 days at Sokode and Natitingou to 11 days at Fada. The coefficient of variation (CV) ranged between 2% at Dapaong and 8% at GRID19, and with a mean CV of 3% for the entire basin, indicating less variation (2%<CV<8%). The CV for the simulated historical varied between 3% at Sokode, Tenkodogo and Natitingou, and 6% at GRID20, with a mean CV of 3% (Asfaw et al., 2018; Alemu & Bawoke, 2019).

In the future period, and under RCP4.5, it is observed that the dry days would range between 152 days at GRID19 and 227 days at GRID3, with a mean for the entire basin that would be around 189 days. The SD would range between 7 days at Natitingou to 18 days at Tenkodogo, with a mean SD of 6 days for the entire basin. In addition, the CV would be in the ranges of 4% at GRID12, GRID13, Mango, and Dapaong, and 9% at GRID20, and a mean CV of 3% in the entire basin, indicating less variation (Asfaw et al., 2018; Alemu & Bawoke, 2019).

In the future period, and under RCP8.5, the dry days would range between 151 days at GRID19 and 226 days at GRID3, and a mean of 190 days for the entire basin. The SD would also range between 6 days at GRID6, GRID7, GRID10, GRID11, GRID13, GRID14, Kara, Mango, Niamtougou, and Sokode, and 10 days at GRID20 and Tenkodogo, and a mean SD of 5 days in the entire basin. The CV would range between 3% at GRID2, GRID3, GRID4, GRID6, GRID7, GRID8, GRID9, GRID10, GRID11, GRID13, Mango and Niamtougou, and 6% at GRID20, and a mean CV of 3% in the entire basin, indicating a less variation (Asfaw et al., 2018; Alemu & Bawoke, 2019).

Table 4. 15: Summary results for number of dry days in Oti River Basin

	Observed (1981-2010)			Sim-historical (1981-2005)			RCP4.5 (2021-2050)			RCP8.5 (2021-2050)		
Station	Mean [days]	SD [days]	CV [%]	Mean [days]	SD [days]	CV [%]	Mean [days]	SD [days]	CV [%]	Mean [days]	SD [days]	CV [%]
GRID1	288	11	4	227	9	4	221	17	8	221	9	4
GRID2	283	9	3	225	9	4	219	15	7	219	7	3
GRID3	287	9	3	232	10	4	227	17	7	226	8	3
GRID4	281	10	3	223	10	4	218	15	7	217	8	3
GRID5	282	10	3	218	8	4	211	13	6	211	8	4
GRID6	280	9	3	216	8	4	210	11	5	210	6	3
GRID7	278	11	4	218	8	4	211	11	5	211	6	3
GRID8	275	11	4	216	8	4	209	11	5	211	7	3
GRID9	274	10	4	212	8	4	208	12	6	210	7	3
GRID10	273	8	3	203	9	4	197	9	5	196	6	3
GRID11	265	11	4	204	7	4	198	9	5	200	6	3
GRID12	263	12	5	198	8	4	194	8	4	195	7	4
GRID13	267	11	4	196	8	4	195	8	4	195	6	3
GRID14	259	11	4	182	7	4	175	8	5	175	6	4
GRID15	246	14	6	175	8	5	170	9	5	170	7	4
GRID16	240	13	5	164	7	5	160	11	7	160	7	4
GRID17	242	14	6	159	7	5	157	12	7	157	7	5
GRID18	234	15	6	171	7	4	167	8	5	168	7	4
GRID19	232	18	8	158	9	5	152	11	7	151	7	5
GRID20	230	17	7	158	10	6	153	13	9	155	10	6
Natitingou	271	18	7	184	6	3	180	7	4	182	7	4
Fada	299	13	4	225	11	5	222	16	7	220	9	4
Tenkodogo	283	8	3	223	7	3	219	18	8	218	10	4
Kete Krachi	285	9	3	163	8	5	155	11	7	156	8	5
Yendi	287	8	3	170	9	5	167	9	6	167	8	5
Dapaong	298	6	2	200	8	4	195	8	4	194	7	4
Kara	272	9	3	177	7	4	173	9	5	175	6	4
Mango	296	8	3	188	8	4	184	8	4	183	6	3
Niamtougou	268	10	4	179	7	4	175	9	5	176	6	3
Sokode	271	8	3	160	6	3	154	12	8	156	6	4
Basin	270	8	3	194	6	3	189	6	3	190	5	3

Note: *SD is standard deviation; CV is Coefficient of variation; Simulated historical*

At the temporal scale, it is observed that the number of dry days (NDD) in the basin during the historical period was between 257 days (2009) and 296 days (1983). For the simulated historical, the dry days in the basin was between 179 days (1992) and 203 days (1996). In the future period and under RCP4.5, the dry days would range between 174 days (2024) and 202 days (2027); and between 182 days (2042) and 200 days (2039) for RCP8.5 (Figure 4.18).

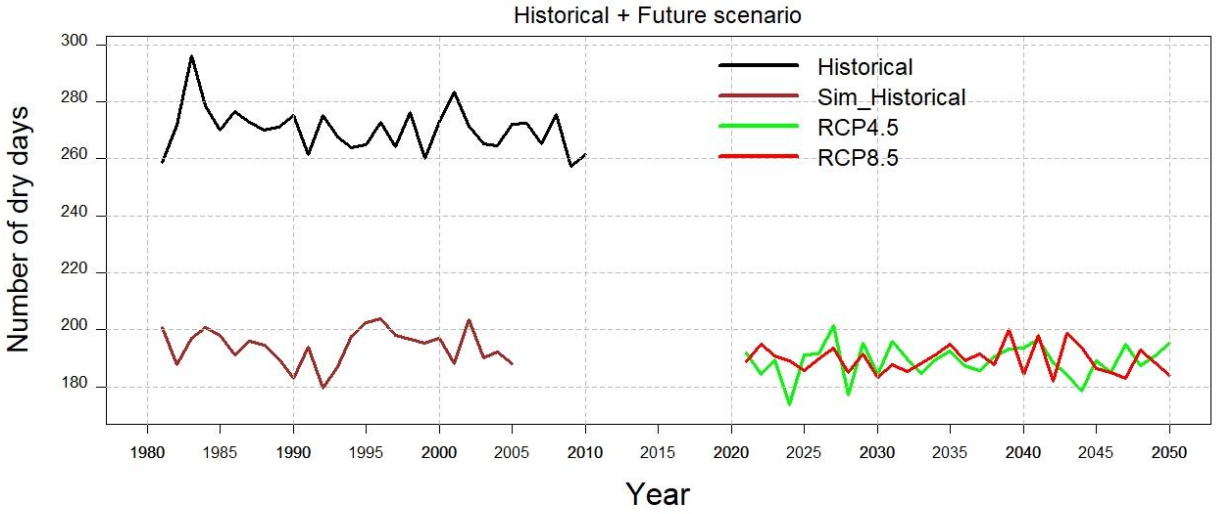

Figure 4. 18: Temporal variations in NDD during the historical (1981-2010), simulated historical (1981-2005) and future periods (2021-2050) under RCP4.5 and RCP8.5 scenarios

It is found that at the spatial scale, the dry days is higher in the upper basin while it is less in the lower basin, and was generally severe due to the historical drought conditions experienced in the basin. In the near-future however, the dry days in the basin would increase from the lower basin towards the upper basin under both RCP4.5 and RCP8.5 scenarios (Figure 4.19).

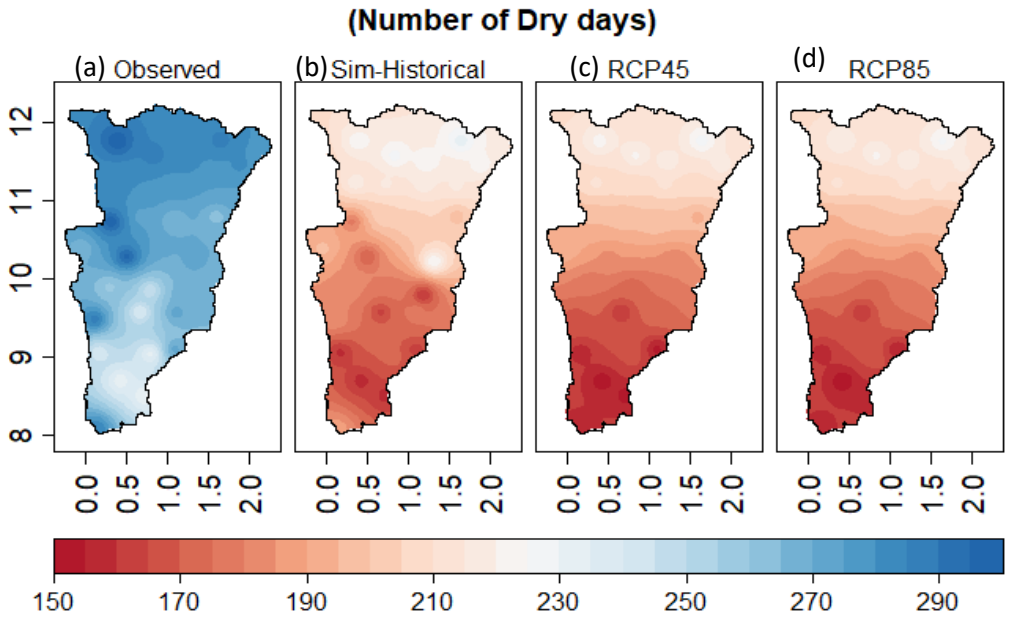

Figure 4. 18: Spatial distribution of NDD in Oti River Basin for (a) observed (1981-2010), (b) simulated historical (1981-2005) and future (2021-2050) under (c) RCP4.5 and (d) RCP8.5 scenarios

For number of dry days trend in the basin, it was revealed that it showed a mixture of non-significant positive and negative trends among the stations except for GRID9, Natitingou, Fada, Yendi and Dapaong that showed significant negative trends during the observed period (Table 4.17). The entire basin also revealed a non-significant negative trend with a magnitude of decrease of 0.26 day per annual. The Simulated-historical period also reveals non-significant decreasing trend in the entire basin, with a magnitude of decrease of 0.09 day per annual. In the future period under RCP4.5 scenario, the stations would show a mixture of non-significant positive and negative trends, and within the entire basin revealing a non-significant positive trend, with a magnitude of 0.08 day per annual. Similarly, the RCP8.5 scenario would also show a mixture of non-significant positive and negative trends among the stations except for GRID12 that would show significant negative trend. The entire basin would also reveal a non-significant negative trend, with a magnitude of decrease of about 0.08 day per annual (Table 4.17).

Table 4. 16: Mann-Kendall trend test and Sen's slope estimates for number of dry days

	Observed (1981-2010)		Sim-historical (1981-2005)		RCP4.5 (2021-2050)		RCP8.5 (2021-2050)	
Station	Z value	Sen's slope	Z value	Sen's slope	Z value	Sen's slope	Z value	Sen's slope
GRID1	-1.14	-0.35	-0.89	-0.21	0.23	0.05	0.16	0.00
GRID2	-1.07	-0.30	-0.56	-0.18	-0.29	0.00	-0.52	-0.08
GRID3	-1.56	-0.33	-0.45	-0.10	1.36	0.19	0.81	0.17
GRID4	-1.32	-0.32	-1.24	-0.31	1.56	0.27	0.25	0.04
GRID5	-0.75	-0.17	-0.02	0.00	0.43	0.10	0.84	0.15
GRID6	-1.07	-0.16	-0.14	-0.03	1.11	0.25	0.61	0.07
GRID7	-0.71	-0.21	-0.80	-0.25	1.06	0.14	-0.32	0.00
GRID8	-0.70	-0.17	-1.34	-0.26	0.59	0.08	-0.82	-0.11
GRID9	**-2.07**	-0.48	-0.28	-0.09	0.75	0.12	-0.36	-0.05
GRID10	-1.45	-0.29	-0.45	-0.15	0.80	0.20	-0.14	0.00
GRID11	-0.86	-0.27	0.75	0.15	0.59	0.10	-0.89	-0.12
GRID12	-1.18	-0.33	0.80	0.13	0.00	0.00	**-2.03**	-0.27
GRID13	0.14	0.00	-0.98	-0.21	0.20	0.04	-1.17	-0.12
GRID14	0.34	0.13	0.12	0.00	-0.52	-0.06	-0.18	0.00
GRID15	-0.14	0.00	-0.26	-0.05	-1.20	-0.21	-0.30	0.00
GRID16	-0.61	-0.20	-0.26	-0.06	-1.27	-0.22	-0.43	0.00
GRID17	-0.43	-0.11	0.56	0.21	0.30	0.00	-0.36	0.00
GRID18	0.14	0.05	0.02	0.00	-0.63	-0.08	-0.18	0.00
GRID19	-0.11	-0.09	0.33	0.10	-1.43	-0.18	-0.84	-0.13
GRID20	-0.07	0.00	0.65	0.18	-0.95	-0.22	-1.05	-0.29
Natitingou	**-3.72**	-1.31	-0.16	0.00	0.04	0.00	-0.72	-0.12
Fada	**-3.81**	-1.10	-0.26	-0.10	-0.27	-0.07	0.00	0.00
Tenkodogo	-1.29	-0.21	-0.23	-0.03	1.40	0.25	0.29	0.00
Kete Krachi	1.57	0.29	0.96	0.25	0.16	0.00	-0.91	-0.15
Yendi	**-2.94**	-0.50	-0.91	-0.29	-1.05	-0.18	-0.16	0.00
Dapaong	**-2.78**	-0.31	0.05	0.00	0.43	0.07	-0.79	-0.17
Kara	-0.54	-0.08	-0.40	-0.11	-0.55	-0.13	-0.21	0.00
Mango	-1.57	-0.30	0.28	0.06	-0.45	-0.08	-1.22	-0.18
Niamtougou	-1.89	-0.37	-0.35	-0.08	-0.73	-0.18	-0.39	-0.05
Sokode	-1.96	-0.31	0.33	0.06	-1.49	-0.23	-0.82	-0.14
Basin	-1.32	-0.26	-0.51	-0.09	0.52	0.08	-0.64	-0.08

Note: *values in bold are significant at 5%; S. slope is Sen's slope; Sim-historical is Simulated historical*

4.5 Historical rainfall anomaly (1981-2010)

Figure 4.20 illustrates the seasonal rainfall anomaly during the historical period (1981-2010). The results exposed the year-to-year variations in seasonal rainfall across the basin. It was found that the highest positive anomaly was +1.66 which was recorded in 1994, indicating a very wet condition, while the highest negative anomaly was -2.29 which was observed in the year 1983 corresponding to extremely dry conditions (McKee et al., 1993). Generally, it is revealed that the early 1980s experienced pronounced positive seasonal rainfall anomalies whereas the 1990s and 2000s experienced moderately wet periods during the rainy season periods. Generally, the rainy season in the historical period experienced 2 very wet years (1994, 2009), 4 moderately wet years (1991, 1998, 1999, 2003), 3 moderately dry years (1982, 1984, 1990), 1 extremely dry year (1983) with the remaining 20 years being near-normal years.

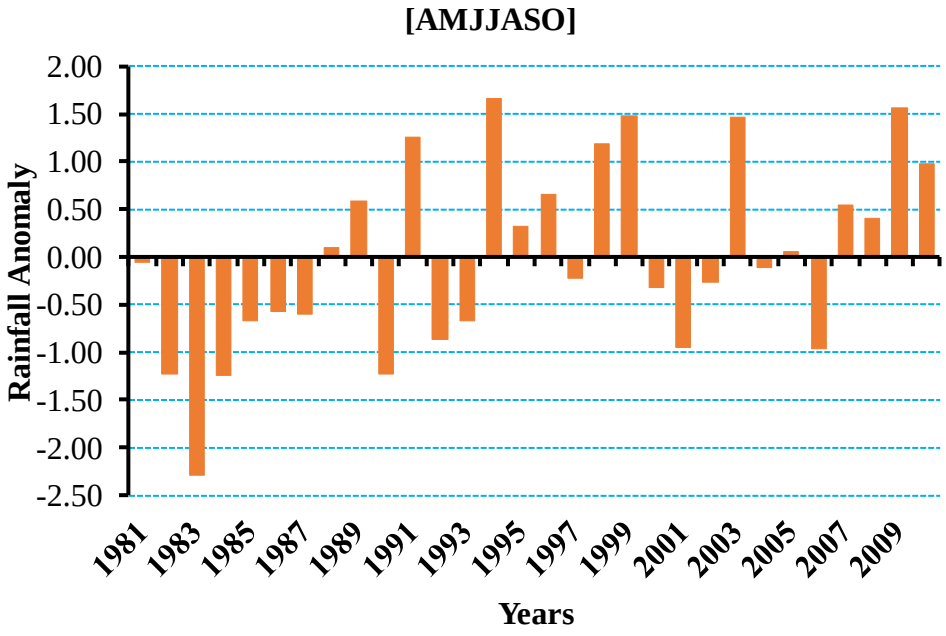

Figure 4. 19: Seasonal rainfall (AMJJASO) anomaly during the historical period (1981-2010)

4.6 Seasonal rainfall anomaly for near-future (2021-2050) under RCP4.5 and RCP8.5

4.6.1 Rainy season (AMJJASO)

Figure 4.21 presents the seasonal rainfall anomaly (AMJJASO) for the near-future period (2021-2050) under RCP4.5 and RCP8.5 scenarios. In the near-future during the rainy season, the negative anomaly would be more pronounced in 2027 (-2.31) while the positive anomaly would be highest in 2037 (+2.13) indicating extremely dry and extremely wet situations respectively under the RCP4.5 scenario. In all, during this period, the basin would experience 1 extremely wet year (2037), 2 very wet years (2024, 2044), 2 moderately wet years (2035, 2036), 3 moderately dry years (2023, 2033, 2047), 1 extremely dry year (2027), and remaining 21 years, near normal.

Under the RCP8.5 scenario, the highest positive anomaly would be recorded in 2028 (+1.77) and the highest negative anomaly would be in 2041 (-2.49) revealing very wet and extremely dry conditions correspondingly (McKee et al., 1993). Generally, under this climate change scenario and period, the basin is anticipated to experience 2 very wet years (2028, 2045), 3 moderately wet years (2033, 2035, 2046), 4 moderately dry years (2022, 2039, 2043, 2049), 1 extremely dry year (2041) and remaining years being near normal.

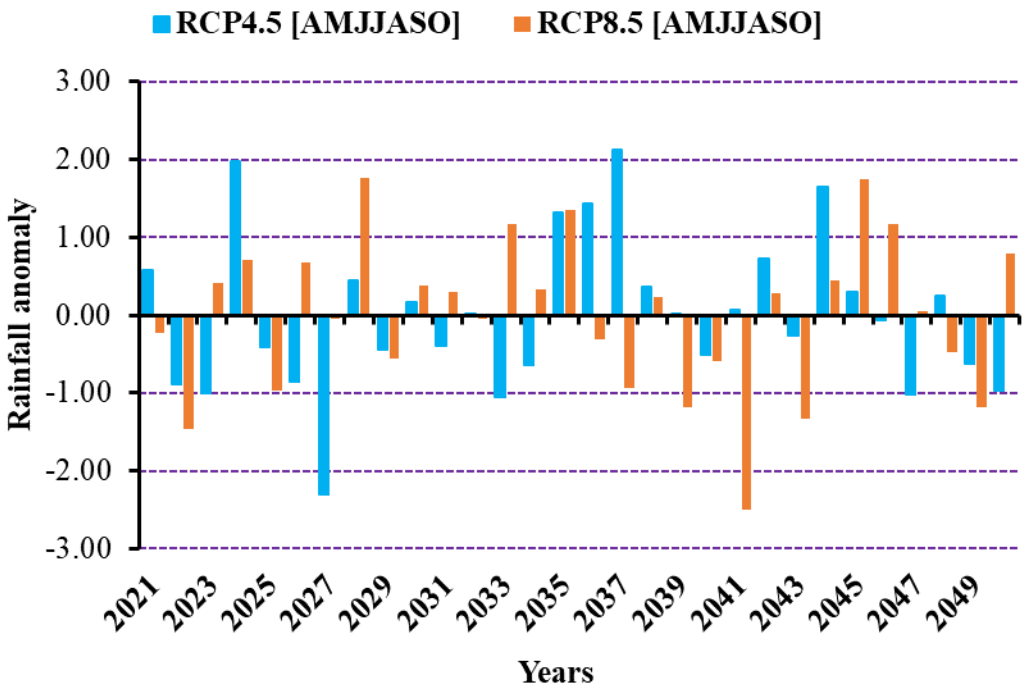

Figure 4. 20: Seasonal rainfall anomaly (AMJJASO) for the near-future period (2021-2050) under RCP4.5 and RCP8.5 scenarios

4.7 Discussion

Climate change and variability impact on water resource constraints is significantly hampered by a lack of spatially complete and poor climatic data, especially in the Oti River Basin (ORB) which falls part of the Volta Basin in West Africa. As a result, satellite-derived rainfall and temperature estimates such as CHIRPS, among others have become an alternative source for regions with scarce and inaccurate stations data. Earlier studies contrasted the availability of in-situ data to sources of gridded climate data (Awotwi et al., 2021). The results of this study, which compared climate station data from the years 1981-2010 with the ability of the CHIRPS and NASA POWER datasets to simulate the current climate of the ORB, demonstrated that both satellite products can accurately reproduce the ORB's climatic pattern and its peak in August as indicated by studies like Agyekum et al. (2018) and Oguntunde et al. (2020). Generally, after evaluation based on metrics such as Pearson correlation, Nash-Sutcliffe efficiency, Bias and Root-mean-square error, the CHIRPS and NASA POWER products proved their suitability for use in climate analysis over the basin. When CHIRPS rainfall data was compared to station rainfall data, it demonstrated a fair amount of success in reproducing the ORB's rainfall pattern, notwithstanding a few instances when it overestimated or underestimated rainfall. The outcomes are in line with findings from observations made

over Ghana, by Atiah et al. (2019) and Larbi et al. (2018), and observations made over Burkina Faso, West Africa by Dembélé and Zwart (2016). These findings show that CHIRPS is proficient in representing rainfall patterns in the ORB, which is mostly due to the benefit it derives from combining a variety of input data and the high-resolution climatology it enjoys (Atiah et al., 2020; Cohen et al., 2012; Gebrechorkos et al., 2018). Similarly, comparing NASA POWER data with station data for the study period, through evaluation metrics such as Pearson correlation, Bias and Root-mean-square error, showed a good agreement between them and could replicate the climate pattern in the basin. Previous studies such as Joseph et al. (2020), Larbi et al. (2018) and Lizumi et al. (2014) have applied NASA POWER datasets in the region and confirmed its universal conformity with ground data and can be used for further studies.

The analysis of annual rainfall indicated that the yearly precipitation quantity in the basin was between 783.4 mm/yr and 1,464.8 mm/yr during the historical, and between 1,105.5 mm/yr and 610.7 mm/yr for the simulated historical period. In the near-future mean annual rainfall amount would range from 640.2 mm/yr to 1,408.3 mm/yr under RCP4.5 scenario whereas that of RCP8.5 would range from 1027.9 mm/yr to 1287.1 mm/yr. The results of this analysis are consistent with the study of Yeboah et al. (2022), which found that annual precipitation in the Volta Basin is anticipated to decrease for the near future (the 2020s), the mid-century (2050s), and the long future (the 2100s) under RCP4.5 and 8.5 (2080s). The West African subregion's rainfed farming may be seriously jeopardized (Owusu & Waylen, 2009). Additionally, Lare & Nicholson (1994) noted how ecosystems could be impacted by insufficient large-scale precipitation, as demonstrated at the locations. The anticipated decline might severely impact the climate-sensitive activities such as agricultural planning (both arable and livestock) and farming output. Unusual rainfall patterns might have an influence on crop cultivation and result in harvest losses because rainfall is a key climatic factor for agricultural productivity Sharma et al. (2022). A decline in the supply of basin-scale irrigation due to freshwater deficit might have disastrous effects on sustainable farming (Sylla et al., 2018), and hence pose major danger to West Africa's food and economic security. Given that access to fresh water is essential to the economic and social growth of the countries that border the basin, it is crucial that existing adaptation strategies be reviewed to ensure that the anticipated changes do not impede the economies of surrounding populations.

With regards to seasonal rainfall (AMJJASO) in the basin, it was revealed that mean rainfall during the rainy season varied between 778.1 mm/yr and 1,324.5 mm/yr during the historical period, and between 608.4 mm/yr and 1,066.6 mm/yr for the simulated historical. In the near-future, the rainfall amount would range from 637.1 mm/yr to 1,350.4 mm/yr under RCP4.5 scenario, and from 753.9 mm/yr to 1,231.6 mm/yr under RCP8.5 scenario. In their study, Agyekum et al. (2018) found a significant decreasing trend in rainy seasonal rainfall with a magnitude of 1.58 mm per season over the study period 1950-2004 in the basin. Contrary to their study, this study showed a non-significant increasing trend during the period 1981-2010 with a magnitude of 5.91 mm per season. One may anticipate a potential impact of this season's rainfall on its discharges given the expected drop in rainfall during the rainy season (Ebodé et al., 2022). As rainfall is a major influencing factor for agricultural production in the Oti River basin, the projected decline in rainfall during the rainy season period poses serious threats to the sector. This change in rainfall, would pose large risks to food security especially in the basin-dependent countries whose economy depends on the basin. Given that the food need in Africa is anticipated to grow by a staggering fivefold by 2050, the persistent hunger may further worsen in the long term (Sultan & Gaetani, 2016).

The analyses of rainfall onset in the basin showed that mean onset of rainfall which used to occur in 128 days (8 May) during the historical period, and 149 days (29 May) for the simulated historical is now projected to occur in 144 days (24 May) under the RCP4.5 scenario, and in 143 days (23 May) under the RCP8.5 scenario in the basin. The findings fall within the results of Dieng et al. (2018) where the recorded mean rainfall onset ranged between 100 to 175 days for the period (1981-2010) over the Savanna region in West Africa. Additionally, the findings for the future period are in agreement with van de Giesen et al. (2010) who projected a forward shift in rainfall onset for 2030-2039 in the basin, and they indicated this forward shift as from April towards May. Thus, showing that farmers now plant 10-20 days later than previously. In addition, a forward shift in rainfall onset has also been projected by Lacombe et al. (2012), Laux et al. (2008) and Jung & Kunstmann (2007). On-time preparation of agricultural land, mobilization of seeds/crops, labor, and equipment will all benefit from accurate onset time predictions, as will the consequences of planting/sowing too early or too late (Omotosho et al., 2000). The late onset of rain in the basin raises concern as this could have severe consequences on the performance of agriculture and water resources in the basin. The late onset of rains will translate into short length of the rainy season, thereby allowing only crops with short growing periods to be cultivated yearly (Ocen et al., 2021).

Stations like GRID1 to GRID9, Tenkodogo and Fada in the upper basin are mostly likely to experience worsened conditions of water scarcity and food insecurity as these areas already faces such situations (Diasso & Abiodun, 2017). Hallegatte & Rozenberg (2017) reported that changes in climate will intensify insecurity in many semi-arid areas, and this effect will manifest itself through decreases in agricultural productivity, price shifts, and extreme climatic occurrences. The timing of rainfall onset is crucial especially for the determination of planting dates in agriculture and hence a late onset could delay planting activities like tillage operation (Mounkaila et al., 2015; Wakjira et al., 2021). To offset the effect of the late onset of rainfall on rainfed agriculture, farmers will need to employ additional coping techniques, such as developing water-efficient agricultural varieties and minimizing non-productive rainwater deficits (Porkka et al., 2021).

The analyses of rainfall cessation in the basin indicated that mean rainfall cessation which used to occur in 302 days (29 Oct) during the historical period, and 281 days (8 Oct) during the simulated historical is now expected to occur in 280 days (7 Oct) under both the RCP4.5 and the RCP8.5 scenarios in the basin. Additionally, increased evaporation can increase the loss of soil moisture required by crops for growth (Batisani & Yarnal, 2010). According to Oruonye et al. (2016), in the tropics, efficient agricultural production is linked to the commencement and end of the rainy season, as well as its variability. As has been noted elsewhere, the early cessation witnessed in the basin could result in low yields of commonly planted crops like maize (Lala et al., 2021; Mosunmola et al., 2020). For example, for optimal yield, a crop like maize requires 500 to 900 mm of uniformly distributed rainfall. As a result, the projected early cessation could result in a moisture shortage, affecting the ideal maturity (Ikpe et al., 2016). Also, early cessations may cause cereal stuffing to be disrupted, limiting production, while late cessations may cause harvesting to be delayed, resulting in higher pre-harvest losses and infections of aflatoxins-producing moulds (Atiah et al., 2021). The livelihood and economy of basin-dependent countries may be jeopardized by early rainfall cessation as crop growth seasons will be cut short due to the early termination, resulting in crops failing to reach functional maturity. The dependence on crop farming for a living may transition into mixed-breed livestock-based farming for those households who obtain their survival from crop-based agriculture (UN, 2020).

The investigation of length of the rainy season (LRS) in the basin showed that mean LRS which used to last for 173 days during the historical period, and 132 days for the simulated

historical is now anticipated to decrease to about 136 days under the RCP4.5 scenario and 137 days under the RCP8.5 scenario in the basin. Thornton et al. (2006), also maintains that depending on the emission scenario and climate model used, Africa, particularly semi-arid areas, might see a 20% decline in LRS by 2050 or more. The predicted decrease in length of the rainy season is evidence of the projected delay in rainfall onset in the basin, and this can impact the overall agricultural process in the production of food crops (Makondo & Thomas, 2020). The shorter LRS projected in the basin could lead to manifestation of long periods of droughts thereby threatening the source of livelihood of the basin-dependent communities. A longer LRS, on the other hand, indicates a favorable contribution to crop yield (Mosunmola et al., 2020). A good understanding of the date of rainfall cessation, enables the prediction of the length of the rainy season, which is most relevant for crop variety selection, crop matching, and cropping sequences (Omotosho et al., 2000). The length of the rainy season is such an important indicator of changes in rainfall volumes, patterns, and temperature (Thornton et al. 2006), hence the observed large decrease in LRS across the basin requires immediate attention.

Regarding the number of wet days (NWD) in the basin, it was revealed that mean wet days was 95 days and 171 days for the historical and simulated historical periods respectively, and that in the near-future mean number of wet days would be around 175 days under both RCP4.5 and RCP8.5 scenarios. Generally, it was observed that the NWD reduced from the lower basin towards the upper basin in the historical period. However, NWD in the lower basin would be more and would decrease from the upper basin downward the lower basin in the near-future period under both RCP4.5 and RCP8.5 scenarios. This might be as a result of the lower basin's proximity to the Volta Lake, which increases rainfall in the region (Jiang, 2003; Roe, 2005). This has been validated by Nicholson (2009), demonstrating the impact of both local-scale (like orography) and large-scale (like atmospheric circulation; convergence and divergence) elements on the NWD. A decrease in the NWD, which could lead to prolonged periods of drought, is considered one of the region's major disasters (Conway, 2008; Sokona & Denton, 2001) while an upsurge could lead to floods (Agyekum et al., 2022). The findings could be that the model tends to be relatively weak in representing the wet days in the basin. The anticipated general increase in the wet days alongside the anticipated decline in annual rainfall is contrary to the findings of Polade et al. (2014). According to Maranan et al. (2019), Sall et al. (2007) and Zhou & Wang (2006), the multi-model mean ensemble may have overemphasized the influence of the summer monsoon flow, which is why it provided a

poor approximation of the spatial distribution of the NWD. It could also be that rainfall may have decreased proportion of total rainfall occurring on wet days (Gunawardhana et al., 2018).

Results from the number of dry days in the basin, showed that mean number of dry days was 270 days and 194 days for the historical and simulated historical periods respectively, and that in the near-future mean number of dry days would be around 189 days under RCP4.5 scenario and 190 days under RCP8.5 scenario. Broadly, NDD was observed to be longer in the upper basin and shorter in the lower basin in the historical period and this seemed extensive largely because of the historic drought conditions of 1983 experienced in the basin and in the region between 1961 and 2005 (Kasei et al., 2010). The findings depicts that the multi-model mean ensemble could not relatively represent the number of dry days well in the basin. The maritime winds' impact and the convergence over the basin may be highlighted by the model's underestimation of the NDD (Agyekum et al., 2022).

Analysis of rainfall anomaly in the basin during the historical period (1981-2010) showed that the basin experienced very wet conditions in the year 1994 with a high positive anomaly of +1.66, and an extremely dry conditions in the year 1983 with a high negative anomaly of -2.29 during the rainy season (AMJJASO). The very wet condition exposed in the basin is confirmed by the study of Agyekum et al. (2022) who evaluated 41 CMIP6 models in simulating extreme precipitation events over the basin for 1985-2014. In their study, they found that the very wet days condition experienced in the basin contributed a mean value of 31% of the annual rainfall received over the basin. The extremely dry condition in the basin is consistent with a research conducted by Kasei et al. (2010) that determined 1983 to be the driest year in the basin. A severe drought affected more than 90% of the basin, and a mild drought existed before 1982. According to the findings, there were significant negative anomalies in the early 1980s. This study links the 1961–2005 West African drought to the previous drought in the basin (Kasei et al., 2010). This resulted in the loss of lives and farm animals in desertlike areas of Burkina Faso (Dembélé & Zwart 2016).

The seasonal rainfall anomaly conducted for the rainy season period for the future period exposed a pronounced negative anomaly (-2.31) in the year 2027 while a high positive anomaly (+2.13) is anticipated in 2037. This discloses that after ten years of experiencing an extremely dry condition, the basin would experience an extremely wet condition in the year 2037 during the wet season period and under the RCP4.5 scenario. Similarly, under the RCP8.5 scenario in the wet season, the basin is projected to record its highest positive

anomaly (+1.77) in the year 2028 indicating a very wet situation, and its highest negative anomaly (-2.49) in the year 2041 also indicating an extremely dry situation in the basin. The anticipated very wet and extremely wet years might result in catastrophic floods, that might endanger lives and valuables, and disruptions in hydroelectric power generation (Agyekum et al., 2022; Klassou & Komi, 2021; Wei et al., 2020). The moderately dry, severely dry, and extremely dry periods in the watershed may contribute to water shortages. Extended dry periods triggered by climate change lead to water deficit, which has a negative impact on crop growth and people's welfare (Zhang et al., 2015).

Chapter 5: Projected Changes in Intraseasonal Rainfall Variability Indicators

This chapter discusses the anticipated changes in annual rainfall, seasonal rainfall, rainfall onset, cessation and length of rainy season, and the number of wet and dry days in the Oti basin.

5.1 Predicted changes in annual rainfall

Table 5.1 presents the projected changes in annual rainfall over the basin during the near-future (2021-2050) relative to the historical period (1981-2010). The analyses revealed that the decrease in mean annual rainfall for the entire basin would be about 103.6mm/yr and 45.9mm/yr in the near-future under RCP4.5 and RCP8.5 scenarios respectively. Under both scenarios, the maximum decrease in annual rainfall is projected to occur at Niamtougou. Although a general decrease is predicted for the whole basin, stations like GRID1, GRID2, GRID5, GRID6, GRID7, GRID10, GRID11, GRID14, Fada, Mango, Tenkodogo and Sokode is projected to experience slight increase in annual rainfall under the RCP8.5 scenario while Sokode would record a slight increase under the RCP4.5 scenario. Generally, it is observed that annual rainfall in the upper basin would greatly experience rainfall decrease, with just a little portion of the middle basin experiencing a severe rainfall decline in rainfall and although the lower basin would also record a decline, this would be moderate under the RCP4.5 scenario. With respect to the RCP8.5 scenario, reveals that annual rainfall decline would be less in the upper basin with moderate decline in lower basin and severe decline in just a small portion of the middle basin (Figure 5.1).

Table 5. 1: Changes projected for mean annual rainfall [in mm] in the near-future (2021-2050)

Stations	Observed [1981-2010]	RCP4.5 [2021-2050]	Change	RCP8.5 [2021-2050]	Change
GRID1	792.9	684.2	-108.7	834.3	41.4
GRID2	815.6	693.4	-122.2	839.2	23.6
GRID3	783.4	640.2	-143.2	758.4	-25
GRID4	853.6	712.7	-141	835.9	-17.7
GRID5	891.6	774.7	-116.8	922	30.5
GRID6	877.2	773.1	-104.1	896.1	18.9
GRID7	886	792	-94	898.7	12.7
GRID8	928.6	829.3	-99.3	915.9	-12.7
GRID9	974.9	866.8	-108.2	927.5	-47.4
GRID10	941.8	885.8	-56	1006.3	64.5
GRID11	943.7	872.7	-71.1	957.5	13.8
GRID12	1074.7	932.2	-142.6	1006.6	-68.1
GRID13	982.5	845.9	-136.6	914.2	-68.3
GRID14	1101.5	1038	-63.4	1117.4	16
GRID15	1200.3	1108.6	-91.7	1124.9	-75.3
GRID16	1239.3	1174.1	-65.2	1193.7	-45.7
GRID17	1330.6	1279	-51.6	1266.1	-64.5
GRID18	1363.5	1164.4	-199.1	1128	-235.5
GRID19	1360.3	1295.4	-64.9	1227.5	-132.9
GRID20	1464.8	1293.5	-171.3	1212.1	-252.7
Natitingou	1187.5	1045.2	-142.3	1091.7	-95.7
Fada	819.4	688.9	-130.5	852.2	32.8
Tenkodogo	819	740.3	-78.7	887.4	68.4
Kete-Krachi	1358.6	1332.6	-26	1249.1	-109.5
Yendi	1210.1	1153.2	-56.9	1148.2	-61.9
Dapaong	1061.5	894.7	-166.8	1012.5	-49
Kara	1289.1	1134.2	-154.9	1149	-140
Mango	1045.2	986.1	-59.1	1096.5	51.3
Niamtougou	1361.9	1067.7	-294.2	1082.3	-279.6
Sokode	1266.8	1408.3	141.5	1287.1	20.3
Basin	1073.8	970.2	-103.6	1027.9	-45.9

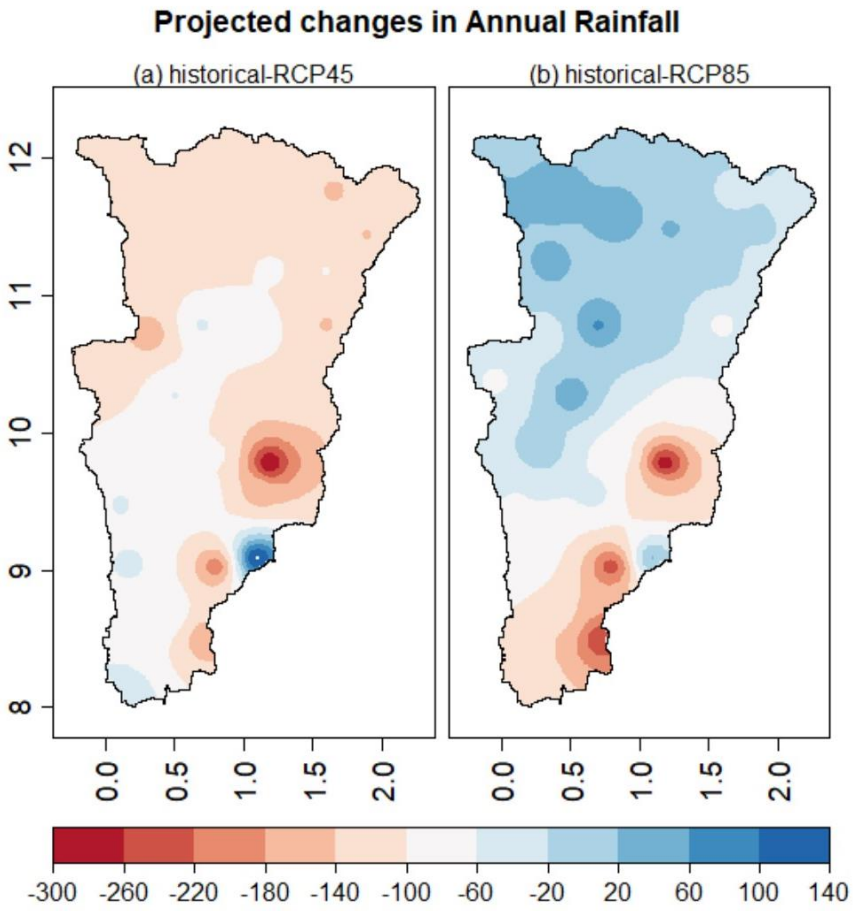

Figure 5. 1: Projected changes in annual rainfall (mm/yr) in Oti basin in the future period (2021-2050) under (a) RCP4.5 and (b) RCP8.5 scenarios

5.2 Seasonal rainfall (AMJJASO)

Table 5.2 illustrates the changes predicted for seasonal (AMJJASO) rainfall in the near-future. From the analysis, it is projected that the mean yearly rainfall for the entire basin during the rainy season would decrease by about 90.8 mm/yr and 34.6 mm/yr under RCP4.5 and RCP8.5 scenarios respectively. With respect to the RCP4.5 scenario, rainy season period would experience a decrease in rainfall amount in the entire basin. Very small portions of the lower basin are however likely to experience a slight recovery up to about 153.8mm/yr, with small portions of the middle basin also experiencing severe decline, up to about 265mm/yr decrease. The RCP8.5 scenario also projects an overall decline in rainfall amount, with very small portions of the middle and upper basin having a little recovery up to about 69.7mm/yr. Small portions of the middle basin extending to the lower basin is also anticipated to have a severe decline up to about 252.3mm/yr of rainfall (Figure 5.2).

Table 5. 2: Changes predicted for mean seasonal (AMJJASO) [in mm] rainfall in the near-future (2021-2050)

Station	Observed [1981-2010]	RCP4.5 [2021-2050]	Change	RCP8.5 [2021-2050]	Change
GRID1	788.3	680.3	-107.9	829.7	41.4
GRID2	809.7	689.4	-120.3	834.1	24.4
GRID3	778.1	637.1	-141.0	753.9	-24.1
GRID4	847.4	708.3	-139.1	830.5	-16.9
GRID5	882.0	767.5	-114.5	912.4	30.4
GRID6	869.1	768.2	-100.9	888.2	19.1
GRID7	879.8	787.3	-92.5	892.0	12.2
GRID8	917.7	823.5	-94.2	907.8	-9.9
GRID9	965.5	859.4	-106.1	919.2	-46.3
GRID10	930.5	875.0	-55.6	993.7	63.2
GRID11	932.3	862.6	-69.8	945.2	12.9
GRID12	1055.4	920.0	-135.3	992.5	-62.9
GRID13	963.0	833.7	-129.3	899.6	-63.4
GRID14	1071.6	1013.4	-58.2	1088.9	17.3
GRID15	1163.6	1079.7	-83.9	1093.5	-70.1
GRID16	1189.6	1132.0	-57.6	1149.6	-40.0
GRID17	1264.4	1225.0	-39.4	1211.3	-53.1
GRID18	1281.3	1124.0	-157.3	1086.9	-194.5
GRID19	1274.4	1239.7	-34.6	1171.3	-103.1
GRID20	1324.5	1227.9	-96.7	1147.6	-177.0
Natitingou	1145.6	1026.5	-119.1	1071.2	-74.5
Fada	808.7	684.7	-124.0	846.9	38.3
Tenkodogo	809.5	732.9	-76.7	879.2	69.7
Kete-Krachi	1273.3	1282.7	9.4	1198.9	-74.4
Yendi	1146.7	1105.7	-41.0	1099.8	-46.9
Dapaong	1037.2	880.1	-157.0	995.4	-41.8
Kara	1233.2	1107.9	-125.3	1120.8	-112.4
Mango	1013.0	966.8	-46.3	1074.7	61.6
Niamtougou	1304.9	1039.9	-265.0	1052.6	-252.3
Sokode	1196.6	1350.4	153.8	1231.6	35.0
Basin	1038.6	947.7	-90.8	1004.0	-34.6

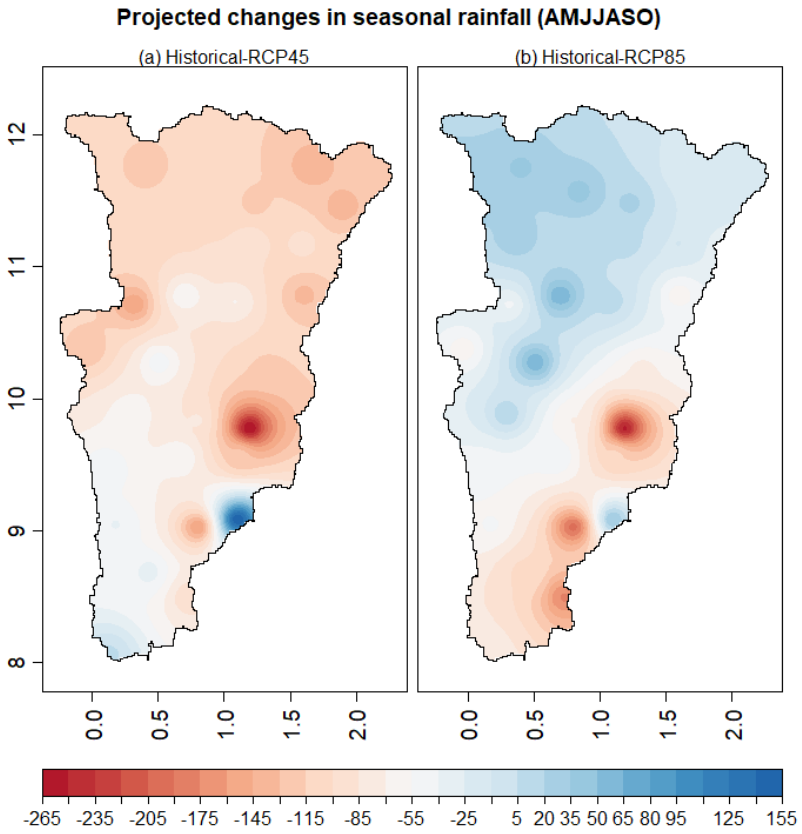

Figure 5. 2: Projected changes in seasonal rainfall (AMJJASO) (mm/yr) in the Oti basin in the future (2021-2050) under (a) RCP4.5 and (b) RCP8.5 scenarios

5.3 Rainfall onset

The changes projected for the near-future (2021-2050) are presented in Table 5.4. It is observed that the onset of rainfall is projected to delay in the future period and under both scenarios. The mean onset of rain is projected to delay by about 16 days under RCP4.5 and 15 days under RCP8.5 scenarios. Although a general delay is predicted for both RCPs, stations like Kete-Krachi, Mango and Sokode are anticipated to experience earlier start of rains by 15, 6 and 5 days respectively under the RCP4.5 scenario whiles the RCP8.5 scenario also project earlier start for Kete-Krachi (8 days) and Mango (3 days). For RCP4.5 and the RCP8.5 scenario, the impacts would be more dramatic overall, but especially in the lower basin. This means that the lower basin would experience a more delayed onset under RCP4.5 and a more delayed onset for the entire basin under the RCP8.5 scenario (Figure 5.3).

Table 5. 3: Changes projected for rainfall onset [in days] in the near-future (2021-2050)

Stations	Observed [1981-2010]	RCP4.5 [2021-2050]	Change	RCP8.5 [2021-2050]	Change
GRID1	145	168	23	159	14
GRID2	146	168	22	159	13
GRID3	145	178	34	163	18
GRID4	145	170	25	155	10
GRID5	138	161	23	154	15
GRID6	139	164	26	152	13
GRID7	140	167	27	160	20
GRID8	138	156	18	149	11
GRID9	135	146	11	149	14
GRID10	132	149	16	149	16
GRID11	135	151	16	153	18
GRID12	127	153	25	151	24
GRID13	124	153	29	145	21
GRID14	116	136	19	143	27
GRID15	117	130	13	135	18
GRID16	107	122	15	129	22
GRID17	103	120	17	125	22
GRID18	102	124	22	128	26
GRID19	101	106	5	119	18
GRID20	98	115	17	114	16
Natitingou	124	134	10	138	14
Fada	152	169	17	160	8
Tenkodogo	143	163	20	159	16
Kete-Krachi	129	114	-15	120	-8
Yendi	124	132	8	138	14
Dapaong	138	160	21	159	20
Kara	123	127	4	132	9
Mango	146	140	-6	143	-3
Niamtougou	118	140	21	140	22
Sokode	113	109	-5	118	4
Basin	128	144	16	143	15

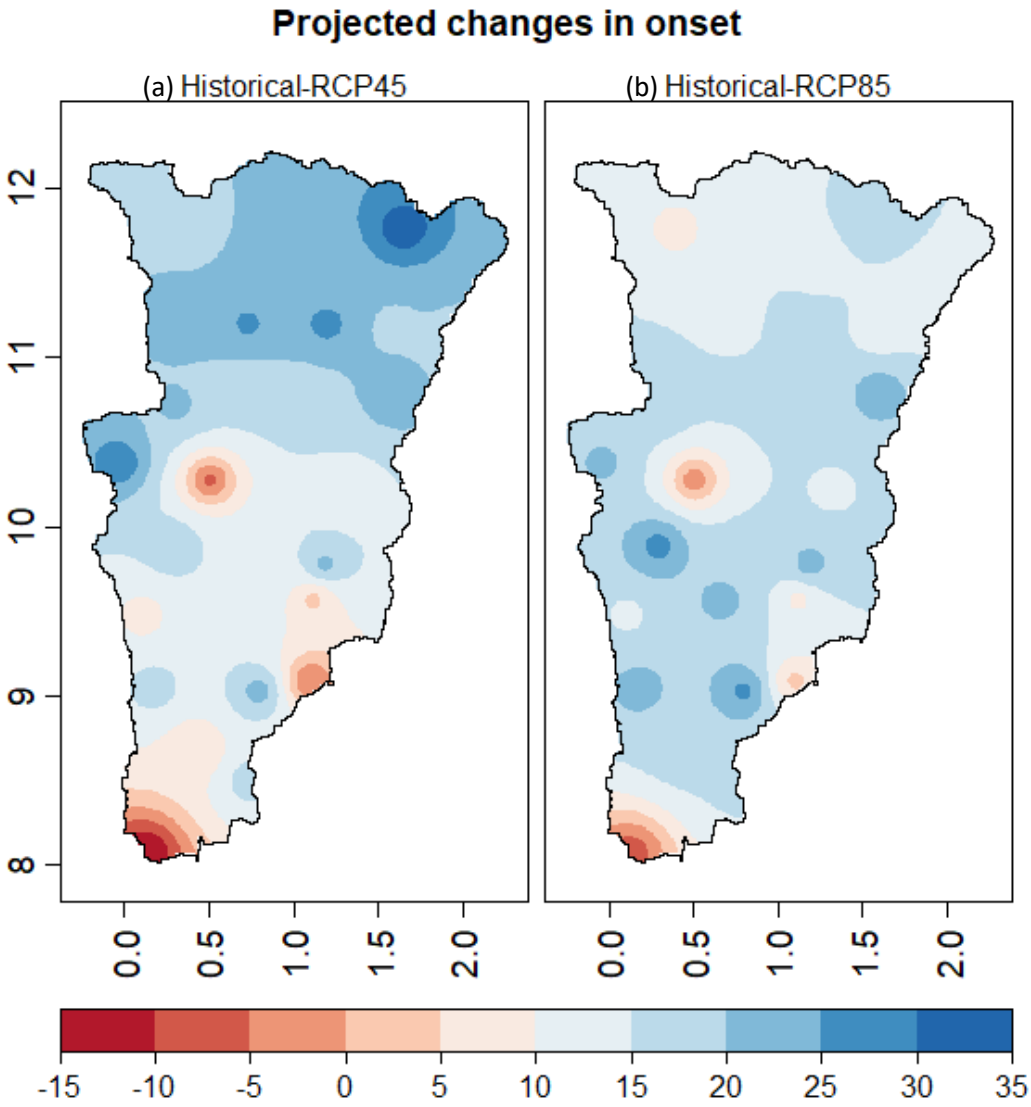

Figure 5. 3: Projected changes in rainfall onset (days) in Oti basin in the future (2021-2050) under (a) RCP4.5 and (b) RCP8.5 scenarios

5.5 Rainfall cessation

Table 5.4 presents the anticipated changes in rainfall cessation in the near-future (2021-250). From the results, the mean cessation is projected to decrease by about 21 days under both RCP4.5 and RCP8.5 scenarios. It is observed that all stations in the basin are expected to experience early termination of rains. Under the RCP4.5, GRID18 is anticipated to experience the earliest termination by about 45 days, whereas GRID5 and GRID3 would experience the least by about 6 days. Under the RCP8.5 scenario however, maximum decrease in cessation would be around 48 days at GRID20, while the least decrease is expected to be around 5 days at GRID2, GRID3 and GRID4. In other words, the basin would experience a shorter rainy

season with the change expected to be more pronounced in the lower basin under RCP4.5, and in the entire basin under the RCP8.5 scenario (Figure 5.4).

Table 5. 4: Projected changes in rainfall cessation [in days] in the near-future (2021-2050)

Stations	Observed [1981-2010]	RCP4.5 [2021-2050]	Change	RCP8.5 [2021-2050]	Change
GRID1	291	275	-16	279	-12
GRID2	282	275	-7	277	-5
GRID3	281	275	-6	275	-5
GRID4	282	276	-7	278	-5
GRID5	283	278	-6	276	-7
GRID6	288	277	-11	277	-11
GRID7	283	276	-7	277	-6
GRID8	285	275	-10	278	-7
GRID9	285	275	-10	278	-7
GRID10	291	279	-12	277	-14
GRID11	289	278	-11	276	-13
GRID12	296	277	-19	278	-19
GRID13	297	278	-19	279	-18
GRID14	307	286	-21	283	-23
GRID15	306	281	-26	282	-24
GRID16	316	285	-32	285	-32
GRID17	323	288	-36	292	-31
GRID18	328	284	-45	281	-47
GRID19	332	290	-42	291	-41
GRID20	338	294	-43	290	-48
Natitingou	303	277	-26	279	-24
Fada	295	275	-19	277	-17
Tenkodogo	284	276	-8	277	-7
Kete-Krachi	328	299	-29	294	-35
Yendi	313	281	-32	280	-32
Dapaong	300	278	-21	278	-22
Kara	314	278	-36	279	-35
Mango	298	279	-18	279	-19
Niamtougou	316	278	-38	279	-37
Sokode	314	282	-31	280	-34
Basin	302	280	-21	280	-21

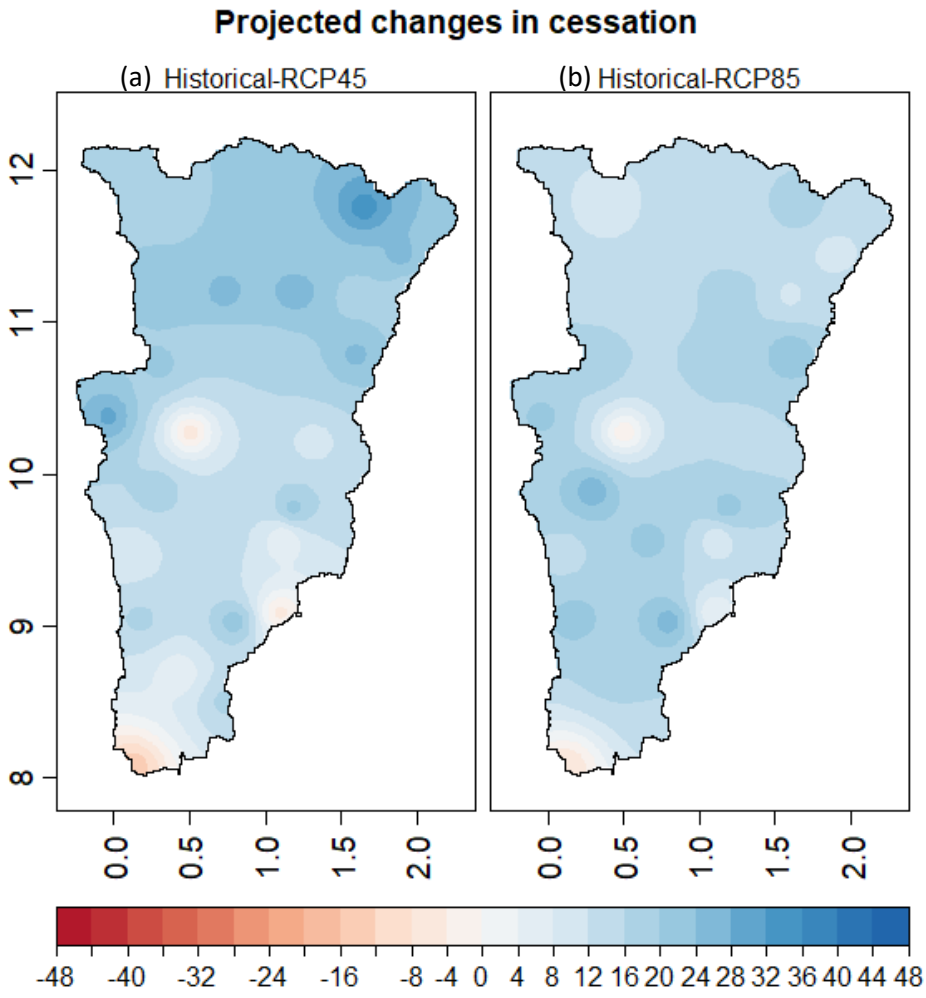

Figure 5. 4: Projected changes in cessation (days) in Oti basin in the future (2021-2050) under (a) RCP4.5 and (b) RCP8.5 scenarios

5.5 Length of the rainy season

Table 5.5 shows the summary results of projected changes in the length of the rainy season for the near-future (2021-2050). The findings reveal a drop in mean LRS days by almost 37 days and about 36 days under RCP4.5 and RCP8.5 scenarios respectively, indicating a shorter rainy season duration in the basin (Figure 5.5). Under the RCP4.5 scenario, GRID18 is anticipated to record the highest reduction in the length of the rainy season of about 67 days whereas the least is expected to occur at Mango (about 13 days). The RCP8.5 scenario also projects the maximum reduction in LRS to occur at GRID18 by about 73 days with the minimum reduction anticipated to be about 15 days at GRID4.

Table 5. 5: Projected changes in length of rainy season [in days] for the near-future (2021-2050)

Stations	Observed [1981-2010]	RCP4.5 [2021-2050]	Change	RCP8.5 [2021-2050]	Change
GRID1	146	107	-39	120	-26
GRID2	136	107	-29	118	-18
GRID3	136	97	-40	113	-24
GRID4	138	106	-32	123	-15
GRID5	145	116	-29	123	-22
GRID6	149	112	-37	125	-24
GRID7	143	109	-34	117	-26
GRID8	148	120	-28	129	-18
GRID9	150	129	-21	129	-21
GRID10	158	131	-28	129	-30
GRID11	155	127	-27	123	-31
GRID12	169	125	-44	126	-42
GRID13	173	124	-49	135	-38
GRID14	190	150	-40	140	-50
GRID15	189	151	-39	147	-43
GRID16	209	163	-46	156	-53
GRID17	220	167	-53	167	-54
GRID18	226	160	-67	153	-73
GRID19	231	184	-47	172	-59
GRID20	239	179	-60	176	-63
Natitingou	179	143	-36	141	-38
Fada	143	106	-37	117	-26
Tenkodogo	142	114	-28	119	-23
Kete-Krachi	200	185	-15	173	-26
Yendi	189	149	-40	142	-47
Dapaong	161	119	-43	119	-42
Kara	191	151	-40	147	-44
Mango	152	139	-13	136	-16
Niamtougou	198	138	-59	139	-59
Sokode	201	174	-27	162	-38
Basin	173	136	-37	137	-36

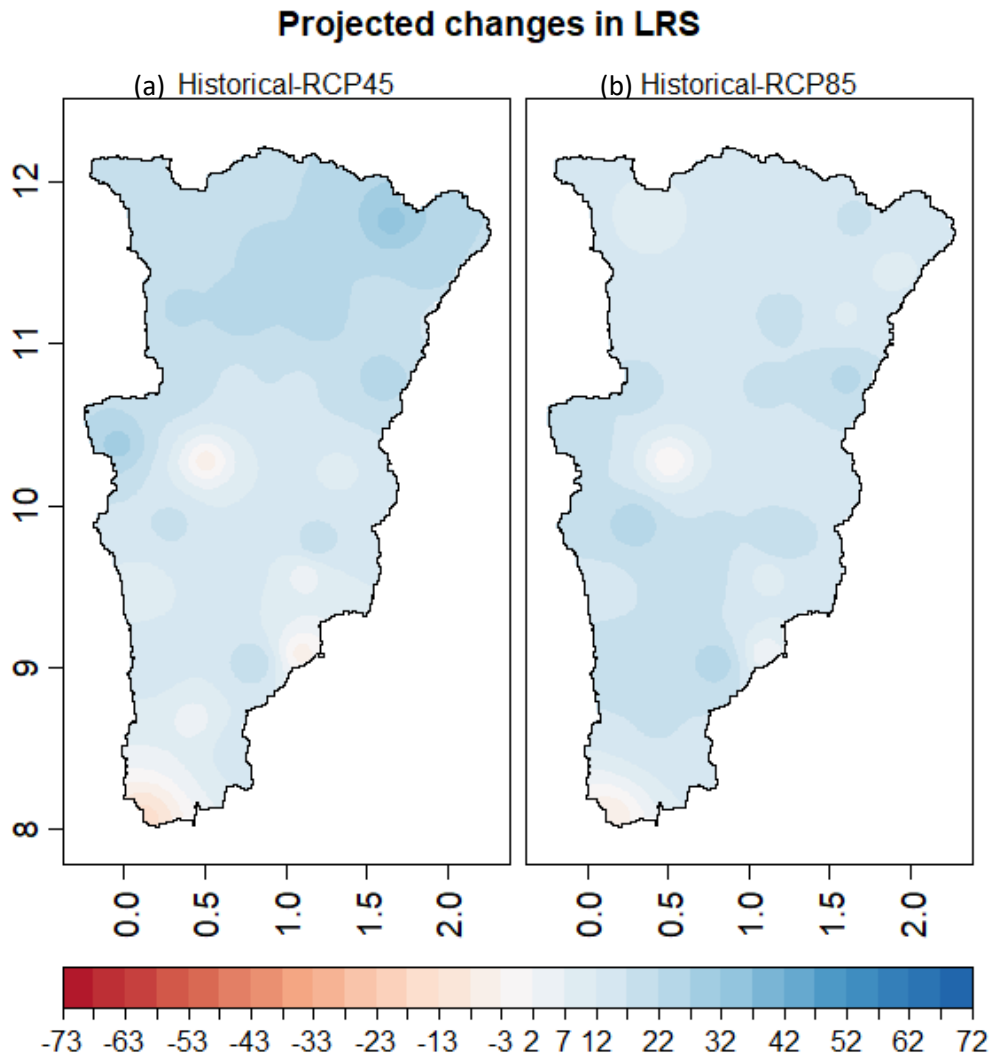

Figure 5. 5: Projected changes in LRS (days) in Oti basin in the future (2021-2050) under (a) RCP4.5 and (b) RCP8.5 scenarios

5.6 Number of wet days

Results for the projected changes in number of wet days are shown in Table 5.6. The results reveal a decrease in wet days in most parts of the basin with few portions in the basin showing a slight increase in wet days. For the entire basin, the mean wet days showed an increase of about 80 days for both RCP4.5 and RCP8.5 scenarios, thus revealing that the models tend to be relatively weak in representing the wet days especially in the parts of the basin that showed a slight increase in the wet days (Figure 5.6).

Table 5. 6: Changes projected for number of wet days [in days] in the near-future (2021-2050)

Stations	Observed [1981-2010]	RCP4.5 [2021-2050]	Change	RCP8.5 [2021-2050]	Change
GRID1	78	141	63	144	66
GRID2	82	143	61	146	64
GRID3	78	135	57	139	61
GRID4	84	145	61	148	64
GRID5	83	152	69	154	71
GRID6	85	154	69	155	70
GRID7	87	153	66	154	67
GRID8	90	155	65	154	64
GRID9	91	155	64	156	65
GRID10	92	167	75	169	77
GRID11	100	166	66	165	65
GRID12	102	170	68	170	68
GRID13	98	170	72	170	72
GRID14	106	190	84	190	84
GRID15	119	196	77	195	76
GRID16	126	206	80	205	79
GRID17	123	209	86	208	85
GRID18	131	198	67	197	66
GRID19	133	214	81	214	81
GRID20	135	213	78	210	75
Natitingou	94	185	91	183	89
Fada	66	181	115	145	79
Tenkodogo	82	143	61	147	65
Kete-Krachi	80	211	131	209	129
Yendi	78	199	121	198	120
Dapaong	67	169	102	171	104
Kara	93	193	100	190	97
Mango	69	181	112	182	113
Niamtougou	97	191	94	189	92
Sokode	94	212	118	209	115
Basin	95	175	80	175	80

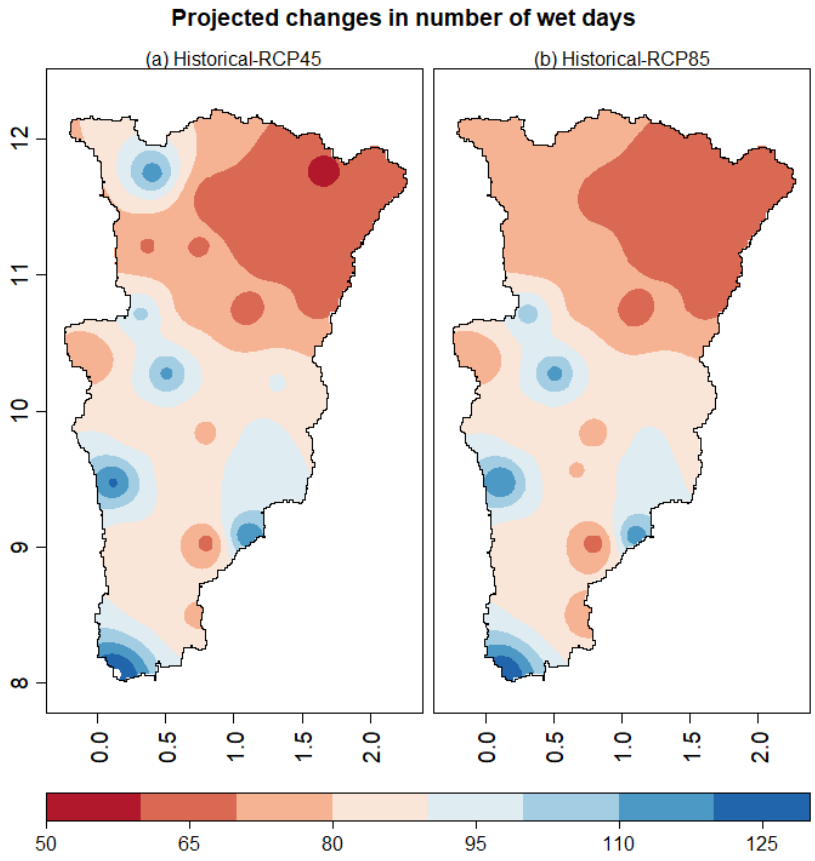

Figure 5. 6: Projected changes in number of wet days in Oti basin in the future (2021-2050) under (a) RCP4.5 and (b) RCP8.5 scenarios

5.7 Number of dry days

Table 5.7 presents the results for projected changes in the number of dry days. The findings reveal an increase in dry days in most parts of the basin with few portions in the basin showing a slight decrease in dry days. For the entire basin, the mean dry days showed a decrease of about 81 days for RCP4.5 scenario and 80 days for RCP8.5 scenario, thus disclosing how weak the model tends to represent the dry days in the basin (Figure 5.7).

Table 5. 7: Changes projected for number of dry days [in days] in the near-future (2021-2050)

Stations	Observed [1981-2010]	RCP4.5 [2021-2050]	Change	RCP8.5 [2021-2050]	Change
GRID1	288	221	-67	221	-67
GRID2	283	219	-64	219	-64
GRID3	287	227	-60	226	-61
GRID4	281	218	-63	217	-64
GRID5	282	211	-71	211	-71
GRID6	280	210	-70	210	-70
GRID7	278	211	-67	211	-67
GRID8	275	209	-66	211	-64
GRID9	274	208	-66	210	-64
GRID10	273	197	-76	196	-77
GRID11	265	198	-67	200	-65
GRID12	263	194	-69	195	-68
GRID13	267	195	-72	195	-72
GRID14	259	175	-84	175	-84
GRID15	246	170	-76	170	-76
GRID16	240	160	-80	160	-80
GRID17	242	157	-85	157	-85
GRID18	234	167	-67	168	-66
GRID19	232	152	-80	151	-81
GRID20	230	153	-77	155	-75
Natitingou	271	180	-91	182	-89
Fada	299	222	-77	220	-79
Tenkodogo	283	219	-64	218	-65
Kete-Krachi	285	155	-130	156	-129
Yendi	287	167	-120	167	-120
Dapaong	298	195	-103	194	-104
Kara	272	173	-99	175	-97
Mango	296	184	-112	183	-113
Niamtougou	268	175	-93	176	-92
Sokode	271	154	-117	156	-115
Basin	270	189	-81	190	-80

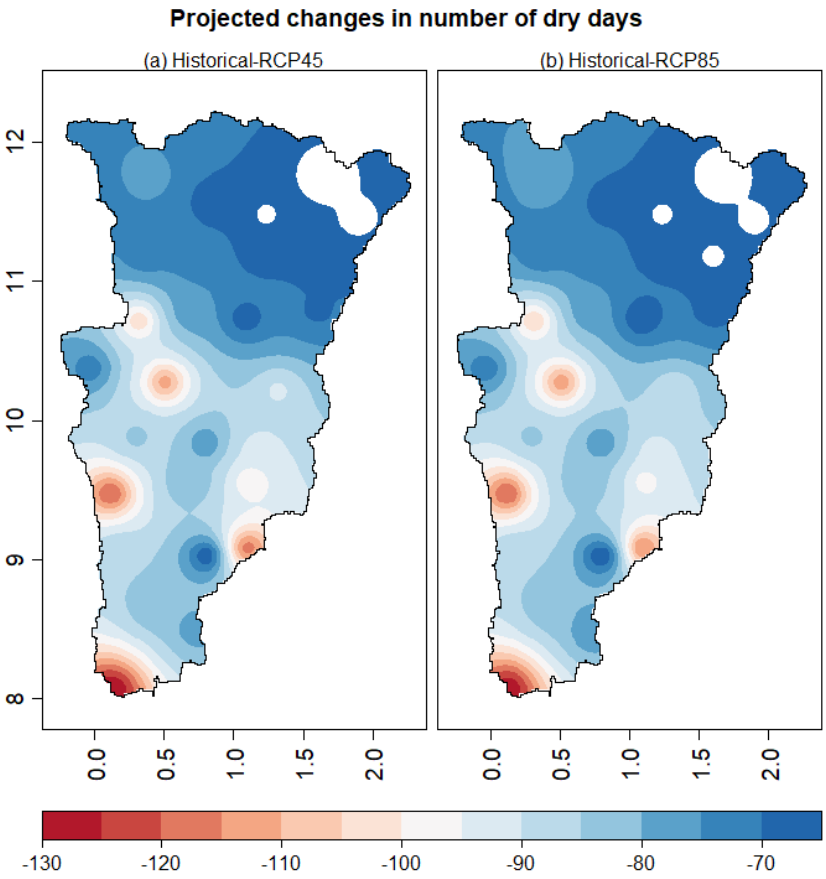

Figure 5. 7: Projected changes in number of dry days in Oti basin in the future (2021-2050) under (a) RCP4.5 and (b) RCP8.5 scenarios

5.9 Discussion

The analysis of projected changes in annual rainfall revealed a future decline in annual rainfall by about 103.6 mm/yr under the RCP4.5 scenarios and by about 45.9 mm/yr under the RCP8.5 scenarios. The results agree with the study of Ekwezuo et al. (2017) who projected a decrease in mean annual rainfall in West Africa over most part of the Guinea Coast under the RCP4.5 scenario for the early Twenty-first century (2010-2035) and the mid Twenty-first century (2040-2065). Although they predicted a decline in rainfall under the RC8.5, they also indicated that some areas in Ghana, Togo, and Benin would experience reasonably stable rainfall, which is in direct contrast to the results of this study. This study found that under the RCP8.5, 7 stations in the upper basin which are also in Burkina Faso (i.e., GRID1, GRID2, GRID5, GRID6 GRID7, Fada, and Tenkodogo), 2 stations in Togo (Mango and Sokode) and 3 stations in the Ghana (GRID10, GRID11 and GRID14) would experience slight increase in their annual rainfall in the range of 12.7 mm/yr to 68.4 mm/yr. These changes predicted under both scenarios, could impact the basin negatively. Obeng-Asiedu (2004) asserts that because

runoff in the basin is very sensitive to rainfall, even slight variations in yearly precipitation can have a significant impact on river flow. Furthermore, predicted changes in rainfall across the basin could limit renewable surface and groundwater resources in basin, increasing demand for water among various sectors Kabir & Golder (2017). The basin's streamflow and water levels could be negatively impacted from the projected decrease. Since rainfall is the primary means of recharging, a decrease in yearly precipitation may indicate a decrease in streamflow in the basin. Already in West Africa, Nicholson & Grist (2001) found that changes in rainfall patterns have influenced runoff in recent years. Mahe et al. (2013) discovered that variations in rainfall have a significant impact on streamflow in West Africa, with a threefold decrease in runoff for every unit decrease in rainfall.

With regards to the seasonal rainfall (AMJJASO), the analysis projected a future decline in annual rainfall by about 90.8 mm/yr under the RCP4.5 and by about 34.6 mm/yr under the RCP8.5 scenarios. Although a decline is projected in the mean rainy season's rainfall under the RCP4.5, the study predicts increase in rainy season's rainfall at 2 stations while under the RCP8.5, an increase is projected for 12 stations. It is important to note that even before the onset of the dry season period, the expected drop in this season's rainfall might lead to a water deficit scenario in the basin (evaporation and soil water reserve). So there is a complete decrease in the amount of rainfall that could result in runoff (Ebodé et al., 2022). Variations in the regional distribution and changing patterns of atmospheric precipitation, which are related to changing climate, may have an impact on the spatial layout of streamflow (Kimaru et al., 2019). This is possible as runoff was found to be particularly responsive to rainfall according to a study on the water balance of the Volta Basin in West Africa (Friesen et al., 2005). The changes observed especially projected decline in mean rainfall in the rainy season under both emission scenarios can be a serious threat to water supplies owing to flooding, which could have an effect on the local inhabitants in the basin.

The projected changes in the onset of rains showed that the mean onset of rainfall would delay by about 16 days under RCP4.5 and 15 days under RCP8.5 scenarios in the entire basin. Despite this projection for the entire basin, both scenarios project earlier start of rains at 3 stations under the RCP4.5 and 2 stations under the RCP8.5 scenarios. The delayed onset anticipated across the entire basin has the tendency to impact the availability of water and its associated hydrological services in the basin. Babalola et al. (2021) stated in their study that a late onset of the rains in the Niger basin would result in a decrease in streamflow volume of

around 39 m^3/s and 40 m^3/s under the RCP4.5 and RCP8.5 scenarios, correspondingly, in the far future (2070–2099). In their investigation, Eisner et al. (2017) also revealed how the Niger basin saw falling discharge at the beginning of the rainy season with a loss of up to 37% under the RCP8.5 scenario.

With regards to cessation of rainfall in the basin, it is anticipated that rainfall would stop early at all the stations in the basin with a mean cessation of about 21 days under both RCP4.5 and RCP8.5 scenarios in the entire. The early cessation means the length of the rainy season in the basin would be shortened by about 37 days and 36 days under RCP4.5 and RCP8.5 scenarios correspondingly. These projections could result in a decreased amount of rainfall in the entire basin and subsequently impact the basin's hydrology. According to Babalola et al. (2021), higher rainfall during the rainy season caused significant increases in streamflow volumes at the Yobe river in Nigeria of roughly +371 m^3/s (+90%) and +191 m^3/s (87%) under RCP4.5 and RCP8.5. Likewise, their research showed that a one-month shift in rainfall start, or a decrease of 32 mm of rain from June to July, transcribed into a decline of 91m^3/s (24%) in streamflow under the RCP8.5 scenarios and a decline of 11 mm rainfall produced a reduction in discharge volume of 40m^3/s (14%) under the RCP4.5 scenarios.

The number of wet days for the entire basin is projected to have slight increase in the number of wet days by a mean of about 80 days for the entire basin whereas the number of dry days would likely decrease by about 81 days (RCP4.5) and 80 days (RCP8.5). In addition, all stations in the basin are anticipated to experience a slight increase in the number of wet days within the range of 57 days to 131 days, with the highest being at Kete-Krachi under the RCP4.5 scenario, and between 61 days and 129 days, under the RCP8.5 scenario. This is possible especially for Kete-Krachi station as it is located adjacent to the Volta Lake (Braimah et al., 2022). The analyses of projected changes in the NWD and NDD in the basin reveals an opposite pattern to the situation where projected decline in mean annual rainfall leads to a decreased NWD and increased NDD paradigm (Polade et al., 2014; Sultan & Gaetani, 2016).

Chapter 6: Intraseasonal Rainfall Variability Impact on Streamflow

This chapter presents the findings obtained from the modelling of streamflow in the Oti basin using HBV model. The results consist of (a) the features of the sub-basins (precipitation and potential evapotranspiration, (b) HBV model calibration and validation, (c) model evaluation and (d) trend analysis for the predicted streamflow under both RCP4.5 and RCP8.5 scenarios and (e) discussion.

6.1 Climate conditions of the sub-basins

Figure 6.1 displays the average yearly precipitation and potential evapotranspiration throughout the historical timespan (1981-2010) in the five sub-basins investigated. The results reveal that during the period 1981-2010, mean annual rainfall and mean annual potential evapotranspiration at Porga were 893.07 mm/yr, and 2369.72 mm/yr respectively. At Arly, mean annual rainfall was 957.96 mm/yr while mean annual potential evapotranspiration was 2411.90 mm/yr. The mean annual rainfall was 1274.67 mm/yr and mean annual potential evapotranspiration was 1914.71 mm/yr at Koumongou. At Sabari, mean annual rainfall and mean annual potential evapotranspiration were 1003.38 mm/yr and 2189.13 mm/yr correspondingly. Saboba, had its mean annual rainfall to be 983.26 mm/yr while its mean annual potential evapotranspiration was 2189.14 mm/yr. With regards to land use in the sub-basins, Porga is 100% savanna. Arly is dominated by savanna with very few areas being barren, grassland and cropland. At Koumongou, this vegetation is largely savanna, with very few areas being grassland, cropland and shrubland. The vegetation types in the sub-basins are described in Table 6.1.

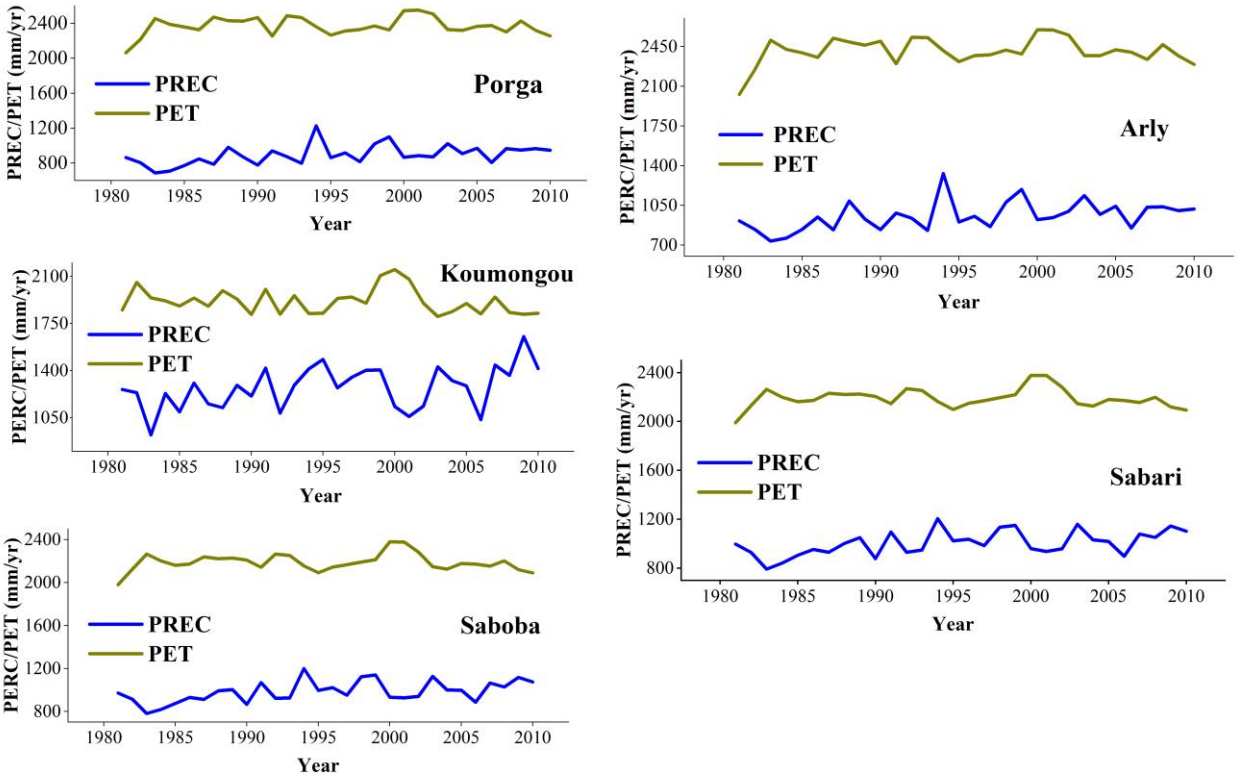

Figure 6. 1: Precipitation and potential evapotranspiration in the sub-basins (1981-2010)

Table 6. 1: Characteristics of the investigated sub-basins

	Sub-basins				
Hydrological variables	**Porga**	**Arly**	**Koumongou**	**Sabari**	**Saboba**
Mean precipitation (mm/yr)	893.07	957.96	1274.67	1003.38	983.26
Mean potential evapotranspiration (mm/yr)	2369.72	2411.9	1914.71	2189.13	2189.14
Mean discharge (m^3/s)	9693.9	788.9	13180.1	67496.4	57772.3
Topography					
Area (sqkm)	23134.6	6487.9	6684.92	60184.1	54039
Minimum elevation (m)	129	159	105	53	90
Maximum elevation (m)	581	643	668	463	209
Mean elevation (m)	212.3	307.7	323.8	155.5	140.1
Slope (degrees)	2.0	3.3	4.6	2.0	1.6
Mean Aridity Index	0.38	0.39	0.67	0.46	0.45
Land use					
Savanna (%)	100	99.6	98.2	100	100
Barren/sparsely vegetated (%)	-	0.18	-	-	-
Grassland (%)	-	0.17	1.45	-	-
Cropland/woodland mosaic (%)	-	0.02	0.24	-	-
Shrubland (%)	-	-	0.1	-	-

NB: Discharge data span from 1981-1991; Precipitation, and potential evapotranspiration data (1981-2010)

Figure 6.2 illustrates the aridity levels of the sub-basins under investigation. The semi-arid, dry sub-humid, and humid zones are the basin's three predominant climatic conditions, according to the aridity index (AI) graph. The distribution pattern of aridity in the sub-basins is consistent with the gradient of aridity found in the Volta basin's eco-climatic divisions (Dembélé et al., 2022). The semi-arid zone's AI ranges from 0.38 to 0.47 and mostly cuts across Porga and Arly. The AI ranges from 0.48 to 0.57 for the dry sub-humid zone, which is primarily found in Koumongou. AI in the humid zone ranges from 0.58 to 0.67. Akpoti et al. (2016) and Oguntunde et al. (2006) have also discovered similar outcomes in the Volta Basin. The findings show that the lowest points in each of the sub-basins - Porga (AI = 0.28), Arly (AI = 0.29), Koumongou (AI = 0.48), Sabari (AI = 0.35), and Saboba (AI = 0.34) were found in 1983. According to the classification system, aridity increases as the AI score decreases. As a result, it was discovered that 1983 was the driest year in each of the sub-basins.

The highest peak of aridity at all five sub-basins is seen to have occurred in 1994 whilst the lowest peak was detected in 1983 with the exception of Koumongou where the highest peak occurred in 2009. Given that AI is a ratio of long-term precipitation to climatic water demand (in this example, potential evapotranspiration), a greater AI value is recorded, as it was in 1983, when precipitation was lower than potential evapotranspiration. All five of the sub-basins' lowest values occurred in 1983, when drought conditions were recorded in the area, with high aridity mostly being observed at Porga and Arly (Kasei et al., 2010). These findings point to increased evapotranspiration rates in comparison to the precipitation that has fallen. Simply said, this indicates that rainfall may not have been sufficient to meet atmospheric water demands, leading to water shortages (Akpoti et al., 2016).

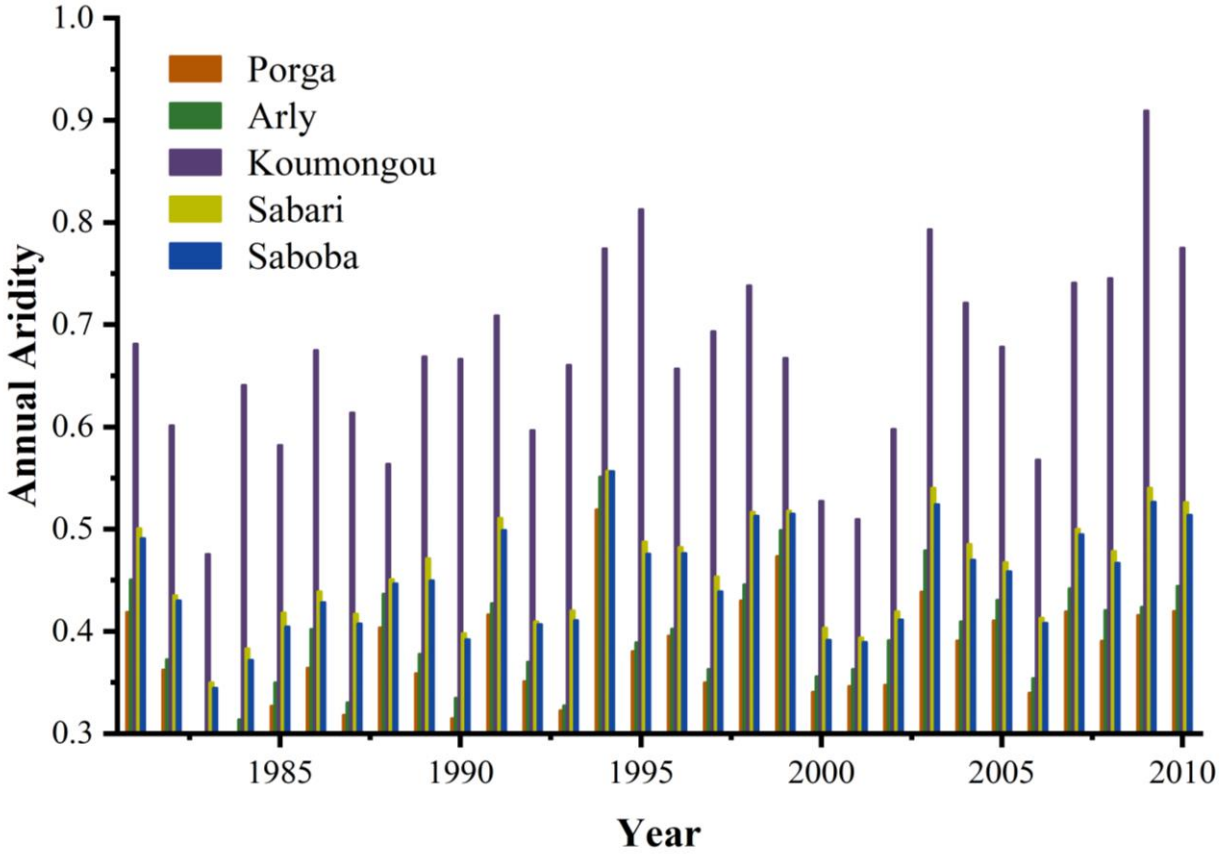

Figure 6. 2: Mean annual values of aridity for the sub-basins (1981-2010)

6.2 HBV model calibration and validation

The comparison between the observed and simulated hydrograph of the HBV model calibration (1981 – 1986) and validation (1987 – 1991) periods performed are shown in Figure 6.3 and Figure 6.4 correspondingly. It can be deduced that the observed and simulated hydrograph of the model in simulating daily streamflow is good for all the sub-basins despite the slight overestimations for low river discharge periods of 1986 for Porga and Arly, and 1981 and 1982 for Saboba during the calibration. The validation period also revealed that although the rising and recession limbs of the hydrograph of the observed and simulated streamflow seems good for all the sub-basins, it could be seen that the model tends to overestimates the peaks in some years at all sub-basins. This may be the consequence of an error in the model, the observed runoff or the slight gaps in the observed runoff. These observations have also been made by Kwakye and Bárdossy (2020) and Götzinger (2007). Regardless of the slight under-and-over estimations seen in the calibration and validation periods, the HBV model was able to simulate well the hydrology of the five sub-basins in the Oti River basin based on the generated Nash-Sutcliffe efficiency (NSE) and Kling-Gupta efficiency values which were ≥ 0.5, making the model suitable for use in the basin.

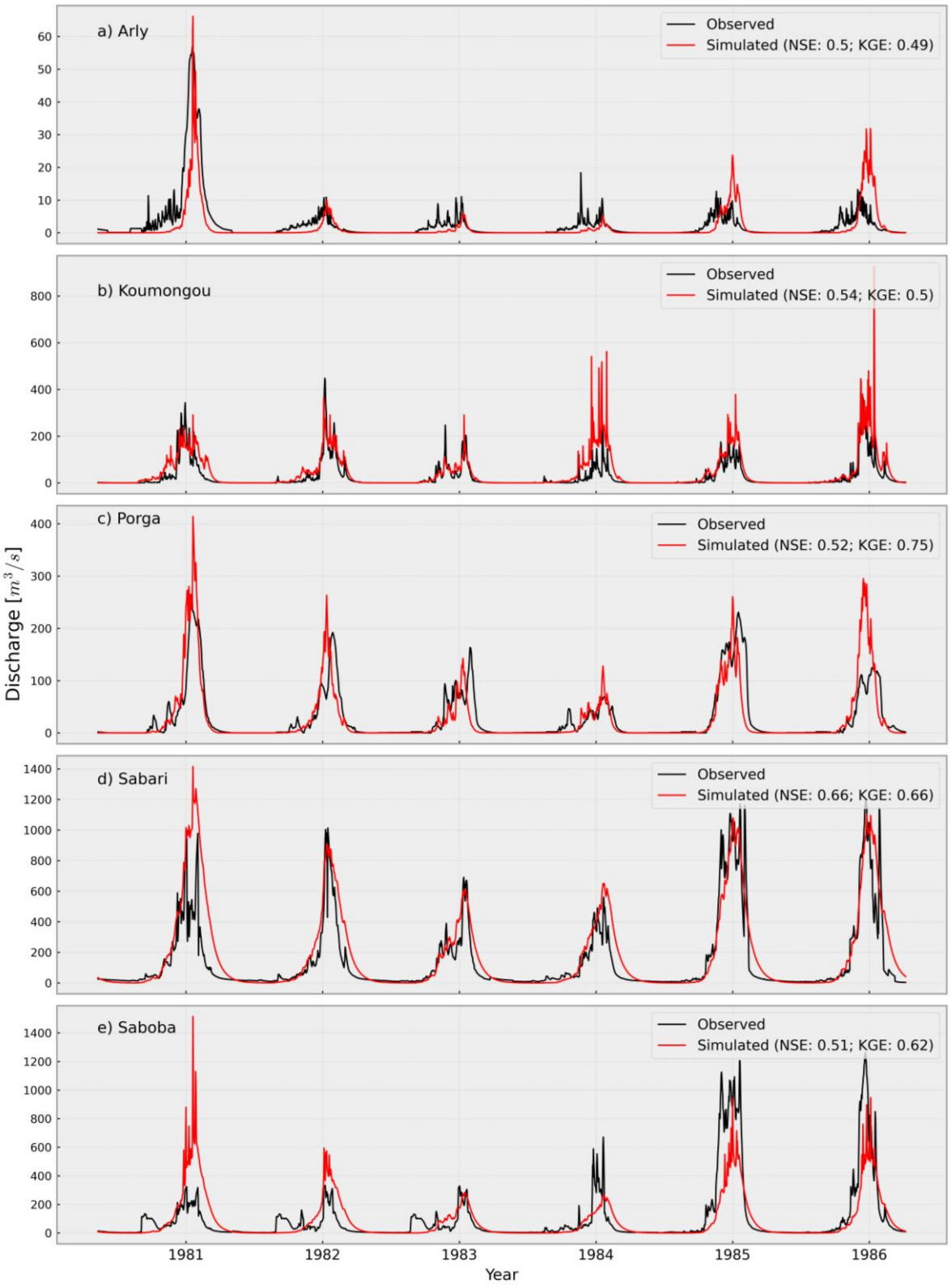

Figure 6. 3: Observed vs. Simulated daily discharge for calibration period (1981-1986)

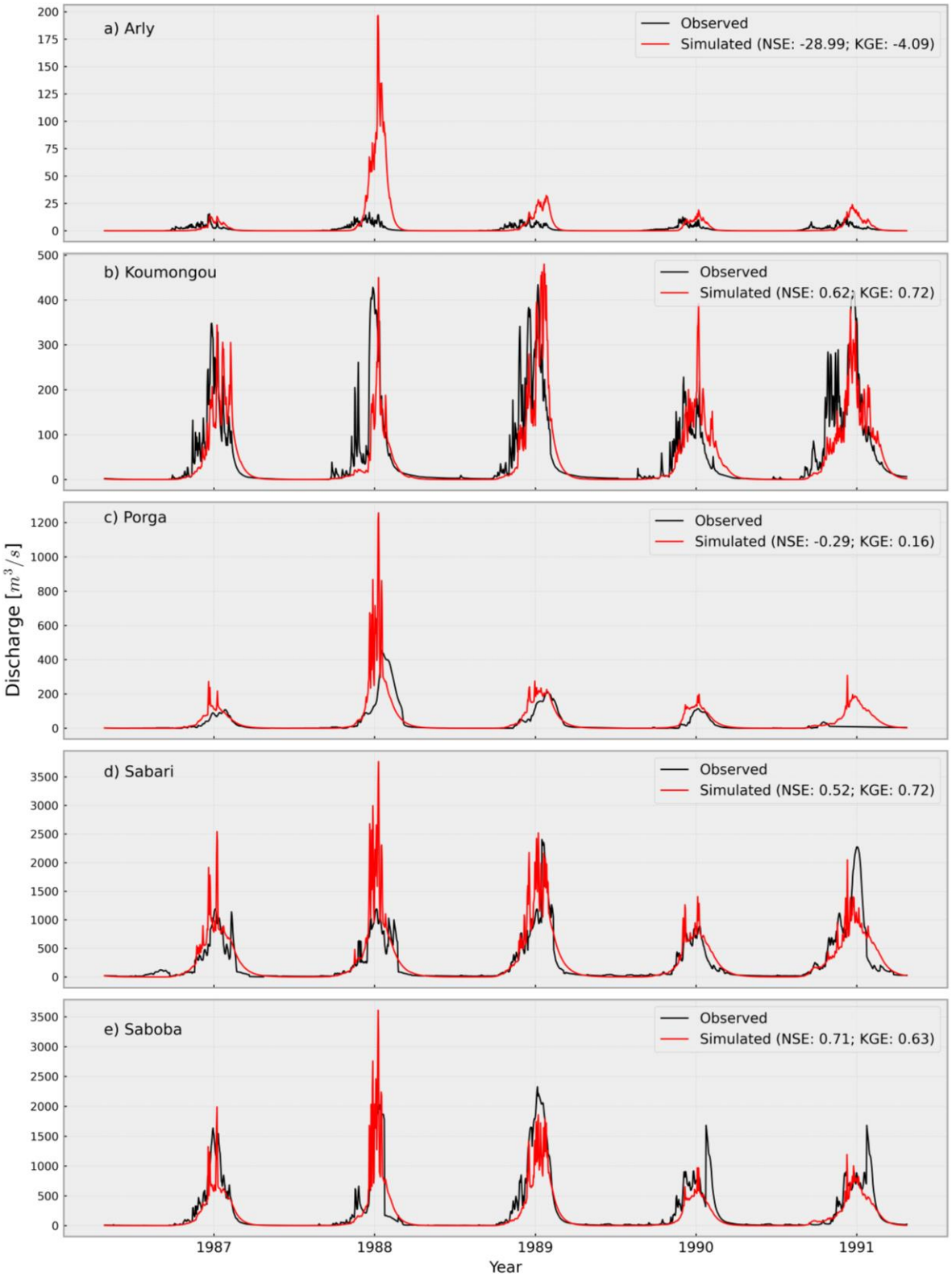

Figure 6. 4: Observed vs. Simulated daily discharge for validation period (1987-1991)

6.3 Optimal parameters of the HBV model after calibration and validation

After applying the hydrologic model to all five subbasins, varied measure of success was obtained. Figure 6.5 presents the results of the best parameters with maximum Nash-Sutcliffe efficiency (NSE) values that were generated for each subbasin. All the exponential parameter in soil routine (BETA) values are seen to be fairly estimated with the least value at Sabari and the maximum value at Arly for the calibration. This could mean that there is less infiltration in the soil of this sub-basin that could facilitate more contribution to runoff as compared to the other sub-basins (Reddy et al., 2020). The values for the maximum soil moisture storage (FC) in the sub-basins are relatively high. Comparing all the sub-basins, the highest and least values were detected at Arly and Porga respectively.

(Figure 6.5). The high value at Arly is contrary to Uhlenbrook et al. (1998) where decreased FC values were estimated for three large basins. The lowest value at Porga could be that this sub-basin had less available water and could cause moisture stress. The availability of water varies between soils in the sub-basins, as well as land use/cover types (Reddy et al., 2020). The recession coefficient of lower groundwater store (K_2) was highest at Koumongou and lowest at Porga. The additional recession coefficient of upper groundwater store (K_0), at Porga, Sabari and Saboba were found to be within the K_0 parameter maximum and minimum limits. However, calibrated values at stations like Arly, and Koumongou were slightly above the parameter range. The validation of the model revealed Porga, Arly and Saboba to be slightly above the K_0 parameter maximum limit, while those of Koumongou and Sabari were within the parameter limits.

The recession coefficient of upper groundwater store is found to decrease at Sabari which is the largest sub-basin. This could be expected because in such large basins there is a slower and more balanced response to precipitation. The limit for potential evapotranspiration (LP) was also well estimated with the maximum value at Arly and the least at Porga. The transfer function parameter (MAXBAS) generally behaved well in all sub-basins although it appeared to decrease for smaller basins like Arly. For the maximum flow from upper to lower tank (PERC), the maximum value was at Sabari which could suggest that the upper layer of this sub-basin releases large amounts of water to the lower layer and hence resulting in more water being stored in the lower layer. The threshold parameter for extra flow from upper zone (UZL) at all sub-basins recorded values that were within the maximum and minimum limits.

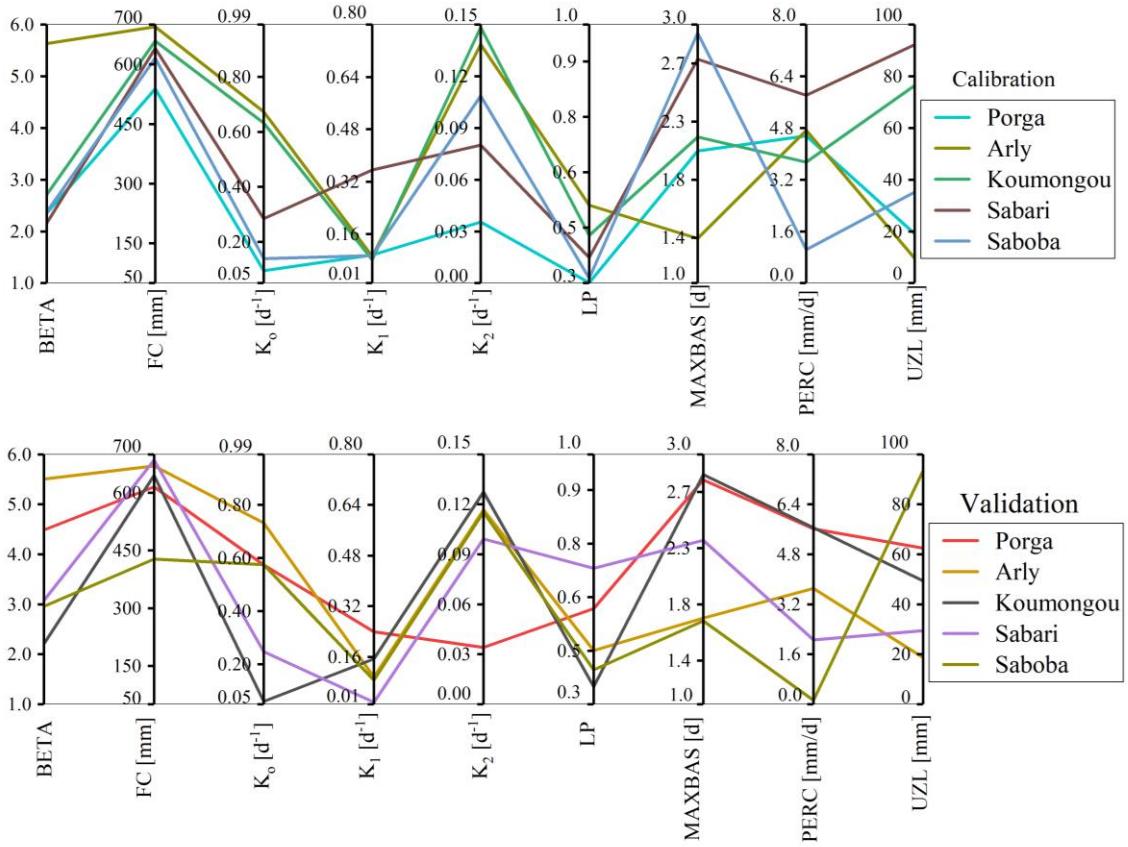

Figure 6. 5: Parallel coordinate plots showing HBV model behavioural parameterisation and their corresponding simulated output values for each sub-basin

6.4 Model's performance evaluation

During the calibration of the model, a variety of behavioural parameters were obtained in all the understudied sub-basins using the NSE threshold of ≥ 0.5. These NSE values were generated from the 20000 simulations performed for each sub-basin. Accordingly, sub-basins with calibration and validation NSE ≥ 0.5 accurately predicted streamflow against the observed. During the calibration, the NSE values were generally high with Sabari having the highest NSE values, followed by Koumongou, Porga, Saboba, with Arly recording the least number of NSE values. The NSE values at each of the sub-basins are; Porga (0.52), Arly (0.50), Koumongou (0.54), Sabari (0.66), and Saboba (0.51) (Figures 6.3 and 6.4). The validation saw NSE values for Saboba (0.71) and Koumongou (0.62) increased indicating stability of the HBV model parameters and hence good prediction in these sub-basins whiles that of Sabari (0.52), Porga (-0.29) and Arly (-28.99) had their NSE values decreased greatly during the validation as compared to their calibration. The KGE values detected for the sub-basins during the calibration are; Arly (0.49), Koumongou (0.5), Porga (0.75), Sabari (0.66)

and Saboba (0.62) whereas those recorded for the validation are; Arly (-4.09), Koumongou (0.72), Porga (0.16), Sabari (0.72) and Saboba (0.63) (Figures 6.3 and 6.4). The general decrease in prediction accuracy from calibration to validation particularly at Arly and Porga shows that the model may have been over-fitted as has been stated by Efstratiadis & Koutsoyiannis (2010). Kwakye and Bárdossy (2020) are of the notion that these errors are caused by the complicated nature of natural mechanisms as well as by misconceptions made during the whole modeling process.

Table 6.2 provides information about the investigated sub-basins' mean monthly streamflow characteristics for the calibration and validation periods. When comparing the validation periods to the calibration periods, it is shown that the average streamflow in Porga and Arly shows reductions of 1.9% and 31.9%, respectively while streamflow at Koumongou, Sabari and Saboba increased by +86%, +66%, and +141%, respectively. The maximum flow is seen to have decreased by 132.3 m^3/s at Arly, whereas it increased by +199 m^3/s at Porga, by +2,697.5 m^3/s at Koumongou, +14,281.6 m^3/s at Sabari and 23,892.6 m^3/s at Saboba. Similarly, the minimum flow decreased at Arly by 0.5 m^3/s, while it increased at Porga, Koumongou, Sabari and Saboba by +2.8 m^3/s, +27.1 m^3/s, 4,243.9 m^3/s and +67.4 m^3/s correspondingly.

Table 6. 2: Characteristics of mean monthly streamflow at the sub-basins for calibration and validation periods

	Porga		Arly	
Factors	Calibration (1981-1986)	Validation (1987-1991)	Calibration (1981-1986)	Validation (1987-1991)
Mean [m^3/s]	815.0	799.3	76.9	52.3
Max [m^3/s]	3515.8	3714.8	358.2	225.9
Min [m^3/s]	6.2	9.0	0.6	0.1
Std. Dev	1296.9	1360.9	109.8	73.6
CV	1.6	1.7	1.4	1.4
	Koumongou		Sabari	
Mean [m^3/s]	789.3	1469.2	4323.8	7185.8
Max [m^3/s]	4093.0	6790.5	19604.8	33886.4
Min [m^3/s]	2.8	29.9	356.6	504.4
Std. Dev	1294.4	2252.1	6306.0	10549.9
CV	1.6	1.5	1.5	1.5
	Saboba			
Mean [m^3/s]	2928.6	7077.3		
Max [m^3/s]	14594.7	38487.3		
Min [m^3/s]	96.0	163.4		
Std. Dev	4435.3	12021.2		
CV	1.5	1.7		

NB: Std. Dev is standard deviation; CV is Coefficient of variation; Max is Maximum; Min is Minimum

6.5 Future streamflow projections

6.5.1 Mean monthly streamflow

Figure 6.6 represents the monthly predictions of streamflow for 2021-2050 under RCPs 4.5 and 8.5 scenarios. It is discovered that streamflow at Porga had its highest peak (20,203.36 m^3/s) in August and its minimum flow (1.79 m^3/s) in February for the observed period (1981-2010). For the simulated historical (1981-2005), the highest peak of streamflow was 19,896.22 m^3/s in August while the minimum flow (1.67 m^3/s) in February. However, future streamflow in the sub-basin shows that flow would start to rise from April and have its highest peak (21,161.78 m^3/s) in August with a slight increase relative to the observed period under the RCP4.5 emission scenario. The lowest flow (1.80 m^3/s) under this scenario is predicted to occur in February. Streamflow is generally projected to increase under the RCP8.5 scenarios with a maximum peak of 30,595.28 m^3/s in the month of August. In addition, the lowest flow (4.58 m^3/s) would occur in February. At the Arly sub-basin, streamflow is predicted to

generally increase under both emission scenarios. Flow in the sub-basin had its highest peak (6,557.69 m^3/s) in August during the observed period (1981-2010) whereas the minimum flow (0.61 m^3/s) was recorded in February. Concerning the simulated historical period (1981-2005), maximum streamflow (6,504.35 m^3/s) also occurred in August and the minimum flow (0.57 m^3/s) was recorded in February.

A similar pattern with a maximum peak of 6,637.39 m^3/s and 9,102.05 m^3/s under the RCP4.5 and RCP8.5 scenarios correspondingly would be experienced in August. The sub-basin is projected to have its lowest flows of 0.67 m^3/s (RCP4.5) and 1.90 m^3/s (RCP8.5) respectively in February. At the Koumongou sub-basin, a maximum peak of 8,230.99 m^3/s in August while a recorded minimum flow of 2.61 m^3/s occurred in February. The simulated historical revealed the highest peak of streamflow (8063.7 m^3/s) to be in August while the minimum flow (2.46 m^3/s) occurred in February. However, in the future period, streamflow is projected to attain a maximum peak (8,971.8 m^3/s) in August under RCP4.5, and 10,632.83 m^3/s also in August, under the RCP8.5 scenarios. The minimum flows are anticipated to occur in the month of February (2.88 m^3/s) and (4.34 m^3/s) under the RCP4.5 and RCP8.5 scenarios respectively.

At Sabari, the maximum peak recorded for the observed period (1981-2010) was 55,357.08 m^3/s and it occurred in August while the minimum flow (14.09 m^3/s) occurred in February. Regarding the simulated historical, the maximum flow (54, 907 m^3/s) was also recorded in August whereas the minimum flow (13.70 m^3/s) occurred in February as well. For the future period, a general increase is projected for both RCP4.5 and RCP8.5 scenarios. The maximum peaks of 62,600.03 m^3/s and 85,628.1 m^3/s under RCP4.5 and RCP8.5 respectively are all anticipated to occur in August. The lowest flows of 15.8 m^3/s (RCP4.5) and 32.01 m^3/s (RCP8.5) are all projected to occur in February. At Saboba, a maximum peak of 49,818.9 m^3/s in August and a minimum flow of 9.22 m^3/s in February was recorded for the observed period. For the simulated historical, a maximum peak of 49,301.49 m^3/s and a minimum flow of 8.56 m^3/s were recorded in August and February respectively. The future period shows increase in streamflow under both RCP4.5 and RCP8.5 scenarios. The maximum peak anticipated under the RCP4.5 is 55,067.7 m^3/s and would occur in August while its minimum flow (9.99 m^3/s) would occur in February. The RCP8.5 would have its maximum peak (76,430.97 m^3/s) also in August while its minimum flow (21.19 m^3/s) would occur in February as well.

It can be deduced that generally, the RCP8.5 projects higher peaks of streamflow at all the sub-basins with the exception of Koumongou where the RCP4.5 projects most of the higher peaks (Figure 6.7).

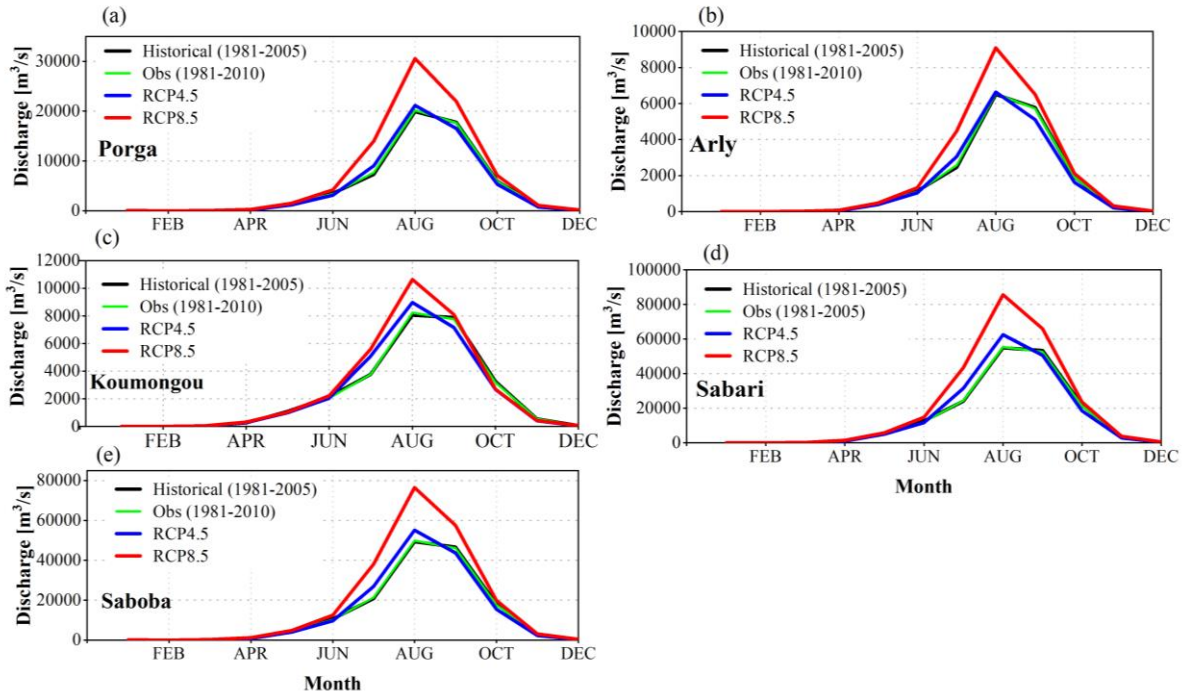

Figure 6. 6: Annual cycle of monthly discharge for the observed (1981-2010), simulated-historical (1981-2005) and future projection (2021-2050) under RCP4.5 and RCP8.5 scenarios

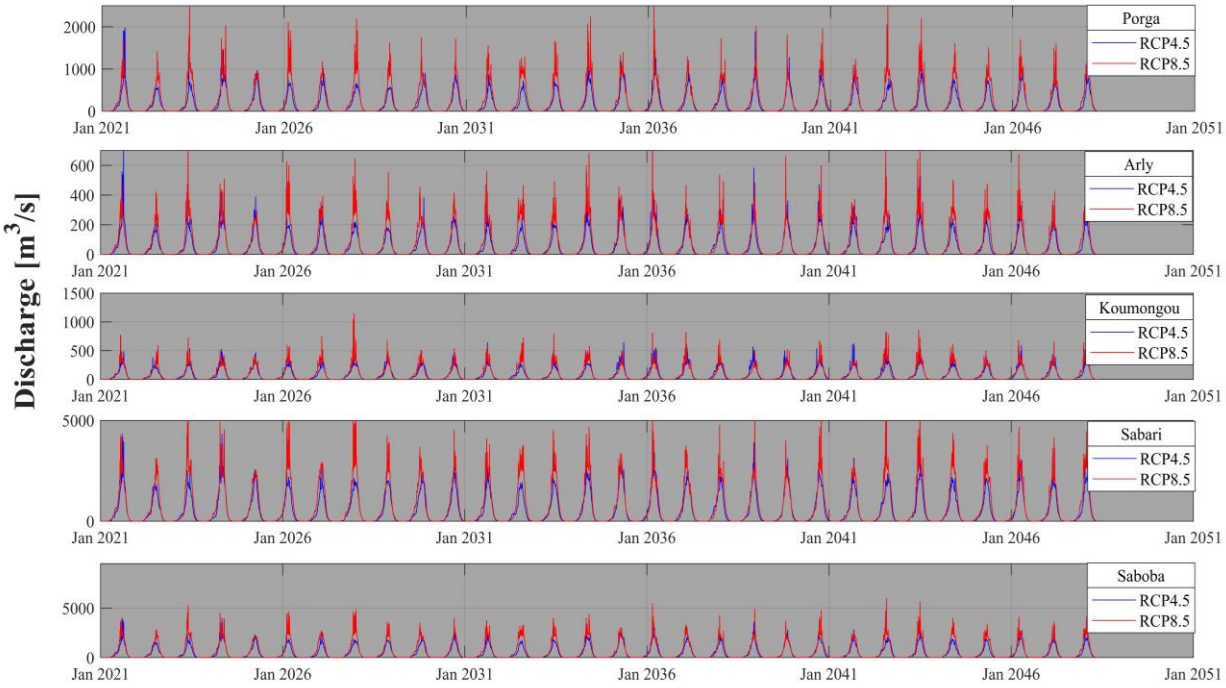

Figure 6.7: Streamflow projections under RCP4.5 and RCP8.5 scenarios (2021-2050)

6.5.2 Mean projected annual streamflow for the sub-basins

Figure 6.7 illustrates the annual projected streamflow at the five sub-basins, and Table 6.4 shows the trend test at the sub-basins. At Porga, and in the near-future, annual maximum streamflow is projected to occur in 2037 with a highest flow of about 6,551.78 m^3/s and a least flow of about 3736.58 m^3/s in 2022 under the RCP4.5 scenarios. By contrast, under the RCP8.5, the maximum flow is predicted to be about 8,346.57 m^3/s in 2035 and a minimum of about 5002.75 m^3/s in 2041. The mean flow would be about 4,770.28 m^3/s (RCP4.5) and 6,732.95 m^3/s (RCP8.5). The trend analysis for the RCP4.5 projects a non-significant increasing trend with a magnitude of about 13.32 m^3/s, whereas a decreasing trend is projected for RCP8.5, with the magnitude of decrease expected to be about 1.98 m^3/s. Arly is anticipated to have its maximum flow to be about 2,084.52 m^3/s (2037) with a minimum flow of about 1,152.52 m^3/s (2022) under the RCP4.5, whereas maximum flow would be around 2,497.22 m^3/s (2045) and minimum flow would be about 1,599.56 m^3/s (2041), under the RCP8.5 scenarios. The mean flow for both scenarios would be about 1,511.84 m^3/s (RCP4.5) and 2,040.19 m^3/s (RCP8.5). The trend analysis for the RCP4.5 and RCP8.5 scenarios projects increasing trends, with magnitudes of about 3.50 m^3/s and 4.63 m^3/s respectively. The maximum flow at Koumongou, under the RCP4.5 scenarios, is projected to be about 2,864.94 m^3/s in 2037, and a minimum flow of about 1,780.59 m^3/s in 2027. Under the RCP8.5 scenarios, however, maximum flow is expected to be around 3,495.89 m^3/s in 2028 and a minimum flow of about 1,948.19 m^3/s in 2040. The mean flow for both scenarios would be about 2,309.20 m^3/s (RCP4.5) and 2,594.40 m^3/s (RCP8.5). An increasing trend is predicted for RCP4.5 and RCP8.5 scenarios with the magnitudes of increase expected to be around 8.54 m^3/s and 2.50 m^3/s respectively.

At Sabari, under the RCP4.5, a maximum flow of about 19,176.24 m^3/s is anticipated to occur in 2037 with a minimum flow of about 12,171.27 m^3/s occurring in 2027. On the contrary, the RCP8.5 predicts the maximum flow to be about 24,440.32 m^3/s in 2028 and a minimum flow of about 15,966.18 m^3/s in 2041. The mean flow for both scenarios would be about 15,348.81 m^3/s (RCP4.5) and 20,433.15 m^3/s (RCP8.5). The RCP4.5 projects an increasing trend with a magnitude of about 31.18 m^3/s, whereas a decreasing trend with a magnitude of about 11.63 m^3/s is projected for the RCP8.5. At Saboba, the maximum flow under the RCP4.5 is expected to be around 16,801.62 m^3/s in 2037 and the minimum flow would be about 10,487.43 m^3/s in 2027. On the other hand, the RCP8.5 projects the maximum flow to be about 21,453.82 m^3/s in 2028 and the minimum flow of about 13,741.2 m^3/s in 2041. The

mean flow for both scenarios would be about 13,183.62 m^3/s (RCP4.5) and 17,832.38 m^3/s (RCP8.5). An increasing trend with a magnitude of about 34.40 m^3/s and a decreasing trend with a magnitude of about 9.03 m^3/s are projected for the RCP4.5 and RCP8.5 respectively.

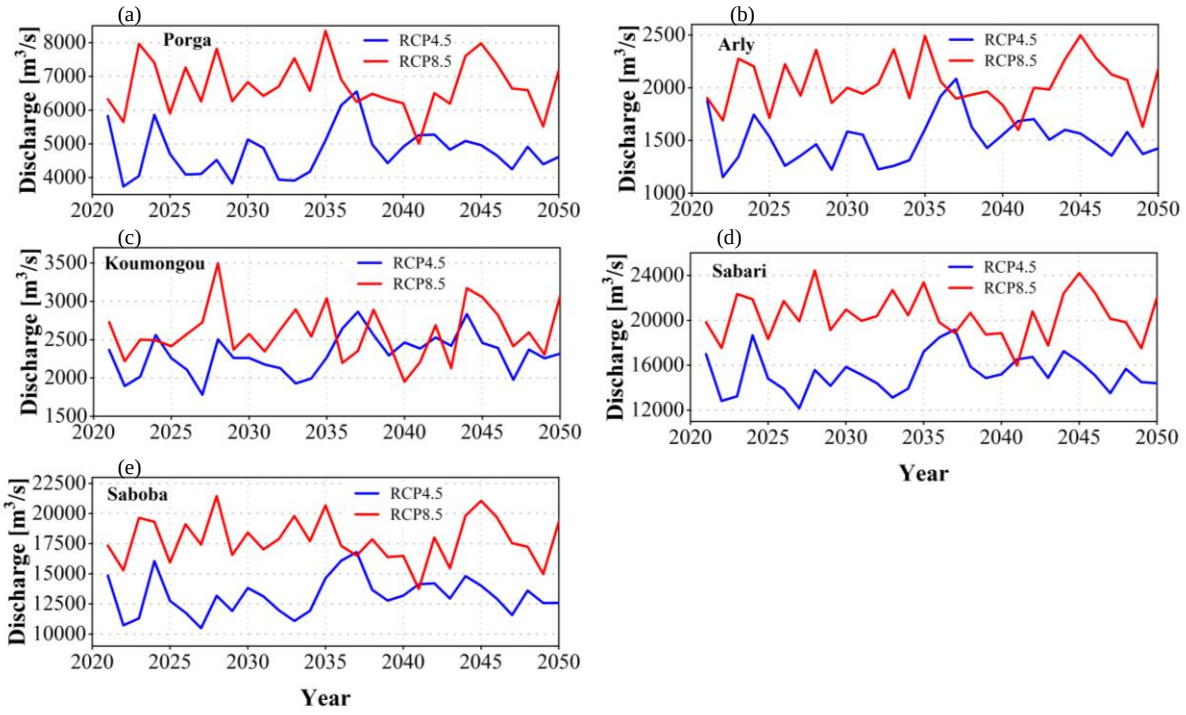

Figure 6. 8: Annual streamflow projections in the near-future at the sub-basins

Table 6. 3: Mann-Kendall trend and Sen's slope estimates for annual streamflow

	Sub-basins				
	Porga	Arly	Koumongou	Sabari	Saboba
RCP4.5					
MK (Z)	0.86	0.82	1.57	0.86	0.93
Sen's	13.32	3.50	8.54	31.18	34.40
RCP8.5					
MK(Z)	-0.07	0.79	0.29	-0.18	-0.36
Sen's	-1.98	4.63	2.50	-11.63	-9.03

6.6 Discussion

On streamflow at the Oti basin, the effect of intraseasonal rainfall variability was examined. The results of this study show that, although somewhat overestimating lower river discharge times in 1981 (Porga, Arly, Sabari, and Saboba), 1982 (Porga and Saboba), 1985 (Arly), and 1986 (Porga, Arly, and Koumongou), during calibration, the HBV was able to replicate the daily streamflow at all the subbasins that were under investigation well. Similar to this, except for the peaks in 1987 (Sabari), 1988 (Porga, Arly, Sabari and Saboba), 1989 (Arly), and 1991 (Porga and Arly), where the modeled peak came later and was marginally higher than the observed, all peak flows were accurately reproduced at all sub-basins in the validation. The results are consistent with Kwakye and Bárdossy (2020) who examined how well the HBV model performed in West Africa's Black Volta basin and found that it overestimated peak values throughout both the calibration and validation periods. These discoveries were also noted by Götzinger (2007) when the model was used in Benin's Ouémé basin (West Africa). These observations could result from a model error, the measured runoff, or the very minor gaps in the recorded runoff (Kwakye and Bárdossy, 2020). Regardless of these observations, the model performed well with NSE values which ranged between 0.50 and 0.75 for the calibration, and -28.99 to 0.71 for the validation. The KGE values were also between 0.49 and 0.75 for the calibration and between -4.09 and 0.72 which generally showed a good agreement between observed and simulated streamflow. Similar results were shown by Meresa & Gatachew (2019) whose calibration and validation of the HBV model recorded NSE values from 0.53 – 0.83 when they studied the impact of climate change on river flow extremes in the Upper Blue Nile River basin in Ethiopia. The model performance during calibration and validation are regarded as adequate and satisfactory according to Moriasi et al. (2015) and Schalla et al. (2023).

With regards to the seasonal streamflow, all the sub-basins seemed to have recorded their highest peaks in September, with average streamflow at each sub-basins indicating increment/reduction for the validation period (1987-1991) relative to the calibration period (1981-1986). For example, the average streamflow at Porga and Arly decreased by 1.9% and 31.9%, respectively, while it increased by approximately 86%, 66%, and 141.7% at Koumongou, Sabari, and Saboba, respectively. The historical rainfall deficits in the Sahelian and Sudano-Sahelian parts of the basin (Paturel et al., 2003) as well as population growth in the West African sub-region, which led to increased water extraction by 31% between 1983 and 1987 and 1998 to 2002, could be responsible for the declines in mean annual streamflow

(Roudier et al., 2014). Additionally, Descroix et al. (2012) and Mahe et al. (2003) confirm that the Sudanian region, where Arly is located, demonstrated a rather more predictable behavior with a two- to three-fold reduction in streamflow during the region's rainfall shortages. Amogu et al. (2010) also draw attention to the fact that Hewlettian saturation surplus discharge predominates in Sudanian regions, which may help to explain the decline in streamflow at Arly. The observed rebound of rainfall in the region's eastern section, according to Lebel & Ali (2009), as well as the favorable Guinean zone in which these sub-basins are located, may have contributed to the increase in streamflow at the three southern sites.

The monthly streamflow projections indicate that in the future, mean streamflow would generally increase at all sub-basins under both RCP4.5 and RCP8.5 scenario, with the exception of Arly which is projected to decrease by about 2.8% under RCP4.5 while it will increase by about 31.17% under RCP8.5. The projected increase in mean streamflow would be around approximately 0.06% (RCP4.5) and 41.2% (RCP8.5) at Porga, 2.7% (RCP4.5) and 15.4% (RCP8.5) at Koumongou, 4.7% (RCP4.5) and 39.4% (RCP8.5) at Sabari, and 3.2% (RCP4.5) and 39.6% (RCP8.5) at Saboba. In all, Sabari would experience the highest increase in streamflow under the RCP4.5 while Porga would have the highest increase under the RCP8.5. With regards to the streamflow peaks, the models project an increase by about 958.4 m^3/s (RCP4.5) and 10,391.9 m^3/s (RCP8.5) at Porga. At Arly, the peak is also anticipated to increase under both RCP4.5 and RCP8.5 by about 79.7 m^3/s and 2,544.4 m^3/s respectively. An increase is projected at Koumongou by about 740.8 m^3/s under RCP4.5, and 2,401.8 m^3/s is expected under RCP8.5. At Sabari, streamflow peak is predicted to increase under both RCP4.5 and RCP8.5 by about 7,242.95 m^3/s and 30,271.02 m^3/s correspondingly. Saboba is also anticipated to experience an increase in peak flow by about 5,248.7 m^3/s (RCP4.5) and 26,611.9 m^3/s (RCP8.5). Across the sub-basins, the predictions appear to be distinct. When compared to Koumongou, Saboba, and Sabari, which are in the southern section and primarily fall into the dry sub-humid and humid climates, it is projected that the changes in mean streamflow will be more pronounced at Arly and Porga, located in a semi-arid climatic zone. The study corroborates with Abubakari et al. (2019) who also projected future monthly streamflow changes between -13% to +32% in the White volta basin in West Africa for the periods 2011-2030 and 2046-2065. The study also agrees with Dembélé et al. (2022) who also projected monthly changes in runoff between -16.5% and +173.9% in the Volta basin for the periods 2021-2050, 2051-2080, and 2071-2100.

The annual scale projects an increase in mean, maximum and minimum streamflow at all sub-basins under both RCP4.5 and RCP8.5. The changes in maximum flow expected at each sub-basin are; +9.01% (RCP4.5) and +38.87% (RCP8.5) at Porga, +5.2% (RCP4.5) and 26.07% (RCP8.5) at Arly, 8.3% (RCP4.5) and +32.2% (RCP8.5) at Koumongou, +10.97% (RCP4.5) and +41.4% (RCP8.5) at Sabari, and +11.16% (RCP4.5) and +41.9% (RCP8.5) at Saboba. The anticipated increase in mean, minimum, and maximum streamflow could be as a result of their position or slope influencing rainfall. The projected increase in mean annual streamflow in the sub-basins is insensitive to the estimated decline of about 103.6 mm/yr (RCP4.5) and 45.9 mm/yr (RCP8.5) in mean annual rainfall in the entire basin (Kwawuvi et al., 2022). This is also supported by the study of Soro et al. (2013), who found that throughout the 1970s and 1980s, a 16.5% decrease in precipitation levels in the Upper Bandama basin (Ivory Coast) led to a 62% drop in discharge at the Tortiya station. Furthermore, Oguntunde et al. (2006) discovered that between 1936 and 1998, a 16% reduction in runoff in the Volta basin was caused by a 10% marked decline in rainfall.

The anticipated reduction in streamflow at Arly under the RCP4.5 may cause ecological issues such worsening of the water-soil quality, river drying up, vegetation decline and sandstorms (Shi et al., 2022). The potential rise in streamflow at Porga, Koumongou, Sabari and Saboba, however, might help agricultural output because it increases the possibility of irrigation by increasing the quantity of ground and surface water (Risal et al., 2022). Additionally, the predicted increase in streamflow may cause the basin to suffer from the continuous loading of dissolved substances and nutrient management challenges (Lenhart et al., 2011; Raymond et al., 2008). Although the anticipated changes don't appear to be too significant, caution is needed to prepare for any shocks and stresses that could be brought on by these changes in the sub-basins.

Chapter 7: General Conclusion and Perspectives

7.1 Conclusions

The importance of rainfall in West Africa cannot be over emphasized. Key systems like ecosystems, hydropower production, and agriculture are totally dependent on rainfall. In spite of this, the sub-region is susceptible to changes in its rainfall. Consequently, analyses were conducted on a number of critical rainfall indicators, such as the total annual rainfall amount, seasonal rainfall total (wet season), the onset of rains, the cessation of rain, the length of the rainy season, and the number of wet and dry days in the Oti River Basin. The modified Hydrologiska Byråns Vattenbalansavedlning (HBV) model was applied in the basin to assess its streamflow and make projections for future period 2021-2050 under the Representative Concentration Pathways, RCP4.5 and RCP8.5 climate change scenarios. These analyses resulted in the comprehension of the (i) historical (1981-2010), and future (2021-2050) intraseasonal rainfall variability in the Oti basin, (ii) the projected changes in these rainfall variability indicators in the future period 2021-2050 under the RCP4.5 and RCP8.5 scenarios relative to the historical period, and (iii) the impact of the variations in rainfall on streamflow as well as future streamflow projections in the basin.

The study found that the CHIRPS data was also fairly capable of simulating the basin's climate patterns, emphasizing its potential for use in subsequent analyses. In the entire basin, it was shown that the rainfall variability indicators, mainly the annual rainfall and seasonal (rainy) rainfall would generally decrease in their amounts in both space and time relative to the observed period. Annual rainfall amount that used to be 1,073.8 mm/yr is likely to decrease by about 103.6 mm/yr (RCP4.5) and 45.9 mm/yr (RCP8.5). Also, seasonal (rainy) rainfall amount which was 1038.6 mm/yr would likely decline to about 947.7 mm/yr (RCP4.5) and 1004 mm/yr (RCP8.5). Although annual and seasonal rainfall amount projects a general decline, the number of wet and dry days in the entire basin shows a general increase and decrease correspondingly in the future according to the model’s ensemble. The basin is likely to experience a forward shift in its onset of rains. Onset would likely shift from 8 May to about 24 May (RCP4.5) and 23 May (RCP8.5). This shift in onset would greatly impact its associated cessation and length of the rainy season in the entire basin such that rainfall in the basin is predicted to terminate early while the length of the rainy season would become shorter relative to the historical period. After 10 years of an exceptionally dry condition in 2027, the basin would probably have an extraordinarily wet condition in 2037 during the wet

season period under the RCP4.5 scenario. Under the RCP8.5 scenario, a very wet condition would likely occur in 2028 while an extremely dry situation is expected in the basin in 2041 during the wet season. However, the RCP8.5 predicts that 2025 would be quite dry and 2037 will be highly wet. These findings do not agree with the hypothesis that in the future period, rainfall variability at the intra-seasonal scale would increase. The study also revealed the climatic features of each sub-basin. Among the five sub-basins, Porga and Arly were found to be highly arid. All the sub-basins, however recorded their lowest aridity values in 1983 when drought hit the region. A better knowledge of the spatiotemporal distribution and fluctuations in rainfall in the Oti basin can be achieved from the study's findings. Crop productivity and food security in the basin may face significant challenges as a result of the expected changes in the rainfall indices. Overall, the research gives an overview that could assist farmers in organizing their agricultural operations and water resource authorities in managing the basin effectively.

The streamflow of the basin was evaluated using both station and gridded data in the HBV hydrologic model. Then, using the historical observed, historical ensembled of the model and the ensembled mean of climate projection from eight bias-corrected regional climate models enforced by RCP4.5 and RCP8.5, the model was used to project future streamflow. Despite the study's minimal over-and-underestimations in peak flows, the model was able to reproduce the daily streamflow in all five sub-basins. Streamflow is simulated to be higher at Koumongou (+86%), Sabari (+66%) and Saboba (+141.7%), while it dropped at Porga and Arly by roughly 1.9% and 31.9%, accordingly. This provided details on how previous rainfall deficiencies in the Sudanian zone of the basin, rainfall recovery, and the favorable characteristics of the Guinean zone might have affected the declines and gains observed.

All five sub-basins' monthly streamflow are expected to increase in the future. Therefore, the study disagrees with the hypothesis that variability in intra-seasonal rainfall would decrease future streamflow. The streamflow is also observed to be influenced by the sub-basins' relative position. At the annual scale, mean streamflow as well as low and peak flows are anticipated to increase at all sub-basins apart from Arly whose peak flow would likely decrease by 2.79% under RCP4.5 emissions scenario. A lack of water for domestic activities, agriculture, and industrial use in the basin may result from the drop in mean streamflow in the Arly sub-basin. If the existing pattern of decreasing streamflow at the subbasin continues, water crisis will worsen and have an impact on the quality of life.

The anticipated decline in rainfall has the tendency to affect to the basin-dependent countries' efforts towards achieving the Sustainable Development Goals (SDGs)1, 2, 3 and 6. The study's findings signals the possible adverse impact on rainfed agriculture in the basin, which could result in the reduction or poor growth of food crops and farm animals, and subsequently increasing the prices of agricultural produce. This situation could increase poverty levels in the basin thereby making it difficult for inhabitants to feed well and for the achievement of the no poverty and zero hunger that the SDGs 1 and 2 indicates. Moreover, the expected increase in streamflow could lead to contamination of the basin's water through the accumulation of dissolved substances and nutrients. This would impact inhabitants' access to safe water (SDG6) for domestic use, and agricultural production, thereby affecting the health and well-being (SDG3) of people who rely on the basin for these needs. Despite the study's many flaws, its findings are crucial for giving us a glimpse into the Oti basin's future climatic conditions and water supply. The findings are essential for developing strategies for the basin's adaptation to a changing climate as well as aiding the countries that depend on the basin to achieve the SDGs 1, 2, 3 and 6.

7.2 Perspectives or future works

Among the many limitations faced in this study was the scarcity and inadequacy of observed climate and streamflow records. This therefore encouraged the integration of Climate Hazards Group Infrared Precipitation with Station data (CHIRPS), National Aeronautics and Space Administration Prediction of Worldwide Energy Resource (NASA POWER) project data for analyses in the Oti basin. Despite the fact that these satellite products showed a reasonable level of precision future studies in the basin can use just climatic data from these products or data that is based only on meteorological station data to determine any variations in results. Furthermore, the study was obliged to calibrate and validate the HBV model on short periods due to the difficulty in obtaining adequate long-term discharge data. Streamflow in the basin could be accurately simulated, but it would be beneficial to run simulations on longer periods of discharge data when they are available.

The climate data used to estimate the input variables for the model was also an integration of station and gridded data, 8 RCMs-GCMs, and focused on only two climate change scenarios (RCP4.5 and RCP8.5). For a better understanding of the hydrology of the basin, it would be advantageous if future studies in the basin included more RCM-GCMs and emission scenarios. Therefore, it is crucial that discharge in the basin be adequately monitored and

recorded in order to support research that offers information for the implementation of effective climate change adaptation measures.

Furthermore, future studies would include full global datasets of Multi-Source Weighted-Ensemble Precipitation (MSWEP) and Gleam datasets and resample these parameters to simulate and project the basin's streamflow. Another improvement could be to emphasize modelling the basin's hydrology for the accessibility of water by taking into account the changes in the basin's land-use and land-cover.

Researchers and the basin's management officials could benefit from a better understanding of the study's discoveries. The discoveries in the onset, cessation, the length of the rainy season, and annual and seasonal rainfall can help policymakers and management authorities identify appropriate interventions to aid in designing climate change resilient management strategies in the basin.

Policymakers and management authorities, can also identify appropriate actions to support the design of climate change resilient management strategies in the basin with the assistance of the findings regarding the onset, cessation, length of the rainy season, annual rainfall, seasonal rainfall, and streamflow projections. It could also facilitate cooperation in development and conservation among the basin-sharing countries, which might avoid transboundary disputes related to water.

References

Abbaspour, K. C., Faramarzi, M., Ghasemi, S. S., & Yang, H. (2009). Assessing the impact of climate change on water resources in Iran. *Water Resources Research*, *45*(10), 1–16. https://doi.org/10.1029/2008WR007615

Abebe, N. A., Ogden, F. L., & Pradhan, N. R. (2010). Sensitivity and uncertainty analysis of the conceptual HBV rainfall-runoff model: Implications for parameter estimation. *Journal of Hydrology*, *389*(3–4), 301–310. https://doi.org/10.1016/j.jhydrol.2010.06.007

Abraham, T., Liu, Y., Tekleab, S., & Hartmann, A. (2022). Prediction at Ungauged Catchments through Parameter Optimization and Uncertainty Estimation to Quantify the Regional Water Balance of the Ethiopian Rift Valley Lake Basin. *Hydrology*, *9*(8). https://doi.org/10.3390/hydrology9080150

Abraham, T., Woldemicheala, A., Muluneha, A., & Abateb, B. (2018). Hydrological Responses of Climate Change on Lake Ziway Catchment, Central Rift Valley of Ethiopia. *Journal of Earth Science & Climatic Change*, *09*(06). https://doi.org/10.4172/2157-7617.1000474

Abubakari, S., Dong, X., Su, B., Hu, X., Liu, J., Li, Y., Peng, T., Ma, H., Wang, K., & Xu, S. (2017). Modelling the spatial variation of hydrology in volta river basin of west Africa under climate change. *Nature Environment and Pollution Technology*, *16*(4), 1095–1105.

Abubakari, S., Dong, X., Su, B., Hu, X., Liu, J., Li, Y., Peng, T., Ma, H., Wang, K., & Xu, S. (2019). Modelling streamflow response to climate change in data-scarce White Volta River basin of West Africa using a semi-distributed hydrologic model. *Journal of Water and Climate Change*, *10*(4), 907–930. https://doi.org/10.2166/wcc.2018.193

Adeniyi, M. O., & Dilau, K. A. (2018). Assessing the link between Atlantic Niño 1 and drought over West Africa using CORDEX regional climate models. *Theoretical and Applied Climatology*, *131*(3–4), 937–949. https://doi.org/10.1007/s00704-016-2018-0

Aguilar, E., Barry, A. A., Brunet, M., Ekang, L., Fernandes, A., Massoukina, M., Mbah, J., Mhanda, A., do Nascimento, D. J., Peterson, T. C., Umba, O. T., Tomou, M., & Zhang, X. (2009). Changes in temperature and precipitation extremes in western central Africa, Guinea Conakry, and Zimbabwe, 1955-2006. *Journal of Geophysical Research Atmospheres*, *114*(2), 1–11. https://doi.org/10.1029/2008JD011010

Agyekum, J., Annor, T., Lamptey, B., Quansah, E., & Agyeman, R. Y. K. (2018). Evaluation of CMIP5 Global Climate Models over the Volta Basin: Precipitation. *Advances in Meteorology*, *2018*, 1–24. https://doi.org/10.1155/2018/4853681

Agyekum, J., Annor, T., Quansah, E., Lamptey, B., & Okafor, G. (2022). Extreme precipitation indices over the Volta Basin: CMIP6 model evaluation. *Scientific African*, *16*. https://doi.org/10.1016/j.sciaf.2022.e01181

Akinsanola, A. A., Ajayi, V. O., Adejare, A. T., Adeyeri, O. E., Gbode, I. E., Ogunjobi, K. O., Nikulin, G., & Abolude, A. T. (2017). Evaluation of rainfall simulations over West Africa in dynamically downscaled CMIP5 global circulation models. *Theoretical and Applied Climatology*, *132*(1–2), 437–450. https://doi.org/10.1007/s00704-017-2087-8

Akinsanola, A. A., & Zhou, W. (2018). Ensemble-based CMIP5 simulations of West African

summer monsoon rainfall: current climate and future changes. *Theoretical and Applied Climatology*, *136*(3–4), 1021–1031. https://doi.org/10.1007/s00704-018-2516-3

Akpoti, K., Antwi, E. O., & Kabo-bah, A. T. (2016). Impacts of rainfall variability, land use and land cover change on stream flow of the Black Volta basin, West Africa. *Hydrology*, *3*(3), 1–24. https://doi.org/10.3390/hydrology3030026

Akumaga, U., & Tarhule, A. (2018). Projected changes in intra-season rainfall characteristics in the Niger River Basin, West Africa. *Atmosphere*, *9*(12), 1983–1985. https://doi.org/10.3390/atmos9120497

Al-Safi, H. I. J., & Sarukkalige, P. R. (2017). Assessment of future climate change impacts on hydrological behavior of Richmond River Catchment. *Water Science and Engineering*, *10*(3), 197–208. https://doi.org/10.1016/j.wse.2017.05.004

Alemu, M. M., & Bawoke, G. T. (2019). Analysis of spatial variability and temporal trends of rainfall in Amhara Region, Ethiopia. *Journal of Water and Climate Change*, *11*(4), 1505–1520. https://doi.org/10.2166/wcc.2019.084

Amekudzi, L. K., Yamba, E. I., Preko, K., Asare, E. O., Aryee, J., Baidu, M., & Codjoe, S. N. A. (2015). Variabilities in rainfall onset, cessation and length of rainy season for the various agro-ecological zones of Ghana. *Climate*, *3*(2), 416–434. https://doi.org/10.3390/cli3020416

Amisigo, B. A., van de Giesen, N., Rogers, C., Andah, W. E. I., & Friesen, J. (2008). Monthly streamflow prediction in the Volta Basin of West Africa: A SISO NARMAX polynomial modelling. *Physics and Chemistry of the Earth*, *33*(1–2), 141–150. https://doi.org/10.1016/j.pce.2007.04.019

Amogu, O., Descroix, L., Yéro, K. S., Breton, E. L., Mamadou, I., Ali, A., Vischel, T., Bader, J. C., Moussa, I. B., Gautier, E., Boubkraoui, S., & Belleudy, P. (2010). Increasing river flows in the Sahel? *Water (Switzerland)*, *2*(2), 170–199. https://doi.org/10.3390/w2020170

Ankrah, J., Monteiro, A., & Madureira, H. (2023). Spatiotemporal Characteristics of Meteorological Drought and Wetness Events across the Coastal Savannah Agroecological Zone of Ghana. *Water (Switzerland)*, *15*(1). https://doi.org/10.3390/w15010211

Annor, T., Lamptey, B., Wagner, S., Oguntunde, P., Arnault, J., Heinzeller, D., & Kunstmann, H. (2017). High-resolution long-term WRF climate simulations over Volta Basin. Part 1: validation analysis for temperature and precipitation. *Theoretical and Applied Climatology*, *133*, 829–849. https://doi.org/10.1007/s00704-017-2223-5

Arnell, N. W., & Gosling, S. N. (2016). The impacts of climate change on river flood risk at the global scale. *Climatic Change*, *134*(3), 387–401. https://doi.org/10.1007/s10584-014-1084-5

Asfaw, A., Simane, B., Hassen, A., & Bantider, A. (2018). Variability and time series trend analysis of rainfall and temperature in northcentral Ethiopia: A case study in Woleka sub-basin. *Weather and Climate Extremes*, *19*(December), 29–41. https://doi.org/10.1016/j.wace.2017.12.002

Atiah, W. A., Amekudzi, L. K., Aryee, J. N. A., Preko, K., & Danuor, S. K. (2020). Validation of satellite and merged rainfall data over Ghana, West Africa. *Atmosphere*, *11*(8), 1–23. https://doi.org/10.3390/ATMOS11080859

Atiah, W. A., Amekudzi, L. K., Quansah, E., & Preko, K. (2019). The Spatio-Temporal Variability of Rainfall over the Agro-Ecological Zones of Ghana. *Atmospheric and Climate Sciences*, *09*(03), 527–544. https://doi.org/10.4236/acs.2019.93034

Atiah, W. A., Muthoni, F. K., Kotu, B., Kizito, F., & Amekudzi, L. K. (2021). Trends of rainfall onset, cessation, and length of growing season in northern ghana: Comparing the rain gauge, satellite, and farmer's perceptions. *Atmosphere*, *12*(12), 1–20. https://doi.org/10.3390/atmos12121674

Attogouinon, A., Lawin, A. E., & Deliège, J. F. (2020). Evaluation of general circulation models over the upper oueme river basin in the republic of Benin. *Hydrology*, *7*(1). https://doi.org/10.3390/hydrology7010011

Ayanlade, A., Radeny, M., Morton, J. F., & Muchaba, T. (2018). Rainfall variability and drought characteristics in two agro-climatic zones: An assessment of climate change challenges in Africa. *Science of the Total Environment*, *630*, 728–737. https://doi.org/10.1016/j.scitotenv.2018.02.196

Babalola, T. E., Oguntunde, P. G., Ajayi, A. E., & Akinluyi, F. O. (2021). Future Climate Change Impacts on River Discharge Seasonality for Selected West African River Basins. In *Intech* (pp. 1–20). https://www.intechopen.com/books/advanced-biometric-technologies/liveness-detection-in-biometrics

Badjana, H. M., Fink, M., Helmschrot, J., Diekkrüger, B., Kralisch, S., Afouda, A. A., & Wala, K. (2017). Hydrological system analysis and modelling of the Kara River basin (West Africa) using a lumped metric conceptual model. *Hydrological Sciences Journal*, *62*(7), 1094–1113. https://doi.org/10.1080/02626667.2017.1307571

Badjana, H. M., Renard, B., Helmschrot, J., Edjamé, K. S., Afouda, A., & Wala, K. (2017). Bayesian trend analysis in annual rainfall total, duration and maximum in the Kara River basin (West Africa). *Journal of Hydrology: Regional Studies*, *13*, 255–273. https://doi.org/10.1016/j.ejrh.2017.08.009

Badjana, H. M., Selsam, P., Wala, K., Flügel, W.-A., Fink, M., Urban, M., Helmschrot, J., Afouda, A., & Akpagana, K. (2014). Assessment of land-cover changes in a sub-catchment of the Oti basin (West Africa): A case study of the Kara River basin. *Zentralblatt Für Geologie Und Paläontologie, Teil I*, *2014*(1), 151–170. https://doi.org/10.1127/zgpi/2014/0151-0170

Badou, D. F. (2016). *Multi-Model Evaluation of Blue and Green Water Availability Under Climate Change in Four-Non Sahelian Basins of the Niger River Basin*. University of Abomey-Calavi (UAC).

Barry, B., Obuobie, E., Andreini, M., Andah, W., & Pluquet, M. (2005). The Volta River Basin. In *The Volta River Basin. Comprehensive assessment of water management in agriculture. Comparative study of river basin development and management.* http://armspark.msem.univ-montp2.fr/bfpvolta/admin/biblio/CA-Volta River basin.doc

Batisani, N., & Yarnal, B. (2010). Rainfall variability and trends in semi-arid Botswana:

Implications for climate change adaptation policy. *Applied Geography*, *30*(4), 483–489. https://doi.org/10.1016/j.apgeog.2009.10.007

Bawden, A. J., Linton, H. C., Burn, D. H., & Prowse, T. D. (2014). A spatiotemporal analysis of hydrological trends and variability in the Athabasca River region, Canada. *Journal of Hydrology*, *509*, 333–342. https://doi.org/10.1016/j.jhydrol.2013.11.051

Beck, H. E., van Dijk, A. I. J. M., de Roo, A., Miralles, D. G., McVicar, T. R., Schellekens, J., & Bruijnzeel, L. A. (2016). Global-scale regionalization of hydrologic model parameters. *Water Resources Research*, *52*(5), 3599–3622. https://doi.org/10.1002/2015WR018247

Berglöv, G., German, J., Gustavsson, H., Harbman, U., & Johansson, B. (2009). *Improvement HBV Model Rhine in FEWS: Final Report* (Issue 112).

Bergström, S. (1992). The HBV model - its structure and applications. *Swedish Meteorological and Hydrological Institute*, *Norrköping*, *4*(4), 1–33.

Bessah, E., Raji, A. O., Taiwo, O. J., Agodzo, S. K., & Ololade, O. O. (2020). The impact of varying spatial resolution of climate models on future rainfall simulations in the pra river basin (Ghana). *Journal of Water and Climate Change*, *11*(4), 1263–1283. https://doi.org/10.2166/wcc.2019.258

Biftu, G. F., & Gan, T. Y. (2001). Semi-distributed, physically based, hydrologic modeling of the paddle river basin, alberta, using remotely sensed data. *Journal of Hydrology*, *244*(3–4), 137–156. https://doi.org/10.1016/S0022-1694(01)00333-X

Blanc, E. (2012). The Impact of Climate Change on Crop Yields in Sub-Saharan Africa. *American Journal of Climate Change*, *01*(01), 1–13. https://doi.org/10.4236/ajcc.2012.11001

Boe´, J., Terray, L., Habets, F., & Martin, E. (2007). Statistical and dynamical downscaling of the Seine basin climate for hydro-meteorological studies. *International Journal of Climatology*, *27*(12), 1643–1655. https://doi.org/10.1002/joc

Braimah, M., Asante, V. A., Ahiataku, M. A., Ansah, S. O., Otu-Larbi, F., Yahaya, B., Ayabilah, J. B., & Nkrumah, F. (2022). Variability of the Minor Season Rainfall over Southern Ghana (1981-2018). *Advances in Meteorology*, *2022*. https://doi.org/10.1155/2022/1861130

Bürger, G., Schulla, J., & Werner, A. T. (2011). Estimates of future flow, including extremes, of the Columbia River headwaters. *Water Resources Research*, *47*(10), 1–18. https://doi.org/10.1029/2010WR009716

Chemnitz, C., & Hoeffler, H. (2011). Adapting African Agriculture to Climate Change. *International Journal Rural Development*, *45*, 32–35.

Chen, L., & Frauenfeld, O. W. (2014). Journal of geophysical research. *Nature*, *119*, 5767–5786. https://doi.org/10.1038/175238c0

Chiew, F. H. S., Zheng, H., & Potter, N. J. (2018). Rainfall-Runoff modelling considerations to predict streamflow characteristics in ungauged catchments and under climate change. *Water (Switzerland)*, *10*(10), 7–9. https://doi.org/10.3390/w10101319

Chokkavarapu, N., & Mandla, V. R. (2019). Comparative study of GCMs, RCMs,

downscaling and hydrological models: a review toward future climate change impact estimation. *SN Applied Sciences*, *1*(12), 1–15. https://doi.org/10.1007/s42452-019-1764-x

Codjoe, S. N. A. (2006). journal on Black Volta human settlement. *Ghana Journal of Development Studies*, *3*(2), 66–82.

Cohen, L. T., Matos, J. P., Boillat, J. L., & Schleiss, A. J. (2012). Comparison and evaluation of satellite derived precipitation products for hydrological modeling of the Zambezi River Basin. *Hydrology and Earth System Sciences*, *16*(2), 489–500. https://doi.org/10.5194/hess-16-489-2012

Collins, W. D., Bitz, C. M., Blackmon, L. M., Bonan, G. B., Bretherton, C. S., Carton, J. A., Chang, P., Doney, S. C., Hack, J. J., Henderson, T. B., Kiehl, J. T., Large, W. G., Mckenna, D. S., Santer, B. D., & Smith, R. D. (2006). The Community Climate System Model, version 2. *Journal of Climate*, *19*, 2122–2143. https://doi.org/10.1175/1520-0442(2004)017<3666:TCCSMV>2.0.CO;2

Conway, G. (2008). The science of climate change in Africa : impacts and adaptation. *Department for International Development, UK*, *1*(2), 1–43. http://eprints.whiterose.ac.uk/id/eprint/78098%0Ahttp://dx.doi.org/10.1007/s10584-007-9249-0%0Ahttp://dx.doi.org/10.1016/j.envsci.2015.10.010%0Ahttp://dx.doi.org/10.1007/s10113-015-0761-x%0Asei-international.org

Coulson, S., Lubeck, M., Mitrovica, J. X., Powell, E., Davis, J. L., & Hoggard, M. J. (2021). The Global Fingerprint of Modern Ice-Mass Loss on 3-D Crustal Motion. *Geophysical Research Letters*, *48*(16), 1–11. https://doi.org/10.1029/2021GL095477

Dang, T. D., Cochrane, T. A., Arias, M. E., Van, P. D. T., & de Vries, T. T. (2016). Hydrological alterations from water infrastructure development in the Mekong floodplains. *Hydrological Processes*, *30*(21), 3824–3838. https://doi.org/10.1002/hyp.10894

Dankers, R., Arnell, N. W., Clark, D. B., Falloon, P. D., Fekete, B. M., Gosling, S. N., Heinke, J., Kim, H., Masaki, Y., Satoh, Y., Stacke, T., Wada, Y., & Wisser, D. (2014). First look at changes in flood hazard in the Inter-Sectoral Impact Model Intercomparison Project ensemble. *Proceedings of the National Academy of Sciences of the United States of America*, *111*(9), 3257–3261. https://doi.org/10.1073/pnas.1302078110

Dembélé, M., Schaefli, B., Giesen, N. Van De, & Mariéthoz, G. (2020). Suitability of 17 gridded rainfall and temperature datasets for large-scale hydrological modelling in West Africa. *Hydrology and Earth System Sciences*, *24*(11), 5379–5406.

Dembélé, M., Vrac, M., Ceperley, N., Zwart, S. J., Larsen, J., Dadson, S. J., Mariéthoz, G., & Schaefli, B. (2022). Contrasting changes in hydrological processes of the Volta River basin under global warming. *Hydrology and Earth System Sciences*, *26*(5), 1481–1506. https://doi.org/10.5194/hess-26-1481-2022

Dembélé, M., & Zwart, S. J. (2016). Evaluation and comparison of satellite-based rainfall products in Burkina Faso, West Africa. *International Journal of Remote Sensing*, *37*(17), 3995–4014. https://doi.org/10.1080/01431161.2016.1207258

Descroix, L., Genthon, P., Amogu, O., Rajot, J. L., Sighomnou, D., & Vauclin, M. (2012). Change in Sahelian Rivers hydrograph: The case of recent red floods of the Niger River in the Niamey region. *Global and Planetary Change*, *98–99*, 18–30. https://doi.org/10.1016/j.gloplacha.2012.07.009

Diasso, U., & Abiodun, B. J. (2017). Drought modes in West Africa and how well CORDEX RCMs simulate them. *Theoretical and Applied Climatology*, *128*(1–2), 223–240. https://doi.org/10.1007/s00704-015-1705-6

Dieng, D., Laux, P., Smiatek, G., Heinzeller, D., Bliefernicht, J., Sarr, A., Gaye, A. T., & Kunstmann, H. (2018). Performance Analysis and Projected Changes of Agroclimatological Indices Across West Africa Based on High-Resolution Regional Climate Model Simulations. *Journal of Geophysical Research: Atmospheres*, *123*(15), 7950–7973. https://doi.org/10.1029/2018JD028536

Dinpashoh, Y., Singh, V. P., Biazar, S. M., & Kavehkar, S. (2019). Impact of climate change on streamflow timing (case study: Guilan Province). *Theoretical and Applied Climatology*, *138*(1–2), 65–76. https://doi.org/10.1007/s00704-019-02810-2

Diodato, N., & Ceccarelli, M. (2005). Interpolation processes using multivariate geostatistics for mapping of climatological precipitation mean in the Sannio Mountains (southern Italy). *Earth Surface Processes and Landforms*, *30*(3), 259–268. https://doi.org/10.1002/esp.1126

Dosio, A., Turner, A. G., Tamoffo, A. T., Sylla, M. B., Lennard, C., Jones, R. G., Terray, L., Nikulin, G., & Hewitson, B. (2020). A tale of two futures: Contrasting scenarios of future precipitation for West Africa from an ensemble of regional climate models. *Environmental Research Letters*, *15*(6), 64007. https://doi.org/10.1088/1748-9326/ab7fde

Driessen, T. L. A., Hurkmans, R. T. W. L., Terink, W., Hazenberg, P., Torfs, P. J. J. F., & Uijlenhoet, R. (2010). The hydrological response of the Ourthe catchment to climate change as modelled by the HBV model. *Hydrology and Earth System Sciences*, *14*(4), 651–665. https://doi.org/10.5194/hess-14-651-2010

Droppers, B., Franssen, W. H. P., Van Vliet, M. T. H., Nijssen, B., & Ludwig, F. (2020). Simulating human impacts on global water resources using VIC-5. *Geoscientific Model Development*, *13*(10), 5029–5052. https://doi.org/10.5194/gmd-13-5029-2020

Dwarakish, G. S., & Ganasri, B. P. (2015). Impact of land use change on hydrological systems: A review of current modeling approaches. *Cogent Geoscience*, *1*(1), 1115691. https://doi.org/10.1080/23312041.2015.1115691

Ebi, K. L., & Bowen, K. (2016). Extreme events as sources of health vulnerability: Drought as an example. *Weather and Climate Extremes*, *11*, 95–102. https://doi.org/10.1016/j.wace.2015.10.001

Ebodé, V. B., Braun, J. J., Nnomo, B. N., Mahé, G., Nkiaka, E., & Riotte, J. (2022). Impact of Rainfall Variability and Land Use Change on River Discharge in South Cameroon. *Water (Switzerland)*, *14*(6). https://doi.org/10.3390/w14060941

Efstratiadis, A., & Koutsoyiannis, D. (2010). Une décennie d'approches de calage multi-objectifs en modélisation hydrologique: Une revue. *Hydrological Sciences Journal*,

55(1), 58–78. https://doi.org/10.1080/02626660903526292

Eisner, S., Flörke, M., Chamorro, A., Daggupati, P., Donnelly, C., Huang, J., Hundecha, Y., Koch, H., Kalugin, A., Krylenko, I., Mishra, V., Piniewski, M., Samaniego, L., Seidou, O., Wallner, M., & Krysanova, V. (2017). An ensemble analysis of climate change impacts on streamflow seasonality across 11 large river basins. *Climatic Change*, *141*(3), 401–417. https://doi.org/10.1007/s10584-016-1844-5

Ekwezuo, C. S., Nnamchi, H. C., & Phil-Eze, P. O. (2017). Projected Changes in Mean Annual Rainfall Pattern Over West Africa during the Twenty First Century. *Pakistan Journal of Meteorology*, *14*(June 2018). http://cmip-pcmdi.llnl.gov/cmip5/.

Elsanabary, M. H., & Gan, T. Y. (2015). Evaluation of climate anomalies impacts on the Upper Blue Nile Basin in Ethiopia using a distributed and a lumped hydrologic model. *Journal of Hydrology*, *530*, 225–240. https://doi.org/10.1016/j.jhydrol.2015.09.052

Elsner, M. M., Cuo, L., Voisin, N., Deems, J. S., Hamlet, A. F., Vano, J. A., Mickelson, K. E. B., Lee, S. Y., & Lettenmaier, D. P. (2010). Implications of 21st century climate change for the hydrology of Washington State. *Climatic Change*, *102*(1–2), 225–260. https://doi.org/10.1007/s10584-010-9855-0

Epule, T. E., Ford, J. D., Lwasa, S., & Lepage, L. (2017). Climate change adaptation in the Sahel. *Environmental Science and Policy*, *75*(March), 121–137. https://doi.org/10.1016/j.envsci.2017.05.018

Fenta, A. A., Yasuda, H., Shimizu, K., Ibaraki, Y., Haregeweyn, N., Kawai, T., Belay, A. S., Sultan, D., & Ebabu, K. (2018). Evaluation of satellite rainfall estimates over the Lake Tana basin at the source region of the Blue Nile River. *Atmospheric Research*, *212*(2017), 43–53. https://doi.org/10.1016/j.atmosres.2018.05.009

Flato, G. J., Marotzke, B. A., Braconnot, P., Chou, S. ., Collins, W., Cox, P., Driouech, F., Emori, S., Eyring, S., Eyring, V., Forest, C., Glecker, P., Guilyardi, E., Jakob, C., Kattsov, V., Reason, C., & Rummukainen, M. (2013). Evaluation of climate models. In T. F. Stocker, D. Quin, G.-K. Plattner, M. Tignor, S. K. Allen, J. Boschung, A. Nauels, Y. Xia, V. Bex, & P. M. Midgley (Eds.), *Climate Change 2013 the Physical Science Basis: Working Group I Contribution to the Fifth Assessment Report of the Intergovernmental Panel on Climate Change* (Vol. 9781107057, pp. 741–866). Cambridge University Press, Cambridge. https://doi.org/10.1017/CBO9781107415324.020

Friesen, J., Andreini, M., Andah, W., Amisigo, B., & Van De Giesen, N. (2005). Storage capacity and long-term water balance of the Volta Basin, West Africa. *IAHS-AISH Publication*, *2*(296), 138–145.

Funk, C., Peterson, P., Landsfeld, M., Pedreros, D., Verdin, J., Shukla, S., Husak, G., Rowland, J., Harrison, L., Hoell, A., & Michaelsen, J. (2015). The climate hazards infrared precipitation with stations - A new environmental record for monitoring extremes. *Scientific Data*, *2*, 1–21. https://doi.org/10.1038/sdata.2015.66

Gan, T. Y., Dlamini, E. M., & Biftu, G. F. (1997). Effects of model complexity and structure, data quality, and objective functions on hydrologic modeling. *Journal of Hydrology*, *192*(1–4), 81–103. https://doi.org/10.1016/S0022-1694(96)03114-9

Gao, Y. (2017). *Dealing with missing data in hydrology-data analysis of discharge and groundwater time-series in Northeast Germany* [Freie University Berlin]. https://simongrund1.github.io/posts/anova-with-multiply-imputed-data-sets/

Gebrechorkos, S. H., Hülsmann, S., & Bernhofer, C. (2018). Evaluation of multiple climate data sources for managing environmental resources in East Africa. *Hydrology and Earth System Sciences*, *22*(8), 4547–4564. https://doi.org/10.5194/hess-22-4547-2018

Giorgi, F., & Gutowski, W. J. (2015). Regional Dynamical Downscaling and the CORDEX Initiative. *Annual Review of Environment and Resources*, *40*, 467–490. https://doi.org/10.1146/annurev-environ-102014-021217

Giorgi, F, Jones, C., & Asrar, G. (2009). Addressing climate information needs at the regional level: the CORDEX framework. ... *Organization (WMO) Bulletin*, *58*(July), 175–183. http://www.euro-cordex.net/uploads/media/Download_01.pdf

Giorgi, Filippo. (2019). Thirty Years of Regional Climate Modeling: Where Are We and Where Are We Going next? *Journal of Geophysical Research: Atmospheres*, *124*(11), 5696–5723. https://doi.org/10.1029/2018JD030094

Gnitou, G. T., Ma, T., Tan, G., Ayugi, B., Nooni, I. K., Alabdulkarim, A., & Tian, Y. (2019). Evaluation of the rossby centre regional climate model rainfall simulations over west africa using large-scale spatial and temporal statistical metrics. *Atmosphere*, *10*(12), 1–25. https://doi.org/10.3390/ATMOS10120802

Götzinger, J. (2007). *Distributed Conceptual Hydrological Modelling - Simulation of Climate , Land Use Change Impact and Uncertainty Analysis, PhD Thesis* [Universität Stuttgart]. http://elib.uni-stuttgart.de/opus/volltexte/2007/3349/pdf/Diss_Goetzinger_ub.pdf

Gulacha, M. M., & Mulungu, D. M. M. (2016). Generation of climate change scenarios for precipitation and temperature at local scales using SDSM in Wami-Ruvu River Basin Tanzania. *Physics and Chemistry of the Earth*. https://doi.org/10.1016/j.pce.2016.10.003

Gunawardhana, L. N., Al-Rawas, G. A., Kwarteng, A. Y., Al-Wardy, M., & Charabi, Y. (2018). Potential changes in the number of wet days and its effect on future intense and annual precipitation in northern Oman. *Hydrology Research*, *49*(1), 237–250. https://doi.org/10.2166/nh.2017.188

Gupta, H. V., Kling, H., Yilmaz, K. K., & Martinez, G. F. (2009). Decomposition of the mean squared error and NSE performance criteria: Implications for improving hydrological modelling. *Journal of Hydrology*, *377*(1–2), 80–91. https://doi.org/10.1016/j.jhydrol.2009.08.003

Guug, S. S., Abdul-Ganiyu, S., & Kasei, R. A. (2020). Application of SWAT hydrological model for assessing water availability at the Sherigu catchment of Ghana and Southern Burkina Faso. *HydroResearch*, *3*, 124–133. https://doi.org/10.1016/j.hydres.2020.10.002

Hadgu, G., Tesfaye, K., Mamo, G., & Kassa, B. (2013). Trend and variability of rainfall in Tigray , Northern Ethiopia : Analysis of meteorological data and farmers ' perception. *Academia Journal of Agricultural Research*, *1*(6), 88–100. https://doi.org/10.15413/ajar.2013.0117

Hallegatte, S., & Rozenberg, J. (2017). Climate change through a poverty lens. *Nature*

Climate Change, *7*(4), 250–256. https://doi.org/10.1038/nclimate3253

Hamlet, A. F., Elsner, M. M. G., Mauger, G. S., Lee, S. Y., Tohver, I., & Norheim, R. A. (2013). An overview of the columbia basin climate change scenarios project: Approach, methods, and summary of key results. *Atmosphere - Ocean*, *51*(4), 392–415. https://doi.org/10.1080/07055900.2013.819555

Hausfather, Z., Drake, H. F., Abbott, T., & Schmidt, G. A. (2020). Evaluating the Performance of Past Climate Model Projections. *Geophysical Research Letters*, *47*(1), 1–10. https://doi.org/10.1029/2019GL085378

Heinzeller, D., Dieng, D., Smiatek, G., Olusegun, C., Klein, C., Hamann, I., Salack, S., Bliefernicht, J., & Kunstmann, H. (2018). The WASCAL high-resolution regional climate simulation ensemble for West Africa: Concept, dissemination and assessment. *Earth System Science Data*, *10*(2), 815–835. https://doi.org/10.5194/essd-10-815-2018

Held, I. M. (2005). The gap between simulation and understanding in climate modeling. *Bulletin of the American Meteorological Society*, *86*(11), 1609–1614. https://doi.org/10.1175/BAMS-86-11-1609

Hirabayashi, Y., Mahendran, R., Koirala, S., Konoshima, L., Yamazaki, D., Watanabe, S., Kim, H., & Kanae, S. (2013). Global flood risk under climate change. *Nature Climate Change*, *3*(9), 816–821. https://doi.org/10.1038/nclimate1911

Hope, K. R. (2009). Climate change and poverty in Africa. *International Journal of Sustainable Development and World Ecology*, *16*(6), 451–461. https://doi.org/10.1080/13504500903354424

Houghton, J. T., Meira, L. G., Filho, B. A., Callander, N., Harris, A., & Kattenburg and K. Maskell (Eds.). (1995). Climate Change 1995. In *Climate Change 1995 - The Science of Climate Change: Contribution of Working Group I to the Second Assessment Report of the Intergovernmental Panel on Climate Change.* (ISBN 0 521 564336 hardback: 0 521 564360 paperback; Vol. 4, Issue 3). https://doi.org/10.1071/pc980275

Huang, S., Hattermann, F. F., Krysanova, V., & Bronstert, A. (2013). Projections of climate change impacts on river flood conditions in Germany by combining three different RCMs with a regional eco-hydrological model. *Climatic Change*, *116*(3–4), 631–663. https://doi.org/10.1007/s10584-012-0586-2

IFRC. (2017). *Emergency Plan of Action Final Report - Ghana: Floods*.

Ikpe, E., Sawa, B. A., Ejeh, L., & Adekunle, M. O. (2016). Adaptation Strategies To Climate Change Among Grain Farmers in Goronyo Local Government Area of Sokoto State. *International Journal of Science for Global Sustainability*, *2*(1), 55–65.

Ilori, O. W., & Balogun, I. A. (2022). Evaluating the performance of new CORDEX-Africa regional climate models in simulating West African rainfall. *Modeling Earth Systems and Environment*, *8*(1), 665–688. https://doi.org/10.1007/s40808-021-01084-w

IPCC. (2007). Synthesis Report. In *Synthesis Report. Contribution of Working Groups I, II and III to the Fourth Assessment Report of the Intergovernmental Panel on Climate Change [Core Writing Team, Pachauri, R. K. and Reisinger, A. (eds.)]. IPCC*. https://doi.org/10.1038/446727a

IPCC. (2012). Managing the Risks of Extreme Events and Disasters to Advance Climate Change Adaptation. In *Summary for Policymakers. In: Managing the Risks of Extreme Events and Disasters to Advance Climate Change Adaptation [Field, C. B. Barros, V. Stocker, T. F. Quin, D. Dokken, D. J. Ebi, K. L. Mastrandrea, M. D. Mach, K. J. Plattner, G. K. Allen, S. K. Tig*.

IPCC. (2014a). *Climate Change 2014 Synthesis Report. Contribution of Working Groups I, II and III to the Fifth Assessment Report of the Intergovernmental Panel on Climate Change [Core Writing Team, R.K. Pachauri and L.A. Meyer (eds.)]*.

IPCC. (2014b). Summary for policymakers. In *Climate Change 2014: Synthesis Report. Contribution of Working Groups I, II and III to the Fifth Assessment Report of the Intergovernmental Panel on Climate Change [Core Writing Team, R. K. Pachauri and L. A. Meyer (eds.)]. IPCC, Geneva, Switzerland.* https://doi.org/10.1017/CBO9781139177245.003

Isaak, D. J., Wollrab, S., Horan, D., & Chandler, G. (2012). Climate change effects on stream and river temperatures across the northwest U.S. from 1980-2009 and implications for salmonid fishes. *Climatic Change*, *113*(2), 499–524. https://doi.org/10.1007/s10584-011-0326-z

Jacob, D., Petersen, J., Eggert, B., Alias, A., Christensen, O. B., Bouwer, L. M., Braun, A., Colette, A., Déqué, M., Georgievski, G., Georgopoulou, E., Gobiet, A., Menut, L., Nikulin, G., Haensler, A., Hempelmann, N., Jones, C., Keuler, K., Kovats, S., … Yiou, P. (2014). EURO-CORDEX: New high-resolution climate change projections for European impact research. *Regional Environmental Change*, *14*(2), 563–578. https://doi.org/10.1007/s10113-013-0499-2

Jain, C. K., & Singh, S. (2020). Impact of climate change on the hydrological dynamics of River Ganga, India. *Journal of Water and Climate Change*, *11*(1), 274–290. https://doi.org/10.2166/wcc.2018.029

Jaiswal, R. K., Ali, S., & Bharti, B. (2020). Comparative evaluation of conceptual and physical rainfall–runoff models. *Applied Water Science*, *10*(1), 1–14. https://doi.org/10.1007/s13201-019-1122-6

Jiang, Q. (2003). Moist dynamics and orographic precipitation. *Tellus A: Dynamic Meteorology and Oceanography*, *55*(4), 301. https://doi.org/10.3402/tellusa.v55i4.14577

Jiménez-Navarro, I. C., Jimeno-Sáez, P., López-Ballesteros, A., Pérez-Sánchez, J., & Senent-Aparicio, J. (2021). Impact of climate change on the hydrology of the forested watershed that drains to lake erken in sweden: An analysis using swat+ and cmip6 scenarios. *Forests*, *12*(12). https://doi.org/10.3390/f12121803

Johnson, F., & Sharma, A. (2011). Accounting for interannual variability: A comparison of options for water resources climate change impact assessments. *Water Resources Research*, *47*(4). https://doi.org/10.1029/2010WR009272

Joseph E, J., Akinrotimi, O. O., Rao, K. P. ., Ramaraj, A. P., Traore, P. S. C., Sujatha, P., & Whitbread, A. M. (2020). *The Usefulness of Gridded Climate Data Products in Characterizing Climate Variability and Assessing Crop Production The Usefulness of Gridded Climate Data Products in Characterizing Climate Variability and Assessing*

Crop Production (CCAFS Working Paper no. 322; Issue November). https://doi.org/10.13140/RG.2.2.27548.31367

Jung, G., & Kunstmann, H. (2007). High-resolution regional climate modeling for the Volta region of West Africa. *Journal of Geophysical Research Atmospheres*, *112*(23), 1–17. https://doi.org/10.1029/2006JD007951

Kabir, H., & Golder, J. (2017). Rainfall Variability and Its Impact on Crop Agriculture in Southwest Region of Bangladesh. *Journal of Climatology & Weather Forecasting*, *05*(01), 1–20. https://doi.org/10.4172/2332-2594.1000196

Kasei, R. A. (2009). *Modelling impacts of climate change on water resources in the Volta Basin, West Africa.* [Rheinischen Friedrich-Wilhelms-Universität Bonn]. http://hss.ulb.uni-bonn.de/diss_online elektronisch publiziert

Kasei, R., Diekkrüger, B., & Leemhuis, C. (2010). Drought frequency in the Volta Basin of West Africa. *Sustainability Science*, *5*(1), 89–97. https://doi.org/10.1007/s11625-009-0101-5

Kiesel, J., Gericke, A., Rathjens, H., Wetzig, A., Kakouei, K., Jähnig, S. C., & Fohrer, N. (2019). Climate change impacts on ecologically relevant hydrological indicators in three catchments in three European ecoregions. *Ecological Engineering*, *127*(December 2018), 404–416. https://doi.org/10.1016/j.ecoleng.2018.12.019

Kimaru, A. N., Gathenya, J. M., & Cheruiyot, C. K. (2019). The temporal variability of rainfall and streamflow into Lake Nakuru, Kenya, assessed using swat and hydrometeorological indices. *Hydrology*, *6*(4). https://doi.org/10.3390/HYDROLOGY6040088

Kjellström, E., Bärring, L., Nikulin, G., Nilsson, C., Persson, G., & Strandberg, G. (2016). Production and use of regional climate model projections – A Swedish perspective on building climate services. *Climate Services*, *2–3*, 15–29. https://doi.org/10.1016/j.cliser.2016.06.004

Klassou, K. S., & Komi, K. (2021). Analysis of extreme rainfall in Oti River Basin (West Africa). *Journal of Water and Climate Change*, *12*(5), 1997–2009. https://doi.org/10.2166/wcc.2021.154

Klassou, Komi S., & Komi, K. (2021). Analysis of extreme rainfall in oti river basin (West africa). *Journal of Water and Climate Change*, *12*(5), 1997–2009. https://doi.org/10.2166/wcc.2021.154

Komi, K., Amisigo, B. A., & Diekkrüger, B. (2016). Integrated flood risk assessment of rural communities in the Oti River basin, West Africa. *Hydrology*, *3*(4), 1–14. https://doi.org/10.3390/hydrology3040042

Komi, K., Neal, J., Trigg, M. A., & Diekkrüger, B. (2017). Modelling of flood hazard extent in data sparse areas: a case study of the Oti River basin, West Africa. *Journal of Hydrology: Regional Studies*, *10*, 122–132. https://doi.org/10.1016/j.ejrh.2017.03.001

Konapala, G., Mishra, A. K., Wada, Y., & Mann, M. E. (2020). Climate change will affect global water availability through compounding changes in seasonal precipitation and evaporation. *Nature Communications*, *11*(1), 1–10. https://doi.org/10.1038/s41467-020-

16757-w

Koutsouris, A. J., Seibert, J., & Lyon, S. W. (2017). Utilization of global precipitation datasets in data limited regions: A case study of Kilombero Valley, Tanzania. *Atmosphere*, *8*(12). https://doi.org/10.3390/atmos8120246

Kumi, N., Abiodun, B. J., & Adefisan, E. A. (2020). Performance Evaluation of a Subseasonal to Seasonal Model in Predicting Rainfall Onset Over West Africa. *Earth and Space Science*, *7*(8), 1–13. https://doi.org/10.1029/2019EA000928

Kunstmann, H., & Jung, G. (2005). Impact of regional climate change on water availability in the Volta basin of West Africa. *Regional Hydrological Impacts of Climatic Variability and Change (Proceedings of Symposium S6), April*, 1–11. papers2://publication/uuid/C9E8B1B8-CEE2-458B-8AF3-9463412A741A

Kwakye, S. . (2016). *Study on the effects of climate change on the hydrology of the West African sub-region*. University of Stuttgart.

Kwakye, S. O., & Bárdossy, A. (2020). Hydrological modelling in data-scarce catchments: Black Volta basin in West Africa. *SN Applied Sciences*, *2*(4), 1–19. https://doi.org/10.1007/s42452-020-2454-4

Kwawuvi, D., Mama, D., Agodzo, S. K., Hartmann, A., Larbi, I., Bessah, E., Limantol, A. M., Dotse, S.-Q., & Yangouliba, G. I. (2022). Spatiotemporal variability and change in rainfall in the Oti River Basin, West Africa. *Journal of Water and Climate Change*, *13*(3), 1–19. https://doi.org/10.2166/wcc.2022.368

Lacombe, G., McCartney, M., & Forkuor, G. (2012). Assèchement du Ghana de 1960 à 2005: Preuve par le test de Mann-Kendall basé sur une technique de rééchantillonnage, aux niveaux local et régional. *Hydrological Sciences Journal*, *57*(8), 1594–1609. https://doi.org/10.1080/02626667.2012.728291

Lala, J., Yang, M., Wang, G., & Block, P. (2021). Utilizing rainy season onset predictions to enhance maize yields in Ethiopia. *Environmental Research Letters*, *16*(5), 1–11. https://doi.org/10.1088/1748-9326/abf9c9

Lane, R. A., Coxon, G., E Freer, J., Wagener, T., J Johnes, P., P Bloomfield, J., Greene, S., J A Macleod, C., & M Reaney, S. (2019). Benchmarking the predictive capability of hydrological models for river flow and flood peak predictions across over 1000 catchments in Great Britain. *Hydrology and Earth System Sciences*, *23*(10), 4011–4032. https://doi.org/10.5194/hess-23-4011-2019

Larbi, I., Hountondji, F. C. C., Annor, T., Agyare, W. A., Gathenya, J. M., & Amuzu, J. (2018). Spatio-Temporal Trend Analysis of Rainfall and Temperature Extremes in the Vea Catchment , Ghana. *Climate*, *6*(87), 1–17. https://doi.org/10.3390/cli6040087

Lare, A. R., & Nicholson, S. E. (1994). Contrasting Conditions of Surface Water Balance in Wet Years and Dry Years as a Possible Land Surface-Atmosphere Feedback Mechanism in the West African Sahel. *Journal of Climate*, *7*(5), 653–668.

Laux, P., Kunstmann, H., & B´ardossy, A. (2008). The impact of the positive Indian Ocean dipole on Zimbabwe droughts Tropical climate is understood to be dominated by. *International Journal of Climatology*, *28*, 329–342. https://doi.org/10.1002/joc

Lebel, T., & Ali, A. (2009). Recent trends in the Central and Western Sahel rainfall regime (1990-2007). *Journal of Hydrology*, *375*(1–2), 52–64. https://doi.org/10.1016/j.jhydrol.2008.11.030

Lebel, Thierry, Cappelaere, B., Galle, S., Hanan, N., Kergoat, L., Levis, S., Vieux, B., Descroix, L., Gosset, M., Mougin, E., Peugeot, C., & Seguis, L. (2009). AMMA-CATCH studies in the Sahelian region of West-Africa: An overview. *Journal of Hydrology*, *375*(1–2), 3–13. https://doi.org/10.1016/j.jhydrol.2009.03.020

Lemoalle, J., & de Condappa, D. (2010). Farming systems and food production in the volta basin. *Water International*, *35*(5), 655–680. https://doi.org/10.1080/02508060.2010.510793

Leng, G. Y., Tang, Q. H., Huang, M. Y., Hong, Y., & Ruby, L. L. (2015). Projected changes in mean and interannual variability of surface water over continental China. *Science China Earth Sciences*, *58*(5), 739–754. https://doi.org/10.1007/s11430-014-4987-0

Lenhart, C. F., Peterson, H., & Nieber, J. (2011). Increased streamflow in agricultural watersheds of the Midwest: implications for management. *Watershed Science Bulletin*, *2*(1), 25–31.

Li, Y., Feng, A., Liu, W., Ma, X., & Dong, G. (2017). Variation of aridity index and the role of climate variables in the Southwest China. *Water (Switzerland)*, *9*(10), 1–14. https://doi.org/10.3390/w9100743

Li, Z., & Jin, J. (2017). Evaluating climate change impacts on streamflow variability based on a multisite multivariate GCM downscaling method in the Jing River of China. *Hydrology and Earth System Sciences*, *21*(11), 5531–5546. https://doi.org/10.5194/hess-21-5531-2017

Lindstrom, G., Johansson, B., Persson, M., Gardelin, M., & Bergström, S. (1997). Development and test of the distributed HBV-96 hydrological model. *Journal of Hydrology*, *201*, 272–288. https://doi.org/10.2166/wst.2009.488

Liu, L., Xu, Z., & Huang, J. (2009). Impact of climate change on streamflow in the Xitiaoxi catchment, Taihu Basin. *Wuhan University Journal of Natural Sciences*, *14*(6), 525–531. https://doi.org/10.1007/s11859-009-0612-z

Lizumi, T., Okada, M., & Yokozawza, M. (2014). A meteorological forcing data set for global crop modeling: Development, evaluation, and intercomparison. *Journal of Geophysical Research: Atmospheres*, *119*, 363–384. https://doi.org/doi:10.1002/2013JD020130.

Lu, G. Y., & Wong, D. W. (2008). An adaptive inverse-distance weighting spatial interpolation technique. *Computers and Geosciences*, *34*(9), 1044–1055. https://doi.org/10.1016/j.cageo.2007.07.010

Luce, C., Staab, B., Kramer, M., Wenger, S., Isaak, D., & McConnell, C. (2014). variability in the Pacific Northwest. *Water Resources Research*, *50*, 3428–3443. https://doi.org/10.1002/2013WR014329.Received

Lutz, A. F., ter Maat, H. W., Biemans, H., Shrestha, A. B., Wester, P., & Immerzeel, W. W. (2016). Selecting representative climate models for climate change impact studies: an

advanced envelope-based selection approach. *International Journal of Climatology*, *36*(12), 3988–4005. https://doi.org/10.1002/joc.4608

Mahe, G., Leduc, C., Amani, A., Paturel, J. E., Girard, S., Servat, E., & Dezetter, A. (2003). Recent increase in the surface runoff the Sudan-Sahel and impact on the water resources. *IAHS-AISH Publication*, *278*, 215–222.

Mahe, G., Lienou, G., Descroix, L., Bamba, F., Paturel, J. E., Laraque, A., Meddi, M., Habaieb, H., Adeaga, O., Dieulin, C., Chahnez Kotti, F., & Khomsi, K. (2013). The rivers of Africa: Witness of climate change and human impact on the environment. *Hydrological Processes*, *27*(15), 2105–2114. https://doi.org/10.1002/hyp.9813

Majumder, S. I. M., Hasan, I., Mandal, S., M., K. I., Md., M. R., N., H. H., & Sultana, I. (2017). Climate Change Induced Multi Hazards Disaster Risk Assessment in Southern Coastal Belt of Bangladesh. *American Journal of Environmental Engineering and Science.*, *Vol. 4*(1), 1–7.

Makondo, C. C., & Thomas, D. S. G. (2020). Seasonal and intra-seasonal rainfall and drought characteristics as indicators of climate change and variability in Southern Africa: a focus on Kabwe and Livingstone in Zambia. *Theoretical and Applied Climatology*, *140*(1–2), 271–284. https://doi.org/10.1007/s00704-019-03029-x

Maranan, M., Fink, A. H., Knippertz, P., Francis, S. D., Akpo, A. B., Jegede, G., & Yorke, C. (2019). Interactions between convection and a moist vortex associated with an extreme rainfall event over southern West Africa. *Monthly Weather Review*, *147*(7), 2309–2328. https://doi.org/10.1175/MWR-D-18-0396.1

McKee, T. B., Doesken, N. J., & Kleist, J. (1993). The relationship of drought frequency and duration to time scales. *Proceedings of the 8th Conference on Applied Climatology*, 179–184. https://doi.org/10.1002/jso.23002

Meresa, H. K., & Gatachew, M. T. (2019). Climate change impact on river flow extremes in the upper blue nile river basin. *Journal of Water and Climate Change*, *10*(4), 759–781. https://doi.org/10.2166/wcc.2018.154

Moriasi, D. N., Arnold, J. G., Liew, M. W. Van, Bingner, R. L., Harmel, R. D., & Veith, T. L. (2007). Model Evaluation Guidelines For Systematic Quantification Of Accuracy In Watershed Simulations. *American Society of Agricultural and Biological Engineers*, *50*(3), 885–900.

Moriasi, D. N., Gitau, M. W., Pai, N., & Daggupati, P. (2015). Hydrologic and water quality models: Performance measures and evaluation criteria. *American Society of Agricultural and Biological Engineers*, *58*(6), 1763–1785. https://doi.org/10.13031/trans.58.10715

Mosunmola, I. A., Samaila, I. K., Emmanuel, B., & Adolphus, I. (2020). Evaluation of Onset and Cessation of Rainfall and Temperature on Maize Yield in Akure, Ondo State, Nigeria. *Atmospheric and Climate Sciences*, *10*(02), 125–145. https://doi.org/10.4236/acs.2020.102006

Mounkaila, M. S., Abiodun, B. J., & Bayo Omotosho, J. (2015). Assessing the capability of CORDEX models in simulating onset of rainfall in West Africa. *Theoretical and Applied Climatology*, *119*(1–2), 255–272. https://doi.org/10.1007/s00704-014-1104-4

Mugalavai, E. M., Kipkorir, E. C., Raes, D., Rao, M. S. (2008). Analysis of Rainfall Onset, Cessation and Length of Growing Season for Western Kenya. Agric For Meteorol 148(6–7):1123–1135. https://doi.org/10.1016/j.agrformet.2008.02.013

Mujere, N., & Moyce, W. (2016). Climate change impacts on surface water quality. *Environmental Sustainability and Climate Change Adaptation Strategies*, *July*, 322–340. https://doi.org/10.4018/978-1-5225-1607-1.ch012

Mul, M., Obuobie, E., Appoh, R., Kankam-Yeboah, K., Bekoe-Obeng, E., Amisigo, B., Logah, F. Y., Ghansah, B., & McCartney, M. (2015). Water resources assessment of the Volta River Basin. In *(IWMI Working Paper 166)* (No. 166; (IWMI Working Paper 166), Vol. 166). https://doi.org/10.5337/2015.220

MWH (Ministry of Works and Housing) (1998). Water resources management study, information building block study. Part II, Vol. 2. Volta Basin System, Groundwater Resources. Report for the Ministry of Works and Housing (MWH). Accra: Nii Consulting Ltd.

Nhemachena, C., Nhamo, L., Matchaya, G., Nhemachena, C. R., Muchara, B., Karuaihe, S. T., & Mpandeli, S. (2020). Climate Change Impacts on Water and Agriculture Sectors in Southern Africa : Threats and Opportunities for Sustainable Development. *Water*, *12*(10), 1–17.

Nicholson, S. E. (2009). A revised picture of the structure of the "monsoon" and land ITCZ over West Africa. *Climate Dynamics*, *32*(7–8), 1155–1171. https://doi.org/10.1007/s00382-008-0514-3

Nicholson, S. E., & Grist, J. P. (2001). A conceptual model for understanding rainfall variability in the West African Sahel on interannual and interdecadal timescales. *International Journal of Climatology*, *21*(14), 1733–1757. https://doi.org/10.1002/joc.648

Nicholson, S. E., & Palao, I. M. (1993). A re-evaluation of rainfall variability in the sahel. Part I. Characteristics of rainfall fluctuations. *International Journal of Climatology*, *13*(4), 371–389. https://doi.org/10.1002/joc.3370130403

Niel, H., Paturel, J. E., & Servat, E. (2003). Study of parameter stability of a lumped hydrologic model in a context of climatic variability. *Journal of Hydrology*, *278*(1–4), 213–230. https://doi.org/10.1016/S0022-1694(03)00158-6

Nikiema, P. M., Sylla, M. B., Ogunjobi, K., Kebe, I., Gibba, P., & Giorgi, F. (2017). Multi-model CMIP5 and CORDEX simulations of historical summer temperature and precipitation variabilities over West Africa. *International Journal of Climatology*, *37*(5), 2438–2450. https://doi.org/10.1002/joc.4856

Obahoundje, S., Diedhiou, A., Ofosu, E. A., Anquetin, S., François, B., Adounkpe, J., Amoussou, E., Kouame, Y. M., Kouassi, K. L., Bi, V. H. N., & Ta, M. Y. (2018). Assessment of spatio-temporal changes of land use and land cover over South-Western African basins and their relations with variations of discharges. *Hydrology*, *5*(4). https://doi.org/10.3390/hydrology5040056

Obuobie, E., & Barry, B. (2010). *Groundwater in sub-Saharan Africa : Implications for food security and livelihoods*.

Ocen, E., de Bie, C. A. J. M., & Onyutha, C. (2021). Investigating false start of the main growing season: A case of Uganda in East Africa. *Heliyon*, *7*(11), 1–16. https://doi.org/10.1016/j.heliyon.2021.e08428

Ogega, O. M., Gyampoh, B. A., & Mistry, M. N. (2020). Intraseasonal precipitation variability over West Africa under 1.5 °c and 2.0 °c global warming scenarios: Results from cordex RCMS. *Climate*, *8*(12), 1–19. https://doi.org/10.3390/cli8120143

Oguntunde, P. G., Abiodun, B. J., Lischeid, G., & Abatan, A. A. (2020). Droughts projection over the Niger and Volta River basins of West Africa at specific global warming levels. *International Journal of Climatology*, *40*(13), 5688–5699. https://doi.org/10.1002/joc.6544

Oguntunde, P. G., Friesen, J., van de Giesen, N., & Savenije, H. H. G. (2006). Hydroclimatology of the Volta River Basin in West Africa: Trends and variability from 1901 to 2002. *Physics and Chemistry of the Earth*, *31*(18), 1180–1188. https://doi.org/10.1016/j.pce.2006.02.062

Okafor, G., Annor, T., Odai, S., & Agyekum, J. (2019). Volta basin precipitation and temperature climatology: evaluation of CORDEX-Africa regional climate model simulations. *Theoretical and Applied Climatology*, *137*(3–4), 2803–2827. https://doi.org/10.1007/s00704-018-2746-4

Omotosho, J. B., Balogun, A. A., & Ogunjobi, K. (2000). Predicting monthly and seasonal rainfall, onset and cessation of the rainy season in West Africa using only surface data. *International Journal of Climatology*, *20*, 865–880. https://doi.org/10.1002/1097-0088(20000630)20:8<865::AID-JOC505>3.0.CO;2-R

Önöz, B., & Bayazit, M. (2003). The power of statistical tests for trend detection. *Turkish Journal of Engineering and Environmental Sciences*, *27*(4), 247–251. https://doi.org/10.3906/sag-1205-120

Oruonye, E. D., Ahmed, Y. M., Gambo, M. N., & Tukura, E. (2016). Effects of Rainfall Variability on Maize Yield in Gassol LGA, Taraba State, Nigeria. *Journal of Agriculture Biotechnology*, *1*(1), 1–8.

Owusu, K., & Waylen, P. (2009). Trends in spatio-temporal variability in annual rainfall in Ghana (1951-2000). *Weather*, *64*(5), 115–120. https://doi.org/10.1002/wea.255

Owusu, Kwadwo, Waylen, P., & Qiu, Y. (2008). Changing rainfall inputs in the Volta basin: Implications for water sharing in Ghana. *GeoJournal*, *71*(4), 201–210. https://doi.org/10.1007/s10708-008-9156-6

Pabón, J. D., & Dorado, J. (2008). Intraseasonal variability of rainfall over Northern South America and Caribbean region. *Earth Sciences Research Journal*, *12*(2), 194–212.

Paturel, J. E., Ouedraogo, M., Mahe, G., Servat, E., Dezetter, A., & Ardoin, S. (2003). The influence of distributed input data on the hydrological modelling of monthly river flow regimes in West Africa. *Hydrological Sciences Journal*, *48*(6), 881–890. https://doi.org/10.1623/hysj.48.6.881.51422

Perrin, C., Michel, C., & Andréassian, V. (2003). Improvement of a parsimonious model for streamflow simulation. *Journal of Hydrology*, *279*(1–4), 275–289.

https://doi.org/10.1016/S0022-1694(03)00225-7

Pervin, L., Gan, T. Y., Scheepers, H., & Islam, M. S. (2021). Application of the hbv model for the future projections of water levels using dynamically downscaled global climate model data. *Journal of Water and Climate Change*, *12*(6), 2364–2377. https://doi.org/10.2166/wcc.2021.302

Polade, S. D., Pierce, D. W., Cayan, D. R., Gershunov, A., & Dettinger, M. D. (2014). The key role of dry days in changing regional climate and precipitation regimes. *Scientific Reports*, *4*, 1–8. https://doi.org/10.1038/srep04364

Porkka, M., Wang-Erlandsson, L., Destouni, G., Ekman, A. M. L., Rockström, J., & Gordon, L. J. (2021). Is wetter better? Exploring agriculturally-relevant rainfall characteristics over four decades in the Sahel. *Environmental Research Letters*, *16*(3). https://doi.org/10.1088/1748-9326/abdd57

Prowse, T. D., Beltaos, S., Gardner, J. T., Gibson, J. J., Granger, R. J., Leconte, R., Peters, D. L., Pietroniro, A., Romolo, L. A., & Toth, B. (2006). Climate change, flow regulation and land-use effects on the hydrology of the Peace-Athabasca-Slave system; Findings from the Northern Rivers Ecosystem Initiative. *Environmental Monitoring and Assessment*, *113*(1–3), 167–197. https://doi.org/10.1007/s10661-005-9080-x

Prudhomme, C., Giuntoli, I., Robinson, E. L., Clark, D. B., Arnell, N. W., Dankers, R., Fekete, B. M., Franssen, W., Gerten, D., Gosling, S. N., Hagemann, S., Hannah, D. M., Kim, H., Masaki, Y., Satoh, Y., Stacke, T., Wada, Y., & Wisser, D. (2014). Hydrological droughts in the 21st century, hotspots and uncertainties from a global multimodel ensemble experiment. *Proceedings of the National Academy of Sciences of the United States of America*, *111*(9), 3262–3267. https://doi.org/10.1073/pnas.1222473110

Qiao, L., Pan, Z., Herrmann, R. B., & Hong, Y. (2014). Hydrological Variability and Uncertainty of Lower Missouri River Basin Under Changing Climate. *Journal of the American Water Resources Association*, *50*(1), 246–260. https://doi.org/10.1111/jawr.12126

Quan, Z., Teng, J., Sun, W., Cheng, T., & Zhang, J. (2015). Evaluation of the HYMOD model for rainfall-runoff simulation using the GLUE method. *IAHS-AISH Proceedings and Reports*, *368*(August 2014), 180–185. https://doi.org/10.5194/piahs-368-180-2015

Ramachandran, A., Khan, Saleem, R., & Palanivelu, K. Prasannavenkatesh, N Jayanthi, A. (2017). Projection of climate change-induced sea-level rise for the coasts of Tamil Nadu and Puducherry, India using SimCLIM: a first step towards planning adaptation policies. *Journal of Coastal Conservation*, *v. 21*(6), 731-742–2017 v.21 no.6. https://doi.org/10.1007/s11852-017-0532-6

Rameshwaran, P., Bell, V. A., Davies, H. N., & Kay, A. L. (2021). How might climate change affect river flows across West Africa? *Climatic Change*, *169*(3–4), 1–27. https://doi.org/10.1007/s10584-021-03256-0

Raymond, P. A., Oh, N. H., Turner, R. E., & Broussard, W. (2008). Anthropogenically enhanced fluxes of water and carbon from the Mississippi River. *Nature*, *451*(7177), 449–452. https://doi.org/10.1038/nature06505

Reddy, H. N., Ranjan, A., & Denis, D. M. (2020). Understanding Sensitivity of the Soil

Moisture Routine Parameters using Integrated Hydrological Modelling System (HBV) in a Small Semi-Arid Agricultural Watershed. *Journal of Water Engineering and Management*, *1*(2). https://doi.org/10.47884/jweam.v1i2pp61-75

Risal, A., Urfels, A., Srinivasan, R., Bayissa, Y., Shrestha, N., Paudel, G., & Krupnik, J. T. (2022). Impact of Climate Change on Water Resources and Crop Production in Western Nepal: Implications and Adaptation Strategies. *Agriculture (Switzerland)*, *12*(7), 1–19. https://doi.org/10.3390/agriculture12071056

Roe, G. H. (2005). Orographic precipitation. *Annual Review of Earth and Planetary Sciences*, *33*, 645–671. https://doi.org/10.1146/annurev.earth.33.092203.122541

Roudier, P., Ducharne, A., & Feyen, L. (2014). Climate change impacts on runoff in West Africa: A review. *Hydrology and Earth System Sciences*, *18*(7), 2789–2801. https://doi.org/10.5194/hess-18-2789-2014

Rummukainen, M., Rockel, B., Bärring, L., Christensen, J. H., & Reckermann, M. (2015). Twenty-first-century challenges in regional climate modeling. *Bulletin of the American Meteorological Society*, *96*(8), 135–138. https://doi.org/10.1175/BAMS-D-14-00214.1

Rusli, S. R., Yudianto, D., & Liu, J. tao. (2015). Effects of temporal variability on HBV model calibration. *Water Science and Engineering*, *8*(4), 291–300. https://doi.org/10.1016/j.wse.2015.12.002

Safeeq, M., Grant, G. E., Lewis, S. L., & Tague, C. L. (2013). Coupling snowpack and groundwater dynamics to interpret historical streamflow trends in the western United States. *Hydrological Processes*, *27*(5), 655–668. https://doi.org/10.1002/hyp.9628

Sahin, S. (2012). An aridity index defined by precipitation and specific humidity. *Journal of Hydrology*, *444–445*, 199–208. https://doi.org/10.1016/j.jhydrol.2012.04.019

Sall, S. M., Viltard, A., & Sauvageot, H. (2007). Rainfall distribution over the Fouta Djallon - Guinea. *Atmospheric Research*, *86*(2), 149–161. https://doi.org/10.1016/j.atmosres.2007.03.008

Samuelsson, P., Jones, C. G., Willén, U., Ullerstig, A., Gollvik, S., Hansson, U., Jansson, C., Kjellström, E., Nikulin, G., & Wyser, K. (2011). The Rossby Centre Regional Climate model RCA3: Model description and performance. *Tellus, Series A: Dynamic Meteorology and Oceanography*, *63*(1), 4–23. https://doi.org/10.1111/j.1600-0870.2010.00478.x

Sawai, N., Kobayashi, K., Apip, Takara, K., Ishikawa, H., Yokomatsu, M., Samaddar, S., Juati, A. N., & Kranjac-Berisavljevic, G. (2014). Impact of climate change on river flows in the Black Volta River. *Journal of Disaster Research*, *9*(4), 432–442. https://doi.org/10.20965/jdr.2014.p0432

Schalla, J., Hartmann, A., Abraham, T., & Liu, Y. (2023). *Uncorrected Proof Global hydrological parameter estimates to local applications : in fl uence of forcing and catchment properties Uncorrected Proof*. *00*(0), 1–16. https://doi.org/10.2166/nh.2023.086

Schewe, J., Heinke, J., Gerten, D., Haddeland, I., Arnell, N. W., Clark, D. B., Dankers, R., Eisner, S., Fekete, B. M., Colón-González, F. J., Gosling, S. N., Kim, H., Liu, X.,

Masaki, Y., Portmann, F. T., Satoh, Y., Stacke, T., Tang, Q., Wada, Y., … Kabat, P. (2014). Multimodel assessment of water scarcity under climate change. *Proceedings of the National Academy of Sciences of the United States of America*, *111*(9), 3245–3250. https://doi.org/10.1073/pnas.1222460110

Seibert, J., & Vis, M. J. P. (2012). Teaching hydrological modeling with a user-friendly catchment-runoff-model software package. *Hydrology and Earth System Sciences*, *16*(9), 3315–3325. https://doi.org/10.5194/hess-16-3315-2012

Sharma, R. K., Kumar, S., Vatta, K., Bheemanahalli, R., Dhillon, J., & Reddy, K. N. (2022). Impact of recent climate change on corn, rice, and wheat in southeastern USA. *Scientific Reports*, *12*(1), 16928. https://doi.org/10.1038/s41598-022-21454-3

Shi, F., Li, X., Wang, Y., Ma, X., Zhu, J., & Zhao, C. (2022). Streamflow Consumption vs. Climate Change in the Evolution of Discharge in the Tarim River Basin, Northwest China. *Water (Switzerland)*, *14*(3), 1–11. https://doi.org/10.3390/w14030392

Singh, K. S., & Marcy, N. (2017). Comparison of Simple and Complex Hydrological Models for Predicting Catchment Discharge Under Climate Change. *AIMS Geosciences*, *3*(3), 467–497. https://doi.org/10.3934/geosci.2017.3.467

Singh, S. K., Augas, J., Pahlow, M., & Graham, S. L. (2020). Methods for regional calibration - a case study using the TopNet hydrological model for the Bay of Plenty region, New Zealand. *Australian Journal of Water Resources*, *24*(2), 153–166. https://doi.org/10.1080/13241583.2020.1821487

Sokona, Y., & Denton, F. (2001). Climate change impacts: Can Africa cope with the challenges? *Climate Policy*, *1*(1), 117–123. https://doi.org/10.3763/cpol.2001.0110

Soro, T. D., Kouakou, B. D., Kouassi, E. A., Soro, G., Kouassi, A. M., Kouadio, K. E., Yéi, M.-S. O., & Soro, N. (2013). Hydroclimatology and land use dynamics of the Upper Bandama watershed in Tortiya (Northern Côte d'Ivoire). *VertigO*, *13*(3), 1–23. https://doi.org/10.4000/vertigo.14468

Stackhouse, P. W., Zhang, T., Westberg, D., Barnett, A. J., Bristow, T., Macpherson, B., & Hoell, J. M. (2018). POWER Release 8.0.1 (with GIS Applications) Methodology (Data Parameters, Sources, Validation) Documentation Date. *NASA Langley Research Center*, *8*, 1–99.

Stanzel, P., Kling, H., & Bauer, H. (2018). Climate change impact on West African rivers under an ensemble of CORDEX climate projections. *Climate Services*, *11*(July 2017), 36–48. https://doi.org/10.1016/j.cliser.2018.05.003

Stern, R. D., Dennett, M. D., & Garbutt, D. J. (1981). The start of the rains in West Africa. *Journal of Climatology*, *1*, 59–68.

Stern, R., Rijks, D., Dale, I., & Knock, J. (2006). *Instant Climatic Guide*. *January*, 1–330. https://www.researchgate.net/profile/Roger_Stern/publication/264879427_Instat_Climatic_Guide/links/566532fb08ae4931cd60a556/Instat-Climatic-Guide.pdf

Suleiman, Y., & Ifabiyi, I. (2015). The role of rainfall variability in reservoir storage management at Shiroro hydropower dam, Nigeria. *AFRREV STECH: An International Journal of Science and Technology*, *3*(2), 18–30. https://doi.org/10.4314/stech.v3i2.2

Sultan, B., & Gaetani, M. (2016). Agriculture in West Africa in the twenty-first century: Climate change and impacts scenarios, and potential for adaptation. *Frontiers in Plant Science*, *7*(AUG2016), 1–20. https://doi.org/10.3389/fpls.2016.01262

Suryoputro, N., Suhardjono, Soetopo, W., & Suhartanto, E. (2017). Calibration of infiltration parameters on hydrological tank model using runoff coefficient of rational method. *AIP Conference Proceedings*, *1887*(September). https://doi.org/10.1063/1.5003539

Sylla, M. B., Pal, J. S., Faye, A., Dimobe, K., & Kunstmann, H. (2018). Climate change to severely impact West African basin scale irrigation in 2 °C and 1.5 °C global warming scenarios. *Scientific Reports*, *8*(1), 14395. https://doi.org/10.1038/s41598-018-32736-0

Taylor, J. C., Van De Giesen, N., & Steenhuis, T. S. (2006). West Africa: Volta discharge data quality assessment and use. *Journal of the American Water Resources Association*, *42*(4), 1113–1126. https://doi.org/10.1111/j.1752-1688.2006.tb04517.x

Taylor, K. E., Stouffer, R. J., & Meehl, G. A. (2012). An overview of CMIP5 and the experiment design. *Bulletin of the American Meteorological Society*, *93*(4), 485–498. https://doi.org/10.1175/BAMS-D-11-00094.1

Taylor, S. (2005). *Taylor Diagram Primer Karl E. Taylor*. *January*.

Tegegn, M. G. (2015). *Analysis of Past and Future Intra-Seasonal Rainfall Variability and its Implications for Crop Production in the North Eastern Amhara Region, Ethiopia.* [Haramaya University]. http://publicacoes.cardiol.br/portal/ijcs/portugues/2018/v3103/pdf/3103009.pdf%0Ahttp://www.scielo.org.co/scielo.php?script=sci_arttext&pid=S0121-75772018000200067&lng=en&tlng=en&SID=5BQIj3a2MLaWUV4OizE%0Ahttp://scielo.iec.pa.gov.br/scielo.php?script=sci_

Tessema, S. M. (2011). Hydrological modeling as a tool for sustainable water resources management: a case study of the Awash River Basin. In *Trita-LWR. LIC NV - 2056* (Issue May). http://kth.diva-portal.org/smash/get/diva2:416594/FULLTEXT01.pdf%0Ahttp://urn.kb.se/resolve?urn=urn:nbn:se:kth:diva-33617

Teutschbein, C., & Seibert, J. (2012). Bias correction of regional climate model simulations for hydrological climate-change impact studies: Review and evaluation of different methods. *Journal of Hydrology*, *456–457*, 12–29. https://doi.org/10.1016/j.jhydrol.2012.05.052

Thornton, P., Jones, P., Owiyo, T., Kruska, R., Herrero, M., Kristjanson, P., Notenbaert, A., Bekele, N., & Omolo, A. (2006). Mapping climate vulnerability and poverty in Africa. In *Report to the Department for International Development*. http://0-search.ebscohost.com.catalog.library.colostate.edu/login.aspx?direct=true&AuthType=cookie,ip,url,cpid&custid=s4640792&db=lah&AN=20073285958&site=ehost-live

Tschakert, P., Sagoe, R., Ofori-Darko, G., & Codjoe, S. N. (2010). Floods in the Sahel: an analysis of anomalies, memory, and anticipatory learning. *Climatic Change*, *103*(3–4), 471–502. https://doi.org/10.1007/s10584-009-9776-y

Twisa, S., & Buchroithner, M. F. (2019). Seasonal and Annual Rainfall Variability and Their. *Water*, *11*(2055), 1–18. www.mdpi.com/journal/water

Uhlenbrook, S., Holocher, J., Leibundgut, C., & Seibert, J. (1998). Using a conceptual rainfall-runoff model on different scales by comparing a headwater with larger basins. *IAHS-AISH Publication*, *248*(248), 297–305.

UN. (2020). Climate change: Exacerbating poverty and inequality. In *World Social Report 2020*. https://doi.org/10.18356/88668942-en

UNEP-GEF Volta Project. (2013). *Volta Basin Transboundary Diagnostic Analysis* (Issue March).

Valerio, C. (2005). Water Law Review Thomas V . Cech , Principles of Water Resources : History , Development , Management , and Policy. *Water Law Review*, *8*(2).

van de Giesen, N., Liebe, J., & Jung, G. (2010). Adapting to climate change in the Volta Basin, West Africa. *Current Science*, *98*(8), 1033–1037.

Wagner, S., Kunstmann, H., Bárdossy, A., Conrad, C., & Colditz, R. R. (2009). Water balance estimation of a poorly gauged catchment in West Africa using dynamically downscaled meteorological fields and remote sensing information. *Physics and Chemistry of the Earth*, *34*(4–5), 225–235. https://doi.org/10.1016/j.pce.2008.04.002

Wakjira, M. T., Peleg, N., Anghileri, D., Molnar, D., Alamirew, T., Six, J., & Molnar, P. (2021). Rainfall seasonality and timing: implications for cereal crop production in Ethiopia. *Agricultural and Forest Meteorology*, *310*, 1–12. https://doi.org/10.1016/j.agrformet.2021.108633

Wei, L., Jiheng, L., Junhong, G., Zhe, B., Lingbo, F., & Baodeng, H. (2020). The Effect of Precipitation on Hydropower Generation Capacity: A Perspective of Climate Change. *Frontiers in Earth Science*, *8*(268), 1–13. https://doi.org/10.3389/feart.2020.00268

Wheeler, T., & Von Braun, J. (2013). Climate change impacts on global food security. *Science*, *341*(6145), 508–513. https://doi.org/10.1126/science.1239402

Wu, J., Yen, H., Arnold, J. G., Yang, Y. C. E., Cai, X., White, M. J., Santhi, C., Miao, C., & Srinivasan, R. (2020). Development of reservoir operation functions in SWAT+ for national environmental assessments. *Journal of Hydrology*, *583*, 124556. https://doi.org/10.1016/j.jhydrol.2020.124556

Xu, C. (2002). Hydrologic Model. In *Satellite Remote Sensing in Hydrological Data Assimilation*. https://doi.org/10.1007/978-3-030-37375-7_3

Yeboah, K. A., Akpoti, K., Kabo-bah, A. T., Ofosu, E. A., Siabi, E. K., Mortey, E. M., & Okyereh, S. A. (2022). Assessing climate change projections in the Volta Basin using the CORDEX-Africa climate simulations and statistical bias-correction. *Environmental Challenges*, *6*(August 2021), 100439. https://doi.org/10.1016/j.envc.2021.100439

Yu, X., Bhatt, G., Duffy, C., & Shi, Y. (2013). Parameterization for distributed watershed modeling using national data and evolutionary algorithm. *Computers and Geosciences*, *58*, 80–90. https://doi.org/10.1016/j.cageo.2013.04.025

Zhang, M., Zhang, J., & Song, Y. (2019). Preliminary Research and Application of MIKE SHE Model in Jialingjiang River Basin. *IOP Conference Series: Earth and Environmental Science*, *304*(2). https://doi.org/10.1088/1755-1315/304/2/022088

Zhang, Q., Sun, P., Li, J., Xiao, M., & Singh, V. P. (2015). Assessment of drought vulnerability of the Tarim River basin, Xinjiang, China. *Theoretical and Applied Climatology*, *121*(1–2), 337–347. https://doi.org/10.1007/s00704-014-1234-8

Zhou, L., & Wang, Y. (2006). Tropical rainfall measuring mission observation and regional model study of precipitation diurnal cycle in the New Guinean region. *Journal of Geophysical Research Atmospheres*, *111*(17), 1–18. https://doi.org/10.1029/2006JD007243

Annex

Annex 1a: Statistical analysis of uncorrected climate models performance in simulating mean monthly rainfall

Climate models	Statistical measures				
	PBIAS (%)	NSE	rSD	RMSE	*r*
CanESM2	-6.8	0.53	0.96	58.66	0.76
CNRM-CM5	-6.8	0.53	0.96	58.66	0.76
EC-EARTH	-6.8	0.53	0.96	58.66	0.76
IPSL-CM5A-MR	-6.8	0.53	0.96	58.66	0.76
MIROC5	-6.8	0.53	0.96	58.66	0.76
MPI-ESM-LR	-6.8	0.53	0.96	58.66	0.76
GFDL-ESM2M	-6.8	0.53	0.96	58.66	0.76
NorESM1-M	-6.8	0.53	0.96	58.66	0.76
Ensemble mean	-6.8	0.53	0.96	58.66	0.76

Annex 1b: Statistical analysis of uncorrected climate models performance in simulating mean monthly temperature

Climate models	Statistical measures				
	PBIAS (%)	NSE	rSD	RMSE	*r*
CanESM2	6.8	-0.38	0.96	2.12	0.82
CNRM-CM5	6.8	-0.38	0.96	2.12	0.82
EC-EARTH	6.8	-0.38	0.96	2.12	0.82
IPSL-CM5A-MR	6.8	-0.38	0.96	2.12	0.82
MIROC5	6.8	-0.38	0.96	2.12	0.82
MPI-ESM-LR	6.8	-0.38	0.96	2.12	0.82
GFDL-ESM2M	6.8	-0.38	0.96	2.12	0.82
NorESM1-M	6.8	-0.38	0.96	2.12	0.82
Ensemble mean	6.8	-0.38	0.96	2.12	0.82

Annex 1c: Comparison at annual scale between observed and simulated (a) rainfall before bias-correction and (b) rainfall after bias-correction

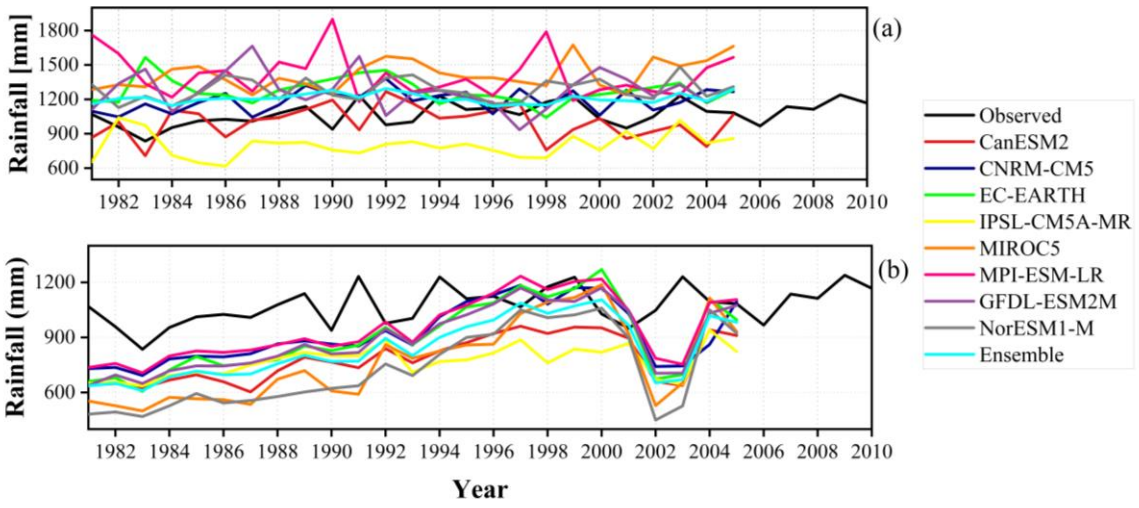

Annex 1d: Comparison at annual scale between observed and simulated (a) temperature before bias-correction and (b) temperature after bias-correction

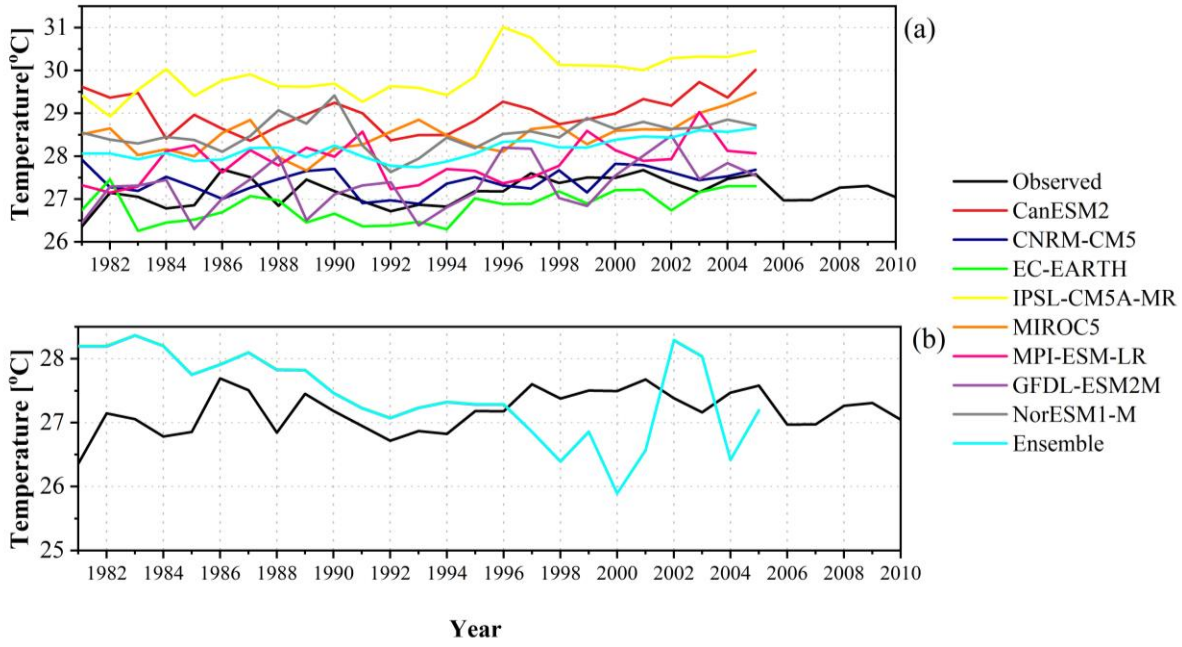

Annex 1e: Basic statistics of rainfall onset in the Oti River Basin for historical and future periods

Station	Observed (1981-2010)		Sim-historical (1981-2005)		RCP4.5 (2021-2050)		RCP8.5 (2021-2050)	
	SD [days]	CV [%]	SD [days]	CV [%]	SD [days]	CV [%]	SD [days]	CV [%]
GRID1	16	10.8	27	16	18	11.0	18	11.2
GRID2	18	12.3	21	12	21	12.7	20	12.7
GRID3	16	11.4	22	13	21	11.7	23	13.9
GRID4	17	11.9	25	14	24	13.9	23	14.7
GRID5	17	12.2	22	14	23	14.0	17	10.8
GRID6	18	12.8	20	13	23	14.2	21	13.8
GRID7	16	11.3	23	14	20	11.7	19	11.8
GRID8	15	11.0	23	14	23	14.7	19	13.1
GRID9	16	11.9	23	15	19	12.8	19	12.8
GRID10	19	14.4	18	12	19	12.7	17	11.7
GRID11	16	11.5	19	12	19	12.9	17	10.9
GRID12	15	12.1	18	12	18	12.0	18	12.0
GRID13	18	14.6	23	16	23	15.0	18	12.3
GRID14	16	13.9	20	13	16	11.5	19	13.1
GRID15	16	13.5	18	12	12	9.1	13	9.7
GRID16	14	12.9	17	12	13	11.0	18	13.8
GRID17	10	9.6	16	12	14	11.8	13	10.6
GRID18	12	12.0	24	18	16	12.6	20	15.7
GRID19	12	11.4	14	12	9	8.5	18	15.3
GRID20	9	8.9	15	12	15	12.8	15	12.8
Natitingou	20	16.1	17	13	25	18.7	22	16.3
Fada	22	14.6	22	13	15	9.1	17	10.9
Tenkodogo	19	13.0	28	17	20	12.4	14	8.9
Kete Krachi	25	19.7	14	11	13	11.5	15	12.5
Yendi	19	15.2	19	13	13	9.8	18	12.9
Dapaong	21	15.2	21	14	21	13.3	14	8.9
Kara	21	17.2	16	13	18	14.1	18	13.8
Mango	29	20.0	20	14	20	14.5	18	12.8
Niamtougou	18	15.3	18	14	20	14.3	17	12.2
Sokode	24	21.1	19	15	9	8.2	18	15.4
Basin	8	6.6	12	8	10	6.9	9	6.3

Note: *SD=standard deviation; CV=coefficient of variation; Sim-historical=Simulated-historical*

Annex 1f: Basic statistics of rainfall cessation in the Oti River Basin for historical and future periods

Station	Observed (1981-2010)		Sim-historical (1981-2005)		RCP4.5 (2021-2050)		RCP8.5 (2021-2050)	
	SD [days]	CV [%]	SD [days]	CV [%]	SD [days]	CV [%]	SD [days]	CV [%]
GRID1	10	3.4	1	0.3	2	0.9	8	2.7
GRID2	8	2.8	2	0.6	2	0.6	7	2.6
GRID3	8	2.9	0	0.0	0	0.0	1	0.4
GRID4	8	2.9	1	0.5	5	1.8	7	2.7
GRID5	8	2.7	1	0.4	6	2.1	5	1.8
GRID6	9	3.1	0	0.0	3	1.3	5	1.9
GRID7	7	2.4	0	0.0	3	1.0	6	2.1
GRID8	10	3.6	1	0.4	1	0.5	7	2.4
GRID9	9	3.1	3	1.1	1	0.4	9	3.1
GRID10	9	3.2	1	0.5	8	2.9	5	1.7
GRID11	8	2.8	0	0.1	7	2.4	3	1.1
GRID12	12	4.0	2	0.6	5	1.9	5	1.8
GRID13	10	3.5	3	1.2	5	1.6	7	2.4
GRID14	9	3.0	7	2.5	9	3.3	10	3.7
GRID15	10	3.2	7	2.6	6	2.2	8	2.7
GRID16	17	5.3	7	2.5	7	2.5	8	2.8
GRID17	10	3.1	10	3.2	11	3.7	11	3.8
GRID18	12	3.6	9	3.0	6	2.2	8	3.0
GRID19	10	3.2	9	3.2	11	3.7	9	3.3
GRID20	12	3.6	9	3.0	9	3.0	8	2.6
Natitingou	11	3.6	6	2.0	4	1.6	8	2.9
Fada	16	5.5	3	1.0	2	0.9	6	2.1
Tenkodogo	9	3.2	1	0.4	4	1.4	6	2.2
Kete Krachi	20	6.0	10	3.3	11	3.7	9	3.0
Yendi	18	5.8	7	2.6	6	2.0	7	2.3
Dapaong	20	6.6	4	1.5	5	1.9	5	1.8
Kara	16	5.1	7	2.4	4	1.4	8	2.9
Mango	14	4.8	4	1.4	7	2.6	9	3.1
Niamtougou	18	5.6	6	2.3	4	1.4	8	2.9
Sokode	17	5.4	9	3.1	9	3.0	6	2.2
Basin	6	1.9	2	0.8	3	1.0	4	1.4

Note: *SD=Standard deviation; CV=Coefficient of variation; Sim-historical=Simulated historical*

Annex 2: List of Publications

- **Daniel Kwawuvi**, Daouda Mama, Sampson K. Agodzo, Andreas Hartmann, Isaac Larbi, Enoch Bessah, Tesfalem Abraham, Sam-Quarcoo Dotse & Andrew Manoba Limantol (2022). An investigation into the future changes in rainfall onset, cessation and length of rainy season in the Oti River Basin, West Africa. *Modeling Earth Systems and Environment*. 8, 5077-5095. https://doi.org/10.1007/s40808-022-01410-w.

- **Daniel Kwawuvi**; Daouda Mama; Sampson K. Agodzo; Andreas Hartmann; Isaac Larbi; Enoch Bessah; Andrew Manoba Limantol; Sam-Quarcoo Dotse; Gnibga Issoufou Yangouliba (2022). Spatiotemporal variability and change in rainfall in the Oti River Basin, West Africa. *Journal of Water and Climate Change*, 13 (3): 1151–1169. https://iwaponline.com/jwcc/article/13/3/1151/87101/Spatiotemporal-variability-and-change-in-rainfall.

Daniel Kwawuvi is a final-year PhD student in Climate Change and Water Resources. Daniel's PhD program is supported by the German Federal Ministry of Education and Research under the West African Science Service Centre on Climate Change and Adapted Land Use (WASCAL) at University of Abomey-Calavi, Republic of Benin. Daniel's doctoral research concerns intraseasonal rainfall variability and its implications on streamflow in the Oti basin of West Africa. He is largely interested in environmental sciences and modelling. Daniel holds a Master of Science degree in Environmental Management from the Pan African University, Life and Earth Sciences Institute, University of Ibadan of Nigeria. He obtained his Bachelor of Science degree in Forest Resources Technology from the Kwame Nkrumah University of Science and Technology of Kumasi, Ghana. Daniel also holds a Certificate in Environmental Management from the Institute of Environmental Assessment of England, and consequently, a Practitioner member of the Institute of Environmental Management and Assessment. Daniel also has a Single Diploma in Occupational Health and Safety Administration from the Institute for Professional and Executive Development, England, UK. Prior to gaining admission for his Bachelor's degree, he attended St. Mary's Boys' Secondary School in Takoradi, Ghana. He also had his basic education at Myohaung Barracks School of Apremdo-Takoradi, Ghana.

***Abstract*:** This study assessed the intraseasonal rainfall variability and its implications on streamflow in the Oti River Basin in West Africa. The specific objectives were to: (i) determine the intra-seasonal rainfall variability and trends for the historical period (1981-2010) and future period (2021-2050) in the Oti basin. (ii) determine the projected changes in intra-seasonal rainfall variability indicators in the Oti basin for the future period (2021-2050) and (iii) To assess the impact of intra-seasonal rainfall variability on streamflow using the Hydrologiska Byråns Vattenbalansavdelning (HBV) model. The analysis was performed using high-resolution and quality-controlled climate data from the Ghana Meteorological Agency, National Meteorological Service of Togo, Meteorological Department of Benin, Climate Hazards Infrared and Precipitation Stations (CHIRPS), and NASA-POWER. The analysis for the future period was performed under RCP4.5 and RCP8.5 scenarios using a multi-model mean ensemble of eight bias-corrected regional climate models based on the quantile-quantile mapping method and from the Coordinated Regional Climate Downscaling Experiment (CORDEX-Africa). The study also used discharge data from the Water Resources Commission, Ghana, Water Resources Directorate (Togo), National Hydrological Service (DGIRH) of Burkina Faso and the Direction Generale de L'eau, Benin. The study revealed a likely decline in mean rainfall in the future by about 103.6 mm/yr (RCP4.5) and 45.9 mm/yr (RCP8.5). It also projected a decline in mean rainfall during the rainy season by about 90.8 mm/yr (RCP4.5) and 34.6 mm/yr (RCP8.5). The study further found a late onset of rains in the basin by about +16 days (RCP4.5) and +15 days (RCP8.5) which would possibly have a rippling effect on rainfall cessation in the basin causing it to occur earlier by a decrease of about 21 days under both RCP4.5 and RCP8.5 scenarios, with regards to the historical period. This subsequently resulted in shortening the length of rainy season by about 37 days (RCP4.5) and 36 days (RCP8.5). The number of wet and dry days are projected to increase and decrease respectively. Additionally, the streamflow of the basin was evaluated and projected for the future using the HBV hydrologic model. The mean multi-model ensemble predicted an increase in mean monthly streamflow at all sub-basins in the future (2021-2050) relative to the historical period (1981-2010) except Arly which is anticipated to have a decrease in its streamflow by about 2.79% (RCP4.5) while it will increase by 31.17% (RCP8.5). The anticipated variations in the rainfall could affect the scheduling of agriculture, its sustainability and could place the basin a water-related stress.

***Key words*:** Oti River Basin, HBV model, rainfall variability, onset, cessation, anomaly

PhD

Daniel KWAWUVI

INTRA-SEASONAL RAINFALL VARIABILITY AND ITS IMPLICATIONS ON STREAMFLOW IN THE OTI BASIN, WEST AFRICA

GRP/CCWR/INE/WASCAL – UAC APRIL, 2023